# UNIVERSIDAD COMPLUTENSE DE MADRID

FACULTAD DE CIENCIAS QUÍMICAS

Departamento de Química Física I



## TESIS DOCTORAL

# Microreología de sistemas viscoelásticos

# Microrheology of viscoelastic systems

MEMORIA PARA OPTAR AL GRADO DE DOCTOR

PRESENTADA POR


**Nuria Mancebo Radio**

Directores

**Francisco Ortega Gómez**
**Ramón González Rubio**


**Madrid, 2017**

UNIVERSIDAD COMPLUTENSE DE MADRID


# MICROREOLOGÍA DE SISTEMAS VISCOELÁSTICOS

**— TESIS DOCTORAL —**

Nuria Mancebo Radio

Madrid, España

2016

UNIVERSIDAD COMPLUTENSE DE MADRID


# MICRORHEOLOGY OF VISCOELASTIC SYSTEMS

**— DISSERTATION —**

Nuria Mancebo Radio

Madrid, Spain

2016

UNIVERSIDAD COMPLUTENSE DE MADRID
FACULTAD DE CIENCIAS QUÍMICAS


# MICROREOLOGÍA DE SISTEMÁS VISCOELÁSTICOS
# MICRORHEOLOGY OF VISCOELASTIC SYSTEMS

Memoria para aspirar al grado de Doctor
In Partial Fulfillment of the Requirements for the Degree of Doctor of Philosophy

Presentada por
by

**Nuria Mancebo Radio**

Directores/Supervised by:
Francisco Ortega Gómez Ramón González Rubio

Este trabajo ha sido llevado a cabo en el Departamento de Química Física I de la Universidad Complutense de Madrid, bajo la dirección de los profesores doctores D. Francisco Ortega Gómez y D. Ramón González Rubio. También se ha trabajado en el laboratorio del profesor doctor D. Miguel Ángel Rubio de la Universidad Nacional de Educación a Distancia.

Durante la Tesis Doctoral se ha realizado una estancia en Alemania en el Departamento de Física, en la Universidad de Constanza, bajo la supervisión del profesor Georg Maret.

La financiación de esta investigación resulta del Ministerio de Ciencia e Innovacción a través de la beca predoctoral FPI.

# Contents

# ESTRUCTURA DE LA TESIS

Con objeto de facilitar la lectura y entendimiento de la presente memoria de tesis doctoral, se ha considerado oportuno incluir en primer lugar esta descripción breve del contenido y distribución de la misma.

En cuanto a la distribución, la tesis doctoral comienza con el índice general del manuscrito. A continuación figura un resumen que pretende dar una idea general del contenido de la misma, introduciendo al lector en el trabajo realizado de una manera sencilla y directa. Seguidamente, se desarrollan los capítulos que la componen, finalizando con una relación de la bibliografía utilizada en los mismos. Se ha preferido incluir la bibliografía al final para no repetir citas bibliográficas y facilitar su localización. Por último, se incluye un breve Curriculum Vitae de la autora de este trabajo.

En lo que respecta al contenido, el primer capítulo consiste en una introducción, que pretende ser un estado del arte de la temática, expone la importancia relativa de la misma, y trata de una manera general el planteamiento del problema que se quiere abordar en esta investigación. El segundo capítulo recoge los objetivos que se han marcado y la metodología a utilizar para lograrlos. Los siguientes capítulos describen las técnicas experimentales empleadas con los detalles del equipo y las medidas de los diferentes experimentos. Los capítulos de resultados constituyen el núcleo de la tesis doctoral y en sus distintos apartados se ha incluido una introducción o antecedentes concretos para ayudar a la comprensión de los temas tratados en cada capítulo. Se agrupan en dos bloques de trabajo de acuerdo con el sistema de estudio en cada uno de ellos. El primer bloque de resultados agrupa el estudio de partículas coloidales en un fluido viscoso newtoniano, el glicerol. En este capítulo se presentan los resultados obtenidos con diferentes tipos de técnicas experimentales macro y microreológicas. Sigue el segundo bloque de resultados donde se profundiza en los sistemas viscoelásticos, centrando la investigación en la técnica de espectroscopía de onda difusa (DWS) por ser el estudio que se pretende realizar y que presenta además un gran interés para los sistemas tratados. En este caso se estudia la matriz en sí y el efecto de las partículas, que da lugar a tres capítulos de resultados según el agente viscoelástico, son la Agarosa, el Pluronic F127 y el Ácido hialurónico. La tesis doctoral finaliza con un capítulo en el que

se recogen las principales conclusiones derivadas del trabajo desarrollado, que pretende resumir las conclusiones parciales de cada capítulo.

Con motivo de la solicitud de la mención de doctorado europeo, determinadas partes de la tesis se han redactado en inglés. Estas partes son: resumen y conclusiones, los apartados de técnicas: reología, microreología y el bloque de resultados segundo que comprende los capítulos de resultados de sistemas viscoelásticos.

# Resumen

# MICROREOLOGÍA DE SISTEMAS VISCOELÁSTICOS

## Introducción

Es importante comenzar encuadrando la tesis globalmente dentro del marco socioeconómico actual y describir su objetivo general, que es la puesta a punto de técnicas microreológicas que permitan obtener información de propiedades de transporte del sistema. El aspecto clave que justifica esta meta es el tipo de sistema a estudiar, un sistema viscoelástico en el que se puedan medir propiedades microreológicas.

Esta tesis se enmarca en el área de la ciencia llamada microreología, que estudia la dependencia del módulo de cizalla complejo de un fluido con la frecuencia utilizando el movimiento de partículas suspendidas en él como información experimental. En los últimos años, ha habido un gran avance en la investigación de estos métodos tanto en lo que se refiere a los métodos experimentales como al análisis teórico de los datos.

La novedad que introduce la microreología es que se trata de escalas de longitud micrométrica, por lo que se necesitan especiales condiciones para su medición, tales como el tamaño de las partículas, además de la ventaja de poder emplear menor cantidad de muestra. Tanto las técnicas activas y pasivas se basan en la medición del desplazamiento cuadrático medio, a partir del movimiento browniano inherente a las partículas sonda. Las principales técnicas de este tipo que se han utilizado y se describen en profundidad en esta tesis son la dispersión de luz dinámica (DLS) y una variante de ésta que es la espectroscopía de onda difusa (DWS). Otras alternativas son la videomicroscopía o el uso de pinzas ópticas o magnéticas.

La dispersión de luz se encuentra dentro del conjunto de técnicas experimentales basadas en la interacción radiación-materia. El campo electromagnético de

la luz incidente induce un momento dipolar oscilante en las moléculas del medio, de manera que la luz irradiada por el dipolo, que se denomina luz dispersada o difundida, tiene la misma frecuencia que la radiación incidente y una intensidad mucho menor, típicamente $10^{-4}$ a $10^{-6}$ veces la incidente. Ésta técnica proporciona información sobre el tamaño, por ejemplo peso molecular de polímeros y radio hidrodinámico de partículas, y de su dinámica como el coeficiente de difusión.

La técnica de dispersión de luz se utiliza en disoluciones diluidas para evitar la dispersión de los fotones por múltiples moléculas o partículas.

DWS es una técnica de dispersión de luz dinámica que funciona en régimen de dispersión múltiple proporcionando la ventaja de poder estudiar fluidos densos y turbios sin necesidad de ajustar los índices de refracción del sistema como en DLS. Permite además obtener propiedades viscoelásticas en un rango de alta frecuencia que no es accesible a los reómetros convencionales.

Con esta técnica se puede estudiar propiedades dinámicas como el coeficiente de difusión y la respuesta tanto elástica como dinámica (viscoelástica) del medio en que se suspenden las partículas a través del desplazamiento cuadrático medio (MSD).

Las propiedades viscoelásticas de los materiales pueden ser determinadas entonces a partir del desplazamiento cuadrático medio de las partículas, obtenidos a partir de las fluctuaciones térmicas del medio.

## Objetivos y resultados

Esta tesis doctoral tiene dos objetivos generales:

a) Poner a punto los distintos tipos de técnicas microreológicas para la caracterización de sistemas viscosos y viscoelásticos;

b) Emplear una técnica microreologíca para investigar los fenómenos de gelificación y las propiedades viscoelásticas de geles. Estos sistemas son muy importantes desde el punto de vista académico y tecnológico.

Se comparan resultados de varias técnicas pasivas de microreología para poder comprobar su consistencia, y a partir de esto aplicar distintas metodologías de análisis de los datos intentando ajustarlos a modelos viscoelásticos.

Con dicha finalidad se han seleccionado cuatro sistemas de estudio, por un lado de tipo viscoso: el glicerol, y por otro lado de tipo viscoelástico. Dentro de los viscoelásticos los siguientes tipos: un gel biológico: la agarosa, un surfactante: el

copolímero Pluronic F-127, y un gel cosmético: el ácido hialurónico.

En este contexto, los resultados en la presente memoria se han estructurado en dos partes según el tipo de comportamiento del sistema:

- **Sistema viscoso** o Newtoniano. Glicerol. Permite iniciar la investigación y comprobación del correcto funcionamiento de los métodos microreológicos al tratarse de un sistema cuyas propiedades reológicas son más predecibles y ajustables a modelos ya descritos en la bibliografía.

Las concentraciones de las mezclas acuosas estudiadas van desde un 5% (w/w) glicerol hasta el glicerol puro.

Las partículas empleadas son de látex de poliestireno de dos tamaños uno de $22 \pm 3$ nm y otro más grandes de $1.00 \pm 0.03\ \mu$m de diámetro.

Tras un tratamiento inicial por dispersión de luz dinámica por el método de cumulantes y el análisis CONTIN, se ha comprobado el comportamiento difusivo tanto del glicerol puro como de sus mezclas acuosas, obteniendo funciones de autocorrelación con caídas exponenciales únicas, de las que se calcula el coeficiente de difusión de la particula en el seno del sistema.

Además, se ha logrado cuantificar el desplazamiento cuadrático medio de las partículas a partir de las funciones de autocorrelación obtenidas de la técnica de dispersión de luz dinámica. Se encontró que es posible realizar un ajuste lineal a un amplio rango temporal, que demuestra el comportamiento viscoso del glicerol.

Los resultados obtenidos por reología mecánica (macroreología) confirman a baja frecuencia el comportamiento viscoso del glicerol, lo que está de acuerdo con los resultados obtenidos por Espectroscopía de onda difusa.

Por videomicroscopía se ha observado igualmente el movimiento browniano que describen las partículas sumergidas en el glicerol, y del cálculo de sus trayectorias se ha obtenido un coeficiente de difusión similar al obtenido por el resto de técnicas microreológicas empleadas. También se ha visto la linealidad en los desplazamientos cuadráticos medios a tiempos iniciales.

- **Sistemas viscoelásticos**. Agarosa, Pluronic F127 y Ácido hialurónico. Se estudia el comportamiento de estos sistemas complejos intentando interpretar los resultados con modelos viscoelásticos como el de Maxwell y otros desarrollados a partir de éste.

Se han utilizado dos tipos de partículas, poliestireno de $977 \pm 2$ nm y dióxido de titanio de $127.0 \pm 0.4$ nm de diámetro.

Cada uno de los geles se prepara de forma manual. Los geles de agarosa se elaboran disolviendo el polvo de agarosa en agua y llevando a ebullición la disolución. La

concentración de agarosa en estos hidrogeles está entre 1 y 5 g/L (0.1-0.5%w/v).

Las disoluciones de Pluronic F127 se estudian en un rango de concentración de 7 a 25%w/v en donde se forman geles. Por debajo no llega a formarse gel. Su preparación necesita temperaturas bajas sin llegar a la conjelación, a diferencia de la agarosa, por lo que se diluye el pluronic F127 en agua fría.

El gel de Ácido hialurónico se prepara disolviendo el polvo en agua fría y después se añade la disolución de la sal. Las concentraciones estudiadas de ácido van desde 1 a 15 g/L, y concentración molar de sal de 0.1 y 0.5 M NaCl y $CaCl_2$.

Para la agarosa se ha visto que presenta un comportamiento muy peculiar e interesante que no muestra el resto de sistemas viscoelásticos analizados y es que parece que interacciona de forma específica con las partículas. Cuando se comparan los resultados obtenidos con diversos tamaños de partículas no se sigue el comportamfiento habitual entre coeficiente de difusión y radio hidrodinámico de las partículas. En efecto dicho coeficiente es menor para partículas de $TiO_2$ que para partículas de poliestireno.

Se ha empleado un modelo de Maxwell extendido para describir mejor la curva de MSD en todo el intervalo de tiempos medido, imprescindible para calcular el módulo complejo de cizalla. Este modelo predice las tres regiones encontradas experimentalmente. Una a tiempos bajos que es la difusión browniana $D_0$, a tiempos intermedios se obtiene el llamado *tamaño de la caja* o *longitud elástica* $\delta$, y a tiempos largos se tiene de nuevo un comportamiento difusivo.

La interacción que ocurre entre las partículas de $TiO_2$ y la agarosa no se observa para el resto de geles estudiados, el pluronic F127 y el ácido hialurónico, cuyos resultados siguen de forma más ordenada los modelos viscoelásticos.

En lo que concierne al Pluronic F127 se obtiene una curva para el MSD frente al tiempo diferente a la obtenida para la agarosa, presentando la agarosa una curva cóncava y el pluronic una convexa. Esto significa una distorsión en los parámetros integrados en el modelo de Maxwell que necesitan de un tratamiento distinto. Es posible hacer un ajuste matemático a la viscosidad de acuerdo a la ecuación de Ahrrenius en la zona viscosa, en cambio en la agarosa se predecía un comportamiento tipo pseudoplástico.

En cuanto al ácido hialurónico, en primer lugar no presenta una influencia de la temperatura tan importante como en los otros sistemas. Sin embargo sí es relavante la fuerza iónica, y por ello se han utilizado distintas sales, NaCl y $CaCl_2$, siendo la última la que presenta un comportamiento viscoelástico más claro. Además del modelo de Maxwell extendido para este caso, se ha utilizado el modelo de Rouse-Zimm, apropiado por las características de la naturaleza del gel debidas a la influencia de la fuerza iónica.

# Conclusiones

A lo largo de este proyecto de Tesis Doctoral se ha estudiado la respuesta mecánica de distintos sistemas utilizando técnicas de dispersión de luz.

La dispersión de luz se puede medir utilizando diversos tipos de técnicas, las activas basadas en manipulación directa de las partículas, como pinzas ópticas, campos magnéticos; y otras técnicas que son las llamadas pasivas y que son las utilizadas en esta tesis que se basan en el movimiento inducido en las partículas por transferencia de cantidad de movimiento y calor. Todas ellas englobadas bajo el mismo fundamento, la medición de las fluctuaciones de intensidad que se producen provocadas por una fuerza externa, una luz láser.

Los sistemas seleccionados han resultado ampliamente caracterizados por estas técnicas, sobretodo por la novedosa y puntera DWS, de la que han derivado resultados satisfactorios que enlazan con los obtenidos por la homóloga técnica macro, la reología.

El análisis de los MSD obtenidos por DWS permite obtener los módulos complejos a partir de la ecuación de Stokes-Einstein.

El mejor modelo viscoelástico que describe el comportamiento no-Newtoniano de los sistemas es el llamado de Maxwell retocado.

La **Agarosa** muestra un comportamiento especial, además de presentar la viscoelasticidad del gel también se observa la reacción del gel con las partículas.

El **Pluronic F127** forma un bucle de gelificación, con una concentración óptima en la que presenta reversión sol-gel.

El **Ácido hialurónico** necesita de una sal para que le proporcione la fuerza iónica necesaria para la formación de un gel con propiedades viscoelásticas.

# Abstract

# MICRORHEOLOGY OF VISCOELASTIC SYSTEMS

## Introduction

This research describes the application of microrheological techniques to study the viscoelasticity of gels as model of weakly ergodic media, during their complex gelation mechanism to make it an interesting prototype for many other gelling systems in order to predict changes in their bulk properties.

Microrheology is founded on the pioneering work of researchers such as Weitz and Mason, [1], [2]. In microrheology, the termal motion of probe particles is interpreted in terms of the mechanical properties of the medium in which they are suspended. The motion of the particles can be quantified with a variety of techniques which can fall into two classes: those involving active manipulation of probe particles within the sample, and those employing passive observation of thermal fluctuations of such probe particles. In either case, the probes used are typically chemically inert spherical beads of between a fraction of a micrometer to several micrometers in diameter. Passive techniques are typically more useful for measuring low values of predominantly viscous moduli, whereas active techniques can extend the measurable range to samples containing significant amounts of elasticity and for carrying out measurements outside the linear regime. Active microrheology methods are, for example, optical and magnetic tweezers, atomic force microscopy. Passive methods are particle tracking, dynamic light scattering, diffusion wave spectroscopy [3], [4].

Microrheological techniques have been shown to provide reliable information in the study of complex fluids. Namely, Diffusing Wave Spectroscopy, DWS, can be used to study turbid samples under controlled temperature conditions. DWS achieves a frequency range far beyond that of conventional rheometers, thus allowing one observing the gels behavior at high frequency.

DWS is an extension of dynamic light scattering, DLS, to the multiple scattering limit. In both cases the intensity fluctuations of the scattered light reflect the dynamics of the scattering medium. The technique extends the analytic power of DLS to opaque samples such us concentrated suspensions, obviating the need to dilute or index match.

Glycerol, agarose, pluronic F127 and hyaluronic acid solutions have been examined in a broad concentration and temperature range. The solutions were doped with microparticles of different size that act both as light scatterers and microrheological probes. The complex shear modulus of the systems has been obtained from the time dependence of the average mean square displacement, MSD, of the particles using the generalized Stokes-Einstein equation.

The viscoelastic model that best describes the non-Newtonian behaviour of these systems is the so called Maxwell fluid, which is a generalization of the previous Maxwell one including additional terms. In order to fit accurately the experimental MSD the dynamic heterogeneity of these complex systems must be properly accounted for.

Three regions for the motion of the probe particles can be appreciated in the MSD. At short times, the dynamic is Brownian, at intermediate times, the mean square displacement remains constant with time, and at longer times it becomes diffusive again.

Microrheological information of complex viscoelastic fluids are provide by DWS and comparing with mechanical measurements at low frequency a good agreement between both techniques was found. The MSD obtained from DWS can be directly inverted using the Stokes-Einstein relation to get the complex shear modulus or a fit with an analytical MSD model derived from a given viscoelastic model can be alternatively used. Using both strategies one can get a more complete dynamic information in the case of complex viscoelastic fluids.

## Objectives and results

The main objective of this Dissertation is two-faced nature, on one hand to study the different types of microrheologycal techniques to understand and characterizate viscous and viscoelastic systems and employ microrheology science to investigate the phenomena of gelling and viscoelastic properties of gels. These systems are very important from the point of view of their application as particles probes and particle stability within it. Both systems are studied in aqueous medium.

Results of several microbiological passive techniques are compared in order to check their consistency and therefore be able to select different methodologies for data analysis adjusting to viscoelastic models.

In this context, this PhD Thesis has been divided into two parts depending on the system behavior:

- **Viscous or Newtonian system**. Glycerol. This allows launching the study and verifying the correct operation of the microreologycal methods, as it is a system whose rheological properties are already more predictable and adjustable to the models.

The concentrations of the aqueous mixtures studied ranging from 5% (w/w) glycerol to the pure glycerol. The particles used are polystyrene latex of two sizes, one of 22± 3 nm and a larger ones of $1.00 \pm 0.03\mu$m in diameter.

After an initial treatment by dynamic light scattering by the cumulant method and the other one CONTIN analysis, it has been proved both the diffusive behavior of pure glycerol and their aqueous mixtures, obtaining autocorrelation functions with exponential fall, that derived of straight lines in the representation of the inverse relaxation time, called decay rate against the square of the wave vector which gives the diffusion coefficient of the particle in the system.

Furthermore, the mean square displacement of the particles has been quantify from the autocorrelation functions obtained from dynamic light scattering. It is found that a linear fit is abble to cover a wide time range, showing the viscous behavior of glycerol.

The results obtained by mechanical rheology confirm at low frequency the viscous behavior of glycerol and making them connect with the results obtained by diffusive wave spectroscopy corroborate this behavior.

By videomicroscopy it was also observed the particles immersed in glycerol describe Brownian motion. Calculating their trajectories, the diffusion coefficient is obtained and becomes similar to that obtained by the other microreologycal techniques used. The mean square displacements are linear.

- **Viscoelastic systems**. Agarose, hyaluronic acid and Pluronic F127. The behavior of these complex systems is studied trying to understand the results adjusting them to a viscoelastic models such as Maxwell and others developed from it.

Two types of particles are used, polystyrene of 977 nm and titanium dioxide 127 nm diameter.

Each type of gels is prepared manually. **Agarose** gels are obtained by dissolving the powder of agarose in water and by boiling the solution. The concentration of

agarose in these hydrogels is between 1 and 5 g/L (0.1-0.5 %w/v).

Solutions of **Pluronic F127** are studying in a concentration range of 7 to 25 %w/v, where gels are formed, below these concentrations the gel is not formed and above is too dense. A self-supporting, gel-like liquid crystalline phase is formed as the temperature is raised to 20°C. Their preparation requires cold, unlike agarose, so the pluronic F127 is diluted in cold water.

The **Hyaluronic acid** gel is prepared first by dissolving the powder in cold water and then the dissolution of the salt is added. Acid concentrations range from 1 to 15 g/L are tested, and molar salt concentration 0.1 to 0.5 M NaCl and $CaCl_2$.

The agarose has shown a peculiar and very interesting behavior that does not show the rest of viscoelastic systems analyzed and it seems that somehow agarose reacts with the particles. When the results obtained with different particle sizes are collecting, instead of following a causal link between the size and microrheological properties, they are affected, so in this Thesis chemical reactions between the gel and tracer particles are considered.

This reaction that occurs between the particles and the agarose not perceived for other gels studied, pluronic F127 and hyaluronic acid, whose results are more orderly viscoelastic models.

Maxwell model is used completed with four parameters to better detail the MSD curve, to improve the three regions that a viscoelasticity curve presents (see Maxwell equation in Agarose chapter).

One parameter is at low times that defines the Brownian diffusion $D_0$, at intermediates times has the parameter $\delta$ that is called *box size* or *elastic length*, and at long times it has a diffusive behavior again having $D_m$. Following the idea of an exponential, the exponent $\alpha$ which allows a better fit in the area of the inflection point of the MSD curve is included.

Regarding the Pluronic F127, the MSD curves are different to that obtained for the agarose, appearing to be inverted, presenting a concave curve Agarose and a convex Pluronic F127. This means a distortion in the parameters involved in the Maxwell model which need different treatment. It is possible to fit the viscosity according to the Ahrrenius equation.

Concerning the Hyaluronic acid, first it has no a strong influence with temperature as it has for the other systems, Pluronic F127 and Agarose. However, ionic force is relavant and makes the gel changes. Therefore, various salts are used, NaCl and $CaCl_2$, being the strongest salt which presents a clearer viscoelastic behavior. Furthermore Maxwell model for this case is also appropriate Rouse-Zimm model.

# Conclusions

Throughout this PhD Thesis the dynamics of different systems, in terms of Scattering Theory, have been studied.

Microrheology is founded on the rheology at smaller length scales. In microrheology, the termal motion of probe particles is interpreted in terms of the mechanical properties of the medium in which they are suspended. The motion of the particles has been quantified with the technique DWS, as a whole study.

Glycerol, Agarose, Pluronic F127 and Hyaluronic acid solutions have been examined in a broad concentration and temperature range. The solutions were doped with microparticles of different size that act both as light scatters and microrheological probes. The complex shear modulus of the systems has been obtained from the time dependence of the average mean square displacement MSD, of the particles using the generalized Stokes-Einstein equation.

The viscoelastic model that best describes the non-Newtonian behaviour of these systems is the so called Maxwell fluid, which is a generalization of the Maxwell one including additional parameters.

DWS provides important microrheological information of complex viscoelastic fluids which compared with mechanical measurements at low frequency found a good agreement. The MSD obtained from DWS can be directly inverted using GSE to get the complex shear modulus or fit with an analytical MSD model derived from a given viscoelastic model. Using both strategies can get more complete dynamic information in the case of complex viscoelastic fluids.

**Agarose** shows a special behavior, agarose gel presents viscoelastic properties and also reacts with the particles, changing the causal behavior and showing new viscoelastic properties.

**Pluronic F127** forms a gelling loop, with an optimum concentration at which a reversal sol-gel can be appreciated.

**Hyaluronic acid** needs a salt which provides the ionic force to become a gel with viscoelastic properties.

# Chapter 1

# Introducción

## 1.1. Antecedentes

Es importante comenzar encuadrando la tesis globalmente dentro del marco socio-económico actual y describir su objetivo general, que es la puesta a punto de técnicas microreológicas que permitan obtener información de propiedades de transporte del sistema. El aspecto clave que justifica esta meta es el tipo de sistema a estudiar, un sistema viscoelástico en el que se puedan medir propiedades microreológicas. Esto es importante desde el punto de vista de la aplicación en sistemas reales como el flujo sanguíneo, el procesado de cremas y geles en cosmética, tecnología de alimentos y farmacia o la amortiguación en un coche, ya que ayuda a resolver en el primer caso el flujo por canal estrecho a alta frecuencia, las propiedades viscoelásticas óptimas en productos cosméticos y farmacéuticos y en el último caso la elevada frecuencia a soportar por la amortiguación de un coche cuando éste va a alta velocidad y con rugosidades en la carretera. El problema químico físico que se pretende ayudar a resolver es el derivado de la alta frecuencia proponiendo para ello un tipo de sistema que la resista, en esta tesis se estudian por un lado el glicerol un sistema que en condiciones normales se comporta como un fluido newtoniano pero que si se sobrepasan ciertos límites pierde su ergodicidad, y por otro lado los propios fluidos viscoelásticos, un gel biológico, la agarosa; un polímero tensoactivo, el pluronic F127, y un gel utilizado en cosmética y medicina, el ácido hialurónico.

El término reología lo acuñó el profesor Bingham por el año 1929, derivado del griego *rheos* que significa fluir. Reología es la ciencia que estudia el flujo y la deformación de materiales como respuesta a una fuerza aplicada. La microreología se ha desarrollado como una nueva familia de técnicas experimentales que consisten en observar cómo se mueve una partícula microscópica en el interior de un fluido para inferir, a partir de dicho movimiento, las propiedades viscoelásticas de éste. La idea de utilizar sondas microscópicas para medir propiedades

mecánicas se remonta a los comienzos del siglo XX, cuando Freundlich y Seifriz [5] propusieron la utilización de partículas magnéticas para estudiar la elasticidad de geles. Sin embargo, ha sido en la última década, a partir de 1995, cuando esta técnica se ha desarrollado realmente, gracias por un lado a las innovaciones tecnológicas introducidas en la video microscopía (cámaras e interfases rápidas, ordenadores con suficiente capacidad de almacenamiento y velocidad de tratamiento de imágenes) y, por otro lado al establecimiento de las herramientas teóricas necesarias, trabajos pioneros son los de Weitz y Mason [1], [2], MacKintosh y Schmidt, [6], [7] entre otros.

Históricamente la microreología surge de los experimentos del biólogo inglés Robert Brown en 1827 que observó al microscopio el devenir de granos de polen en agua. Fue Albert Einstein en 1905 quien desarrolló una teoría para explicar del movimiento aleatorio de las partículas que supuso la primera demostración indirecta de la existencia de las moléculas [8], [9]. En el artículo que publicó Einstein empleaba la teoría del calor en vigor para describir cómo la transmisión de calor, incluso a temperatura ambiente, provocaría que las moléculas de líquido estuviesen en continuo movimiento. Este movimiento haría a su vez que cualquier partícula suspendida en el líquido estuviera sometida a colisiones en direcciones arbitrarias. Si bien el movimiento de la partícula sería al azar, Einstein demostró que se podía determinar una dirección preferente para el movimiento. Desde el punto de vista matemático, el tratameinto es equivalente al del 'camino del borracho', que va para allá y después para acá, tropieza con el banco, cruza la calle tres veces, se abraza a la farola, pero en términos generales se dirige hacia su casa. Una observación del borracho permite determinar la zona hacia la que se dirige y hacer predicciones sobre el tiempo que tardará en llegar incluso sin saber exactamente con cuantos objetos tropezará durante el trayecto. Se puede obviar el azar a corto plazo para hacer predicciones acerca de lo que sucederá a largo.

En 1908, el francés Jean Baptiste Perrin llevó a cabo el experimento que confirmaba el movimiento de las partículas pasado a llamarse movimiento browniano, para ello estudió la forma en la que las partículas sedimentan en el agua por la influencia de la gravedad. La sedimentación encuentra la oposición de los choques de las moléculas desde abajo, por lo que el movimiento Browniano se opone a la atracción gravitatoria. Perrin usó este descubrimiento para calcular el tamaño de las moléculas de agua basándose en las ecuaciones de Einstein. Por este trabajo recibió el premio Nobel de física en 1926. El movimiento Browniano es relevante cuando las dimensiones de la partícula se comparan a la transmisión de calor en el medio.

Las técnicas microreológicas pueden dividirse en dos tipos: métodos activos que implican la manipulación de la sonda con campos externos: magnéticos, pinzas

ópticas, microscopía de fuerza atómica; y métodos pasivos que se basan en el movimiento inducido en la sonda por la agitación térmica [3], [4].

En las técnicas pasivas, en lugar de utilizar una perturbación externa para mover la partícula sonda, se utiliza el movimiento Browniano intrínseco de las partículas debido a las fluctuaciones térmicas propias del sistema. Uno de los problemas, de utilizar el movimiento Browniano como fuerza deformadora, es que la energía térmica viene fijada y limitada a $k_BT$, por tanto la deformación sólo será suficientemente grande para generar movimientos de las partículas detectables en materiales relativamente blandos, como por ejemplo disoluciones de polímeros y geles. En cualquier caso, las técnicas de detección más modernas permiten, en principio, resoluciones espaciales cercanas al nanómetro extendiendo por tanto la utilización de esta técnica a sistemas más duros. Son métodos pasivos el seguimiento de partículas, la dispersión de luz dinámica y la espectroscopía de onda difusa, que se explicarán en detalle en capítulos posteriores.

## 1.2. Reología y Viscoelasticidad

La reología es la ciencia del flujo y la deformación de la materia. En la obra de Barnes *Una introducción a la reología* definen flujo como una deformación, de la cual por lo menos una parte no es recuperable. En el libro *Physical properties of polymers* [10], se dice que la deformación significa un cambio o variación en la forma del sistema. La relación entre el esfuerzo y la deformación es una propiedad constitutiva de cada material que relaciona los esfuerzos con las deformaciones. El rango de comportamiento reológico sigue los extremos clásicos de sólido ideal y fluido ideal. Robert Hooke en 1678 desarrolla su *True theory of elasticity* que define el comportamiento ideal de un sólido (elasticidad). La ley de Hooke describe el comportamiento ideal mecánico relacionando esfuerzo $\sigma$ y deformación $\gamma$ a través de una constante de proporcionalidad que es el módulo de rigidez G. La fuerza de recuperación de un muelle es directamente proporcional a la tensión a que es sometido 1.1.

$$\sigma = G\gamma \tag{1.1}$$

En el otro extremo se encuentra el líquido ideal (viscosidad). Isaac Newton en 1687 estudió los líquidos y el flujo estable simple de cizalla en su libro *Principia*. La ley de Newton describe el comportamiento fluido ideal mediante una ecuación que relaciona esfuerzo y velocidad de deformación $\dot{\gamma}$ a través de una constante de proporcionalidad llamada viscosidad $\eta$. La resistencia que surge de la falta de deslizamiento en el interior del líquido, en las mismas condiciones experimentales, es proporcional a la velocidad con la que unas partes del líquido se mueven unas

respecto a otras 1.2.

$$\sigma = \eta\dot{\gamma} \tag{1.2}$$

Las leyes de Hooke y Newton son leyes lineales, expresan la proporcionalidad directa entre esfuerzo y deformación o entre esfuerzo y velocidad de deformación, para todo el intervalo de esfuerzos. La mayoría de los materiales con los que se suele trabajar obedecen estas leyes para un rango limitado de esfuerzos, más allá del cual las relaciones 1.1 y 1.2 incluyen términos no lineales.

En la mayoría de los casos los materiales tienen un comportamiento viscoelástico intermedio entre el sólido ideal con un comportamiento elástico puro (Sólido Hookeniano) y el líquido/fluido ideal con una respuesta puramente viscosa (Líquido Newtoniano).

Para un material viscoelástico (que posee propiedades viscosas y elásticas en diversos grados), los esfuerzos internos son función de la deformación instantánea (deformación, velocidad de deformación, etc), y también de la historia de la deformación. En el caso, en que tanto el esfuerzo como la deformación sean infinitesimales, las relaciones entre ambas magnitudes a lo largo del tiempo se puedan describir mediante ecuaciones diferenciales, y se estará definiendo un comportamiento viscoelástico lineal, lo cual implica que en un determinado ensayo la relación entre la deformación y el esfuerzo es únicamente función del tiempo y no depende de la magnitud del esfuerzo.

La respuesta de un material viscoelástico va a variar de la siguiente manera:

- para tiempos bajos (altas frecuencias) se comporta como un sólido.

- a tiempos altos (bajas frecuencias) la respuesta es similar a la de un líquido.

En un experimento de reología oscilatoria, los parámetros viscoelásticos se integran en el módulo complejo que mide la resistencia del material a ser deformado, tiene dos componentes, el módulo elástico G' y el módulo viscoso G".

$G^* = G' + iG''$

El módulo elástico o de almacenamiento mide la elasticidad del material, es decir, la aplicación de fuerzas externas provoca una deformación en la materia, realizándose un trabajo que se acumula como energía interna de deformación. Estas transformaciones son reversibles, cuando cesa la fuerza, el sistema recupera la forma y dimensión original, mientras que la energía acumulada se transforma en trabajo.

$G' = G^* cos\delta$

El módulo viscoso o de pérdidas mide la capacidad del material para disipar

energía. La energía que se pierde en forma de calor. La materia se deforma por la acción de una fuerza pero el trabajo realizado se disipa en forma de calor. Cuando la acción de la fuerza cesa, el estado de deformación permanece. Delta $\delta$ da cuenta de la diferencia de fase entre la tensión y la deformación

$G'' = G^* sin\delta$

La tangente de delta mide la energía disipada en relación a la almacenada $Tg\delta = G''/G'$

## 1.3. Geles poliméricos

Las redes poliméricas están formadas por cadenas macromoleculares entrecruzadas unas con otras a través de enlaces de tipo químico o físico [11]. Cuando dichas redes se encuentran hinchadas por un disolvente el material resultante es denominado gel. La definición topológica más aceptada de gel es la de una red tridimensional constituida de elementos básicos conectados entre sí de alguna forma e hinchados por un disolvente [12]. Esta definición implica que un gel debe comportarse como un sólido cuando se aplica una tensión. Este hecho da lugar a la definición mecánica de gel: un gel debe caracterizarse por presentar módulo elástico a frecuencia cero. Los geles poliméricos son una forma interesante de materiales blandos que responden a perturbaciones externas muy pequeñas. Estos materiales se hinchan o deshinchan como respuesta a pequeños cambios en determinados parámetros como son: la adición de sales al medio, el cambio de pH, de la temperatura, el cambio de disolvente, etc. Ejemplos de este tipo de sistemas son las confituras, gelatinas o los yogures que, desde el punto de vista químico-físico, se pueden clasificar dentro de este grupo de materiales. La aplicación de los geles se ha diversificado en multitud de campos de la ciencia y la tecnología durante las últimas décadas. Muy conocida es su utilización como lentes de contacto, recubrimientos de superficies, soporte para moléculas activas, geles para el cabello o los modernos desarrollos de sistemas inteligentes que responden a diferentes tipos de estímulos, como son los músculos artificiales, sensores, ferrogeles, sistemas de liberación controlada de medicamentos, etc. El impulso para el rápido desarrollo científico en este campo fue proporcionado por la observación, por primera vez, del fenómeno del colapso de los geles por T.Tanaka en 1978 [13]. Este fenómeno consiste en una disminución brusca del volumen del gel en varios órdenes de magnitud en respuesta a pequeñas variaciones de parámetros externos como pueden ser la temperatura, el pH, la fuerza iónica, campos magnéticos o eléctricos, etc. Los geles poliméricos no sólo pueden absorber y mantener volúmenes de líquido considerables, sino que también se puede forzar

al gel a expulsar los líquidos absorbidos de una manera regulada, mediante el control de las variables mencionadas anteriormente.

El gel es un estado de la materia que no es ni líquido ni sólido; o por el contrario, es ambos: líquido y sólido a la vez. Es mucho más fácil describir un gel que definirlo, porque su definición precisa debe referirse a la estructura molecular y al concepto de conectividad. Cualquier gel consta de, al menos, dos componentes: una red molecular tridimensional (de naturaleza polimérica o no) y el líquido que la hincha. Como resultado posee tanto las propiedades cohesivas de los sólidos, como las propiedades de transporte difusivo de los líquidos. Los geles son blandos, desde el punto de vista elástico y altamente activos, desde el punto de vista osmótico. Esta dualidad es la que confiere a los geles sus interesantes propiedades de absorción y reológicas que son la base de numerosas aplicaciones importantes. Los geles poliméricos se clasifican en función del tipo de entrecruzamiento que crea la red tridimensional (geles químicos o físicos), en función de la naturaleza del polímero (geles de biopolímeros o de polímeros sintéticos), en función de la forma y tamaño de la configuración del gel (macro y microgeles) y en función del tipo de disolvente (hidrogel, aerogel, xerogel, gel liotrópico u organogel). De interés particular son los hidrogeles, es decir, geles poliméricos que se hinchan extensivamente en agua. Los hidrogeles más comunes son los constituidos por polielectrolitos: su alto grado de hinchamiento en agua es debido a la presión osmótica ejercida por los contraiones. Estos geles absorben agua en relaciones que pueden alcanzar varios cientos de gramos de agua, por gramo de polímero seco. Sin embargo, algunos geles neutros como, por ejemplo, los basados en poliacrilamida, poli(óxido de etileno) o poli(alcohol vinílico), también tienen una gran afinidad por el agua, pero su grado de hinchamiento es siempre mucho menor que el de los geles cargados. Los hidrogeles, debido a sus características estructurales (tamaño de malla mesoscópico) y a sus propiedades químicofísicas, son un medio ideal para llevar a cabo la síntesis de compuestos de tamaño nanométrico.

Una de las clasificaciones principales de los geles es la que los clasifica en geles químicos y geles físicos según el proceso por el que los elementos de la red se conectan entre sí. En los geles químicos las uniones tienen lugar por enlaces covalentes. Estos geles son irreversibles por calentamiento, pues al calentarlos para conseguir la ruptura de los enlaces covalentes que forman la red, se provoca la degradación irreversible del polímero, lo que impide la reformación de un sistema similar. En los geles físicos la unión entre cadenas tiene lugar mediante interacciones de Van der Waals, electrostáticas, enlace de hidrógeno, ácido-base, etc. Esto tiene dos consecuencias:

i) para ser estables, los enlaces débiles requieren que haya cooperatividad, lo que implica que el dominio de las uniones no es de tipo puntual, sino que se extiende

en el espacio y

ii) la energía implicada en este tipo de uniones es del orden de $k_BT$ por lo que los geles son reversibles por calentamiento, es decir, son termorreversibles.

### 1.3.1. Gelificación

Gelificación es el proceso mediante el cual se forma un gel. El proceso de gelificación depende de muchos factores físicos y químicos como la adición de catalizadores, influencia de la fuerza iónica, concentración, temperatura, etc [14].

Existen dos teorías que tratan de explicar la gelificación, teoría clásica desarrollada por Flory [15], [16] y Stockmayer [17] y teoría de percolación. La primera se basa en la distribución de los pesos moleculares de las especies presentes en el sol, pero presenta problemas porque no considera la formación de nuevas estructuras en el crecimiento de los agregados, por lo tanto según este modelo la gelificación produce un aumento de densidad. La segunda permite predecir la evolución de las propiedades del sistema, de manera consistente con los resultados experimentales, es decir, explica la transición sol-gel a densidad constante.

La teoría de percolación es una teoría multidisciplinaria, aplicable a varias ramas de la ciencia (farmacia, biología, química, física) que estudia sistemas caóticos, en los cuales los componentes están distribuidos aleatoriamente en una red, evaluando la probabilidad de ocupación de los componentes en el sistema, con el fin de estudiar propiedades, parámetros o predecir comportamientos en la proximidad del umbral de percolación [18]. La teoría de Percolación permite estudiar fenómenos críticos que se presentan en sistemas caracterizados por la existencia de un punto crítico, en el cual ciertas propiedades del sistema cambian [19]. La teoría de percolación define el de umbral de percolación, cuando al partir de valores bajos de probabilidad de ocupación de los puntos de la red por un determinado componente, va aumentando este parámetro hasta que llega un momento en que existe un cluster que se extiende desde la parte inferior a la superior y desde la izquierda a la derecha de la muestra (Figura 1.1. A este cluster se le denomina cluster infinito o percolante (la sustancia en cuestión percola el sistema), y al porcentaje al cual existe la máxima probabilidad de obtener por primera vez el cluster infinito se le denomina probabilidad crítica o umbral de percolación ($p_c$).

La ecuación que describe el comportamiento del sistema en las inmediaciones del umbral de percolación, se conoce como ecuación fundamental de la teoría de percolación.

$$X = S \cdot (p - p_c)^q \tag{1.3}$$

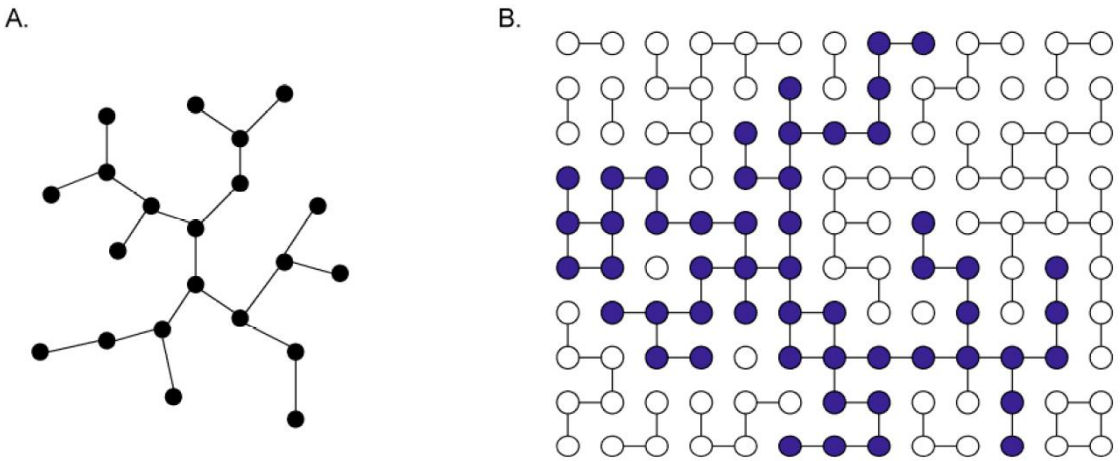


**Figure 1.1:** Diagrama que ilustra la red que predice la teoría de (A) Flory-Stockmayer theory y (B) la teoría de percolacion. Los monómeros se representan por círculos y los enlaces por las líneas conectoras. El grupo de círculos azules en la teoría de percolación indica la formación del cluster en el punto crítico de formación del gel. Dibujo adaptado de Winter y Mours 1997 [20].

donde X es una propiedad cualquiera del sistema; S es un factor de proporcionalidad; $p$ es la probabilidad de ocupación del sistema; $p_c$ es la probabilidad crítica o umbral de percolación y $q$ es el exponente crítico.

Esta ecuación es válida cerca del umbral de percolación ($\pm 10\% p_c$) aunque en la práctica el ajuste de los datos experimentales a la ecuación resulta adecuado en intervalos de probabilidad mucho más amplios [21]. Uno de los descubrimientos más interesantes de la teoría de percolación es la universalidad de los exponentes críticos. A pesar de que existe un gran número de problemas diferentes y de redes de percolación, los exponentes críticos son los mismos para todos los sistemas con el mismo número de dimensiones (bi- o tridimensional). Este descubrimiento no ha podido ser demostrado aún matemáticamente, pero está apoyado por los estudios realizados hasta el momento. Desde el punto de vista físico, este hecho se atribuye a que la macroestructura del cluster principal, en las inmediaciones del umbral de percolación es idéntica en todas las redes que tengan el mismo número de dimensiones, aunque la microestructura sea diferente en cada una de ellas. Por tanto el exponente crítico depende sólo del número de dimensiones del sistema [22, 23].

## 1.4. Glicerol

### 1.4.1. Aspectos generales

El glicerol (1,2,3-propanotriol) es un líquido viscoso, sin color ni olor y con un sabor dulce, que se obtiene tanto de forma natural de las grasas y aceites durante el

proceso de obtención de jabones y ácidos grasos, así como de la transesterificación durante el proceso de producción de biodiesel como a partir de la petroquímica. A la hora de nombrarlo se suele usar de forma indistinta los sinónimos glicerina y glicerol. Constituye una de las sustancias químicas más versátiles y valiosas conocidas. Es completamente soluble en agua y alcoholes, muy poco soluble en disolventes comunes como el éter o el dioxano y totalmente insoluble en hidrocarburos. Además es altamente estable bajo condiciones de almacenamiento normales, compatible con muchos otros materiales químicos, no irritante en su variedad de usos y sin efectos medioambientales negativos conocidos. La molécula de glicerina tiene tres grupos hidroxilo que son los responsables de su solubilidad en agua y su naturaleza higroscópica [24]. Se trata de una molécula altamente flexible formando enlaces de hidrógeno, lo que explica su alto punto de ebullición (290°C a presión atmosférica) y su alta viscosidad. En la tabla 1.1 se muestran las propiedades fisicoquímicas más importantes del glicerol.

### 1.4.2. Aplicaciones del glicerol

En función del grado de purificación, se pueden alcanzar diferentes calidades de glicerina: grado técnico ($>$ 90 % pureza) o grado farmacéutico ($>$ 99,5 % de pureza). La glicerina de grado farmacéutico presenta precios elevados en el mercado, ya que se usa como componente en fármacos, perfumes, cosméticos, productos de cuidado personal y productos alimenticios. Por otro lado, podemos encontrar glicerinas de grado técnico con un amplio intervalo de purezas [26].

En el proceso de refino de la glicerina, la destilación a vacío y las separaciones sólido-líquido y líquido-líquido constituyen las principales unidades de operación [26]. En la Figura 1.2, se muestra un diagrama del proceso formado por dos columnas de destilación, un separador líquido-líquido y un equipo de filtración

**Table 1.1:** Propiedades quimicofísicas del glicerol a 25°C [25]

| | |
|---|---|
| Estructura 3D | 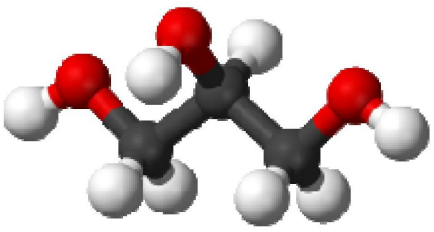 |
| Formula molecular | $C_3H_5(OH)_3$ |
| Peso molecular | 92.09 |
| Densidad (kg m-3) | 1261 |
| Viscosidad (Pa·s) | 0.945 |
| Índice de refracción $n_D$ | 1.4730 |

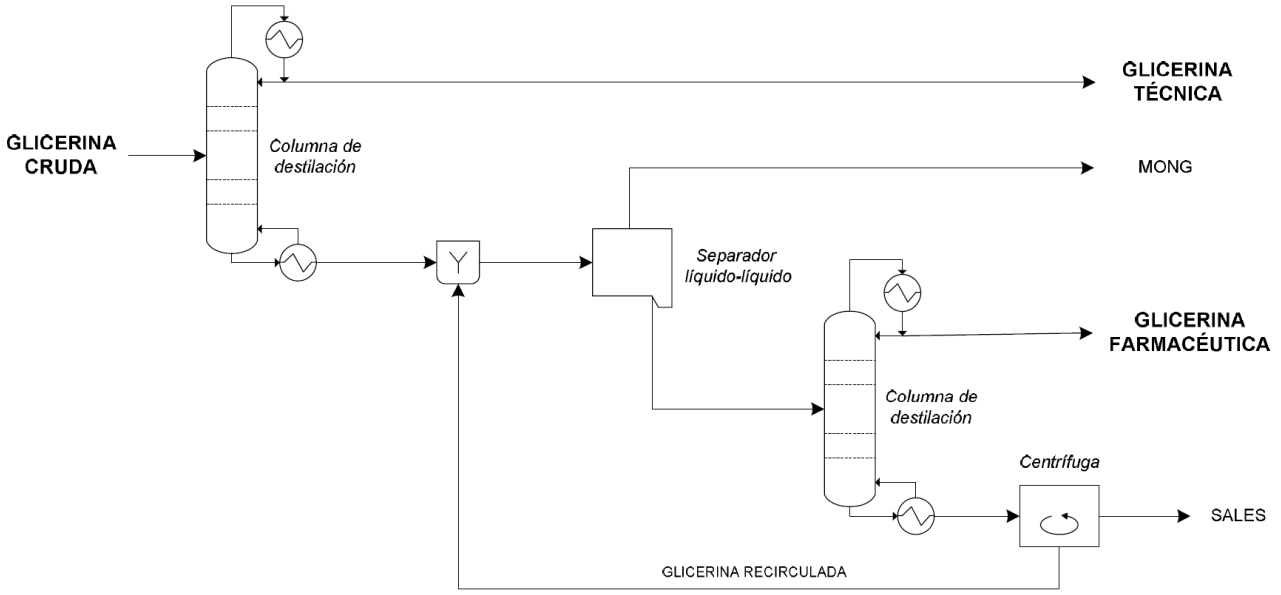


**Figure 1.2:** Esquema del proceso de refinado de la glicerina cruda

o centrifugación. La glicerina cruda que proviene de las plantas de producción de biodiésel se introduce en una primera columna de destilación obteniendo, por la parte superior, una glicerina de grado técnico o industrial libre de sales pero con cierto contenido en agua. La corriente inferior se lleva a un separador líquido-líquido donde se retirará la materia orgánica que no es glicerina constituida principalmente por ésteres metílicos, glicéridos, ácidos grasos libres y productos de oxidación de la polimerización de glicerina. En la segunda columna de destilación se opera a vacío para conseguir reducir la temperatura de operación durante la destilación y evitar de este modo la degradación de la glicerina (en presencia de sales y sosa caústica, la temperatura de ebullición de la glicerina puede llegar a los 220°C). De esta forma, se obtiene una glicerina grado farmacéutico libre de sales y agua. Las sales pueden ser retiradas mediante filtración o centrifugación de la corriente inferior de la columna de destilación, recirculando de nuevo al proceso la glicerina filtrada.

El glicerol presenta una amplia variedad de aplicaciones tradicionales, tales como emulgente, suavizante, plastificante, estabilizante y humectante para tabaquería, pastelería y heladería; en cremas corporales, enjuagues bucales e innumerables preparados farmacéuticos y cosméticos; como medio protector para congelación de glóbulos rojos, esperma, corneas y otros tejidos; en tintas de impresión, resinas de pinturas; mezclas anticongelantes; y como materia prima para la nitroglicerina, resinas alquílicas y poliuretanos (Figura 1.3). La función principal de la glicerina en la mayoría de las aplicaciones es la de absorber la humedad del ambiente y en ocasiones proporcionar suavidad. Por otro lado, la efectividad de la glicerina como plastificante y lubricante hace que sea usado en una amplia variedad

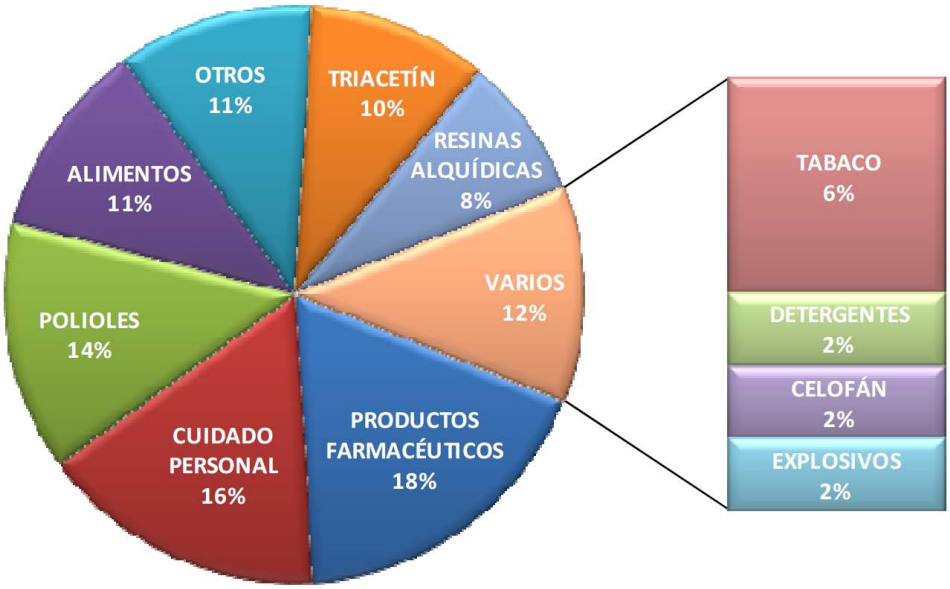


**Figure 1.3:** Volúmenes y usos industriales de la glicerina [27]

de aplicaciones, especialmente en el procesado de alimentos al tratarse de un compuesto no tóxico.

El uso de la glicerina dentro de la industria farmacéutica y cosmética es el más conocido y el que da mayor valor a la glicerina. Hoy en día, los bajos precios de la glicerina pueden abrir numerosos mercados nuevos en la producción de polímeros, éteres y otros compuestos. En un futuro cercano, el potencial de conversión de materias renovables en sustancias químicas de alto valor puede facilitar el desplazamiento de los productos de origen fósil. La conversión de glicerina en hidrógeno o gas de síntesis puede contribuir al uso de energías renovables y limpias.

## 1.5. Agarosa

La agarosa es un polisacárido lineal formado por moléculas de galactosa unidas a través de enlaces $\alpha$ 1-4 y $\beta$ 1-3 que se extrae de la pared celular de varias especies de algas rojas.

La agarosa es soluble en agua a temperaturas superiores a 90°C cuando se produce la fusión de la agarosa en polvo disuelta en agua, es insoluble en disolventes orgánicos y tiene la capacidad de formar geles termoreversibles. Debido a sus características, la agarosa, es un producto indispensable en una gran cantidad de técnicas de biología molecular, bioquímica, cultivos celulares, microbiología y biología celular para la preparación de geles que permitan separar moléculas de ADN u otros compuestos mediante electrofóresis, además de ser utilizada para fijar moléculas en su estructura como antígenos o anticuerpos.

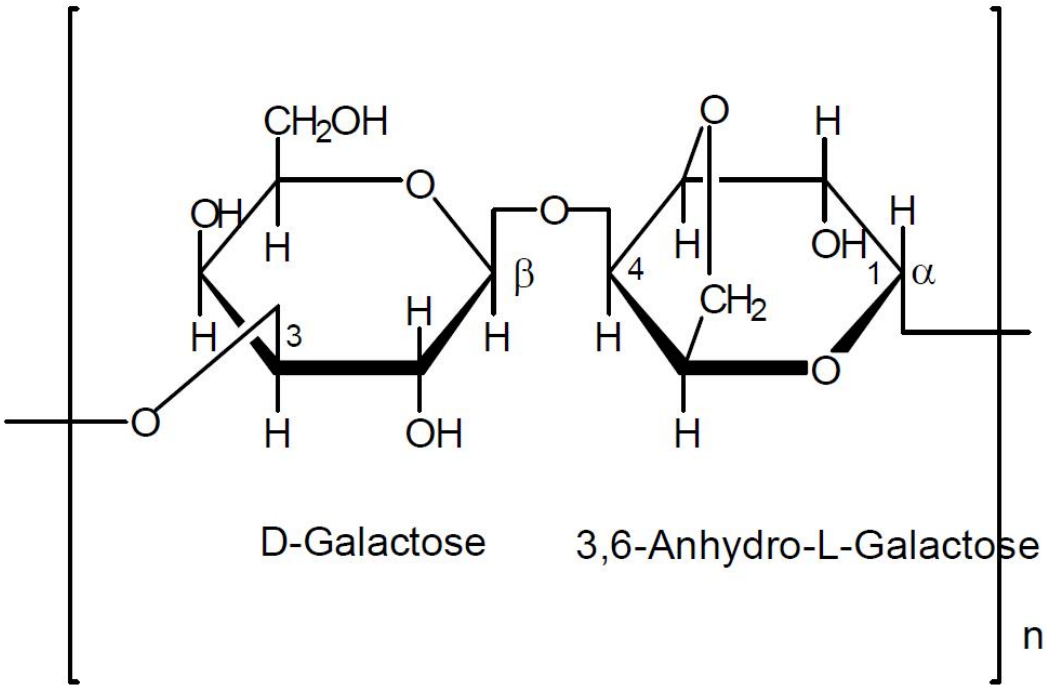


**Figure 1.4:** Estructura química de la agarosa

La agarosa cuando gelifica posee una estructura de doble hélice. Esta estructura se reúne para formar una estructura tridimensional que retiene las moléculas de agua en sus intersticios y forma, así, geles termorreversibles. La propiedad de gelificación de la agarosa es debida a los tres átomos de hidrógeno ecuatorial en los residuos de 3,6-anhidro-L-galactosa, que limitan la molécula para formar una hélice. La interacción de las hélices causa la formación del gel.

La gelificación ocurre a temperaturas muy inferiores a la temperatura de fusión. Una disolución de agarosa forma un gel al ser enfriado a partir de una temperatura de 40°C.

## 1.6. Pluronic F127

Con el término Pluronic se identifica a un copolímero de bloque genérico constituido por dos unidades de óxido de polietileno o polietilenglicol (EO), separadas por una unidad central de óxido de polipropileno o polipropilenglicol (PO), con una estructura $[EO]_x[PO]_y[EO]_x$.

Comercialmente están disponibles distintas variedades de Pluronic y en un amplio rango de pesos moleculares y longitudes de los bloques constituyentes. Los distintos tipos de Pluronic, así como su nomenclatura, se presentan en la Figura 1.5

La nomenclatura para los derivados de Pluronic comienza con las letras L (para

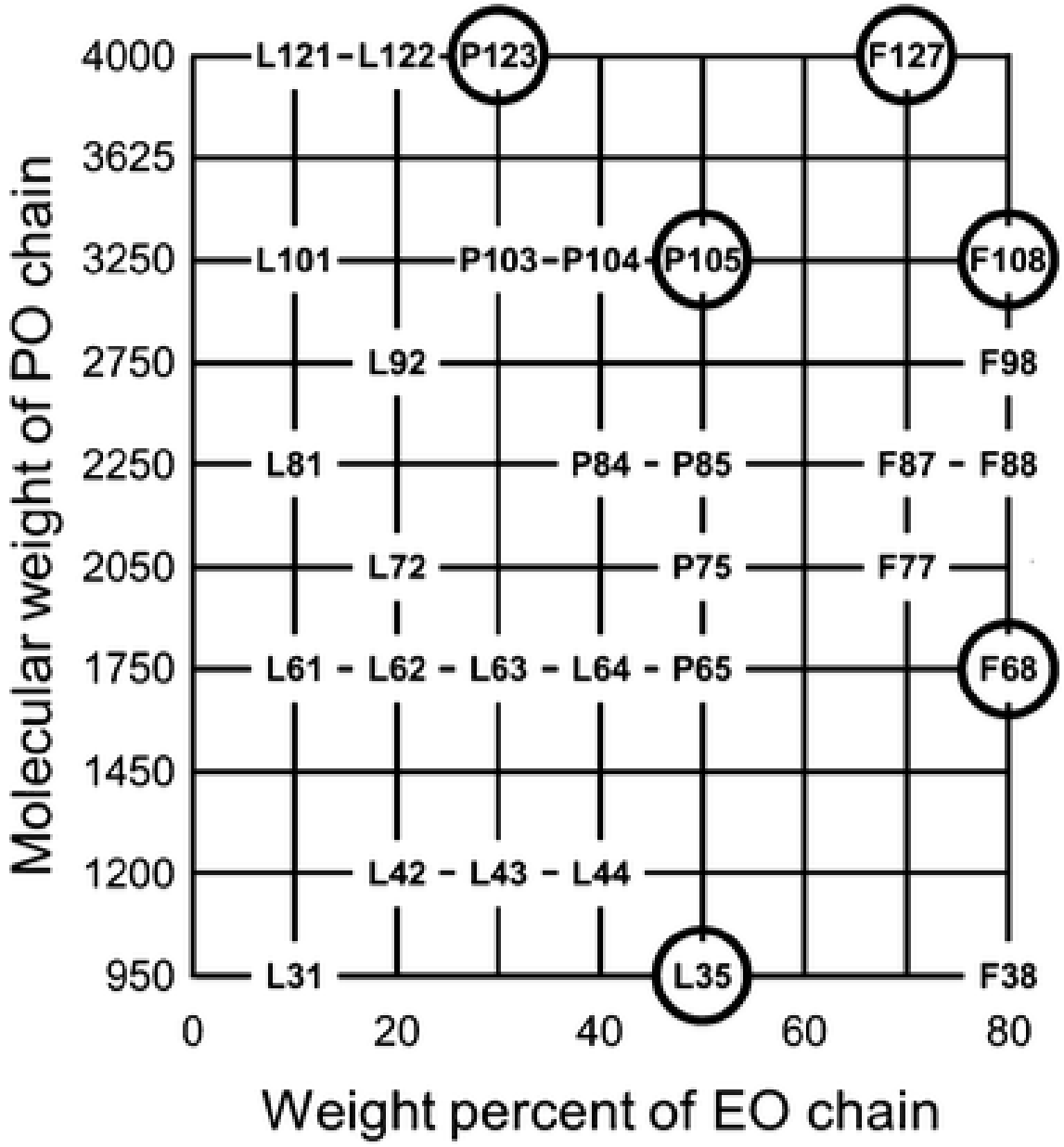


**Figure 1.5:** Tipos de Pluronic

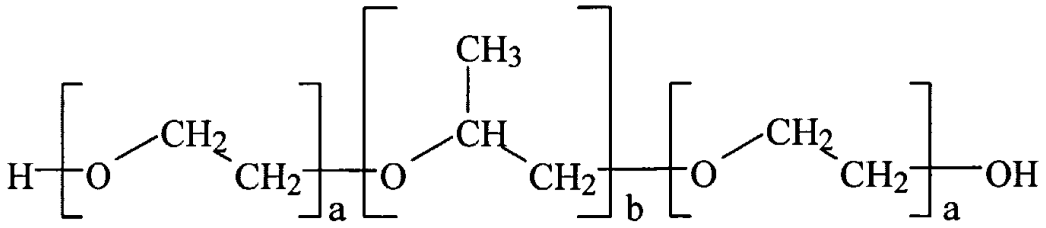


**Figure 1.6:** Estructura química del Pluronic F127

Pluronic en estado líquido), P (para Pluronic en pasta) o F (para Pluronic en estado sólido, en forma de copos). Los dos primeros números son indicativos del peso molecular de la cadena hidrófoba de óxido de polipropileno, y van desde el número 3 para el copolímero con el menor peso molecular de óxido de polipropileno hasta el número 12 para el de mayor peso molecular de óxido de polipropileno (eje vertical en la Figura 1.5). El último número se refiere al porcentaje de óxido de polietileno, y va desde el 1 para el menor porcentaje de óxido de polietileno hasta 8 para el mayor porcentaje de óxido de polietileno (eje horizontal en la Figura 1.5).

La variedad de Pluronic aquí estudiada es el Pluronic F127 (Figura 1.6). El número 12 hace referencia a que se trata de un copolímero bloque con un peso molecular del bloque de óxido de polipropileno de 4000 g/mol, mientras que el número 7 hace referencia a la presencia de un 70% de óxido de polietileno en la molécula.

El Pluronic F127 tiene actividad como surfactante no iónico soluble a bajas temperaturas y forma agregados micelares. Su fórmula molecular aproximada es $[EO]_{106}[PO]_{70}[EO]_{106}$ con un peso molecular de 13400 g/mol.

La mayoría de los copolímeros tipo Pluronic presentan las siguientes características generales:

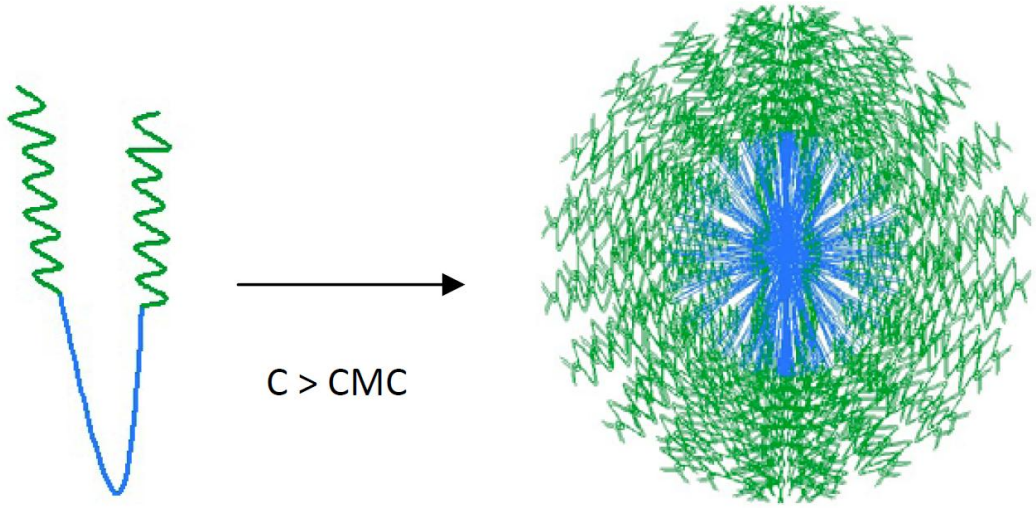


**Figure 1.7:** Esquema de la estructura micelar del Pluronic en agua, a concentraciones por encima de su Concentración Micelar Crítica. En color azul se representa el núcleo hidrófobo de PO y en color verde la corona hidrófila de EO

- En disoluciones acuosas son capaces de autoorganizarse formando micelas, las cuales consisten en un núcleo hidrófobo de óxido de polipropileno y una corona hidrofila de óxido de polietileno (Figura 1.7). La autoorganizacion en micelas se produce a partir de una determinada concentracion, denominada Concentracion Micelar Critica (CMC), que se define como la concentracion mínima de material necesaria para dar lugar a micelas termodinamicamente estables. Otro parámetro fundamental es la Temperatura Micelar Crítica (CMT) o temperatura de Krafft que es la temperatura a partir de la cual se forman las micelas, siempre que el polímero se encuentre por encima de su CMC. El valor de la CMC del Pluronic F127 es de 950-1000 ppm ($\sim 25^{o}C$) [28].

- Las disoluciones acuosas a bajas concentraciones de Pluronic, debido a su capacidad de autoorganizacion en forma de micelas por encima de la CMC y debido a la presencia de su nucleo hidrófobo y su corona hidrófila, se han utilizado como sistemas de encapsulación de fármacos tanto hidrófobos, para mejorar su solubilidad en medio acuoso, como hidrófilos, para mejorar el tiempo de residencia en el torrente sanguíneo.

- Algunas de las variedades de Pluronic disueltos en agua a altas concentraciones presentan gelificación termorreversible a partir de una determinada concentración. Los factores que determinan el punto de gelificación, así como a la temperatura de transición sol-gel, son el peso molecular del polímero, su arquitectura molecular (longitud de los bloques y secuencia de bloques) y la presencia de especies iónicas en la disolución [29].

El mecanismo de la gelificación de Pluronic aun sigue siendo un tema que despierta controversia. Se han propuesto distintos mecanismos que tratan de explicar la

transición sol-gel de este copolímero bloque, que se comentan a continuación.

Rassing y Attwood [30] explicaron la gelificación del Pluronic por cambios intrínsecos en las propiedades micelares, como el número de agregación (número de moléculas que forman las micelas) y la simetría micelar.

Vadnere et al. [31] atribuyeron la transición sol-gel a un cambio de entropía debido a la presencia de moléculas de agua ordenadas próximas a las cadenas hidrófobas de PO. La presencia de moléculas de agua ordenadas alrededor de las cadenas hidrófobas minimiza el contacto agua-cadena hidrófoba. Para polímeros que presentan temperatura de transición sol-gel, el aumento de temperatura permite la deshidratación de las cadenas hidrófobas, provocando un aumento del desorden en las moléculas de agua y por tanto un aumento de la entropia ($\Delta$S), lo que hace que sea un proceso favorable (Energia de Gibbs, $\Delta$G$<$0). En esta situacion, las interacciones agua-polímero se hacen desfavorables mientras que se favorecen las interacciones agua-agua y polímero-polímero. Este fenómeno, que se conoce como efecto hidrofóbico es probablemente el mecanismo más aceptado para la explicación de la gelificación de disoluciones de Pluronic [32].

Años mas tarde, Wanka et al. [33] propusieron la gelificación como una organización tridimensional estructurada. Las moléculas de polímero se autoorganizan en micelas por debajo de la temperatura de transición sol-gel y por encima de la CMC. Al aumentar la temperatura hasta la temperatura de transición sol-gel, se produce el empaquetamiento de micelas en una estructura ordenada formando mesofases liotrípicas cristal líquido [34].

Si bien al proceso de gelificación se le ha prestado atencion, la transicion gel-sol en un calentamiento posterior ha sido poco estudiada. No obstante, se ha propuesto que la transición gel-sol puede estar relacionada con el hinchamiento que experimentan las cadenas de EO en las micelas, al aumentar la solubilidad con el incremento de temperatura [35].

Estas características del Pluronic junto a su biocompatibilidad, hacen que se emplee en productos de uso cotidiano tales como champus, enjuagues bucales, desmaquillantes limpiadores faciales, cremas antiacne, cremas antiinflamatorias, etc.

En disolución acuosa el Pluronic F127 en un intervalo de concentración desde 18 a 30%w/v a baja temperatura (0-5$^{o}$C) es un líquido de baja viscosidad ($<$2 poise), pero a medida que la temperatura aumenta se forma un gel consistente con estructura cúbica cristalina.

## 1.7. Ácido hialurónico

Dentro de la familia de polímeros llamados glucosaminoglicanos se encuentra el acido hialuronico (HA). El ácido hialurónico es por su naturaleza un carbohidrato no reductor y forma parte de la matriz extracelular del tejido conectivo. Es un polisacárido de elevada masa molecular, su unidad estructural fue definida por Weissman y Meyer in 1954 [36] y está constituida por dos tipos de unidades monoméricas, ácido glucurónico y N-acetilglucosamina [-4)-$\beta$-D-glucuronopiranosil-$\beta$(1.3)-2-acetamido-2-dexosi-D-glucopiranosido-(1]. (Figure 1.8).

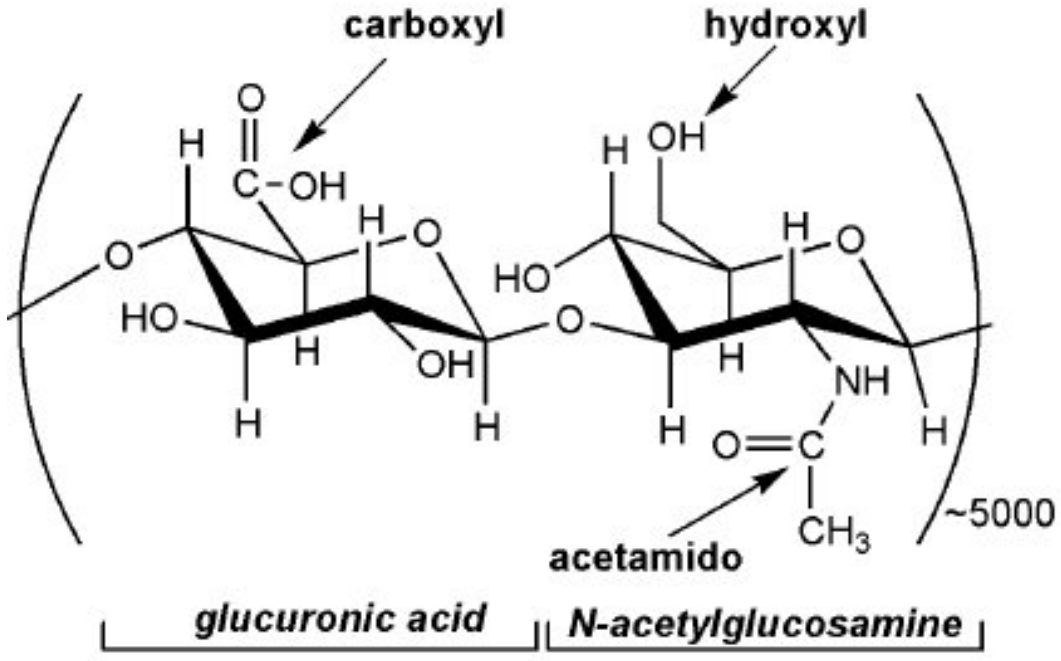


**Figure 1.8:** Estructura del ácido hialurónico

El ácido hialurónico posee estructura primaria, secundaria y terciaria [37],[38]. La estructura primaria está dada por la secuencia del dímero constituido entre el ácido glucurónico y la N-acetilglucosamina. La estructura secundaria, se establece por las interacciones intramoleculares mediante enlaces de hidrógeno, provocando que la cadena lineal del polisacárido se tuerza y forme una doble hélice y la estructura terciaria está caracterizada por tres posibles puntos de contacto intermolecular que son: 1) cadenas antiparalelas unidas a grupos hidrófobos, 2) cadenas paralelas mediante interacciones por enlaces de hidrógeno y 3) cadenas entrecruzadas por interacciones por enlaces de hidrógeno e interacciones con los posibles centros hidrófobos [39], [40]. Estos tipos de interacciones explican la

gran mayoría de las propiedades de interés asociadas a este polisacárido como son: viscoelasticidad, poder hidratante, cicatrizante y antinflamatorio, así como una barrera que dificulta la difusión de los gérmenes, por lo que se le atribuye propiedades bacteriostáticas.

Como se plantea, las propiedades viscoelásticas como el poder hidratante del ácido hialurónico está relacionado con su estructura. En los tejidos biológicos se manifiesta, al formar redes poliméricas comportándose como un medio gelatinoso que sirve de base para las funciones del tejido conjuntivo. Estas redes poliméricas, tienen la posibilidad de retener agua en su interior como si fuera una esponja. En el caso de la piel, es responsable de su capacidad hidratante y por ello es tan usado en cosmética para combatir el envejecimiento.

El ácido hialurónico se localiza en diferentes tipos de tejidos en el ser humano, en la piel actuando como defensa del organismo, al formar parte de la barrera química, impidiendo la penetración o el desarrollo de microorganismos o partículas extrañas y participa en la reparación de la misma, en el fluido sinovial de las articulaciones y tejidos de los cartílagos contribuyendo a la flexión de las articulaciones, humor vítreo, en las células dendríticas, en las membranas de los tejidos gestantes y el cordón umbilical humano, etc.

La función del ácido hialurónico en la piel y en el cartílago es retener agua y procurar elasticidad y tono a los tejidos, mientras que en los líquidos de las articulaciones, actúa como un lubricante y protege las células de los choques físicos del exterior, y de las infecciones bacterianas. Debido a su naturaleza altamente hidrofílica, el ácido hialurónico constituye un constituyente ideal para la preparación de lociones cosméticas. Soluciones muy purificadas de HA se utilizan también como medio de soporte en cirugía ocular (Patente USA No. 4.141.973) o como un líquido de sustitución en las articulaciones en el caso de situaciones patológicas particulares.

La producción del ácido hialurónico de alto peso molecular, que posee propiedades viscoelásticas superiores a las de las fracciones de bajo peso molecular, es por tanto de considerable interés, en vista especialmente de la necesidad de absorber variaciones mayores en la presión, tal como las que tienen lugar in vivo en las articulaciones.

En cuanto a su obtención, existen dos procedimientos para el aislamiento del ácido hialurónico, obtención por vía enzimática y a partir de fuentes naturales.

La extracción de ácido hialurónico a partir de fuentes animales presenta varias desventajas debido a la disponibilidad limitada del material en bruto, la dificultad de extraer grandes cantidades de ácido hialurónico de alto peso molecular de los tejidos animales, donde sólo se encuentran trazas de él, a menudo en forma de

complejos con proteínas u otros mucopolisacáridos, y el peligro de contaminación vírica. Por estas razones, muchos investigadores se han vuelto hacia la producción de HA a partir de un origen microbiológico.

La producción de HA mediante estreptococos se demostró primero por Forrest y col., [41], y posteriormente por otros investigadores, por ejemplo, Roseman y col., [42]; [43]; Patente USA No 2.975.104; y Sugahara y col., [44]. Estos investigadores demostraron que el ácido hialurónico que se encontraba en las cápsulas de muchas cepas de los estreptococos del grupo A y del grupo C es el mismo que el del origen animal. Estos microorganismos pueden asimilar glucosa u otras fuentes de carbono y, bajo condiciones medioambientales particulares, producen ácido hialurónico como un metabolito secundario. La síntesis del ácido hialurónico por los estreptococos está, sin embargo, influenciada por muchos factores genéticos y nutricionales.

Los estreptococos se encuentran entre las bacterias más exigentes desde un punto de vista nutricional. La literatura describe muchos tipos de medios de cultivo que favorecen la producción de ácido hialurónico por estos microorganismos, que normalmente incluyen hidratos de carbono, aminoácidos, vitaminas, sales inorgánicas, y algunos factores de crecimiento. Generalmente, la glucosa se utiliza como una fuente de carbono, mientras que la fuente de nitrógeno puede ser orgánica o inorgánica, incluyendo peptona, extracto de levadura, productos de caseína hidrolizada, productos de soja hidrolizada, aminoácidos, sulfato amónico, cloruro amónico, fosfato amónico, urea, glutamina, etc. Ciertas sales inorgánicas pueden también añadirse al medio, tales como sulfatos, clorhidratos, carbonatos, nitratos, fosfatos, y acetatos de calcio, potasio, sodio, magnesio, manganeso, hierro, cobre, y zinc. Finalmente, la adición de vitaminas y aminoácidos puede también mostrarse ventajosa para el crecimiento bacteriano.

Algunos medios nutritivos específicos para los estreptococos ya se venden comercialmente, tales como la Infusión Corazón Cerebro y el Caldo Todd-Hewitt. Otros se han descrito en patentes relacionadas con la producción del ácido hialurónico mediante fermentación, tales como la Patente USA No. 4.517.295, Patente USA No. 2.975.104, Patente USA No. 4.784.990, Patente USA No. 4.897.349, y la Patente Europea No. 0 244 757. Muchos de estos medios, sin embargo, no se utilizan porque requieren componentes caros, y no son por tanto apropiados para objetivos industriales. Por lo tanto, el producto HA obtenido mediante la fermentación utilizando estos costosos medios complejos, no es ventajosamente económico comparado con el obtenido a partir de fuentes animales.

Otro problema asociado con la producción de ácido hialurónico a partir de las fuentes bacterianas es la utilización, en algunos casos, de cepas de estreptococos

que son patogénicos en el hombre, tales como S. pyogenes. Sin embargo, la producción de ácido hialurónico mediante fermentación, aparte de facilitar la obtención de grandes cantidades de polímeros con un peso molecular más alto que el obtenido a partir de los tejidos animales, permite también la purificación del HA mediante procedimientos menos complicados que los requeridos para otros materiales de partida. Los procedimientos de purificación conocidos, que se han descrito en numerosas patentes, permiten el aislamiento del ácido hialurónico de alto peso molecular, a menudo con un alto grado de pureza. Estos procedimientos necesitan habitualmente grandes cantidades de solventes o de otros productos tóxicos, tales como el cloruro de cetilpiridina, requiriendo también por tanto numerosos pasos antes de producir el ácido hialurónico altamente purificado para utilización en el campo farmacéutico. Todos estos factores crean problemas relacionados con el medio ambiente y el coste.

# Chapter 2

# Objetivos

El objetivo principal de esta tesis tiene naturaleza bifronte, consiste por un lado en aplicar los distintos tipos de técnicas microreológicas para la comprensión y caracterización de sistemas viscosos y viscoelásticos, así como emplear la microreología para investigar los fenómenos de gelificación y propiedades viscoelásticas de geles. Estos sistemas son muy importantes desde el punto de vista de su aplicación como portadores de partículas y de estabilidad de las partículas en su seno. Ambos sistemas se estudiarán en medio acuoso. Se compararán resultados de varias técnicas pasivas de microreología para poder comprobar su consistencia y se pondrán a punto distintas metodologías de análisis de datos de microreología.

Esta tesis se ha dividido en dos grandes bloques de resultados en función del sistema de estudio. De este modo, la primera etapa consiste en la obtención de datos microreológicos en un sistema viscoso que comprende el bloque de resultados primero. La segunda etapa, el mismo proceso pero en sistema viscoelástico, será desarrollada en el bloque de resultados segundo.

La metodología de trabajo a utilizar en todos los sistemas a estudiar tiene un patrón de actuación semejante:

1.- Se selecciona el sistema responsable del comportamiento viscoelástico y el disolvente de acuerdo a criterios quimicofísicos. Uno de los requisitos principales es que el índice de refracción de la matriz sea lo más parecido posible al del agente viscoso o viscoelástico; pero existen otros criterios de selección que se explicarán de manera detallada en cada capítulo.

2.- Se procede a su preparación de acuerdo a una metodología seleccionada con criterios bibliográficos y de experimentación propia.

3.- Finalmente se estudian las propiedades microreológicas de los sistemas de acuerdo a una metodología científica puesta a punto específicamente para cada sistema seleccionado. La finalidad de esta investigación es explicar y tratar de

forma adecuada los datos para diversos sistemas viscoelásticos y con ello obtener propiedades de transporte mediante técnicas de microreología.

En esta tesis se describe la aplicación de diversas técnicas de microreología, en especial, la técnica de espectroscopía de onda difusa (DWS por sus siglas en inglés) en el estudio de la viscoelasticidad de geles.

Los sistemas probados son: agarosa, pluronic F-127 y ácido hialurónico que presentan un complejo mecanismo de gelificación que los hace ser unos interesantes prototipos para el estudio y comparación con otros sistemas que gelifiquen con el fin de predecir qué tipo de cambios se producen en sus propiedades.

# Chapter 3

# Rheology

Rheology is the study of how materials deform or flow, in response to an external stress, $\sigma$, [45] . A Newtonian or viscous fluid will flow with a constant rate of deformation, or strain rate. The ratio between the stress and the strain rate reveals the fluid viscosity. Under a constant stress, an elastic solid will deform to a constant strain, and the ratio, stress/strain is the elastic or storage modulus, G'; and the product *viscosity·frequency* is the viscous or loss modulus, G". Rheological data are often reported in terms of the complex shear modulus $G^* = G'(\omega) + iG''(\omega)$. In general, materials can behave both solid and fluid like and, therefore, are viscoelastic. These properties often depend on the frequency of the measurement as well as the magnitude of the applied stress [46], [47].

Viscosity of fluids are affected by:

- Shear rate

- Time of shearing

- Temperature

- Pressure

Newtonian fluids are characterized by their viscosity which depends only on temperature and pressure and does not vary with shear rate.

- Examples: water, oil, milk, honey, soft drinks sugar and salt solution, etc.

Non-Newtonian fluids are any liquid that show deviation from Newtonian behavior. So the viscosity is dependent on shear rate but may be dependent or independent on the time of shearing. The Non-newtonian fluids are classified into time dependent and Non-newtonian time independent fluids. Figure 3.1 shows the several behaviours of one fluid.

- Non-newtonian time dependent fluids: Pseudoplastic, Dilatant, Bingham plastic.

- Non-newtonian time Independent fluids: Thixotropic and Rheopectic.

- Examples: ketchup, salad dressing, lithographic ink, mayonnaise, skin cream, hair gel, toothpaste, custard and shampoo, etc.

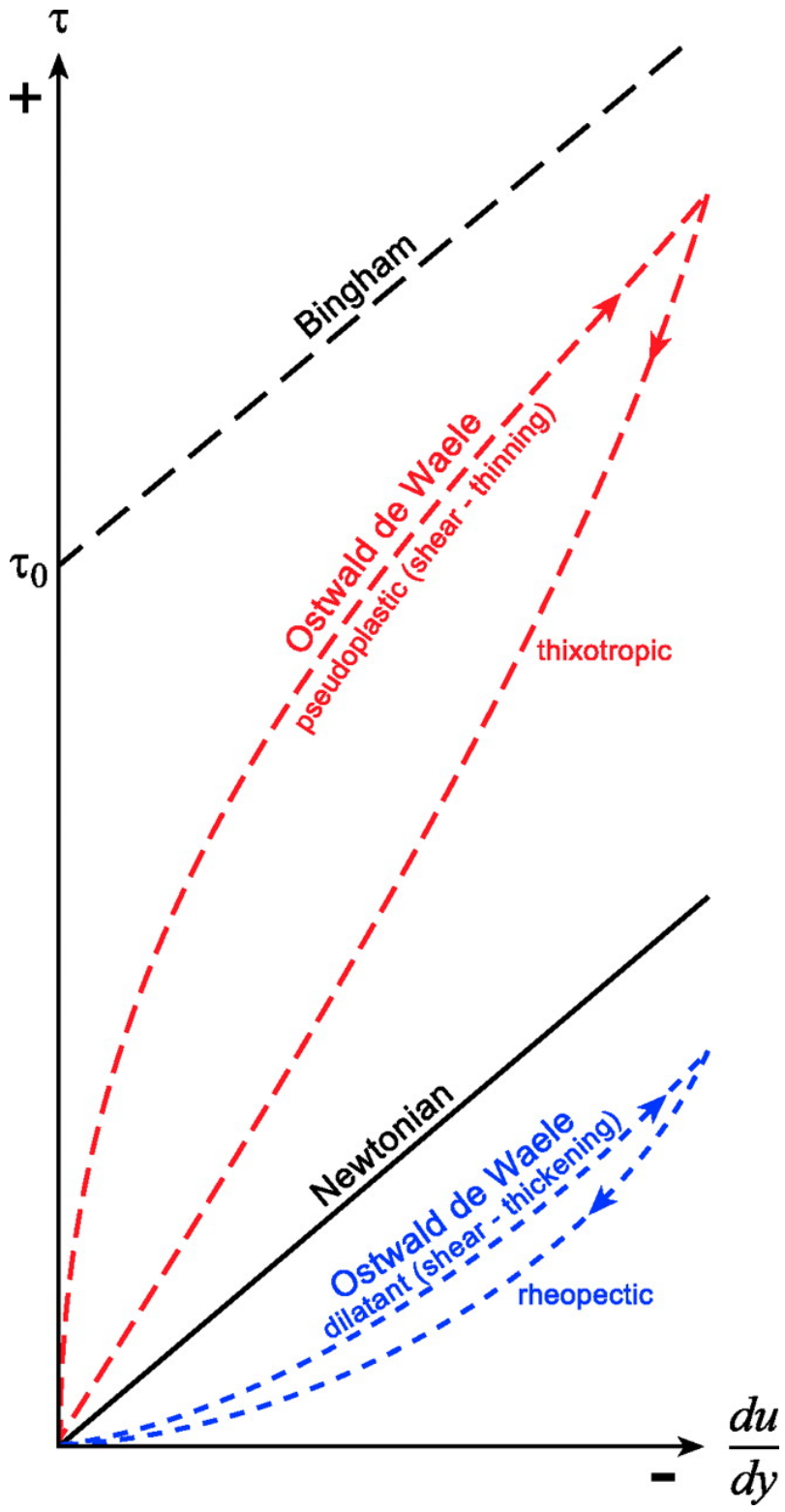


**Figure 3.1:** Summary plot showing variations in rheological behaviour. The case of Newtonian flow where the shear stress ($\tau$) is proportional to rate of shear strain ($du/dy$). The plot shows two variants of Ostwald de Waele flow, pseudoplastic (shear thinning), and dilatant (shear thickening). Both classes show reversible (thixotropic and rheopectic) behaviour defined by hysteresis loops. Bingham fluids possess an apparent inherent yield strength ($\tau_0$).

Traditional rheometers (bulk rheometers) characterize the rheological properties of a material by applying a force (shear stress) to the material and measuring the resulting deformation (strain), or viceversa. Typically, this is done by sandwiching a material between two surfaces, one stationary and one that is free to move, and then applying a torque to the mobile surface. Rotational experiments in which a constant strain or strain rate are applied are ideal for measuring the elasticity or viscosity of elastic solids or Newtonian fluids, respectively. However, in this project we are interested in studying the gelation of hydrogels, which exhibit both solid-like and liquid-like characteristics as they pass through the sol-gel transition. Therefore, we use dynamic or oscillatory tests, since the relaxation response of these materials is dependent on the time scale (frequency) of the applied shear stress.

The shear strain $\gamma(t)$ in a mechanical rheometer is obtained by applying a small amplitude oscillatory,

$$\gamma(t) = \gamma_0 sin\,(\omega t) \tag{3.1}$$

where $\gamma_0$ is the amplitude and $\omega$ is the frequency of oscillation, and measuring the resultant shear stress.

The upper range is limited by the onset of inertial effects, when the oscillatory shear wave decays appreciably before propagating throughout the entire sample. If the shear strain amplitude is small, the structure is not significantly deformed and the material remains in equilibrium; in this case, the affine deformation of the material controls the measured stress.

The time-dependent stress is linearly proportional to the strain, and is given by:

$$\sigma(t) = \gamma_0 \left[G'\,(\omega)\, sin\,(\omega t) + G''\,(\omega)\, cos\,(\omega t)\right] \tag{3.2}$$

$G'$ is the response in phase with the applied strain and is called the elastic or storage modulus, a measure of the storage of elastic energy by the sample. $G''$ is the response out of phase with the applied strain, and in phase with the strain rate, and is called the viscous or loss modulus, a measure of viscous dissipation of energy.

Rheological data are reported in terms of the complex shear modulus defined as

$$G^*(\omega) = G'(\omega) + iG''(\omega) \tag{3.3}$$

In the fluid phase, $G''(w) > G'(w)$, and $G'(w)$ approaches 0 while $G''(w)/w$ approaches a a constant as $w \to 0$. In the gel phase, $G''(w) < G'(w)$, and as

$w \to 0$, $G'(w)$ approaches a constant while $G''(w)/w$ goes to $\infty$. At the gel point, both $G'(w)$ and $G''(w)$ behave as $w^n$ over a broad range of frequencies, with the same power-law exponent $n$ [48][Chambon and Winter (1985)].

### Rheological measurements

The mechanical response of the gels was measured with a torsion shear stress rheometer (CVOR, Bohlin Instruments), with temperature control provided by a Polyscience circulating bath with 0.01°C temperature stability.

All of the measurements were made in the cone-plate geometry with stainless steel fixtures of 40 mm diameter and 1° cone angle. The experiments were made by placing the samples of hot agarose solutions on the plate was had been previously heated to a temperature approximately 10 °C above the gelation temperature. In order to avoid evaporation a thin film of low viscosity silicone oil (FLUKA; viscosity at 25 °C is 5 cSt) was spread around the open surface of the sample rim.

The dynamic moduli of the samples were obtained through oscillatory stress controlled measurements in the frequency range between 0.1 and 50 Hz. The amplitude of the oscillation was controlled so that the strain remained always within the linear regime that had been previously located by means of a torque sweep at a fixed frequency of 1Hz.

# Chapter 4

# Viscometry

The viscosity of the solutions of the pure glicerol and glycerol-water mixtures was mesaured using an Ubbelohde capillary viscometer (Figure 4.1) connected to a water bath. The method involves the determination of the time required for a given volume of liquid to flow through the plumb lines in the capillary of the viscometer under a controlled temperature given by a suitable bath in which the viscometer was immersed. The viscometer in vertical alignment located in the support is placed in the bath. The Hagen-Poiseuille law describes the capillary flow for Newtonian fluids:

$$\eta = \frac{\pi R^4 P}{8Ql} \tag{4.1}$$

Where Q is the volumetric flow rate through the capillary; P is the pressure head forcing the liquid through the capillary (usually, just the hydrostatic pressure of the liquid itself); R is the radius of the capillary; l is the length of the capillary; and, $\eta$ is the viscosity. The bulb volume in the Ubbelohde viscometer is fixed, thus, the flow rate, Q, is just inversely proportional to the time between marks. Since P is usually the hydrostatic pressure, which is proportional to the density of the fluid, the viscosity is obtained by:

$$\eta = c\rho t \tag{4.2}$$

where c is the viscometer constant. The Poiseulle equation does not consider one factor: the pressure drop due to the motion of the fluid itself. The necessary adjustment is called the kinetic energy correction. If this factor is taken into consideration, the revised Poiseuille relation has the form:

$$\frac{\eta t}{\rho} = A + Bt^2 \tag{4.3}$$

The parameters A and B are constants of the particular viscometer, and can be determined calibrating the viscometer with pure liquids of known viscosity.

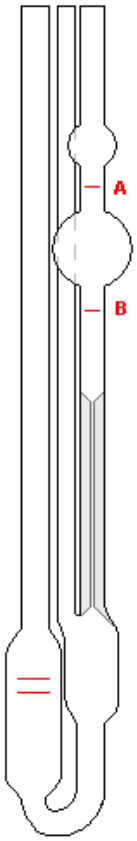


**Figure 4.1:** Ubbelohde viscometer

# Chapter 5

# Microrheology

## 5.1. Dynamic Light Scattering DLS

### 5.1.1. Theory of Dynamic Light Scattering DLS

Light scattering is set into the wide range of experimental techniques based on radiation-matter interaction. The electromagnetic field of the incident light induces an oscillating dipole moment in the molecules of the medium. The light emitted by the dipole, called scattered light has the same frequency as the incident light beam and a much lower intensity, typically $10^{-4}$ to $10^{-6}$ times the incident. However, due to the motion of the particles an optical Doppler effect occurs for the resting observer. The frequency of the scattered light is shifted by a small portion that is proportional to the velocity of the particle. Thus, the scattered light intensity is not constant but fluctuates about a mean value.

In 1930 Gross [49] obtained the first spectrum of light scattered by a liquid. His appearance was like in Figure 5.1 with the double peak predicted by Brillouin in 1914, it also shows the existence of a central band known as Rayleigh with its maximum centered on the frequency of the incident radiation.

If a light beam impinges on particles they interact with the electromagnetic radiation and the light is scattered. The radiation is made up by electric and magnetic fields that oscillate with the same frequency, $\omega_i$, but as the magnetic field effect on the matter is much smaller than the electric one, it can be ignored. The incident electric field, $\vec{E_i}$, moves the molecular charges inducing an oscillating electric dipole moment, $\vec{\mu} = \alpha\vec{E_i}$ where $\alpha$ is the polarizability tensor.

The incident light that illuminates the particles can approximately be described as a plane wave of wavelength $\lambda$, frequency $\omega_i$ and amplitude $E_0$ at a point $\vec{r}$ where the incident electric field is defined:

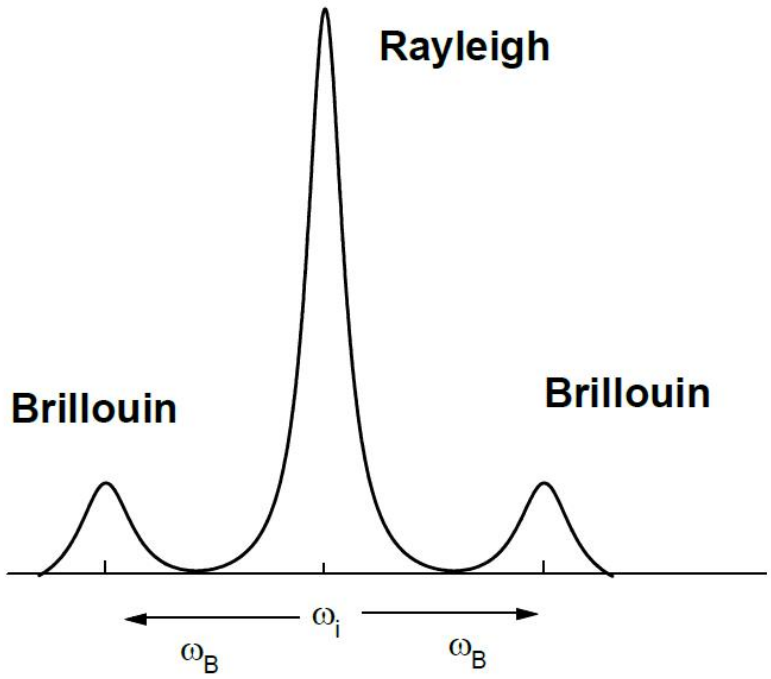


**Figure 5.1:** Scheme of the spectrum of the scattered light by a liquid

$$\vec{E_i} = E_0 exp\, i\left(\vec{k_i}\cdot\vec{r} - \omega_i \cdot t\right) \tag{5.1}$$

where $\vec{k_i}$ is the incident wave vector defined as:

$$\vec{k_i} = \frac{2\pi n_0}{\lambda_i} \tag{5.2}$$

being $n_0$ the medium refractive index.

Figure 5.2 shows a light scattering geometry, where $k_i$ and $k_d$ are the directions of propagation of the incident wave and the scattered wave that reaches the detector, respectively and $k_t$ is the transmitted wave. The angle between $k_t$ and $k_d$ is called the scattering angle $\theta$.

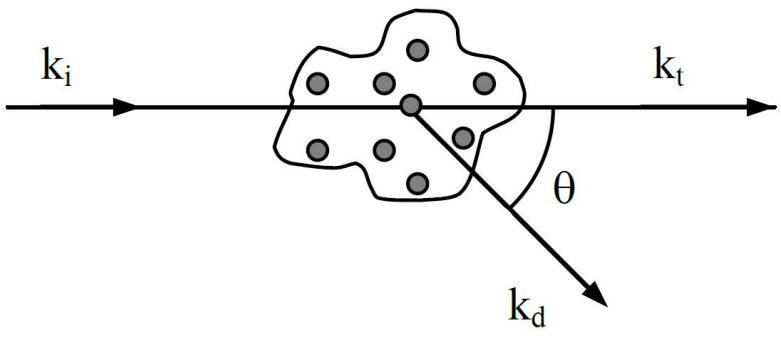


**Figure 5.2:** Schematic ilustration of a scattering geometry

The scattering wave vector $\vec{q}$ is defined as $\vec{q} = \vec{k_d} - \vec{k_i}$ and its magnitude can be expressed as follows

$$q = \frac{4\pi n_0}{\lambda_i} sin\left(\frac{\theta}{2}\right) \tag{5.3}$$

The Brownian motion of a particle is characterized by its mean-square displacement $\left\langle \Delta r^2(t) \right\rangle$ or MSD. In the case of 3D free diffusion this is a linear function of time:

$$\left\langle \Delta r^2(t) \right\rangle = 6Dt \tag{5.4}$$

where $D$ is the diffusion coefficient. For a spherical particle with hydrodynamic radius R in a solvent with viscosity $\eta$, the diffusion coefficient is related to the particle radius by the Stokes-Einstein relation, where $k_B$ is the Boltzmann constant and T is the temperature

$$D = \frac{k_B T}{6\pi\eta R} \tag{5.5}$$

The Stokes-Einstein relation is strictly valid for very diluted solution of spherical particles diffusing in a continuous, nonelastic Newtonian medium with Stokes friction. Many complex media, however, such as semidilute polymer solutions, are viscoelastic. In this case, the mean-square displacement is determined by both the elastic and the viscous response of the medium, and the dynamics of the particle depends strongly on the time scale at which it is probed. The elastic response of the medium is more important at short times, while the viscous response dominates at longer times. In a light scattering experiment, when a laser passes through a sample containing scatterers, it introduces a phase shift which results from a path length difference in the scattered light. The scattered light from different regions in the scattering volume interferes to form a scattering pattern which consists of both constructive and destructive interference of the scattered light. The regions of constructive interference show up as a bright spots and are called speckles. In general the scatterers are able to undergo random motion around their mean positions which causes the phase shifts to fluctuate with time, which results in the speckles to change intensity over time. The average intensity of these speckles over time as a function of the scattering vector, $I(q)$, provides information regarding the size, shape and spatial orientation of the scatterers, and is known as static light scattering. On the other hand, measuring the fluctuations in the intensity of the speckles provides information regarding the dynamics of the scatterers, and it is known as dynamic light scattering.

As the particles diffuse and rearrange in the sample, the intensity of light that reaches the detector fluctuates in time. In the simplest case, each photon is scattered only once within the illumination volume directly into the detector. The

intensity fluctuations are measured as a function of time, $I(t)$, and the normalized intensity autocorrelation function, $g^{(2)}(t)$, is calculated

$$g^{(2)}(t) = \frac{\langle I(t)\, I(t+\tau)\rangle}{\langle I(t)\rangle^2} \tag{5.6}$$

where the intensity at a particular time is correlated with the intensity measured at a later delay time for any scattering wave vector, q and the angular brackets denote time average.

Time averaged intensity is equal to the ensemble averaged intensity, the measured intensity autocorrelation function is converted into electric field autocorrelation function $g^{(1)}(t)$

$$g^{(1)}(t) = \frac{\langle E(t)\, E^*(t+\tau)\rangle}{\langle E(t)\rangle^2} \tag{5.7}$$

where E is the scattered electric field and E* the complex conjugate. For ergodic samples both functions are related by the Siegert relation

$$g^{(2)}(t) = 1 + \beta \left| g^{(1)}(t) \right|^2 \tag{5.8}$$

where $\beta$ is the coherence factor that depends on the experimental setup and for fiber based optical detection systems it is very close to 1.

Only in the case of a dilute collection of monodisperse Brownian particles with a mean square displacement, MSD, given by Einstein equation,$MSD = 6Dt$, for a wavevector $q$ and $\beta = 1$, then:

$$g^{(2)}(t) - 1 = e^{-2\Gamma t} = e^{-2Dq^2 t} \tag{5.9}$$

$$g^{(1)}(t) = e^{\tau t} = e^{-Dq^2 t} \tag{5.10}$$

where t is the lag time, and $\Gamma$ is the decay rate related to the diffusion coefficient $D$ by

$$\Gamma = \frac{1}{\tau} = Dq^2 \tag{5.11}$$

where $\tau$ is the relaxation time and q is the magnitude of the scattering vector. The hydrodynamic radius, $R_h$, of the particles can be obtained from the Stokes-Einstein relation.

$$R_h = \frac{k_B T}{6\pi\eta D} \tag{5.12}$$

The technique of dynamic light scattering, DLS, has been established as a powerful method for investigating dynamic processes. By measuring the temporal

fluctuations of the scattered light it is possible to obtain information about the dynamics of the scattering medium. When the sample is polydisperse only the average of the decay rate or hydrodynamic radius can be obtained and this will be discussed in the Data Analysis section. The use of dynamic light scattering in microrheology is based in the following equation

$$g^2(t) - 1 = exp\left(-\frac{MSD \cdot q^2}{3}\right) \tag{5.13}$$

Which is the intensity autocorrelation function of a dilute collection of monodisperse Brownian particles with a mean square displacement, MSD, given by Einstein equation, MSD=6Dt, for a wavevector $q$. This equation can be traced back to Berne and Pecora´s book [50]. This equation can be inverted to extract the MSD from experimental autocorrelation functions according to

$$MSD = \left(-\frac{3}{q^2}\right) ln(g^2(t) - 1) \tag{5.14}$$

Recently G.D.J.Phillies has proposed that the above inversion can only be used if the probe particles are strictly monodisperse and there is a true Brownian motion. If the intensity autocorrelation function $g^2(t)$ is not a single exponential then it will depend not only on the MSD but also on all the higher moments $MSD^n$ and there will be a dependence with the wave vector $q$ [51].

### 5.1.2. DLS Experimental equipment

Light scattering experiments were performed using an Argon ion laser (wavelength =514.5 nm) at various scattering angles between 30° and 150°, corresponding to scattering vectors $q$ from 8.4 $^{-1}$ to 31.4 $^{-1}$, for n=1.3320 corresponding to the refractive index of water at 25°C.

Dynamic light scattering measurements were carried out with the same setup described above, with an ALV/DLS/SLS-5000 (ALV GmbH; Langen, Germany) equipment using an ALV-5000/EPP and ALV-60X0 Multiple Tau Digital Correlator to calculate the intensity correlation function. The temperature was 25.0°C controlled by a thermostatic bath. A picture of the equipment is shown in 5.3.

A goniometer holds the sample and defines the scattering geometry.

The detail of the laser passing through the sample is observed in Figure 5.4.

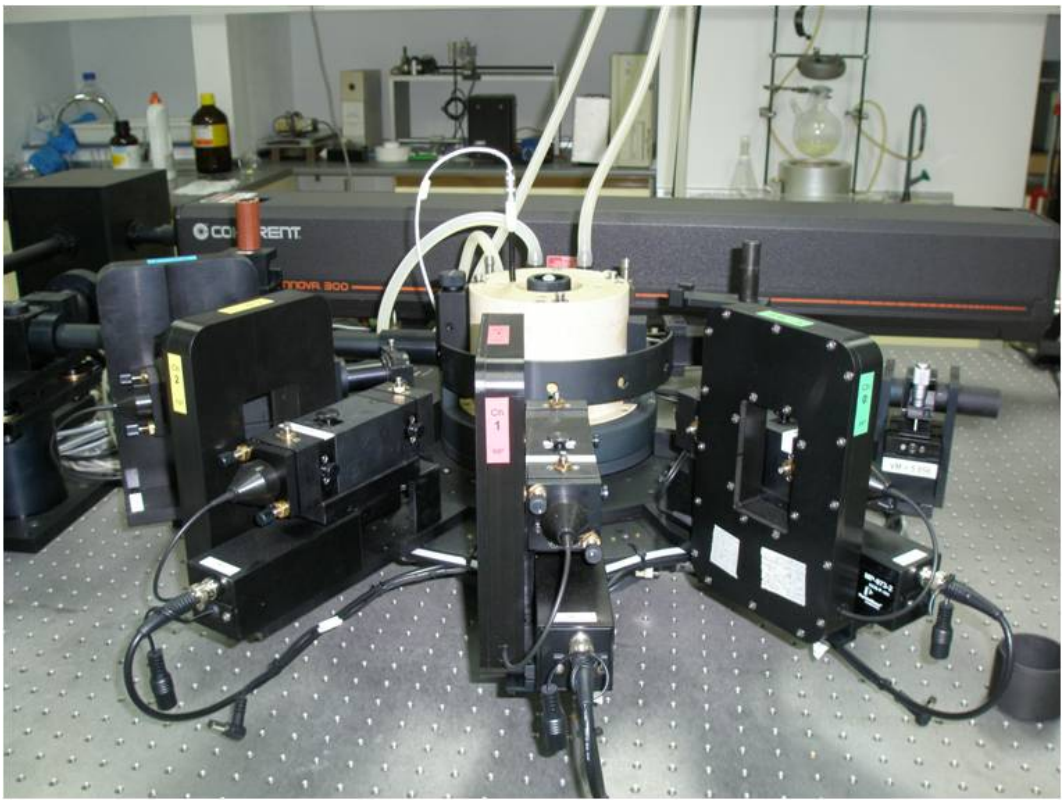

**Figure 5.3:** Light scattering equipment

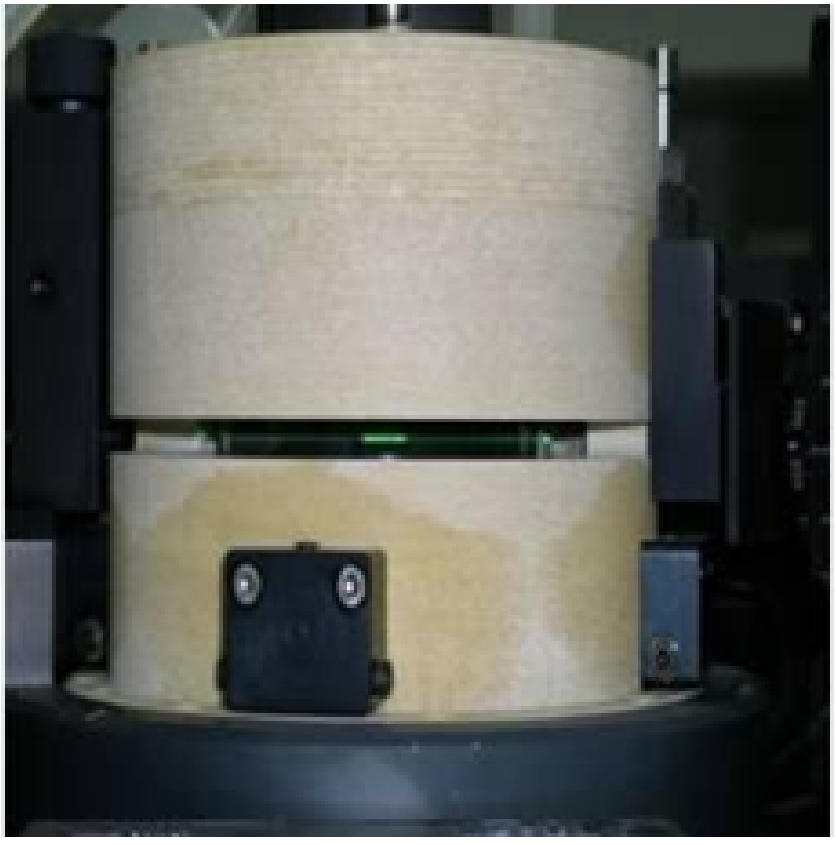

**Figure 5.4:** Laser passing through the sample

One centimeter cylindrical cells are used for measurements at multiple scattering angles and are positioned such that the laser beam passes through the center of the cell, and are placed in a bath filled with toluene which has a refractive index nearly equal to that of glass, in order to reduce the refraction and scattering at the cell surface. Cells were cleaned in acetone vapor before used. Data acquisition and analysis was attained via the ALV Correlator Software V.3.0. The software includes cumulant analysis (linear, second and third cumulants), inversion via CONTIN, a nonlinear fitting method where nonlinear model functions can be selected.

A typical DLS system comprises of six main components. First of all a laser is used to provide a light source to illuminate the sample particles within a cell. Most of the laser beam passes straight through the sample, but some is scattered by the particles within the sample. A detector is used to measure the intensity of the scattered light. As a particle scatters light in all directions, it is (in theory), possible to place the detector in any position and it will still detect the scattering. The intensity of the scattered light must be within a specific range for the detector to successfully measure it. If too much light is detected then the detector will become overloaded. To overcome this an attenuator is used to reduce the intensity of the laser and hence reduce the intensity of the scattering.

The appropriate attenuator position is automatically determined by the ALV/DLS/SLS-5000 during the measurement sequence.

The scattering intensity signal for the detector is passed to a digital signal processing board called a correlator. The correlator compares the scattering intensity at successive time intervals to derive the rate at which the intensity is varying.

This correlator information is then passed to a computer, where the specialist ALV software will analyse the data and derive diffusion and size information.

A schematic diagram of the light scattering apparatus with the components described above is shown in Figure 5.5. The argon ion laser beam at a wavelength of 514.5 nm and a power up to 200 mW is focused by a system of mirrors and lens at the centre of the goniometer. A beam splitter divides the laser beam into two parts: the incident and the reference beams. The sample cell in the middle of the goniometer is surrounded by an index matching bath in order to avoid light coming from reflection and refraction at the cell walls. The photomultiplier detector is placed on the goniometer arm and records the scattering intensity. It can be moved to different scattering angles ranging from $30^{o}$ to $150^{o}$. The scattered light is focused by lens on the pinhole in front of the photomultiplier. The photomultiplier works in the photon-counting mode. Single photo-electron is

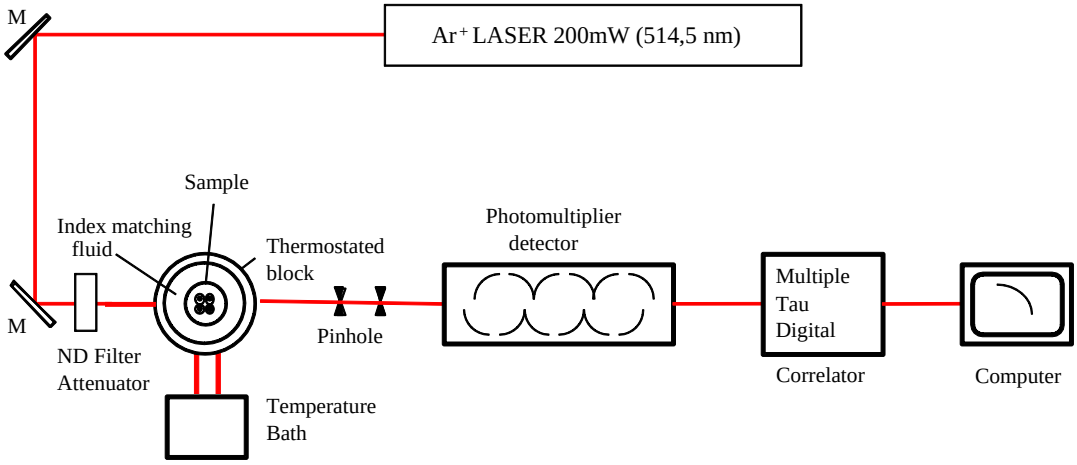


**Figure 5.5:** Schematic flux diagram of the experimental DLS equipment; M:mirror; ND: neutral density filter

first accelerated by a suitably electric field and then hits the intermediate metal electrodes known as dynodes which provide amplification between $10^5$ and $10^7$ altogether. Finally, the photon counts are transferred to the correlator.

Mean display screen of the ALV Correlator Software is shown in Figure 5.6. There are four live data windows: Correlation function, Count Rate, Residuals and Distribution.

### The cumulant data analysis

A Cumulant analysis of the correlation function is performed by the ALV software following the Koppel method [52].

The analysis of the cumulant expansion of the correlation function is performed by fitting a polynom up to third order to the function $ln(g^{(2)}(t)-1)$. The polynomial coefficients are converted into the coefficients of the cumulant expansion of the field correlation function

$$ln\, g^{(1)}(t) = lnA - \Gamma t + \frac{\mu_2}{2}t^2 - \frac{\mu_3}{6}t^3 \tag{5.15}$$

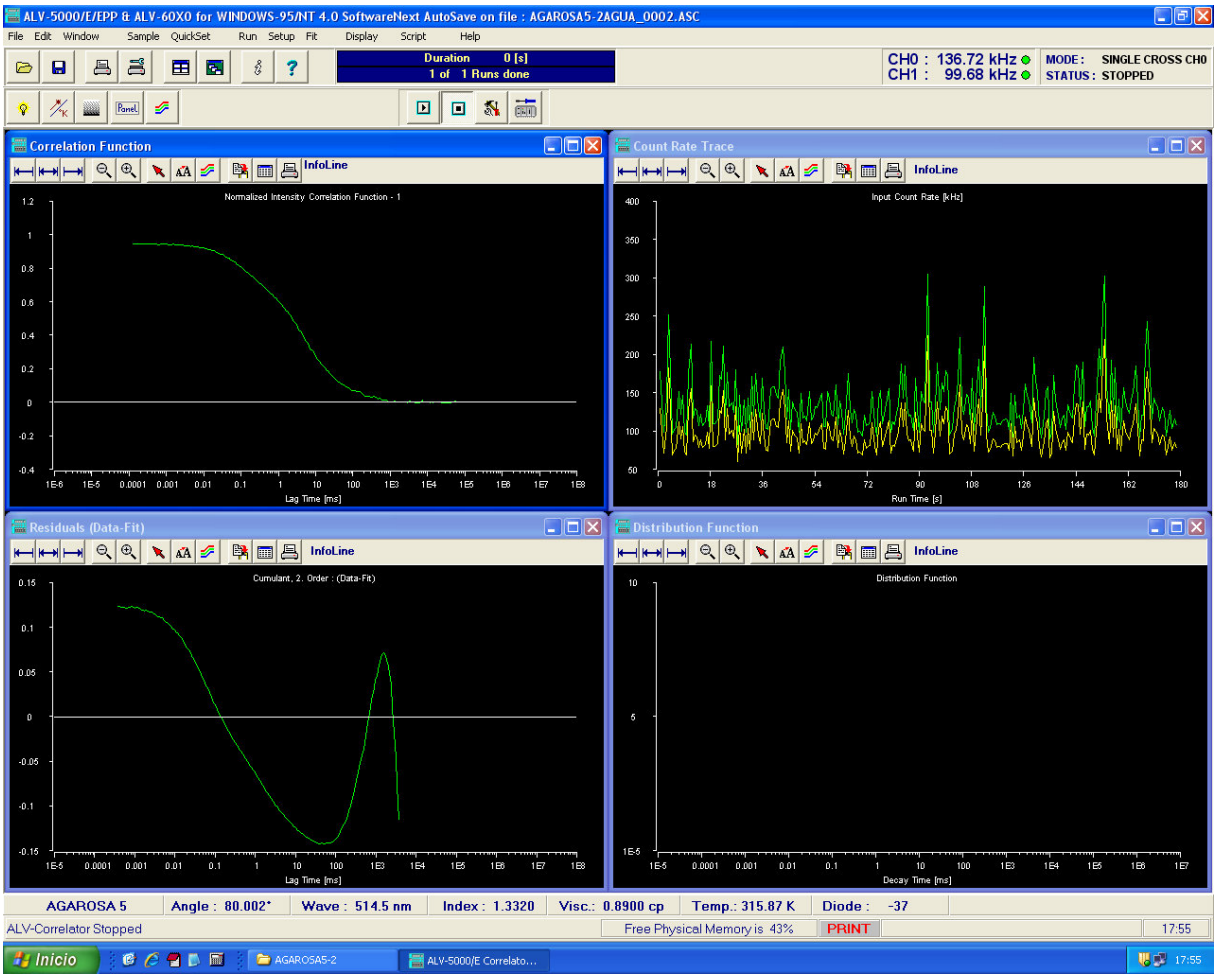


**Figure 5.6:** Main display screen by ALV correlator software

The fit parameters are displayed in a table, first the amplitude A, followed by the time $\tau$ $(1/\Gamma)$, $\mu^2$, $\mu^3$. Time unit is always in milliseconds (ms) and the unit of $\mu^2$ and $\mu^3$ are therefore $1/ms^2$ and $1/ms^3$.

The mean apparent hydrodynamic radius is calculated from the time of 1st. to 3rd. order fitting and the width of the radius distribution $(w)$ as well as the polydispersity index (PDI) are calculated from the second moment $\mu_2$ of 2nd. and 3rd. order fitting according to the following formulas (Stokes-Einstein equation):

$$R_h = \frac{k_B T}{6\pi\eta\Gamma} q^2 \tag{5.16}$$

$$\Gamma = \frac{1}{\tau} = D \cdot q^2 \tag{5.17}$$

$$w = \frac{\sqrt{\mu_2}}{\Gamma} R_h \tag{5.18}$$

$$PDI = \frac{\sqrt{\mu_2}}{\Gamma^2} \tag{5.19}$$

The cumulant analysis window is like the represented in Figure 5.7. On the right the intensity autocorrelation function (ICF) is represented, and on the left the cumulant fit with the order of residuals, the fit results for one to third order cumulant, and the hydrodynamic radius, width (from $\mu^2$) and Polydispersity index.

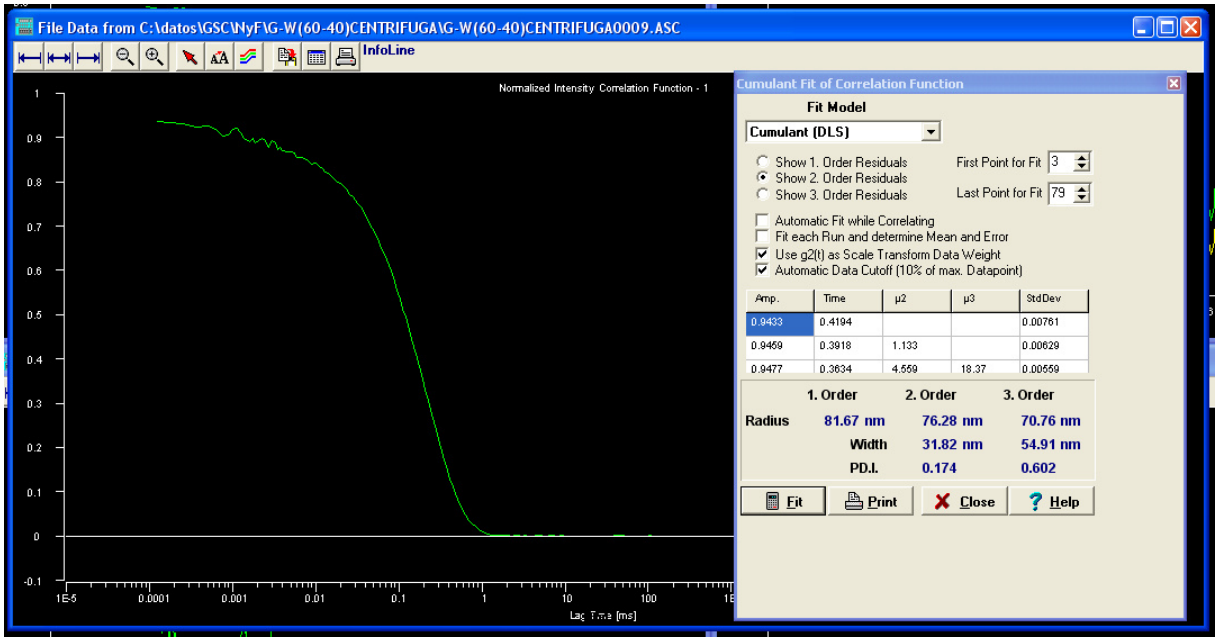


**Figure 5.7:** Cumulant display screen by the ALV correlator software with four data windows: Correlation function, Count Rate, Residuals and Distribution

### Data analysis using regularized methods

ALV-NonLin data analysis fits an integral type model function to the correlation function using a constrained regularization method. For dynamic light scattering data the mathematical background of regularization is described in great detail for the CONTIN program by Provencher. [53],[54],[55]. The following nonlinear fit model is used: Where $G(\Gamma)d\Gamma$ denotes the decay rate distribution function that is an intensity weighted distribution function of characteristic times of fluctuations responsible for the scattering of light. The method gives good estimates for the widths and peaks of multimodal distributions when the data has good signal to noise. The routine REPES, [56], has formal similarities to CONTIN. In contrast to CONTIN which uses the $g^{(1)}(t)$ values extracted from the measured $g^{(2)}(t)$ values, Siegert relation referenced 5.8, REPES directly minimizes the sum of the squared differences between experimental and calculated intensity correlation functions, $g^{(2)}(t)$, using a constrained regularization method. The regularized fit gives the residuals which should be uniformly random and the distribution function which should consist in a narrow peak for monodisperse samples. Figure 5.8 shows these windows.

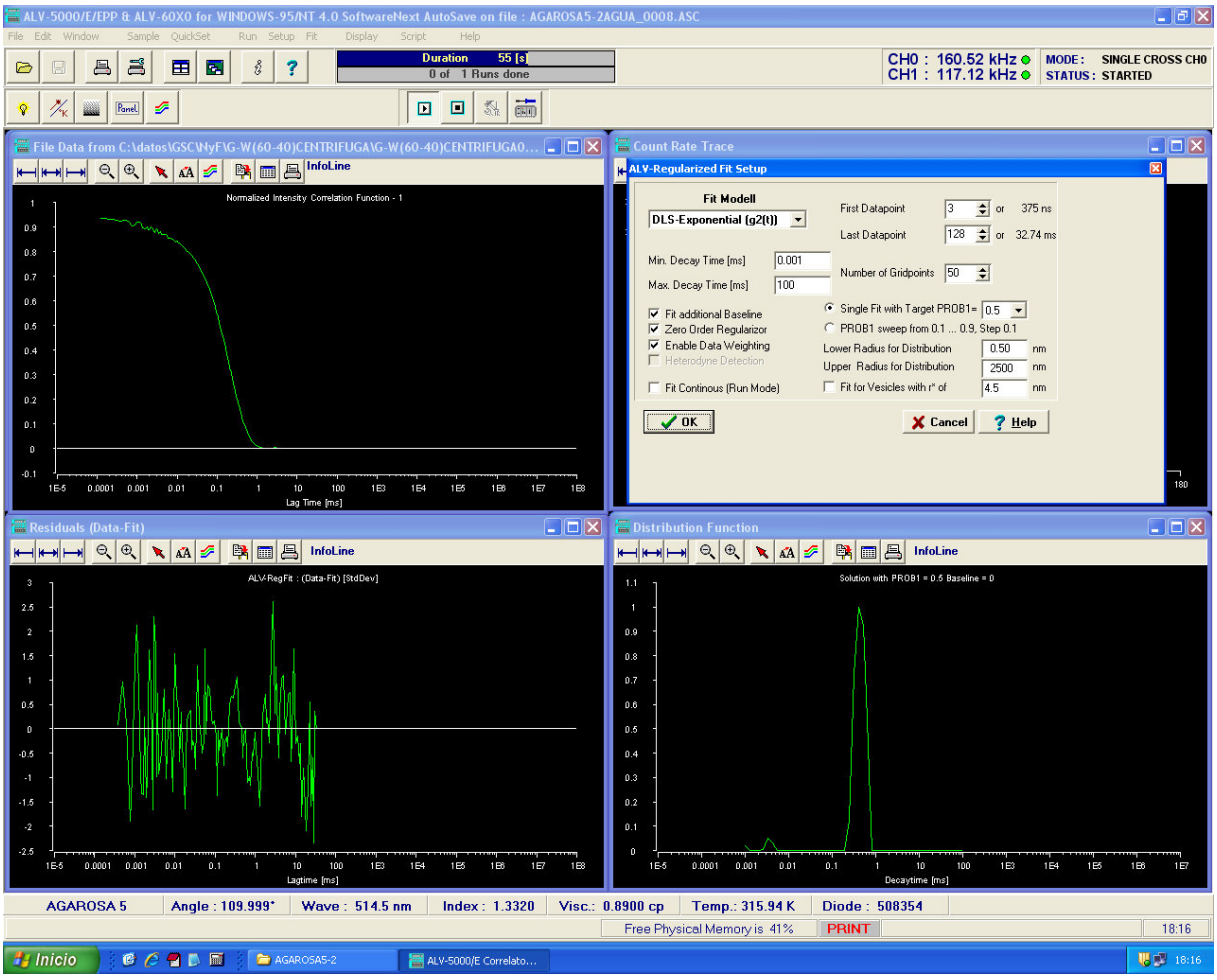


**Figure 5.8:** Regularized fit display screen by the ALV correlator software

## 5.2. Diffusing wave spectroscopy DWS

### 5.2.1. Theory of Diffusing wave spectroscopy DWS

Diffusing wave spectroscopy, DWS, is an extension of dynamic light scattering, DLS, to the multiple scattering limit [57], [58] (Maret, 1987; Pine, 1988). Therefore, DWS is very similar to conventional dynamic light scattering. In both cases the intensity fluctuations of the scattered light reflect the dynamics of the scattering medium. The technique extends the analytic power of DLS to opaque samples such us concentrated suspensions, obviating the need to dilute or index match.

DWS is a multiple scattering technique, where the mean square displacement of probe particles is measured using time correlation functions. The intensity autocorrelation function $g^{(2)}(t)$ is obtained by collecting the scattered intensity from a single speckle over a sufficiently long collection period. The field autocorrelation function $g^{(1)}(t)$ is related to the measured $g^{(2)}(t)$ through the Siegert relation 5.8. In DLS, the characteristic decay time of the correlation function is related to the dynamics of the medium through the length scale set by the scattering wavevector. The decay of the temporal autocorrelation function of the multiple scattering light measured with DWS results from a change in phase of the scattered light. In DWS the total path length of the light through the sample must change by one wavelength to cause the change in phase and thus the fluctuation in the intensity. The calculation of this phase change entails two fundamental approximations. The first approximation is the description of the light propagation through the scattering medium. In the limit of very high multiple scattering, each photon is scattered a very large number of times, and its path can be described as a random walk. The simplest description of the light propagation is to use the diffusion approximation. The second fundamental approximation in DWS is in the treatment of the effect of the dynamics of the scatterers on the phase of the light. Since each photon is scattered a large number of times and it is transported through the medium, the details of individual scattering events are insignificant. In particular, the conservation of scattering momentum at every point along the full path can be neglected. Instead, the individual scattering events are approximated by the contribution of an average scattering event. Then the knowledge of the path length obtained by the diffusion approximation determines the number of these average scattering events that contribute to each path.

The Figure 5.9 represents the multiple scattering of light by particles.

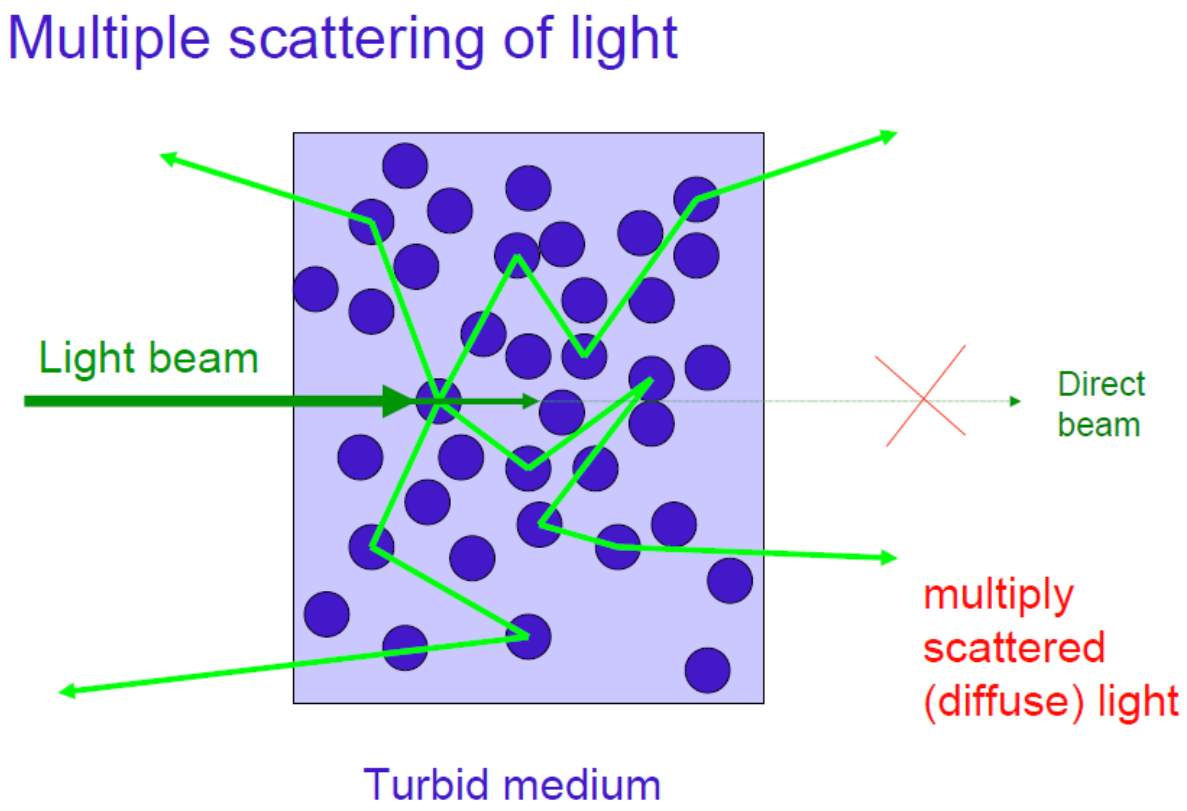


**Figure 5.9:** Scheme of the multiple scattering of light that occurs in the DWS

The use of the diffusion approximation to describe the propagation of light ensures that the scattering wavevector, which relates the incident and detected light, has little relevance to the resultant correlation function, because the light has undergone such a large number of intermediate scattering events. Therefore, unlike DLS, the angle between the incident and detected light is not important in DWS. The wave vector dependence is lost as the photons average over all possible angles, resulting in only two experimental geometries: transmission and backscattering.

In the multiple scattering limit, see Figure 5.10 there are two length scales that characterize light scattering and transport: the mean free path $l$ between scattering events, and the transport mean free path $l^*$. The mean free path is the average distance between scattering events and, in dilute suspensions, is given by

$$l = \frac{1}{\rho\sigma} \tag{5.20}$$

where $\rho$ is the number density of particles and $\sigma$ is the total scattering cross-section for a single particle in suspension.

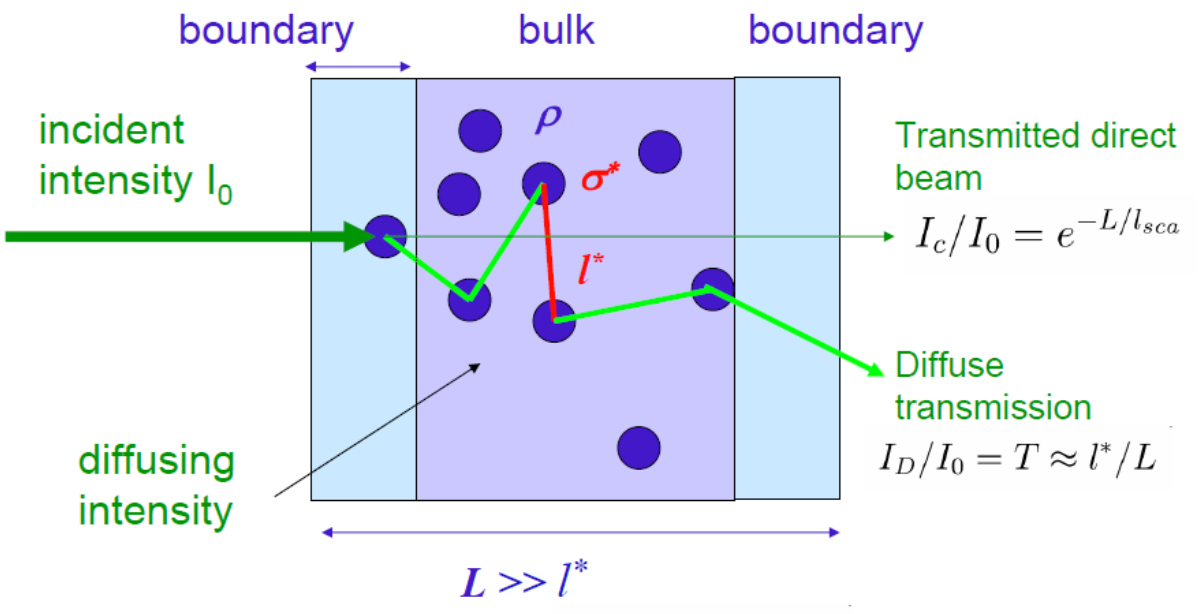


**Figure 5.10:** Definition of the transport mean free path $l^*$ in the multiple scattering of light phenomenon

The transport mean free path $l^*$ is the length scale for which the direction of light propagation is randomized; it is related to the mean free path by

$$l^* = \frac{l}{\langle 1 - cos\theta \rangle} \tag{5.21}$$

In the limit of small particles, the single particle scattering is isotropic and the direction of light is randomized after a single scattering event and $l^* = l$. For larger particles, the scattering reaches high point in the forward direction so that several scattering events are required, on average, to randomize the direction of propagation, in this case, $l^* > l$. The mean free path and transport mean free path can be determined experimentally by measuring the transmission coeficient of a plane wave of light through a suspension of thickness L. If $L \leq l$, most of the trasmitted light is unscattered light. If $L >> l^*$, then none of the transmitted light is unscattered. In this limit, light propagation is diffusive and the photons perform a random walk of step length $l^*$. In general, several scattering events are required to randomize the direction of propagation, implying that $l \leq l^*$. When $L >> l^*$, the system is considered to be in the highly multiple scattering limit.

Measurements of the temporal autocorrelation function of the fluctuating intensity of the speckle pattern yields detailed information on the mean-squared displacement MSD of scatterers with time by the relations 5.22 and 5.23

$$g^1(t) = \int_{l*}^{\infty} P(s) \cdot e^{-\frac{2t}{\tau} \cdot \frac{s}{l^*}} \, ds \tag{5.22}$$

where $\tau = k^2 D^{-1}$. For long light paths, the total path legth through the sample is gicen by s=Nl, *P(s)* is the distribution of the path lengths of the photons in the sample and it is calculated with the diffusion model taking into account the experiment geometry.

$$g^2(t) - 1 = \left( \int_0^\infty P(s) \cdot e^{-\frac{s}{l^*} \cdot k^2 \cdot MSD} \, ds \right)^2 \tag{5.23}$$

with $k$ the wave vector of the light in the medium $k = 2\pi n/\lambda$.

For transmission through a slab, that is, the plane wave limit, and uncorrelated diffusion (diluted suspensions) the field correlation function can be expressed as

$$g^1(t) = \frac{\left(\frac{L}{l^*} + \frac{4}{3}\right) \sqrt{k_0^2 MSD}}{sinh\left[\left(\frac{L}{l^*} + \frac{4}{3}\right) \sqrt{k_0^2 MSD}\right]} \tag{5.24}$$

The analog expression for the intensity autocorrelation function is

$$g^2(t) - 1 = \beta \left[ \frac{\left(\frac{L}{l^*} + \frac{4}{3}\right) \sqrt{k_0^2 MSD}}{sinh\left[\left(\frac{L}{l^*} + \frac{4}{3}\right) \sqrt{k_0^2 MSD}\right]} \right]^2 \tag{5.25}$$

This is the equation used to get $l^*$ from DWS measurements of suspensions of particles of known size.

### 5.2.2. DWS Experimental equipment

Diffusing wave spectroscopy experiments were done in the transmission geometry, see Figure 5.11. The red laser emission at 658 nm is focused by a system of mirrors and lens at the centre of the sample cell. A polarization analyzer is placed before the detection system. Multiple scattered light is collected by an optical fiber and then split by a fiber optic beam splitter and directed to the high quantum efficiency avalanche photodiode (APD) modules operating in Geiger mode. These units provide digital pulses in accordance with the arrival time of individual photons to the detector. Finally, the photon counts are transferred to the correlator.

The structure of the DWS software have a graphical user interface organized by three tabbed windows: Measure, Parameters and Analyze.

To start a measure previous it is neccessary to do a calibration by first measuring a non-absorbing reference sample to know the transport mean free path. This reference sample consist in a monodisperse microparticles aqueous suspension with

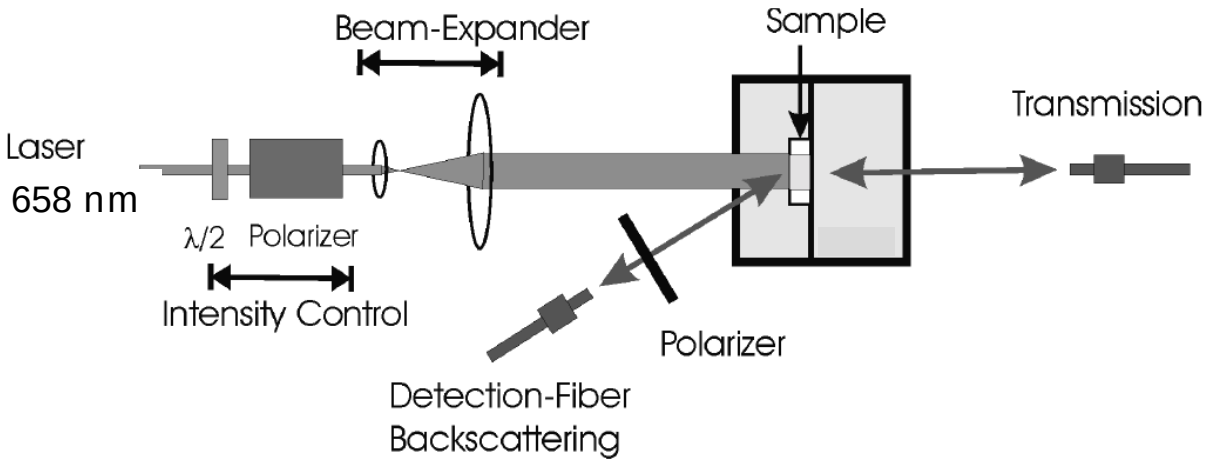


**Figure 5.11:** Set up of the experimental DWS equipment

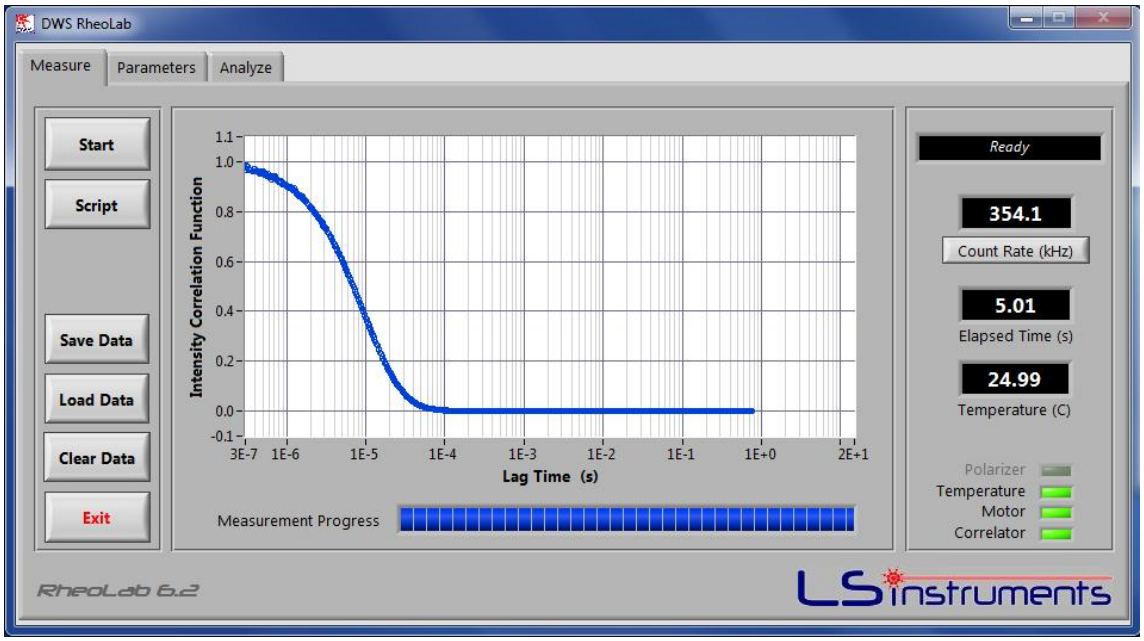


**Figure 5.12:** calibration test correlator software

a known particle size and that is sufficiently turbid such that ($L/l^* > 10$) where L is the sample cuvette thickness.

The software determines the transport mean free path of the reference sample from analysis of the intensity autocorrelation function using the known viscosity of the calibration solvent and the known particle size, the Figure 5.12 shows a current calibration test.

The measured intensity correlation function (ICF) for the calibration sample is displayed while a fit to the data is shown to calculate the transport mean free path, as shown in Figure 5.13.

Upon completion of a measurement, the DWS solftware programm displays the measured intensity correlation function and calculates the mean square

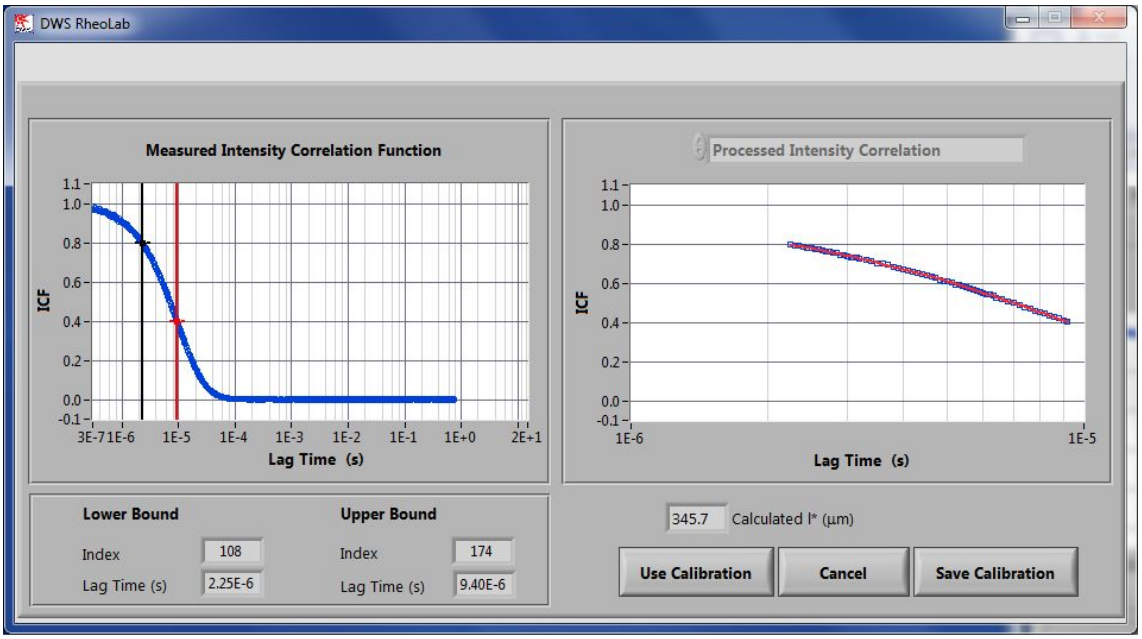


**Figure 5.13:** Calculus of l* by the correlator software

displacement and the viscoelastic moduli. It is possible to selected and well-fit the MSD over the region of interest. When performing a microrheology analysis, it is importat that always first have a look at the MSD form since the data from this is used to calculate the viscoelastic spectrum. The viscoelastic moduli are determined using the generalized Stokes-Einstein relation following the approach of Mason et al.

## 5.3. Video Microscopy

Video based particle tracking is a complementary technique which is used to measure the dynamics of the embedded probes in many types of systems. This technique is not practical to average over thousands of beads, as in a light scattering experiment, nevertheless it is very useful to probe local structures that might be present in the samples.

The trajectories of the particles are identified with their motion in the medium which are tracked by a camera attached to a microscope, so the method name is videomicroscopy.

A Brownian particles trajectory r(t) is parameterized by its self-diffusion coefficient D through the Einstein-Smoluchowsky equation with $d$ the number of the spatial dimension

$$MSD = \left\langle \Delta r(t)^2 \right\rangle = \left\langle \left| r\left(t_0 + t\right) - r\left(t_0\right) \right|^2 \right\rangle = 2dD\tau \tag{5.26}$$

Particle trajectories, are saved as data files containing the x and y coordinates and frame number for each particle identified. Frame numbers can be converted to absolute time using the frame rate of image capture. More important than absolute time is the separation time between images, known as the time lag. The averaged mean-squared displacement MSD is calculated as a function of time lag, and can be used to calculate rheological properties such as the viscosity with the equation of Stokes Einstein for a Newtonian fluid and viscoelastic moduli, as presented in the introductory chapter.

The set-up particle tracking consists in a video camera Hamamatsu photonics UK, about 30 frames per second that is connected to the microscope Nikon Eclipse 80i. The images can be procesed to calculate the MSD and therefore analize the data and extract the microrheologic properties.

## 5.4. Microrheology techniques summary

The experimental techniques described above provide us with complementary ways to measure the dynamics of the embedded probes and to obtain microrheological information spanning almost seven decades in frequency. Figure 5.14 shows the different ranges of time scales that can be probed using DWS, DLS and particle tracking techniques. The diagram also shows the frequency range typically accessible using a conventional rheological experiment. There is a significant overlap between the various microrheological techniques themselves which will help in comparing results between the different types of measurement. We are therefore well suited to extensively test the validity of the microrheological measurements on model polymer solutions, where a low concentration of probe particles are added to the solution and the thermal motion of these particles are used to determine the viscoelastic response of the host polymer solution.

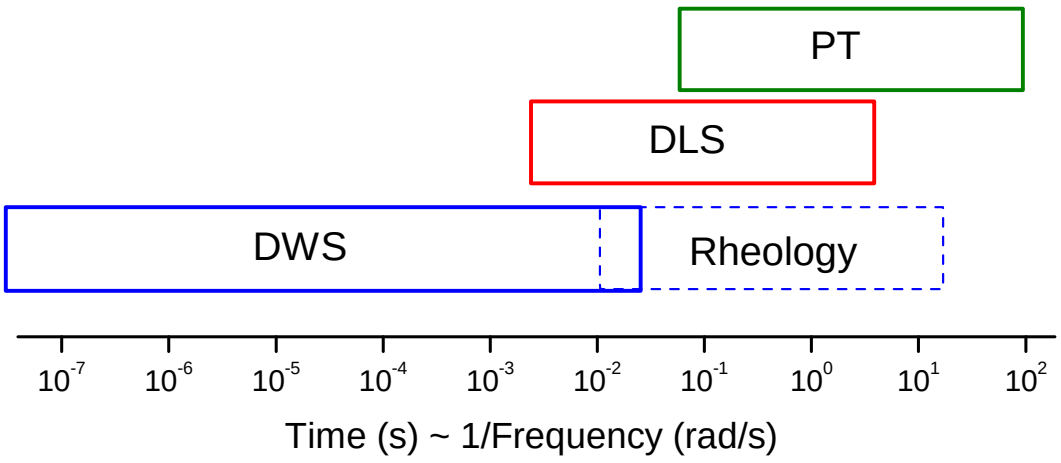


**Figure 5.14:** Typical frequency ranges accessible using the different experimental techniques

# Part I

# PRIMER BLOQUE DE RESULTADOS. SISTEMA VISCOSO: GLICEROL Y MEZCLAS ACUOSAS

# Chapter 6

# GLICEROL

En este apartado de la discusión de resultados se aborda el estudio del sistema glicerol-agua por la técnica de dispersión de luz dinámica (DLS), de la que se obtienen los resultados que se describirán a continuación. El objetivo de este capítulo de resultados es proporcionar los detalles técnicos necesarios y suficientes para que los resultados puedan ser reproducidos. El capítulo se estructura en cuatro apartados según las técnicas empleadas. Primeramente, una explicación del procedimiento experimental de preparación del sistema de estudio. A continuación, la descripción y análisis de los resultados obtenidos.

## 6.1. Medidas de dispersión de luz dinámica

### 6.1.1. Preparación de disoluciones

Para la preparación de las disoluciones de glicerol se partió del reactivo comercial de Sigma-Aldrich (Alemania) con pureza superior al 99% y se diluyó en agua mili-Q a temperatura ambiente 23 ± 2ºC. Seguidamente se añadieron las partículas homogeneizando la disolución resultante mediante ultrasonidos. Finalmente las muestras se centrifugan 60 minutos a 5000 rpm antes de realizar la medida para su estabilización.

Las propiedades físicas del agua como del glicerol se recogen en la tabla 6.1.

**Table 6.1:** Propiedades físico químicas de agua y glicerol a 25ºC. [Marcus., 1985] [25]

| PRODUCTO | Dendidad (kg/m$^3$) | $\eta$ (Pa s) | n$_D$ | Mw(g·mol$^{-1}$) |
|---|---|---|---|---|
| Agua | 997.048(1) | 0.000890(1) | 1.3325(1) | 18.02(1) |
| Glicerol | 1261(1) | 0.945(1) | 1.4730(1) | 92.09(1) |

Las concentraciones de las mezclas estudiadas fueron 5, 20, 30, 50, 60, 70, 80, 90 % (w/w) glicerol y glicerol puro. Las células con la muestra para su medida se

preparan disolviendo 0.1 mL de la suspensión acuosa de partículas de latex de poliestireno en 1 mL de la mezcla de glicerol-agua, recalculando con esta nueva adición la concentración final de la mezcla.

Las sondas son partículas esféricas de poliestireno (8%w/v) de $22 \pm 3$ nm y $1.00 \pm 0.03\,\mu$m de diámetro suministradas por Invitrogen (USA).

## 6.2. Resultados obtenidos por DLS

### 6.2.1. Coeficiente de difusión y radio hidrodinámico de las partículas de poliestireno

La disolución de partículas que se estudió mediante DLS se prepara disolviendo las partículas de latex de poliestireno comercial en agua para obtener una concentración adecuada a las características de la medida en DLS, completamente transparente.

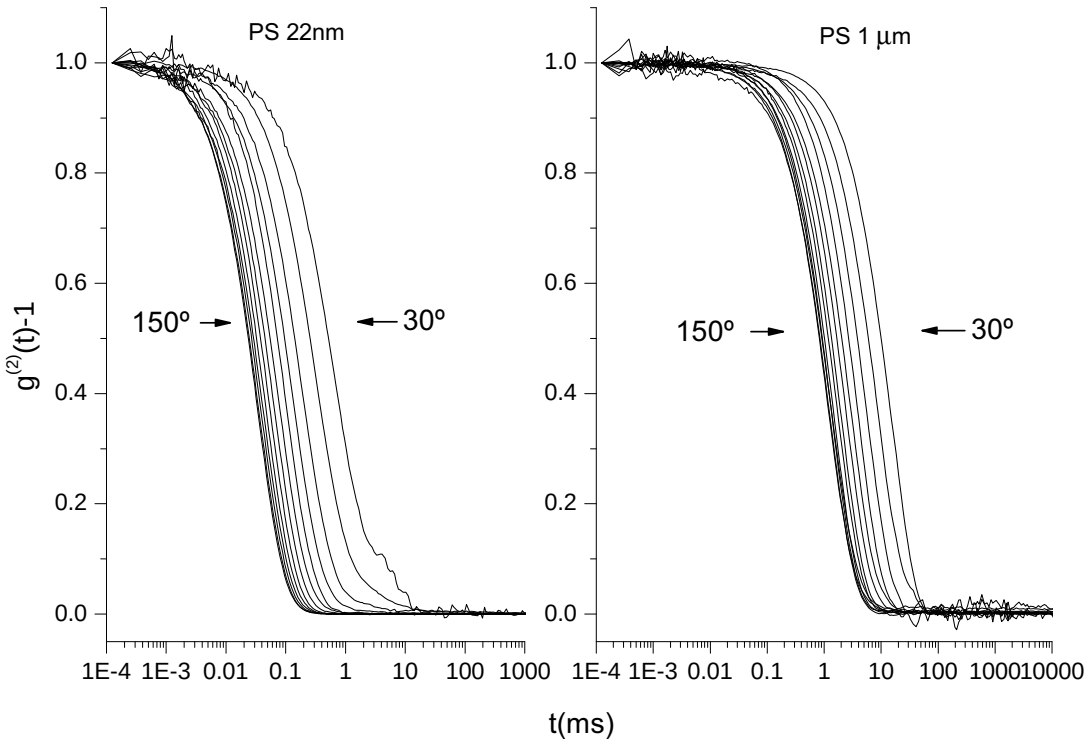


**Figure 6.1:** ICF partículas PS en agua a 25°C para ángulos de observación entre 30° y 150°

La Figura 6.1 muestra las funciones de autocorrelación de intensidades normalizadas para el sistema de partículas suspendidas en agua.

Las curvas presentan caídas exponenciales, características de partículas coloidales monodispersas inmersas en un fluido simple, el agua. Se observa como a medida que aumenta el ángulo de observación la curva correspondiente decae a tiempos más cortos. Cuanto mayor sea el ángulo, tanto mayor es el vector de onda, relacionados por la ecuación 5.3. Además, este análisis junto con la relación de Siegert, ecuación **??**, y el modelo de un único decaimiento exponencial (ecuaciones 5.10 y 5.11) permiten deducir que las funciones de autocorrelación de intensidad obtenidas a mayor ángulo decaen antes.

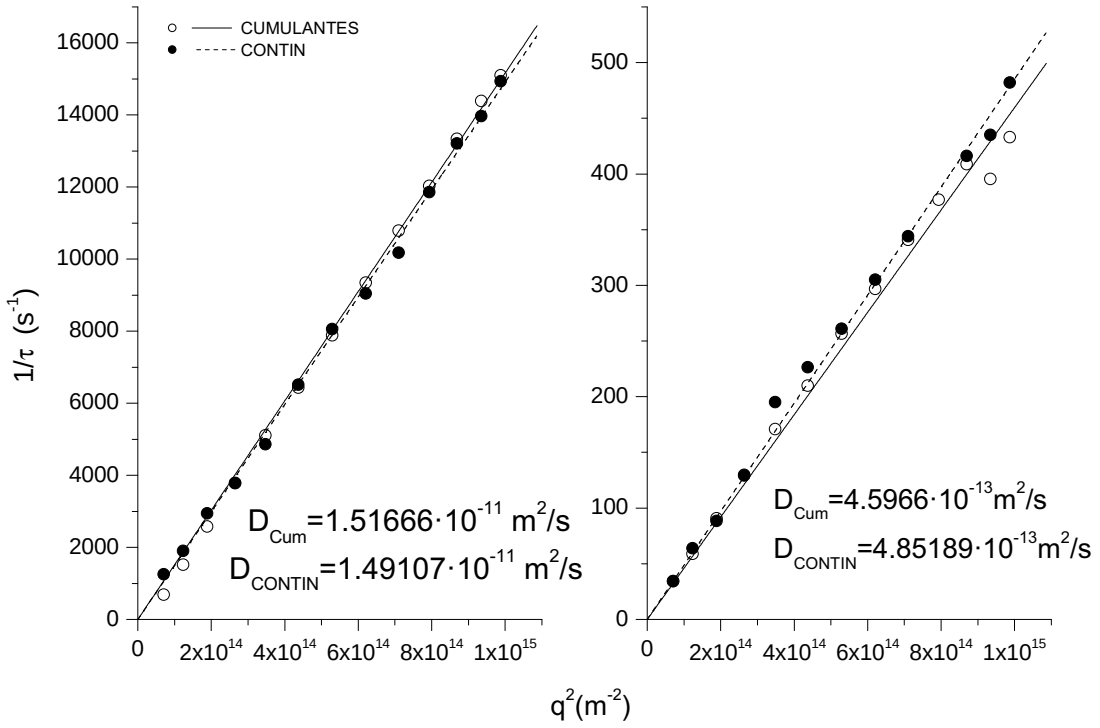


**Figure 6.2:** Dependencia del tiempo de relajación con el vector de onda. Izquierda:partículas de latex de 22 nm de diámetro; derecha: 1 micra de diámetro. (○) ajuste lineal cumulantes(●) ajuste lineal CONTIN

A partir de las funciones de autocorrelación de intensidades se puede obtener el coeficiente de difusión de las partículas en el medio. El ajuste de las curvas al método de cumulantes o al método CONTIN permite determinar el tiempo de relajación $\tau$ para cada uno de los ángulos de observación medidos en la muestra. De este modo, el cálculo del coeficiente de difusión se obtiene del valor de la pendiente al representar el inverso del tiempo de relajación, llamado tasa de decaimiento frente al cuadrado del vector de onda, según la relación 5.11. El valor del coeficiente de difusión de las partículas de 22 nm de diámetro que se obtienen al realizar la representación de la Figura 6.2 es de $(1,52 \pm 0,01)10^{-11}m^2/s$ según el método de Cumulantes y de $(1,49 \pm 0,01)10^{-11}m^2/s$ según CONTIN; para las partículas de una micra de diámetro los resultados son $(4,60 \pm 0,01)10^{-13}m^2/s$

por cumulantes y $(4,85 \pm 0,01)10^{-13} m^2/s$ por CONTIN, resultados ambos para los dos tamaños de partícula muy próximos entre sí que verifican la robustez del método y el carácter monodisperso de las partículas de poliestireno utilizadas.

Las partículas de látex de poliestireno cumplen las condiciones de tener un único centro dispersor por partícula ya que su diámetro es mucho menor que la longitud de onda, presentar geometría esférica y ser un sistema diluido, por lo tanto es válido aplicar la ecuación de Stokes-Einstein 5.19, y obtener de esta forma el radio hidrodinámico de las partículas. La tabla 6.2 contiene los resultados derivados que se obtienen del análisis por Cumulantes y el análisis CONTIN.

**Table 6.2:** Coeficiente de difusión y radio hidrodinámico de PS

| | Diámetro $22 \pm 3$ nm | | Diámetro $1.00 \pm 0.03\ \mu m$ | |
|---|---|---|---|---|
| | $10^{11} D$ (m2/$s$) | $R_h(nm)$ | $10^{13} D$ (m2/$s$) | $R_h(nm)$ |
| Cumulantes | $1.52 \pm 0.01$ | $16.2 \pm 0.2$ | $4.60 \pm 0.01$ | $534 \pm 16$ |
| Regularizado | $1.49 \pm 0.01$ | $16.5 \pm 0.2$ | $4.85 \pm 0.01$ | $506 \pm 13$ |

### 6.2.2. Efecto del ángulo de observación

En las Figuras 6.3 y 6.4, se observan las funciones de autocorrelación normalizadas correspondientes a mezclas glicerol agua de contenidos 20%w y 60%w de glicerol respectivamente.

En la correspondiente a la mezcla glicerol-agua (20-80)%(w/w) (Figura 6.3), se puede visualizar a ángulos bajos que las curvas presentan desviaciones del carácter exponencial debido a las trazas de polvo que de manera fortuita aparecen en las muestras aun siendo extremadamente cuidadosos en su preparación. Las curvas obtenidas correspondientes a la mezcla glicerol-agua (60-40)%(w/w) (Figura 6.4) son claro ejemplo de medidas ideales con caídas monoexponenciales.

Una característica significativa del movimiento browniano en DLS es que las partículas pequeñas dispersan luz en todas direcciones y se mueven más rápido que las partículas grandes que al moverse más lentamente, la dispersión de luz que producen no es igual en todas direcciones sino que tienden a dispersar mayor intensidad de luz a ángulos de observación pequeños. Esto es lo que se observa cuando partículas de polvo, que tienen el tamaño de micrómetros, interfieren en las medidas a bajos ángulos. La Figura 6.5 muestra la función de correlación para partículas grandes y pequeñas. Como puede observarse, la tasa de decaimiento de la función de correlación está relacionada con el tamaño de partícula (ecuaciones 5.11 y 5.19) produciéndose el decaimiento más rápido para partículas pequeñas que para grandes.

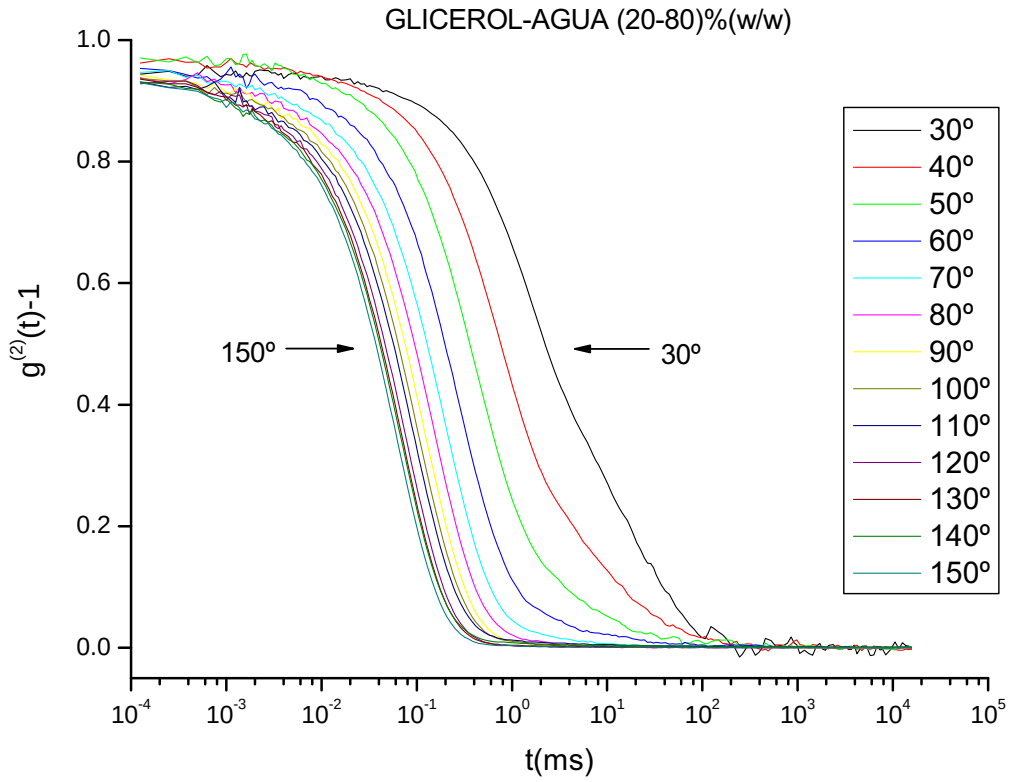


**Figure 6.3:** ICF Mezcla glicerol-agua (20-80)%(w/w) con parículas PS de 22 nm a 25°C para ángulos de observación comprendidos entre 30° y 150°

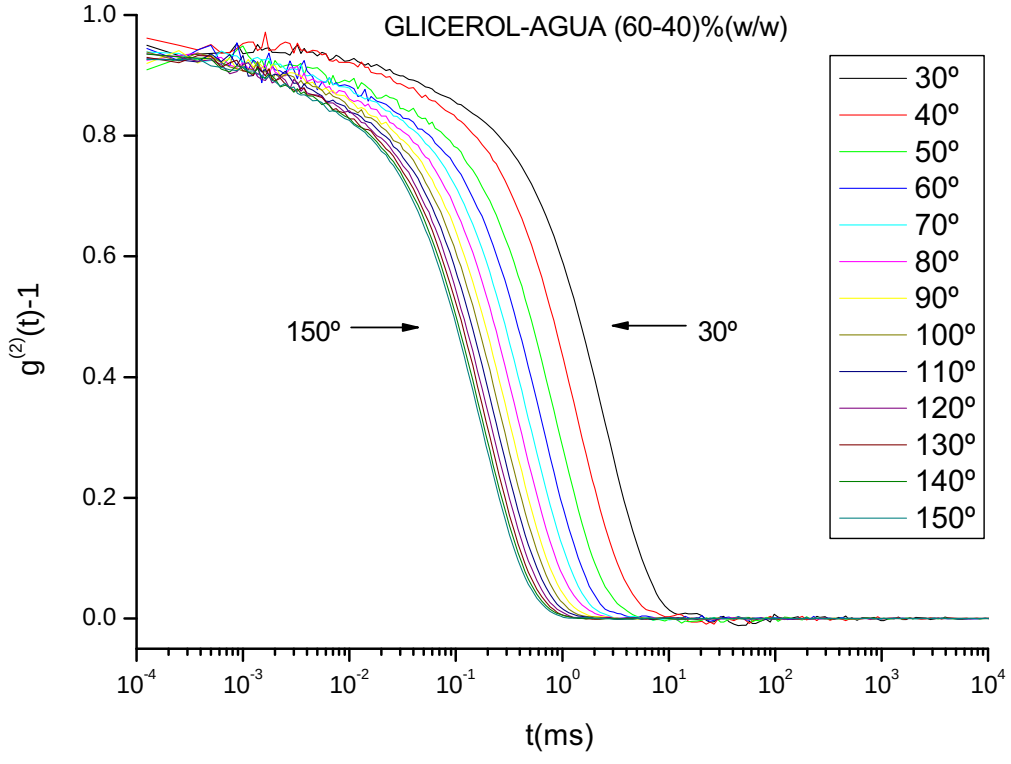


**Figure 6.4:** ICF Mezcla glicerol-agua (60-40)%(w/w) con parículas PS de 22 nm a 25°C para ángulos de observación comprendidos entre 30° y 150°

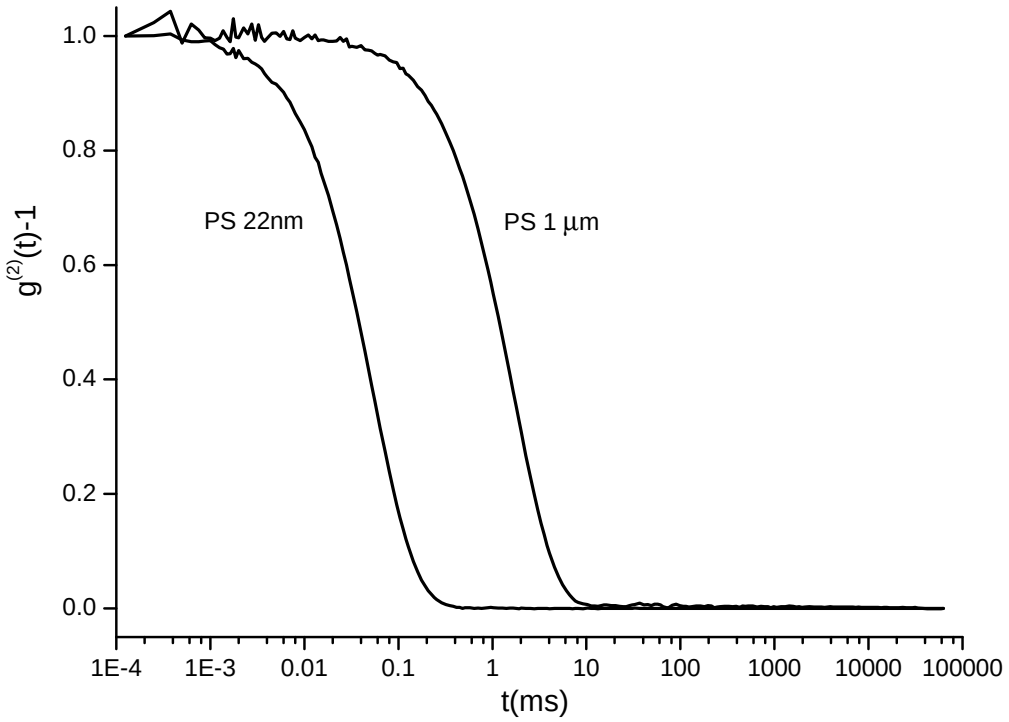


**Figure 6.5:** Función de autocorrelación de intensidades para partículas pequeñas de 22 nm y grandes de 1 micra de diámetro, en agua a 25°C para un ángulo de observación de 100°

### 6.2.3. Coeficientes de difusión

La Figura 6.6 muestra los ajustes lineales de los inversos de tiempo de relajación frente al cuadrado del vector de onda correspondientes a cada una de las mezclas glicerol-agua estudiadas. A la izquierda de la gráfica se representan las rectas pertenecientes a porcentajes de glicerol desde 0%w a 60%w, y a la derecha los restantes porcentajes hasta 100%w glicerol. Se trata de rectas que pasan por el origen cumpliendo el modelo descrito por la ecuación 5.11, con una tasa de decaimiento mayor para las mezclas de bajo contenido en glicerol, que corresponden a mayores coeficientes de difusión y por consiguiente a una menor viscosidad. La tasa de decaimiento va disminuyendo según se aumenta el contenido de glicerol en la mezcla obteniéndose progresivamente coeficientes de difusión menores y valores de viscosidad de la mezcla mayores. Cuanto mayor sea el contenido de glicerol en la mezcla, tanto mayor es su viscosidad.

Así mismo, a partir del tamaño de la partícula calculado con la ecuación de Stokes-Einstein en el apartado primero de estos resultados, junto con los valores de los coeficientes de difusión obtenidos ahora, permiten el cálculo de la constante C que recoge el valor de la operación matemática de todos los términos invariables

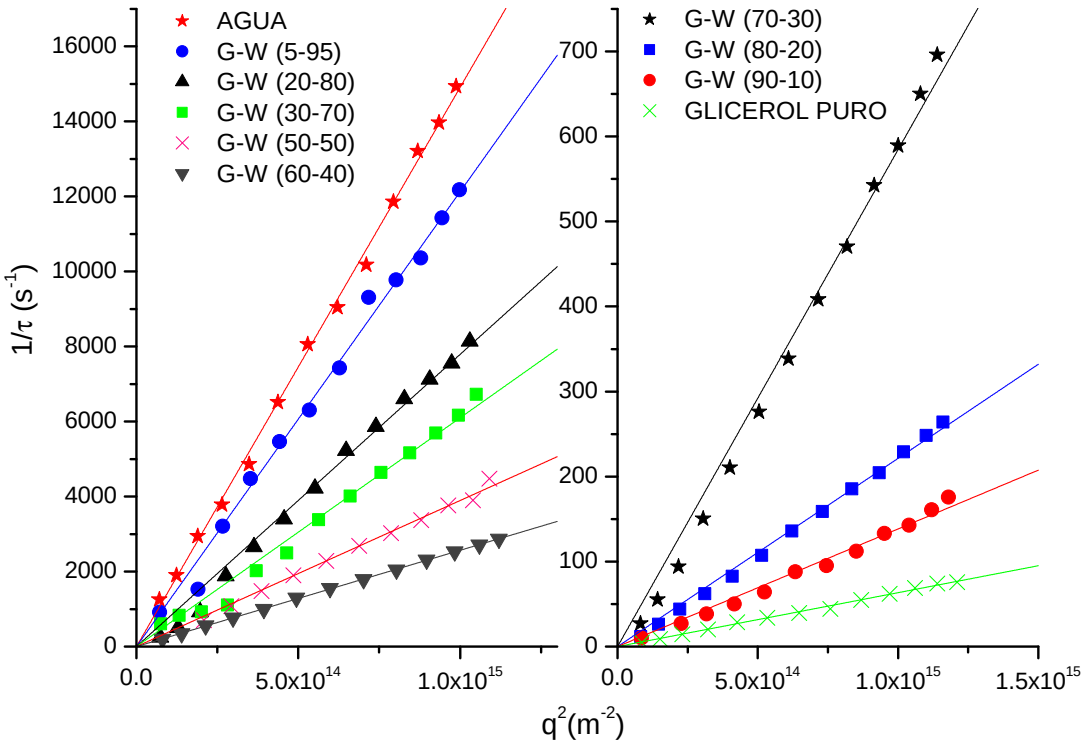


**Figure 6.6:** Evolución de los ajustes para los distintos porcentajes de glicerol estudiados a 25°C para ángulos de observación comprendidos entre 30 y 150°. G-W: Glicerol-Water

involucrados, con la que se puede calcular la viscosidad para cada mezcla en función de su coeficiente de difusión. A continuación, se muestran las expresiones con las que se puede determinar el parámetro C anteriormente explicado y la viscosidad.

$$R_h = \frac{k_B T}{6\pi\eta D_0} \rightarrow C = \frac{k_B T}{6\pi R_h} \rightarrow \eta_i = \frac{C}{D_i} \tag{6.1}$$

Mediante el tamaño de partícula calculado $R_h$ que es de 16,2 nm, el valor de la contante C es de $(1{,}35 \pm 0{,}03)\cdot 10^{-14}$ K/m. Y a partir de ahí se obtienen cada uno de los valores de viscosidad según la relación 6.1 que se recogen en la tabla 6.3.

Otra forma de comprobar que el sistema glicerol-agua tiene un comportamiento difusivo consiste en hacer la representación de la función de autocorrelación de intensidades normalizada $g^{(2)}(t) - 1$ frente al producto del cuadrado del vector de onda por el tiempo de relajación, $q^2 \cdot t$ , como se contempla en la Figura 6.7. En ella se observa que la distribución de las funciones de autocorrelación definen una curva maestra, debido al comportamiento difusivo del sistema, que hace que la función de autocorrelación de intensidades sea proporcional a la tasa

de decaimiento, y ésta a su vez al cuadrado del vector de onda, según la ecuación 5.11. Por ello la multiplicación del cuadrado del vector de onda por el tiempo se relaciona directamente con el coeficiente de difusión.

**Table 6.3:** Coeficiente de difusión y viscosidad de las diferentes mezclas glicerol-agua a 25°C

| %w Glicerol | D ($m^2/s$) | $10^3\eta$ (Pa s) |
|---|---|---|
| 0 | $(1.52 \pm 0.01)10^{-11}$ | $0.89 \pm 0.02$ |
| 4.8 | $(1.21 \pm 0.01)10^{-11}$ | $1.11 \pm 0.02$ |
| 19.1 | $(7.79 \pm 0.01)10^{-12}$ | $1.73 \pm 0.03$ |
| 28.6 | $(6.10 \pm 0.01)10^{-12}$ | $2.21 \pm 0.04$ |
| 47.7 | $(3.89 \pm 0.01)10^{-12}$ | $3.46 \pm 0.07$ |
| 57.2 | $(2.57 \pm 0.01)10^{-12}$ | $5.25 \pm 0.1$ |
| 66.7 | $(5.85 \pm 0.01)10^{-13}$ | $23.1 \pm 0.4$ |
| 76.3 | $(2.21 \pm 0.01)10^{-13}$ | $61 \pm 1$ |
| 85.8 | $(1.39 \pm 0.01)10^{-13}$ | $97 \pm 2$ |
| 92.7 | $(6.47 \pm 0.01)10^{-14}$ | $208 \pm 4$ |

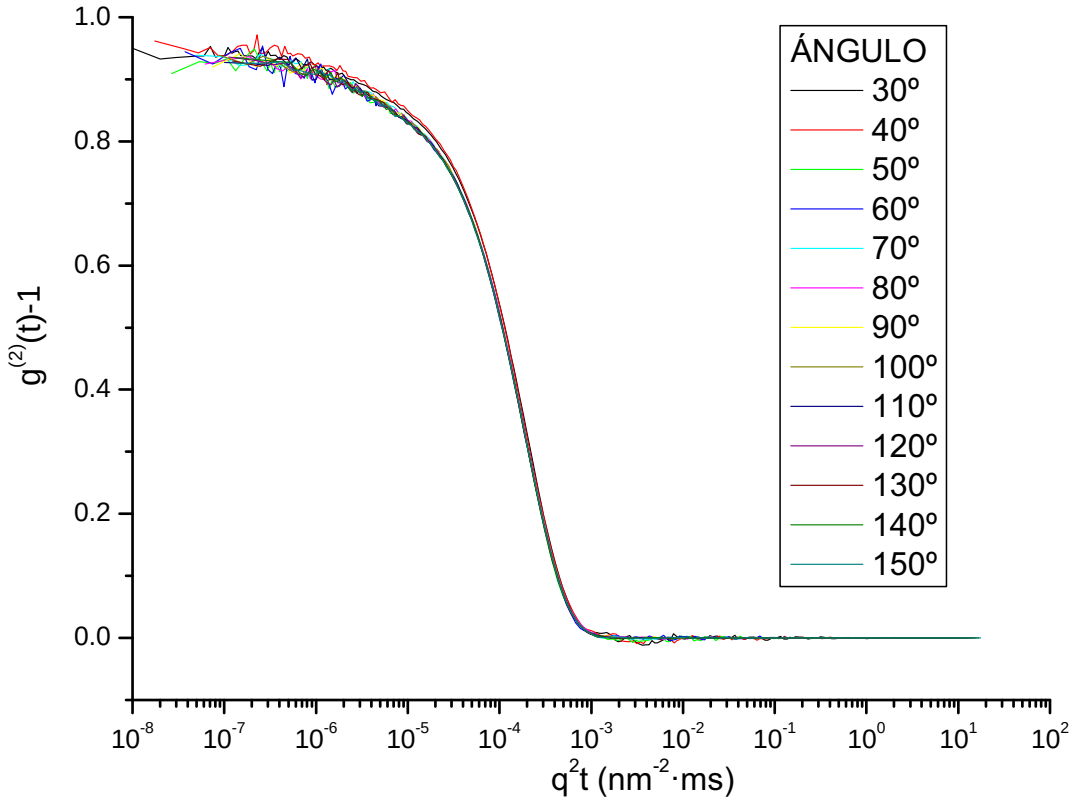


**Figure 6.7:** Evolución de los ajustes para un porcentaje de glicerol-agua (60-40)%(w/w) a 25°C para ángulos de observación comprendidos entre 30º y 150º

Las ecuaciones 6.2 y 6.3 relacionan respectivamente el MSD con las funciones de autocorrelación de campo $g^{(1)}(t)$ y de intensidades $g^{(2)}(t) - 1$:

$$g^1(t) = exp\left(-\frac{MSD \cdot q^2}{6}\right) \tag{6.2}$$

$$g^2(t) - 1 = exp\left(-\frac{MSD \cdot q^2}{3}\right) \tag{6.3}$$

En la Figura 6.8, se muestran $g^{(1)}(t)$ y MSD para la mezcla glicerol-agua (60-40)(%w/w). De la pendiente de la curva de MSD, $1.580(1) \cdot 10^{-14}\ m^2/ms$, se obtiene el coeficiente de difusión, ya que la pendiente es seis veces el coeficiente de difusión, teniendo de ello un valor para el coeficiente de difusión de $2.63(1) \cdot 10^{-12}\ m^2/s$, que concuerda con los calulados a partir de los ajustes del inverso del tiempo de ralajación frente al cuadrado del vector de onda que se han mostrado antes en la Figura 6.6 y que se recogen en la Tabla 6.3.

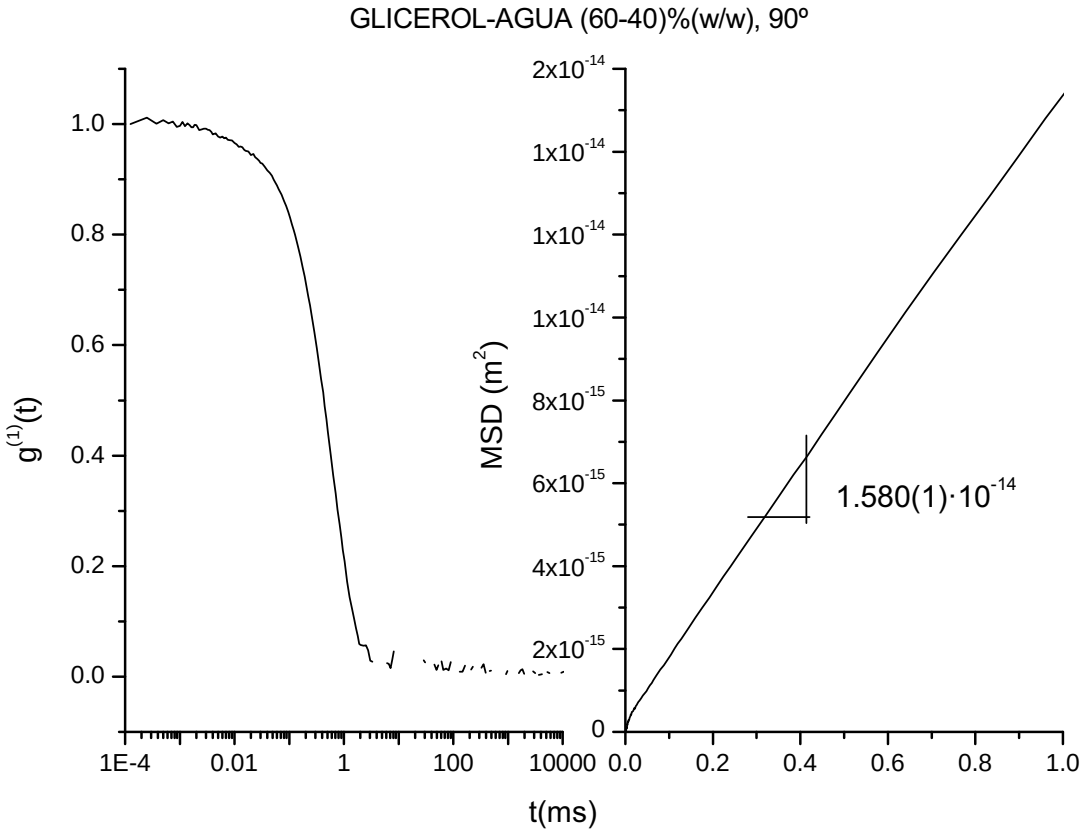


**Figure 6.8:** Función de autocorrelación de campo normalizada y desplazamiento cuadrático medio para un porcentaje de glicerol-agua (60-40)%(w/w) a 25°C para un ángulo de observación de 90º

Phillies pluso de manifiesto [51] que las ecuaciones 6.2 y 6.3 solo son correctas si se trata de un sistema lo suficientemente diluido de partículas monodispersas con movimiento browniano, donde las funciones de autocorrelación son decaimientos exponenciales. Ocurre, en caso contrario, que si las funciones de autocorrelación no son exponenciales la función de autocorrelación depende no sólo del desplazamiento cuadrático medio sino también de sus múltiplos, y por tanto del vector de onda $q$. Se observa en la Figura 6.9 que los datos obtenidos no presentan esta anomalía descrita por Phillies.

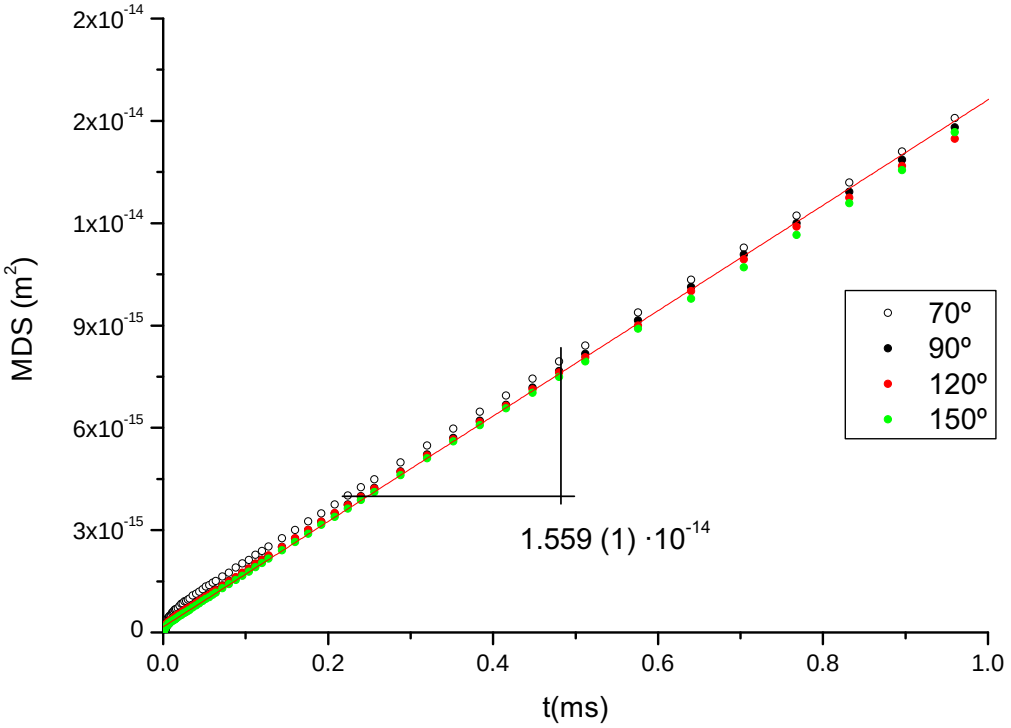


**Figure 6.9:** Desplazamiento cuadrático medio frente al tiempo de relajación para un porcentaje de glicerol-agua (60-40)%(w/w) a 25°C para algunos ángulos de observación. Ajuste lineal realizado para los datos de 90°

### 6.2.4. Efecto de la concentración

En la Figura 6.10 se muestran las funciones de autocorrelación de intensidades normalizadas obtenidas de las muestras de glicerol agua con partículas de 22 nm de diámetro fijando un ángulo de observación determinado, 100°. El espectro presenta las curvas de las funciones de autocorrelación de intensidades típicas del sistema newtoniano en estudio y que vienen siendo corroboradas en los apartados anteriores. Se puede ver como la curva correspondiente al glicerol puro cae la última ya que es la muestra más viscosa y por tanto en la que las partículas

presentan menor coeficiente de difusión.

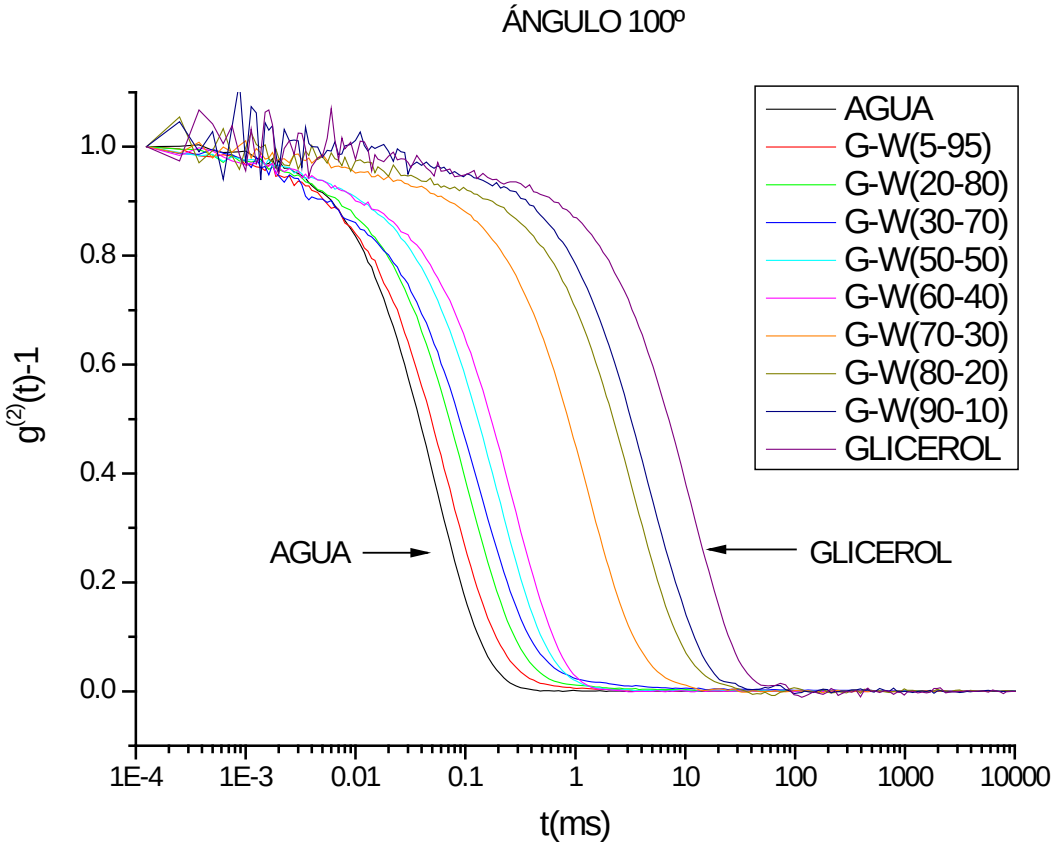


**Figure 6.10:** Evolución de las funciones de autocorrelación de la mezcla glicerol agua con partículas PS de 22 nm a 25°C para un ángulo de observación de 100°.G-W: Glicerol-Water

## 6.3. Viscosimetría

En este apartado se aborda el estudio del sistema glicerol-agua por viscosimetría, cuyo objetivo es la determinación experimental de la viscosidad de disoluciones acuosas de glicerol y de glicerol puro.

Se prepararon disoluciones de glicerol a partir del reactivo comercial y se diluyó en agua a temperatura ambiente 23 ± 2°C.

Para abordar el tratamiento datos es necesario calcular la densidad de cada una de las mezclas mediante la ecuación 6.5 asumiendo aditividad de las densidades, donde $\rho_i$ es la densidad de cada dilución, $\rho_0$ es la densidad del disolvente y $\rho_1$ la densidad de la disolución inicial.

$$\rho_i = \rho_1 \frac{V_1}{V_i} + \rho_0 \frac{V_i - V_1}{V_i} \tag{6.4}$$

$$V_i = V_1 + V_A \tag{6.5}$$

Para el cálculo de la viscosidad de la disolución, se trasvasa un volumen conocido $V_1$ de 12 mL al viscosímetro y se mide su tiempo de caída. El proceso consiste en añadir sucesivamente volúmenes conocidos de disolvente (siendo $V_A$ el volumen añadido acumulado) e ir midiendo el tiempo de caída. Las constantes A y B de calibrado del viscosímetro [ecuación 4.3] se obtienen midiendo el tiempo de paso de un líquido puro de densidad y viscosidad conocida, el agua. A partir de ellas junto con los tiempos medidos se obtiene la viscosidad. Los resultados se muestran en la tabla 6.4. El valor de las constantes de calibrado resultantes son A=0 $m^2$ y B=$(1.86 \pm 0.06) \cdot 10^{-8} m^2/s^2$

**Table 6.4:** Medida de viscosidad de las diferentes mezclas glicerol-agua a 25°C

| t(s) | Dendidad (kg/m$^3$) | $10^3\eta$ (Pa s) | %w Glicerol |
|---|---|---|---|
| $48 \pm 1$ | $997.1 \pm 0.3$ | $0.89 \pm 0.05$ | 0 |
| $60 \pm 1$ | $1017 \pm 3$ | $1.14 \pm 0.06$ | $9.53 \pm 0.03$ |
| $70 \pm 1$ | $1035 \pm 2$ | $1.35 \pm 0.06$ | $17.41 \pm 0.03$ |
| $100 \pm 1$ | $1063 \pm 1$ | $1.97 \pm 0.08$ | $29.66 \pm 0.04$ |
| $153 \pm 1$ | $1094.3 \pm 0.7$ | $3.1 \pm 0.1$ | $42.45 \pm 0.05$ |
| $279 \pm 1$ | $1129.0 \pm 0.6$ | $5.8 \pm 0.2$ | $55.84 \pm 0.06$ |
| $607 \pm 1$ | $1162.0 \pm 0.5$ | $13.1 \pm 0.4$ | $67.82 \pm 0.07$ |
| $739 \pm 1$ | $1167.8 \pm 0.5$ | $16.0 \pm 0.5$ | $69.87 \pm 0.07$ |
| $1111 \pm 1$ | $1179.8 \pm 0.4$ | $24.4 \pm 0.8$ | $74.00 \pm 0.07$ |
| $1560 \pm 1$ | $1189.0 \pm 0.4$ | $34 \pm 1$ | $77.13 \pm 0.07$ |
| $2642 \pm 1$ | $1202.3 \pm 0.4$ | $59 \pm 2$ | $81.57 \pm 0.07$ |
| $3496 \pm 1$ | $1217 \pm 2$ | $79 \pm 3$ | $86.3 \pm 0.1$ |
| $5745 \pm 1$ | $1229 \pm 2$ | $131 \pm 4$ | $90.5 \pm 0.1$ |
| $31217 \pm 1$ | $1261.0 \pm 0.3$ | $732 \pm 23$ | $100.00 \pm 0.09$ |

La Figura 6.11 presenta la evolución de la viscosidad de las mezclas y los componentes puros a una temperatura de 25°C, obtenidos mediante medida con viscosímetro y por dispersión de luz. Los datos calculados de viscosidad por ambos procedimientos son similares, por lo que la técnica de dispersión de luz resulta un método adecuado para la obtención de los valores de viscosidad.

Se puede ajustar la curva a la ecuación de Vogel-Fulcher-Tammann-Hesse (6.6), formulada empíricamente para describir la variación de la viscosidad con la temperatura para polímeros [Riande., 2000] [59].

$$ln\eta = a_0 - \frac{b_0}{c - c_0} \tag{6.6}$$

donde $a_0, b_0, c_0$ son parámetros. Aquí se va a ajustar en función de la concentración, mediante un ajuste no lineal del logaritmo neperiano de la viscosidad frente al porcentaje en peso de glicerol. Por tanto, la viscosidad se determina en función del contenido de glicerol en la mezcla. Mediante el ajuste

de los datos a la ecuación 6.6 se obtienen las funciones interpoladas 6.7 y 6.8 para cada método, viscosimetría y dispersión de luz, siendo $c$ el tanto por ciento en peso de glicerol.

$$Viscosimetra\ ln\eta = -10.2(0.2) - \frac{467(7)}{c - 146(2)} \tag{6.7}$$

$$DLS\ ln\eta = -11(1) - \frac{675(8)}{c - 161(2)} \tag{6.8}$$

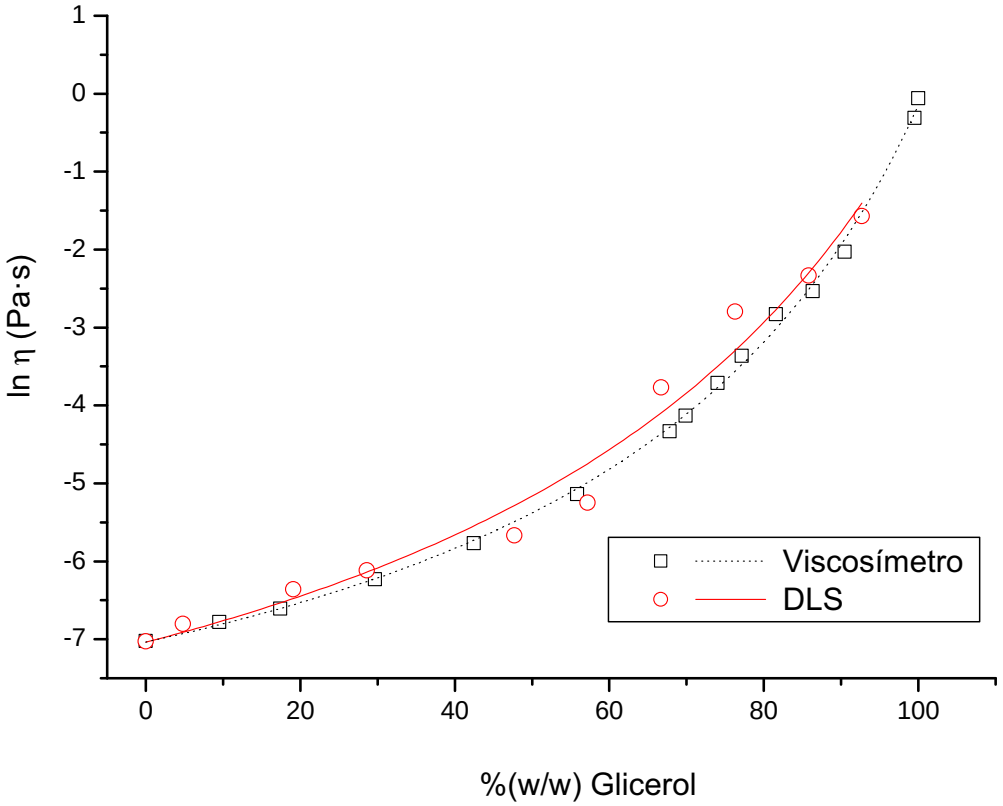


**Figure 6.11:** Ajuste no lineal a la curva de viscosidad de las mezclas glicerol-agua obtenidas por dispersión de luz y mediante el viscosímetro a 25°C

## 6.4. Resultados obtenidos por DWS y reología

Para realizar las medidas por DWS, se necesita que las partículas tengan una concentración lo suficientemente alta para lograr la turbidez de la muestra y que se produzca la dispersión múltiple. Las partículas empleadas son de poliestireno de 977 nm de diámetro dispersas en agua. Se ha utilizado una concentración de partículas de 1%v/v.

Las medidas de reología con reómetro Bohlin se han realizado con las mezclas de glicerol-agua directamente colocadas sobre el soporte empleado. Se ha utilizado una geometría cono-plato de 2,5º y diámetro de plato de 40 mm. Además el sistema de termostatización para el reómetro empleado en estas medidas consiste en un horno de aire, cuya temperatura mínima para obtener una medida aceptable son los 25ºC, por ello para los siguientes sistemas viscoelásticos que se estudian en la tesis se procedió a cambiar el sistema de termostatización por un baño refrigerado con agua para poder tener temperaturas más bajas.

Los resultados que se obtienen por reología confirman a baja frecuencia el comportamiento viscoso del glicerol, solapándose las curvas del módulo viscoso G2 ($G''$) (definido en la ecuación 3.3) en el intervalo de intersección de la técnica micro DWS y la macroreológica reómetro a frecuencias intermedias. Por DWS se puede observar que a elevada concentración de glicerol y alta frecuencia la linealidad que caracteriza el comportamiento viscoso se va perdiendo demostrando con esto que el glicerol también puede comportarse como un sistema con cierta viscoelasticidad, la no ergodicidad, cuando se le somete a condiciones extremas (Figura 6.12).

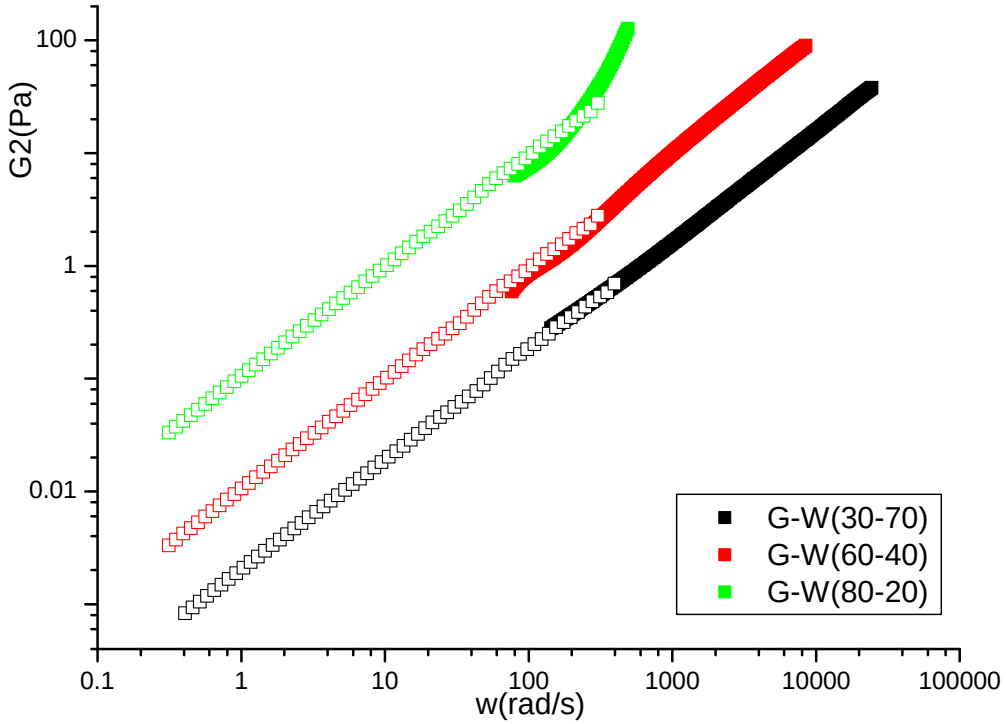


**Figure 6.12:** Valor del módulo viscoso G2 para diferentes mezclas glicerol agua obtenidas mediante reología (puntos huecos) y DWS (puntos rellenos)

De igual manera, se ha procedido empleando el reómetro a obtener los valores de

viscosidad del glicerol puro y de mezclas acuosas hasta el límite de medida del sistema que es detectable por el equipo llegando hasta un 50%w/w de glicerol en función de la temperatura, por eso los datos reflejados en la tabla 6.5 llegan hasta la concentración del 50%w/w de glicerol.

**Table 6.5:** Viscosidad de las diferentes mezclas glicerol-agua en función de la temperatura

| T (°C) | 100%w Glicerol | %w 90 | %w 80 |
|---|---|---|---|
| 30 | $0.65 \pm 0.03$ | $0.120 \pm 0.004$ | 0.058±0.001 |
| 35 | $0.48 \pm 0.01$ | $0.098 \pm 0.003$ | 0.049±0.001 |
| 40 | $0.32 \pm 0.01$ | $0.0717 \pm 0.0004$ | 0.038±0.001 |
| 45 | $0.22 \pm 0.01$ | $0.0553 \pm 0.0009$ | 0.0317±0.0003 |
| 50 | $0.168 \pm 0.005$ | $0.0448 \pm 0.0007$ | 0.0265±0.0002 |
| 55 | $0.126 \pm 0.004$ | $0.0366 \pm 0.0006$ | 0.0223±0.0001 |

| T (°C) | %w 70 | %w 60 | %w 50 |
|---|---|---|---|
| 30 | 0.017±0.001 | 0.0062±0.0005 | 0.0017±0.0004 |
| 35 | 0.015±0.001 | 0.0061±0.0007 | $0.003 \pm 0.001$ |
| 40 | 0.014±0.001 | 0.0063±0.0009 | $0.002 \pm 0.001$ |
| 45 | 0.0125±0.0005 | 0.007±0.001 | $0.002 \pm 0.001$ |
| 50 | 0.0117±0.0004 | 0.006±0.002 | $0.003 \pm 0.001$ |
| 55 | 0.0113±0.0005 | 0.007±0.003 | $0.005 \pm 0.003$ |

## 6.5. Resultados obtenidos por Videomicroscopía

Mediante las medidas de videomicroscopía se obtiene la trayectoria de la partícula en el seno del sistema. En la Figura 6.13 se puede observar como la partícula de poliestireno describe un movimiento browniano al estar sumergida en la mezcla glicerol agua con contenido de glicerol de un 90%w. El tiempo de grabación de la película es de 10 min.

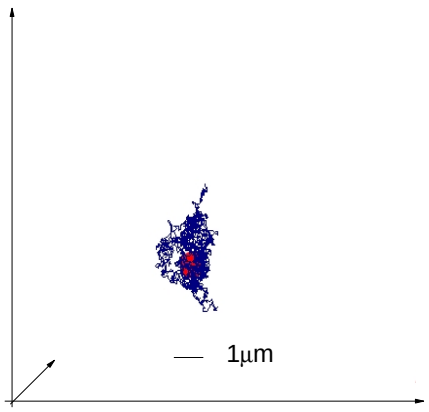


**Figure 6.13:** Trayectoria de una partícula de 1 micra de diámetro en la mezcla acuosa de glicerol 90%w

El cálculo del desplazamiento cuadrático medio obtenido a partir de la trayectoria de la partícula permite analizar la difusión de la misma en el seno del fluido y minimizar el posible movimiento de deriva debido a corrientes o caminos preferenciales. Se han obtenido dos tipos de desplazamientos cuadrático medio, el denominado desplazamiento cuadrático medio absoluto y el desplazamiento cuadrático medio relativo.

El desplazamiento cuadrático medio absoluto en dos dimensiones de la trayectoria de las partículas en el seno de un fluido, el glicerol se calcula como:

$$MSDabs = \left\langle \Delta x^2 (t) \right\rangle + \left\langle \Delta y^2 (t) \right\rangle = 4Dt \tag{6.9}$$

El desplazamiento cuadrático medio relativo será entonces:

$$MSDrel = \left\langle \Delta r_i^2 \right\rangle + \left\langle \Delta r_j^2 \right\rangle = 4Dt + 4Dt = 8Dt \tag{6.10}$$

que permite una medida de la trayectoria de la partícula $i$ en función del movimiento de las vecinas $j$ y es posible por tanto una eliminación de los movimientos de deriva. Se cumple además que el desplazamiento cuadrático medio relativo es el doble del absoluto.

$$MSDrel = 2 \cdot MSDabs \tag{6.11}$$

Los desplazamientos cuadráticos absoluto (Figura 6.14) y relativo (Figura 6.15) que se obtienen presentan la linealidad característica del sistema viscoso.

El movimiento de las partículas en el fluido, se trata de una difusión browniana, con una variabilidad estadística, de ahí que el tiempo de adquisición de las películas sea elevado, para reducir el error aleatorio.

Se puede calcular el coeficiente de difusión a partir de la pendiente del MSD, la viscosidad mediante la ecuación de Einstein y así comparar su valor con el resto de técnicas empleadas.

La comparación de resultados por todas las técnicas macro y microreológicas se recoge en la tabla 6.6 observándose una buena correlación de los datos. Los resultados obtenidos por reología al estar al límite de la viscosidad mínima adecuada requerida en el reómetro, para la concentración de 30%w glicerol no se llega a poder medir, pues como se observa en la tabla 6.5 los datos obtenidos a concentraciones bajas de 60 y 50%w de glicerol, presentan una mayor variabilidad con lo que la fiabilidad a estas concentraciones es menor.

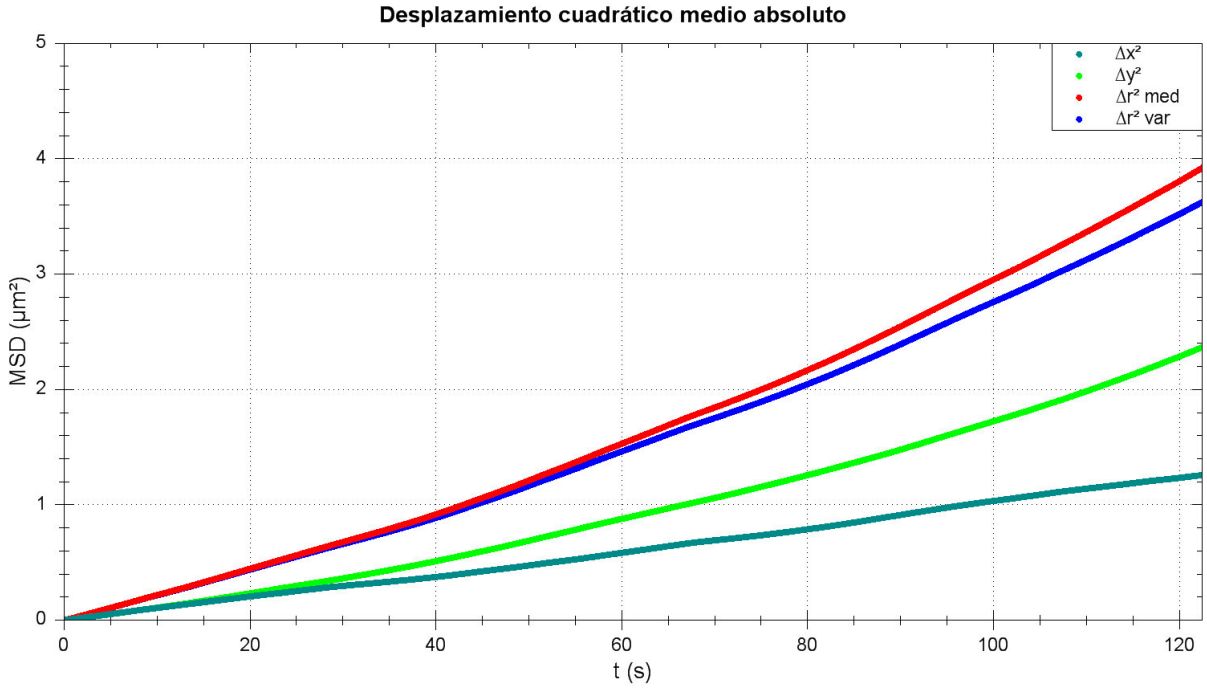


**Figure 6.14:** MSD absoluto de una partícula de 1 micra de diámetro en la mezcla acuosa de glicerol 90%w

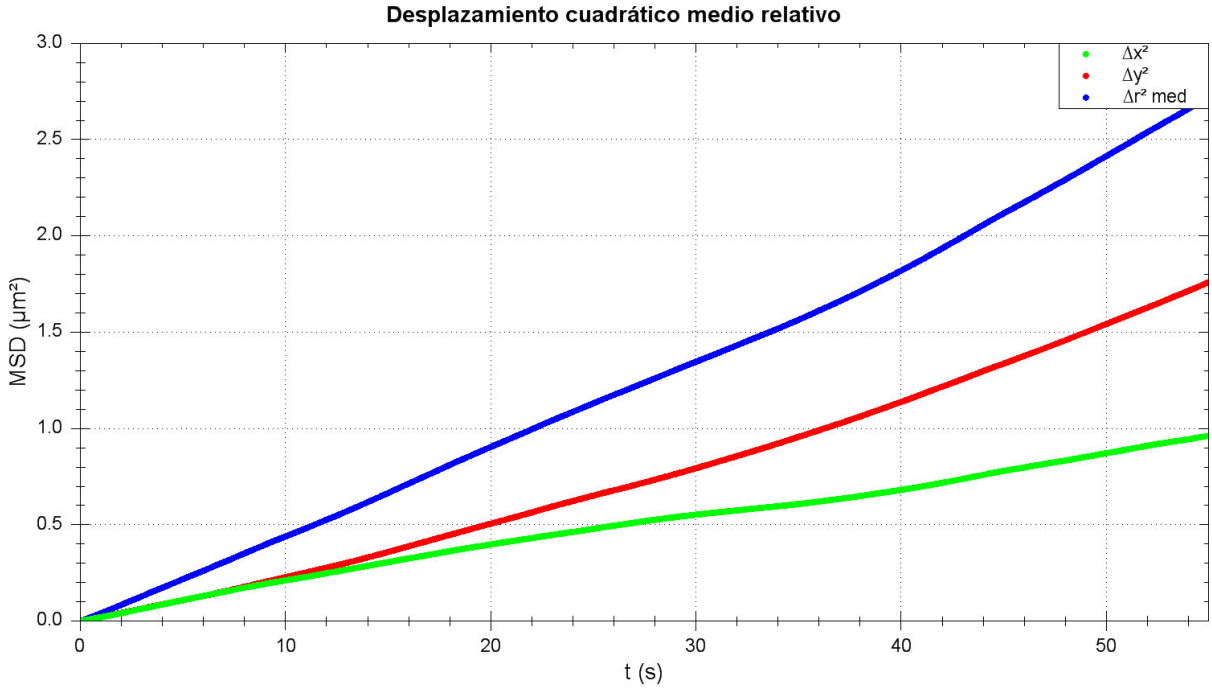


**Figure 6.15:** MSD relativo de una partícula de 1 micra de diámetro en la mezcla acuosa de glicerol 90%w

**Table 6.6:** Viscosidad $\eta$ en Pa·s en función de la concentración de glicerol en la mezcla glicerol-agua a 25°C

| %w G | Reómetro | DWS |
|---|---|---|
| 30 | - | $0.00156 \pm 0.00005$ |
| 60 | $0.007 \pm 0.001$ | $0.01 \pm 0.01$ |
| 80 | $0.06 \pm 0.01$ | $0.075 \pm 0.01$ |

| %w G | DLS | Videomicroscopía | Viscosímetro |
|---|---|---|---|
| 30 | $0.00221 \pm 0.00005$ | $0.00166 \pm 0.00004$ | $0.00197 \pm 0.00004$ |
| 60 | $0.01 \pm 0.01$ | $0.009 \pm 0.004$ | $0.009 \pm 0.002$ |
| 80 | $0.08 \pm 0.01$ | $0.08 \pm 0.02$ | $0.06 \pm 0.01$ |

## 6.6. Conclusiones Sistema Glicerol

En este capítulo se ha estudiado un sistema viscoso desde el punto de vista de una aplicación inicial de técnicas de reología micro y macro, además de servir como modelo para los siguientes sistemas más complejos.

Tras un tratamiento de los datos inicial por el método de cumulantes y el análisis CONTIN se ha comprobado el comportamiento difusivo de las mezclas acuosas con glicerol, obteniendo funciones de autocorrelación con caídas exponenciales únicas, de las que se deriva la obtención de líneas rectas en la representación del inverso del tiempo de relajación, llamado tasa de decaimiento frente al cuadrado del vector de onda cuyo significado es el coeficiente de difusión de la particula en el seno del sistema.

Además, se ha logrado cuantificar el desplazamiento cuadrático medio de las partículas a partir de las funciones de autocorrelación obtenidas de la técnica de dispersión de luz dinámica. Se encontró que es posible realizar un ajuste lineal a un amplio rango temporal, que demuestra el comportamiento viscoso del glicerol.

El glicerol es un fluido de los llamados newtonianos que ha proporcionado excelentes resultados que permiten enlazar con aquellos sistemas en los que se pretende profundizar, los viscoelásticos. Se ha visto también que si se somete al glicerol a condiciones extremas, como altas frecuencias, presenta propiedades viscoelásticas. Además de ello, cualquier sistema viscoso se considera no ergódico cuando no se miden tiempos suficientemente largos pues si no se ha promediado el tiempo suficiente, significa que el promedio en el tiempo no es igual al promedio en el colectivo, y por tanto se convierte en un mal promedio en el tiempo. Las medidas por dispersión de luz dinámica han demostrado que para el glicerol es suficiente con medir un tiempo lo suficientemente corto porque la dispersión de las partículas que contribuyen en ese corto tiempo no ha llegado a alcanzar la posición de equilibrio. Por lo tanto, el glicerol no es orgódico en un intervalo de

tiempos cortos.

Los resultados obtenidos por reología mecánica confirman a baja frecuencia el comportamiento viscoso del glicerol y haciendolos enlazar con los resultados obtenidos por Espectroscopía de onda difusa vienen a corroborar este comportamiento del glicerol tanto el ergódico como el no ergódico a altas frecuencias y elevada concentración de glicerol.

Por videomicroscopía se ha observado igualmente el movimiento browniano que describen las partículas sumergidas en el glicerol, y del cálculo de sus trayectorias se ha obtenido un coeficiente de difusión similar al obtenido por el resto de técnicas microreológicas empleadas. También se ha visto la linealidad en los desplazamientos cuadráticos medios a tiempos iniciales.

# Part II

# SEGUNDO BLOQUE DE RESULTADOS. SISTEMAS VISCOELÁSTICOS

# Chapter 7

# MICRORHEOLOGY OF AGAROSE SOLUTIONS

## 7.1. Introduction

The non-Newtonian behaviour and dynamic viscoelasticity of a series of aqueous solutions of agarose are measured with microrheological techniques (Diffusing Wave Spectroscopy) and compared with macrorheological measurements (mechanical rheology).

Agarose is a natural polymer from the fraction of cell-wall polysaccharides known as agar which is extracted from red marine algae. Structurally, it is a linear polymer consisting of alternating D-galactose and 3,6-anhydro-L-galactose units (see section Agarosa in the Introduction). For our intended light scattering studies on agaroses we have decided to use a single solvent, water, because it is the common solvent for agarose in many applications and due to the importance of it use like aqueous mixes and the refractive index influence.

## 7.2. Experimental Details

A complete explanation of the experimental details used in this section is given here in order to simplify the comprehension. First, the preparation method of the gels is detailed. Next, since the configuration of the experimental techniques analysis varies from that explained in the previous chapter, a full description of the method employed is provided.

### 7.2.1. Preparation of the agarose gels

Low sulfate content agarose (<0.15%) was supplied by Sigma-Aldrich (Agarose for routine use) and it was used as received without further purification. Solutions were prepared with filtered milli-Q water (resistivity > 18.2 MΩ).

Gels were prepared following the boiling water bath method. We have studied agarose hydrogels with agarose concentration in the range between 1 and 5 g/L (0.1-0.5%w/v). The preparation method involved three steps. First, the appropriate mass of agarose powder was dispersed in deionized water at ambient temperature. The solution was placed in a magnetic stirrer for one hour in order for the agarose to become hydrated and reduce foaming. Second, the solution was heated to 100°C, under continuous stirring, to achieve the complete dissolution of the agarose. Third, the solution was permanently kept at a temperature of, approximately, 15°C above the gelation temperature to ensure that the experiments always started from the sol phase.

### 7.2.2. DWS measurements

Two different types of monodisperse spherical particles are used as probes for the DWS measurements: Polystyrene with diameter 977 nm (kindly provided from Polymat, a center for macromolecular design and engineering from the University of the Basque Country) and titanium dioxide particles with diameter 127 nm (Degusa, Germany). They were dispersed in water to obtain a suitable particle concentration for the DWS measurements.

The choice of the tracer particle concentration is connected to the cuvette size. The cornerstone of accurate DWS measurements is ensuring applicability of the diffusion approximation which requires that L>5l*, where L is the thickness of the cuvette and l* is the transport mean free path and it es the length scale over wich the photon is fully randomized. In the case of dilute systems l* is inversely proportional to the tracer particle concentration. Furthermore l* is dependent on the refractive index of the solvent. l* is a constant parameter that enters in the DWS analysis and has to be determined independently. It is chosen a set of reference samples, with different concentrations of particles dispersed in water.It was used a tracer particle concentration of approximately 1%v/v for the polystyrene beads samples and 5%v/v for $Ti0_2$ particles.

Diffusing wave spectroscopy experiments are done in the transmission geometry. The red emission at 658 nm of a diode laser is focused by a system of mirrors and lens at the centre of the sample cell. A polarization analyzer is placed before the detection system. Multiply scattered light is collected by an optical fiber, split by

a fiber optic beam splitter, and directed to the high quantum efficiency avalanche photodiode (APD) modules operating in Geiger mode. These units provide digital pulses in accordance with the arrival time of individual photons to the detector. Finally, the photon counts are transferred to the correlator (a sketch is shown in Figure 5.11).

### 7.2.3. Rheometer measurements

The low frequency mechanical response of the gels was measured with a torsion shear stress rheometer (CVOR, Bohlin Instruments), with temperature control provided by a Polyscience (Model) circulation bath with 0.01 °C temperature stability. All of the measurements were made in the cone-plate geometry with stainless steel fixtures of 40 mm diameter and 1° cone angle. The experiments were made by placing the samples of hot agarose solutions on the plate which had been previously heated to a temperature approximately 10 °C above the gelation temperature. In order to avoid evaporation a thin film of low viscosity silicone oil (FLUKA) was spread around the open surface of the sample rim. The dynamic moduli of the samples were obtained through oscillatory stress controlled measurements in the frequency range between 0.1 and 50 Hz. The amplitude of the oscillation was controlled so that the strain remained always within the linear regime that had been previously located by means of a torque sweep at a fixed frequency of 1Hz.

## 7.3. Microrheology

In this section, the microrheological properties extracted for the agarose solutions are described. Two types of particles are measured to see their infuence in the results, as explained in the DWS measurements section above.

### 7.3.1. Autocorrelation functions

Agarose microrheological properties were measured at different concentrations from 1 to 5 g/L. Figures 7.1, 7.2, 7.3, 7.4, 7.5 show the evolution of the intensity autocorrelation function $[g^{(2)}(t) - 1]$, shorted as ICF, in the different agarose gel concentrations as a function of temperature with the polystyrene 977 nm diameter particles. As long as the temperature is low, the transition from sol to gel occurs and the initial exponential decay, typical for a system that undergoes diffusion due to Brownian motion, change and the correlation functions no longer decay to zero due to the slower motion of the clusters formed during the sol-gel transition.

Figure 7.6 shows the same conditions of the DWS technique and system but using titanium dioxide particles 127 nm diameter. In this case a second decay is observed at high temperatures. This is typical in non ergodic systems.

Then using both intensity autocorrelation functions of PS and $TiO_2$, Figure 7.7, it is possible to see the difference between them. ICF with $TiO_2$ at high temperature, 40°C, corresponding to liquid state, has a light sooner decay and also a second decay that with PS particles does not appear. The same ones ICF at low temperature, 34°C, for the gel, both ICF have the same decay form to a lag time of 0.01 s approximately, and then the system with $TiO_2$ does not decay so far like that for PS, but none of them arrive at zero like at high temperature.

This differences observed are due to the lower size of the $TiO_2$ particles that have a higher diffusion coefficient. In this way long time features that cannot be observed with the PS particles are clearly seen with the $TiO_2$ ones, as pointed out by a comparison of ICF figures with PS particles and Figure 7.6 with $TiO_2$ particles. Nevertheless, at low temperatures even the ICF of the smallest particles do not decay to zero.

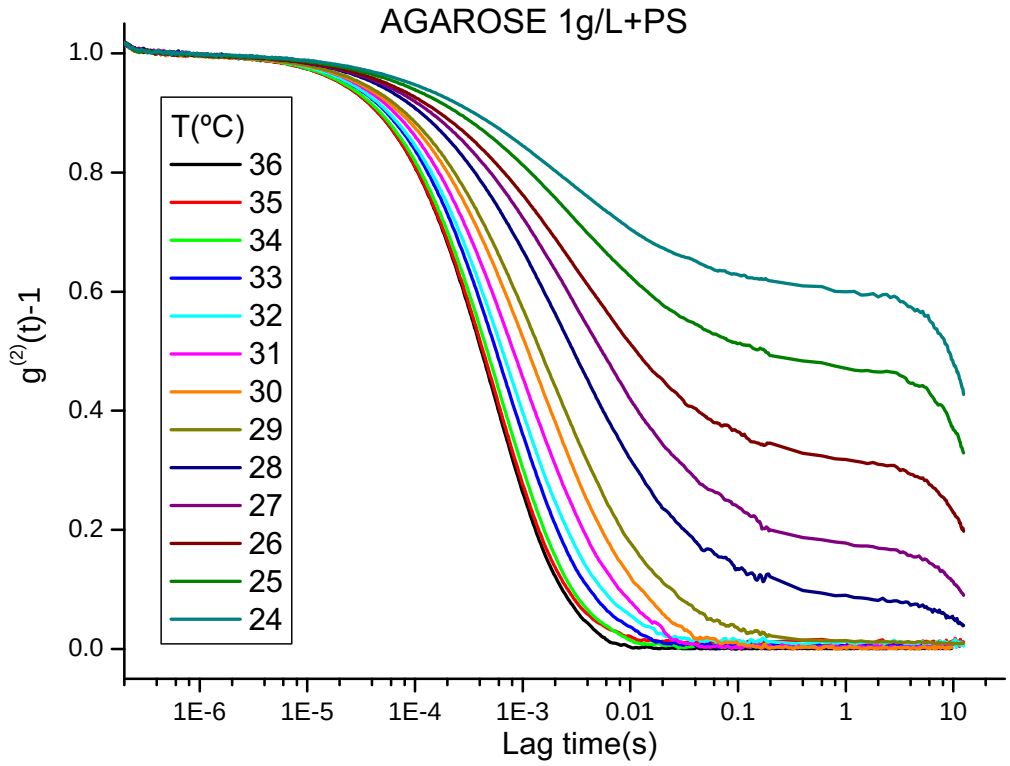


**Figure 7.1:** ICF vs t for an agarose concentration of 1g/L with PS particles in the range of the gel temperature

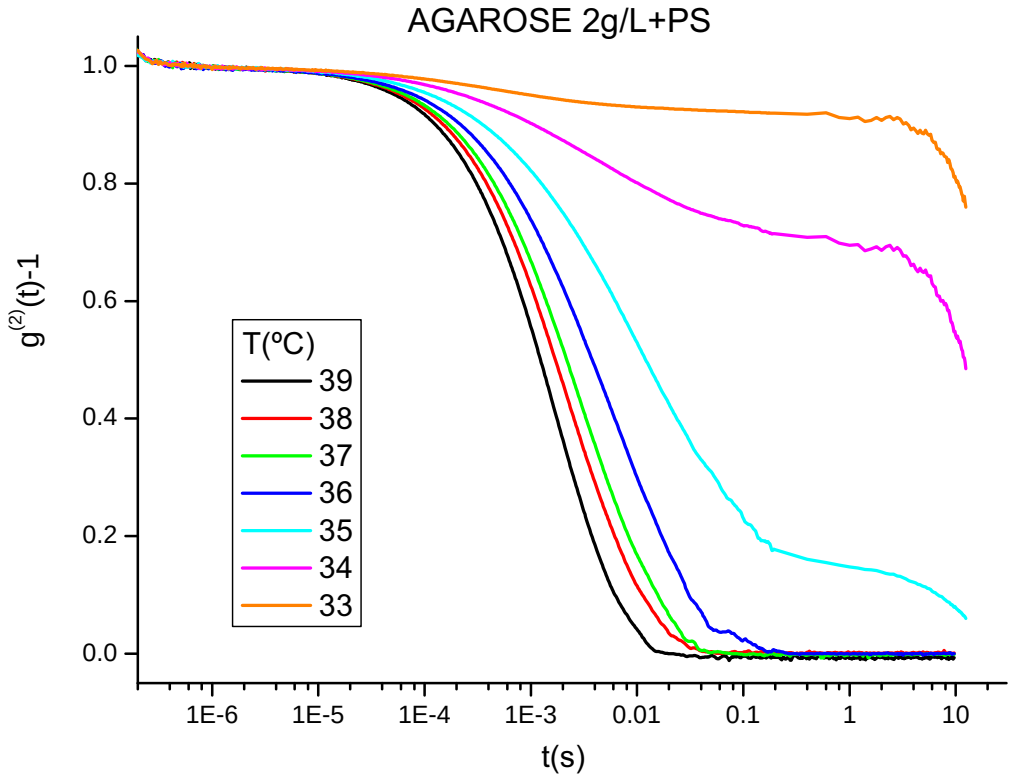


**Figure 7.2:** ICF vs t for an agarose concentration of 2g/L with PS particles in the range of the gel temperature

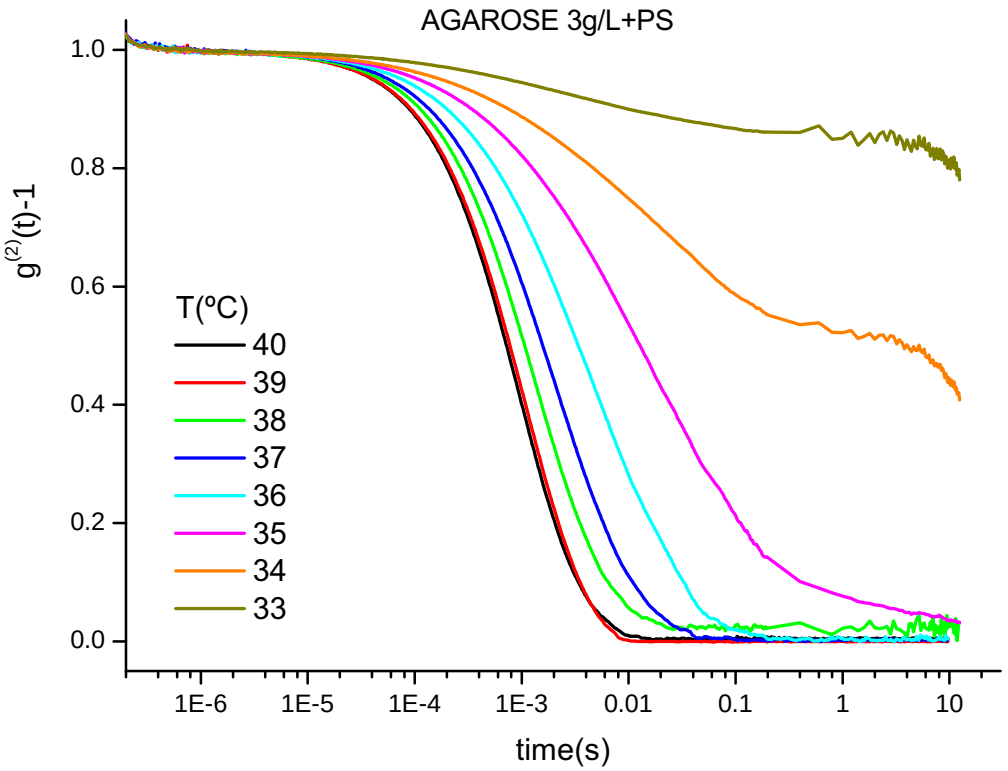


**Figure 7.3:** ICF vs t for an agarose concentration of 3g/L with PS particles in the range of the gel temperature

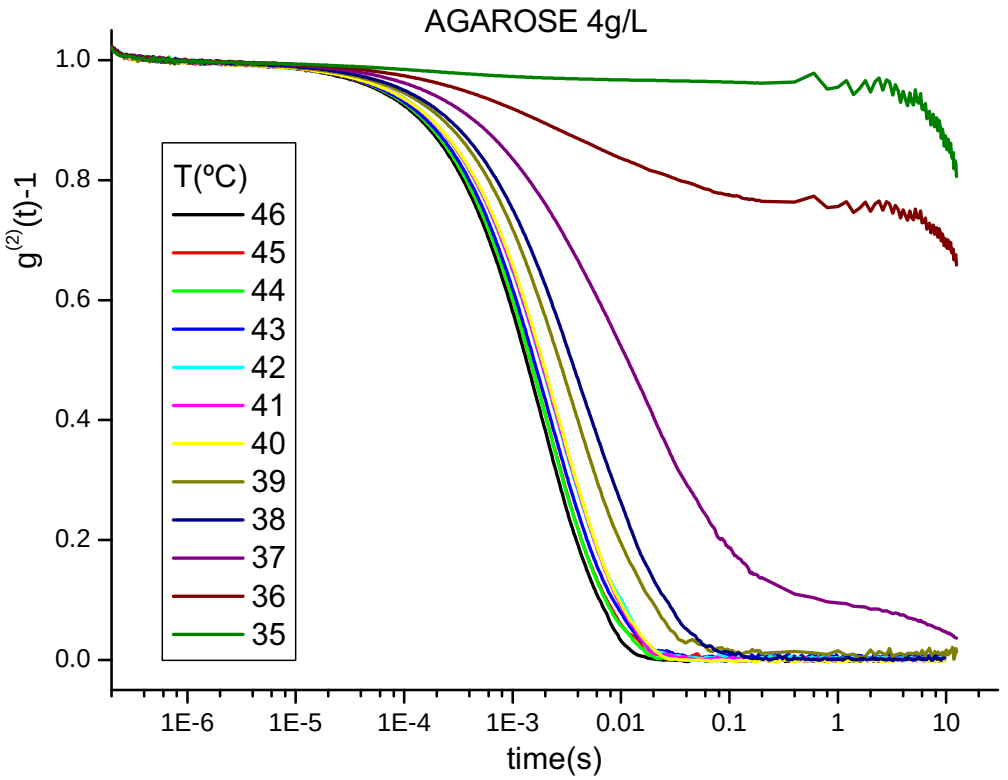


**Figure 7.4:** ICF vs t for an agarose concentration of 4g/L with PS particles in the range of the gel temperature

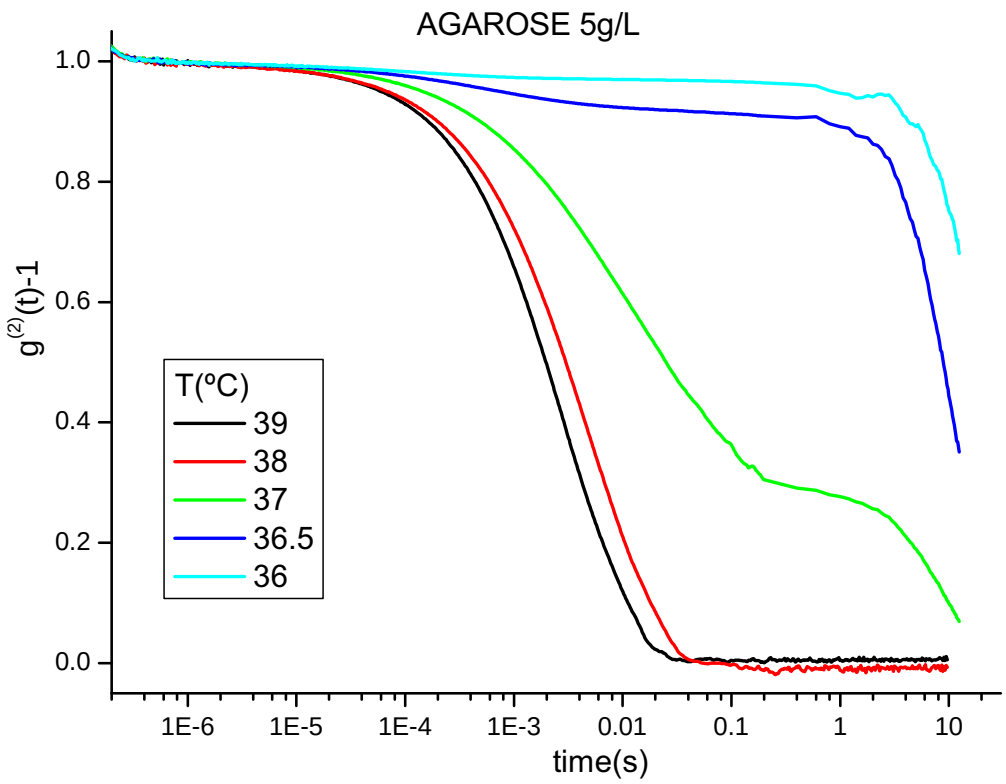


**Figure 7.5:** ICF of the agarose gel 5 g/L with PS particles in the range of the gel temperature

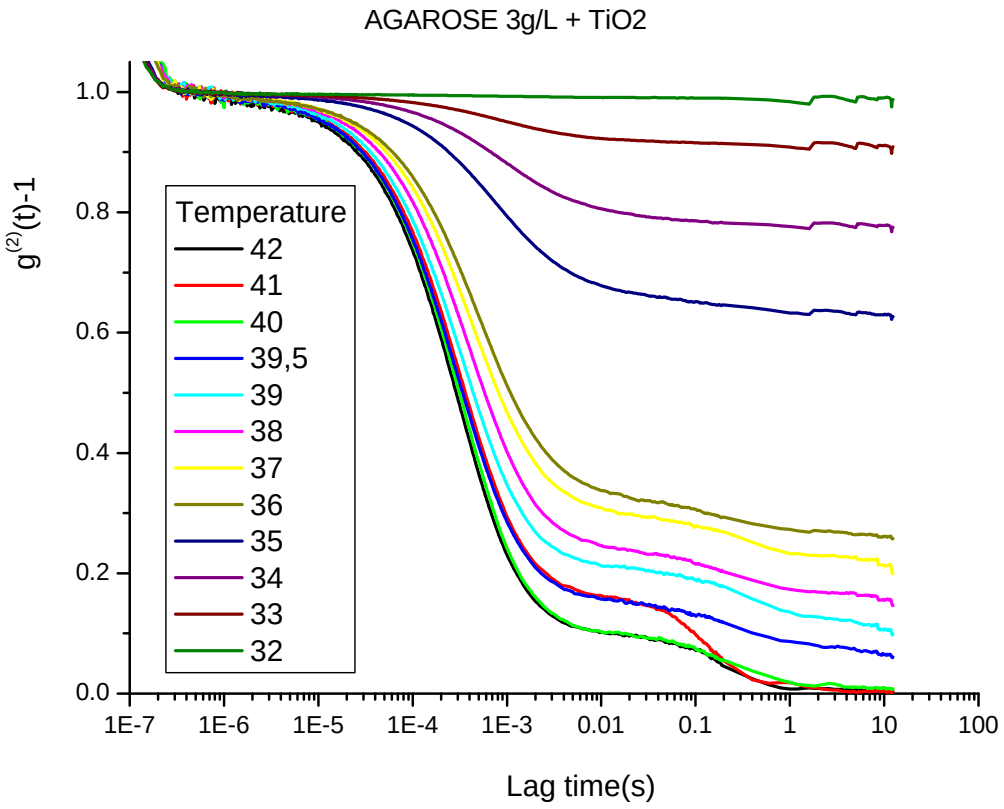


**Figure 7.6:** ICF for agasore 3g/L with $TiO_2$ particles

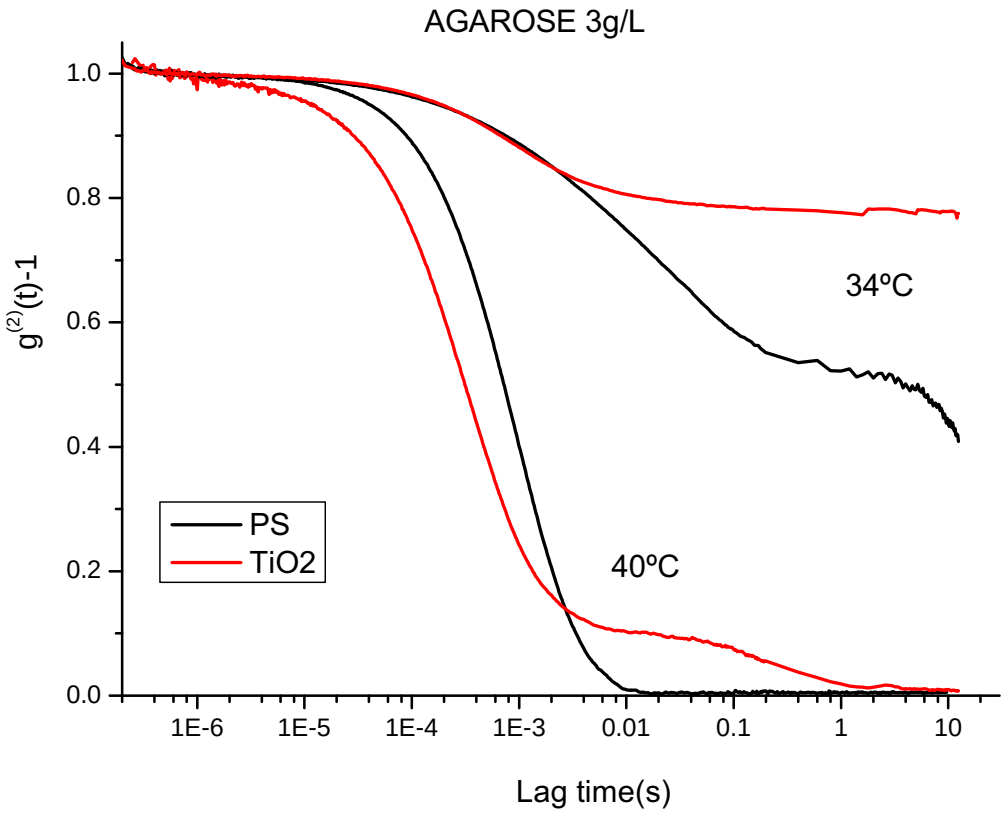


**Figure 7.7:** ICF for the PS and $TiO_2$ particles in agarose 3g/L, at 40°C and 34°C

### 7.3.2. Mean square displacement MSD

The data MSD of the polystyrene particles in the agarose, shown in Figures 7.8 to 7.12 are logarithmically spaced and cover a large range in time. Like single scattering experiments, the intensity of a single coherence area is detected; fluctuations in intensity reflect the dynamics of the scattering medium and the mean squared displacement of the particles can be obtained.

MSD derived from the autocorrelation function given by expression 5.23, the measured ICF includes contributions from a distribution of path lengths, P(s), and the result of the measurement is the weighted average [58].

$$g^2(t) - 1 = \left( \int_0^\infty P(s) \cdot e^{-\frac{s}{l^*} \cdot k^2 \cdot MSD} \, ds \right)^2 \tag{7.1}$$

The path length distribution P(s) depends on the size and shape of the sample, the place where light enters the sample, and the point from wich the outgoing light is collected. For example, consider the case of light incident on the face of a slab of thickness L and collected from a point on the opposite face, as show in Figure 5.10. Thus nearly all the photons leaving the sample will have scattered $\approx (L/l^*)^2(l^*/l)$ times, corresponding to $n_c = (L/l^*)^2$ random walk steps, and will have travelled a total distance of $s_c \sim n_c l^*$. Since all photons scatter approximately the same number of times, $g^1(t)$ will decay nearly exponentially, assuming diffusive particle motion. In contrast, consider the case of light incident over a broad area on the face of a very thick slab and collected from a point near the centre of the illuminated area on the same face, like it occurs in backscattering geometry, see Figure 5.11. Some photons enter the sample and scatter only a few times before leaving and being collected; other photons scatter many times before bwing collected. Thus there will be a very broad distribution of photon path lenghts through the sample and a correspondingly broad distribution of decay times. For this geometry it is expected $g^1(t)$ is highly non-exponential.

For a point source and point detector in an infinite medium P(s) is [58]

$$P(s) = \sqrt{\frac{v r_{sd}^2}{4\pi D}} exp\left( \sqrt{\frac{v\mu_a r_{sd}^2}{D}} \right) s^{-3/2} exp\left( -\frac{v\mu_a r_{sd}^2}{4Ds} \right) exp\left(-\mu_a s\right) \tag{7.2}$$

Here $r_{sd}$ is the separation between the source and detector, $D$ the particle diffusion coefficient, $\mu_a$ the absorption coefficient. Photons arriving at time t after the incident pulse will have travelled a distance $s = vt$ through the sample, where $v$ is the average speed of light within the medium, [60].

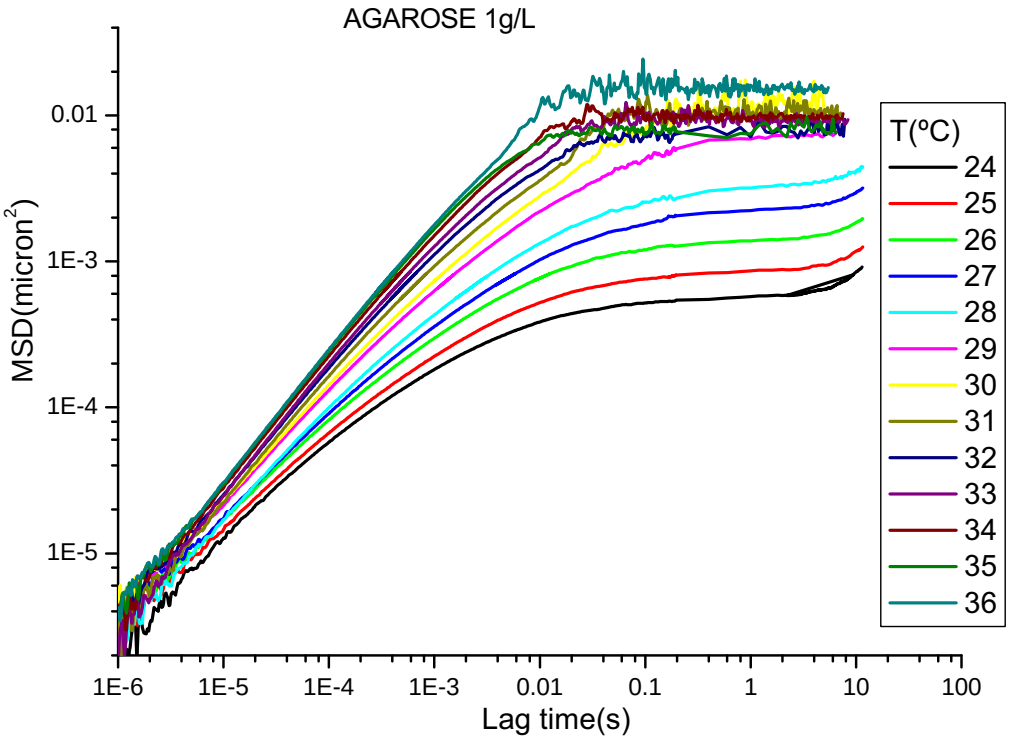


**Figure 7.8:** MSD of PS particles of 977 nm diameter at a volume fraction of 1 in agarose gel of 1g/L in the range of the gel temperature 24-36°C

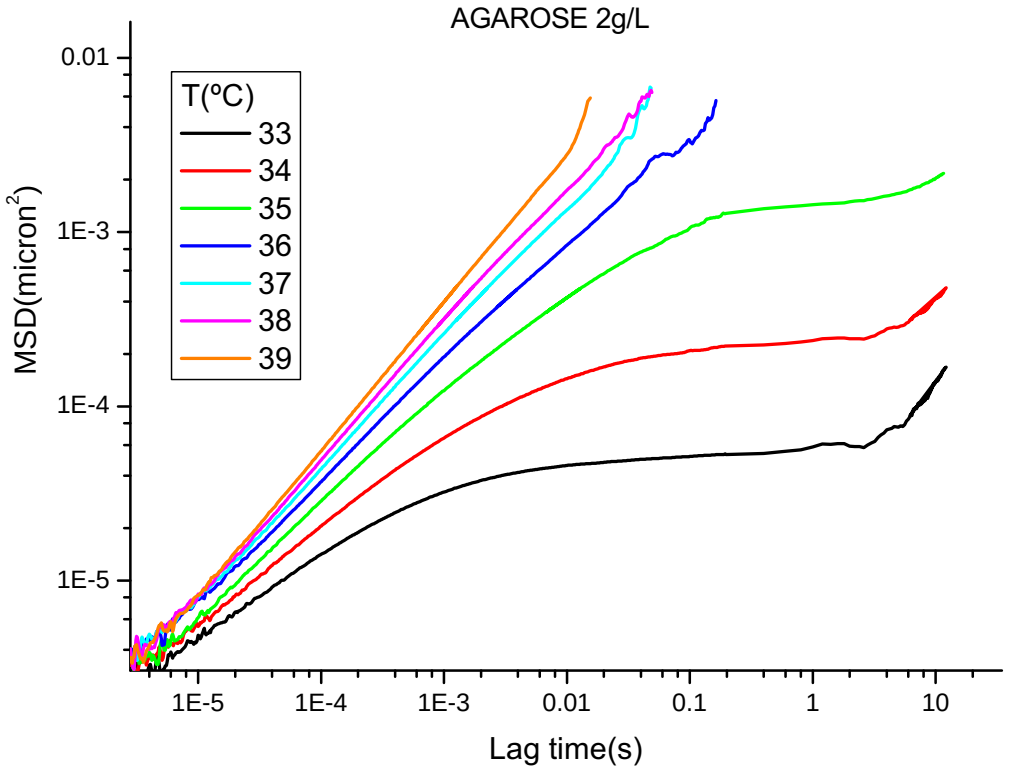


**Figure 7.9:** MSD of PS particles of 977 nm diameter at a volume fraction of 1 in agarose gel of 2g/L in the range of the gel temperature 33-39°C

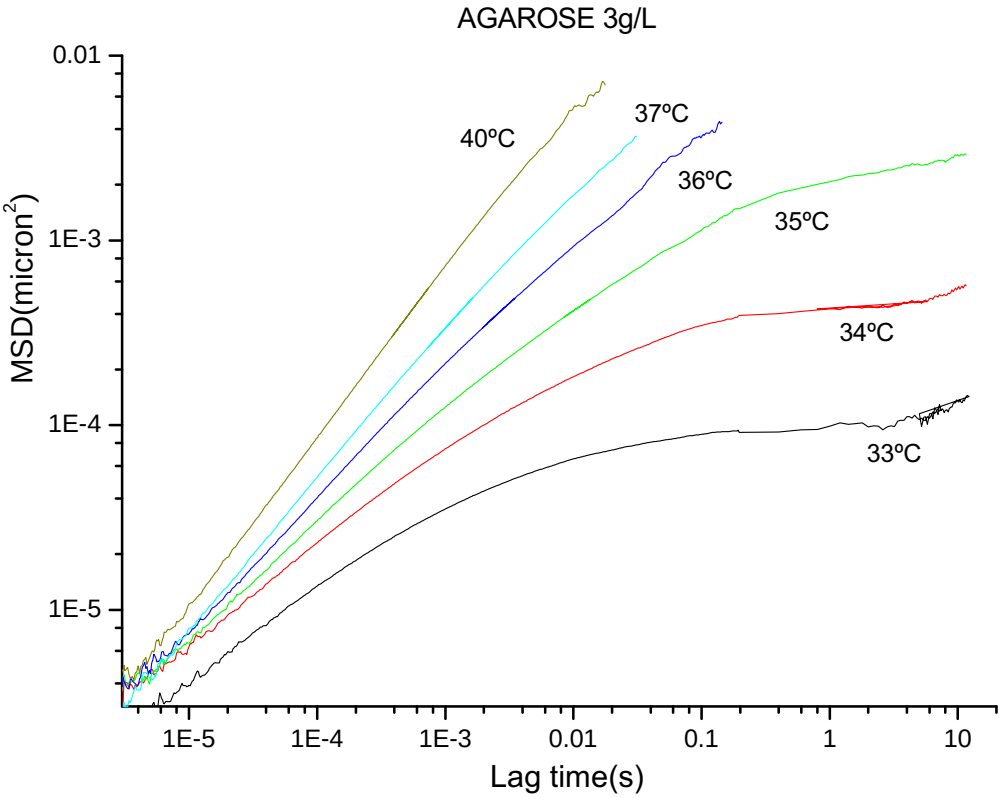


**Figure 7.10:** MSD of PS particles of 977 nm diameter at a volume fraction of 1 in agarose gel of 3g/L in the range of the gel temperature 33-40°C

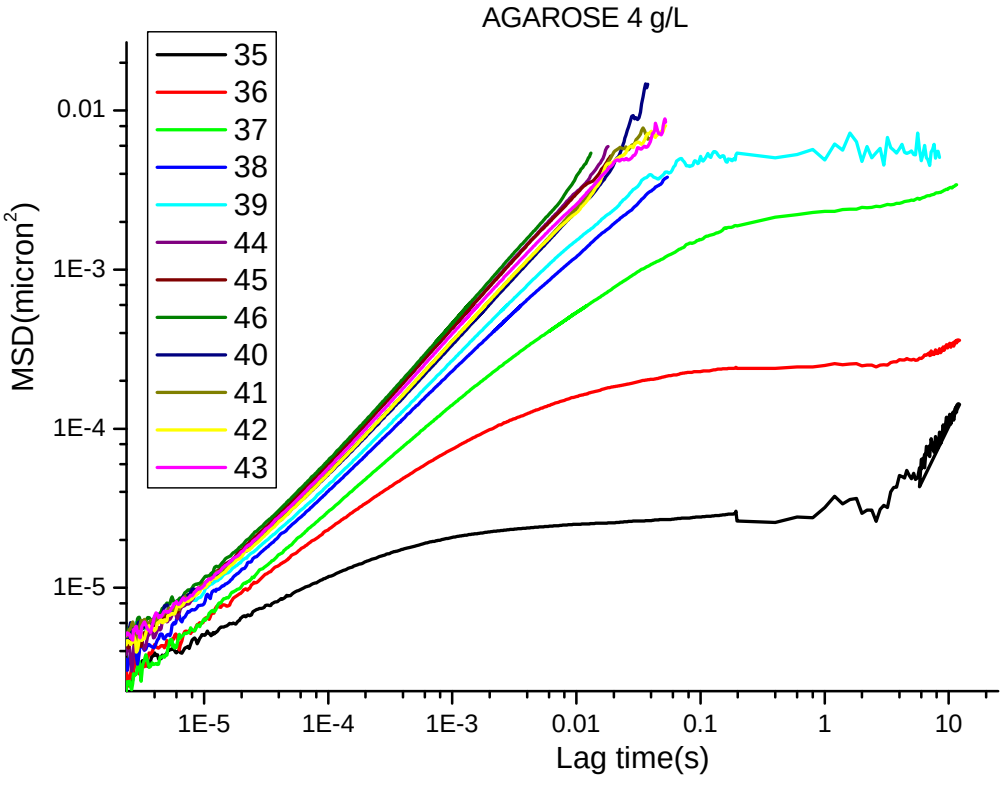


**Figure 7.11:** MSD of PS particles of 977 nm diameter at a volume fraction of 1 in agarose gel of 4g/L in the range of the gel temperature 35-43°C

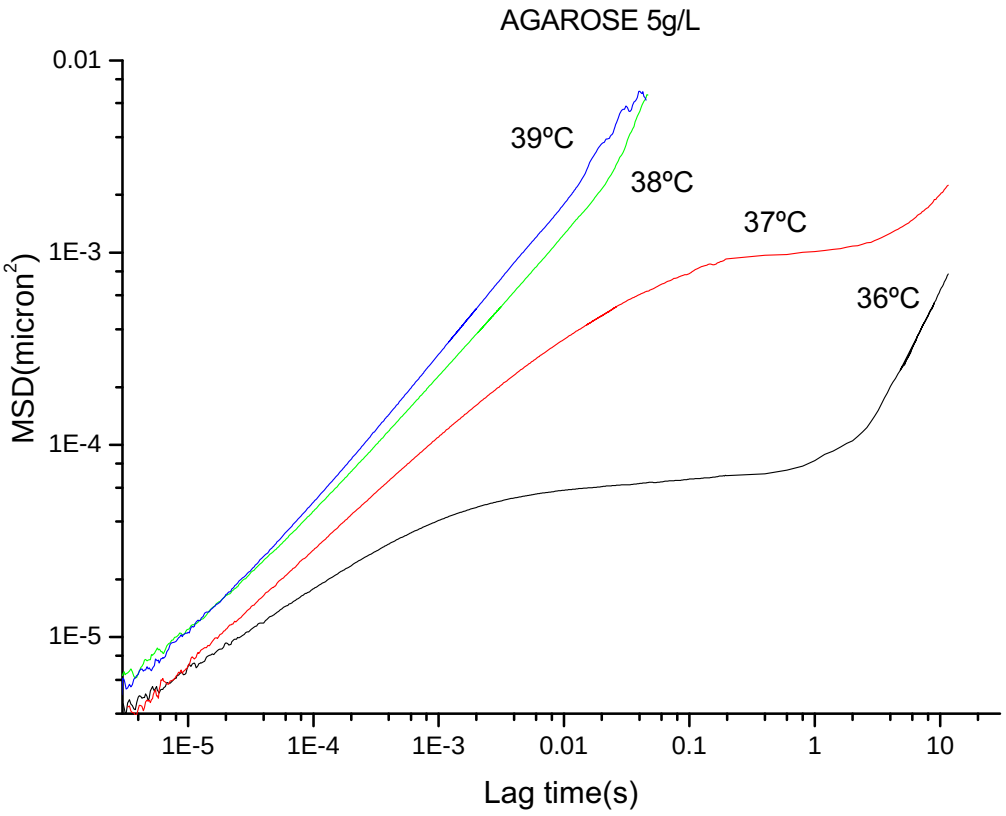


**Figure 7.12:** MSD of PS particles of 977 nm diameter at a volume fraction of 1 in agarose gel of 5g/L in the range of the gel temperature 36-39°C

At the earliest times MSD rises diffusively, then becomes subdiffusive and saturates at long times, for the very longest times there is another rise that suggest some rearrangement of the colloidal particles structure is ocurring.

When the smaller particles of $TiO_2$ are used, the second decay observed in the intensity autocorrelation function is corresponded with the increase in the last part of the MSD curve as Figure 7.13 relates.

Then using both MSD curves of PS and $TiO_2$, Figure 7.14, it is possible to compare the two situations. MSD at high temperature, 40°C, corresponding to the sol state, the MSD slope with PS is near to one that means a Newtonian behavior for the agarose. Using the $TiO_2$, the MSD curve has the three regions described a extended Maxwell model for the MSD in viscoelastic systems. The same ones MSD at low temperature, 34°C, for the gel state, both curves represent the three regions showing a viscoelastic gel behavior.

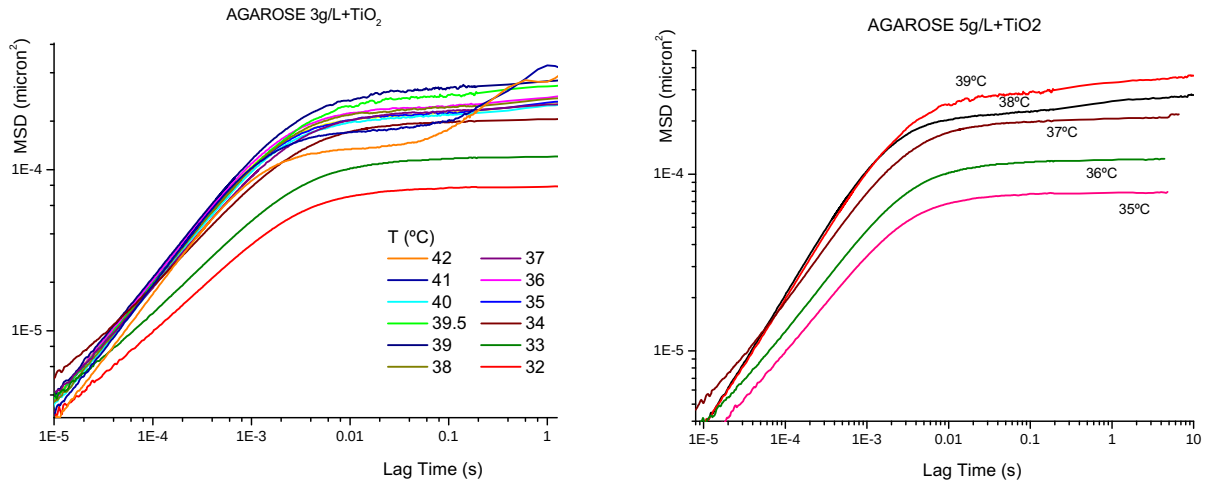


**Figure 7.13:** MSD of the agarose gels at 3 and 5 g/L with $TiO_2$ particles of 127 nm diameter at a volume fraction of 1 at various temperatures in the near of the gelling point

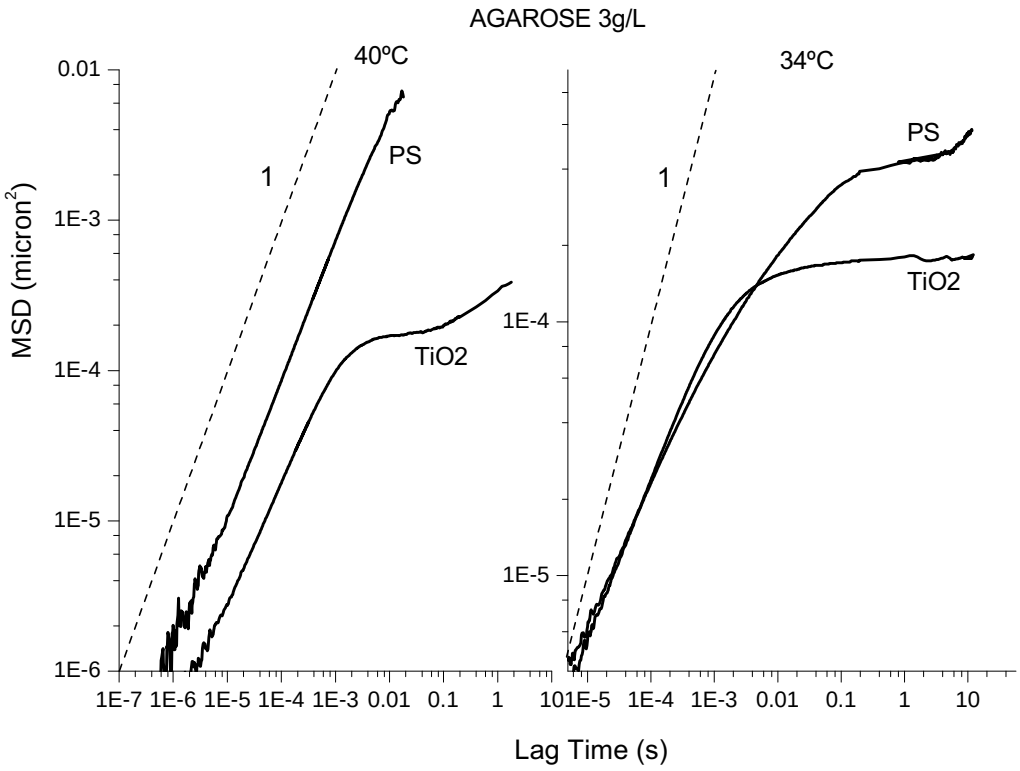


**Figure 7.14:** MSD for the PS and $TiO_2$ particles in agarose 3g/L, at 40°C and 34°C

### 7.3.3. Effect of particle characteristics

To understand the nature of the different form ot the ICF and MSD curves obtained with the two particles tested, PS and $TiO_2$, a different size of particles of PS is measure in the agarose, PS 400 nm diameter.

The results concerning the PS particles are as expected according to Stokes-Einstein equation, so Figure 7.15 shows for the intensity autocorrelation functions and MSD of the two particles in water.

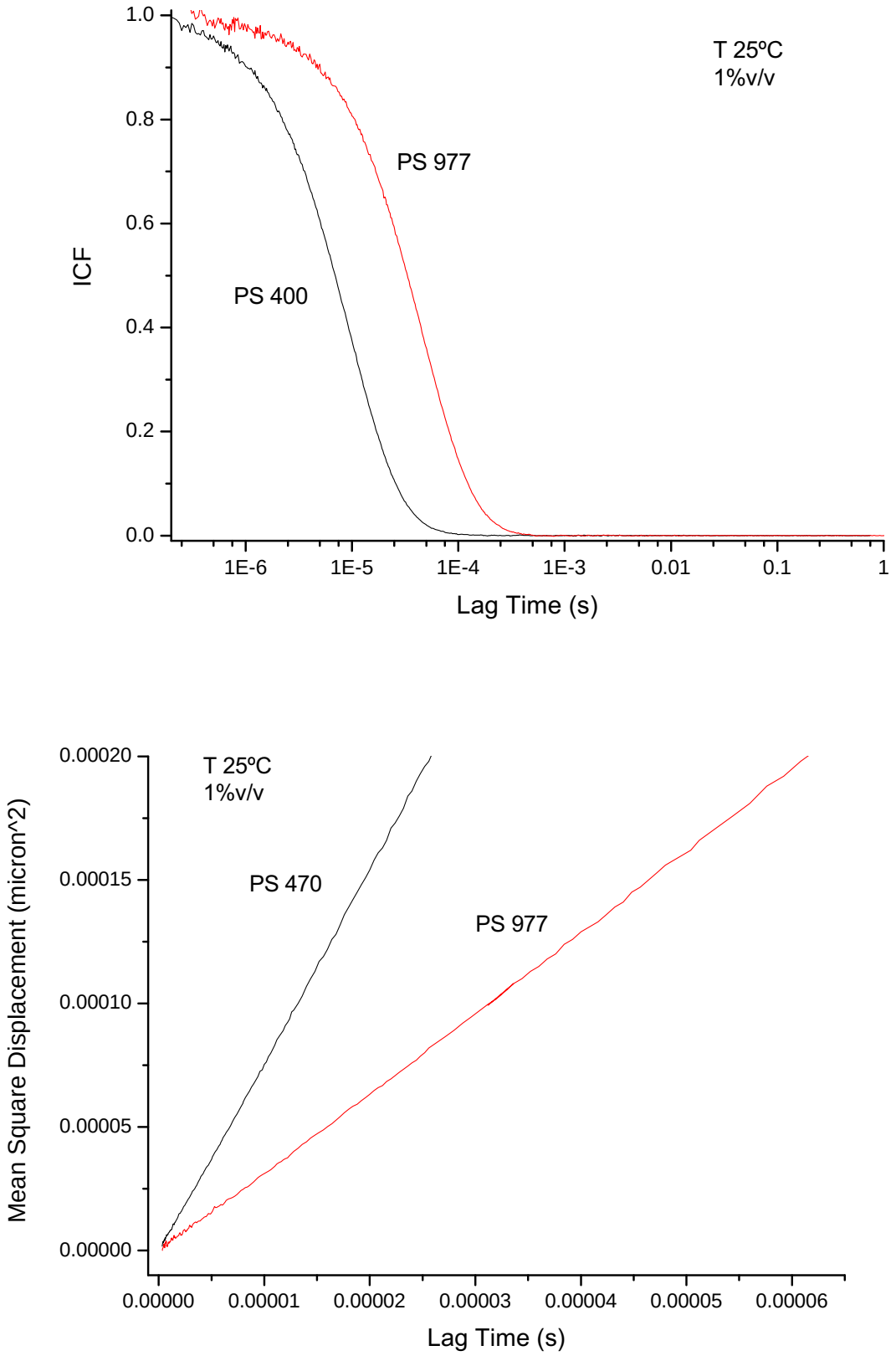


**Figure 7.15:** ICF(up) and MSD (down) for the PS of 400 nm and 977 nm in diameter in water, at 25°C and a volume fraction of 1%v/v

The diameter ratio is proportional to the inverse of the ratio of diffusion coefficients, so the relation 7.3 collects.

$$\frac{d_{977}}{d_{470}} \approx \frac{D_{470}}{D_{977}}; \frac{977nm}{470nm} = 2.08 \pm 0.5 \approx \frac{7.84\frac{\mu m^2}{s}}{3.21\frac{\mu m^2}{s}} = 2.44 \pm 0.3 \tag{7.3}$$

When each one of these particles are tested in the agarose, $TiO_2$ particles describe an unusual behavior that is not in concordance with the Stokes-Einstein equation, Figure 7.16. $TiO_2$ particles move slower in the agarose gel. This means an interaction of the particles in the agarose red that gives a different viscoelastic behavior as the expected by the PS particles ones.

The fact can be a rearrangement of the $TiO_2$ particles with the OH groups in the agarose.

So agarose gel has a structure of large pores, which allows the retention of molecules inside, reducing their mobility [61].

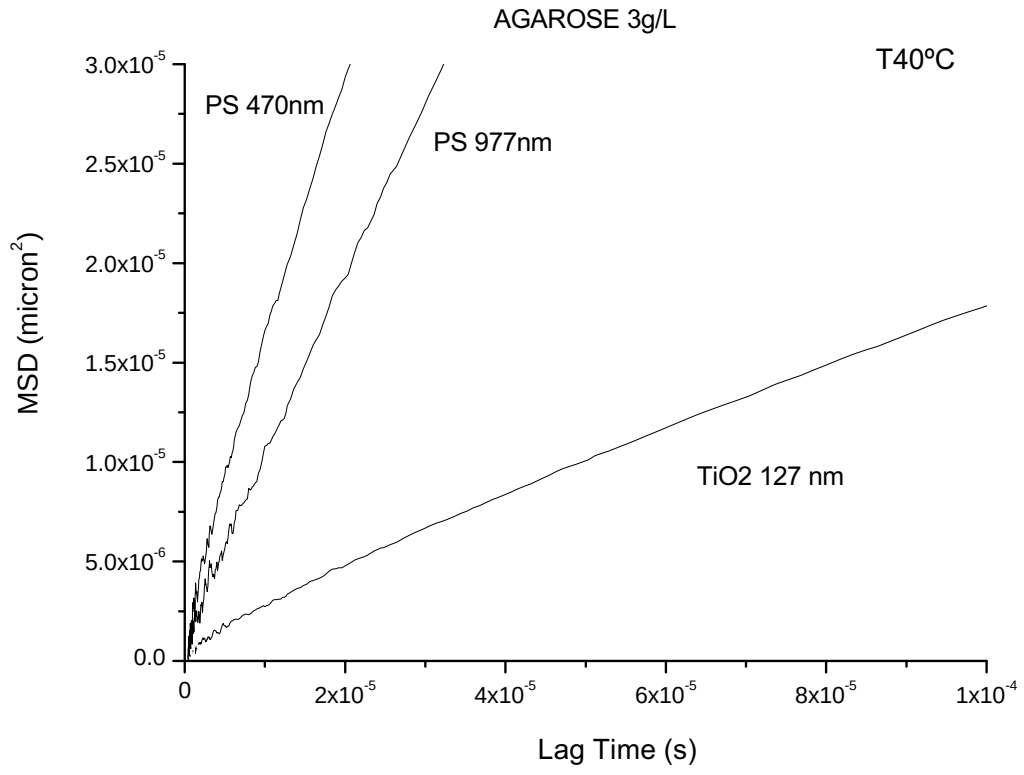


**Figure 7.16:** MSD for the PS of 400 nm and 977 nm and $TiO_2$ 127 nm in diameter in agarose, at 40°C

### 7.3.4. Microrheology estimation viscoelastic moduli

The mean squared displacement of a probe particle embedded in a complex fluid is directly related to the mechanical response of the medium surrounding the particle, both the dissipation of energy due to the viscous response and the storage of energy due to the elastic response. In a purely viscous material, the probe particle will diffuse freely due to thermal fluctuations, and its mean squared displacement will increase linearly with time. In a homogeneous elastic system, the particle motion deforms the surrounding medium, converting kinetic energy into stored elastic energy. In this case, the particles mean squared displacement will reach a plateau value when the stored energy is of order $k_BT$, where $k_B$ is the Boltzmann constant and T the temperature. The particle will thus be trapped by the surrounding medium and undergo thermally induced oscillations about an equilibrium position. By balancing thermal and elastic energies [Gardel et al in book [62]; Mason et al. [63]; van den Ende et al. [64], the linear viscoelastic moduli of the medium is obtained from the $\left\langle \Delta r^2(t) \right\rangle$ (MSD) by using the generalized Stokes-Einstein equation (GSE) 7.7.

Different representations can be used to obtaine the viscoelastic sprectrum $\tilde{G}(s)$, in the Laplace frequency domain, the complex shear modulus $G^*(\omega)$, in the Fourier frequency domain.

$$\widetilde{G}(s) = \frac{k_BT}{\pi \cdot R \cdot s \left\langle \Delta \widetilde{r}^2(s) \right\rangle} \tag{7.4}$$

where $\left\langle \Delta \tilde{r}^2(s) \right\rangle$ is the Laplace transform of the mean square displacement $\left\langle \Delta r^2(t) \right\rangle$ (MSD), $k_B$ is the Boltzmann's constant, T is the temperature and R is the sphere's radius.

This equation has been derived by calculating the ensemble-averaged velocity autocorrelation funcions resulting from a generalized Langevin equation 7.5 in a viscoelastic medium using a local memory function, consistent with energy equipartition and the fluctuation-dissipation theorem.

$$m\frac{dv(t)}{dt} = f_R(t) - \int_0^t \gamma(t-t')\, v(t')\, dt' \tag{7.5}$$

$f_R(t)$ denotes the random forces acting on the particle and includes the contribution from both direct forces between the particles and the stochastic Brownian motion. The random force $f_R(t)$ accelerate and decelerate the colloidal particles in random directions. Therefore, the ensemble average of the fluctuating force is equal to zero.

The integral term represents the viscous damping of the fluid, and incorporates a generalized time-dependent memory function $\gamma(t)$. Energy stored in the medium leads to profound changes in the temporal correlations of the stochastic forces acting on the particle at thermal equilibrium, taking into account the fluctuation-dissipation theorem and delta-function correlation of a purely viscous fluid, becoming

$$f_R(t)f_R(t') = 2I\gamma k_B t\delta(t-t') \tag{7.6}$$

where I es the unit matrix, $\gamma$ is the drag coefficient.

Using equation 7.7, it can be determined the macroscopic viscoelasticity of the material from the local response assuming the bulk stress relaxation has the same behavior as the local relaxations that affect the bead dynamics, in the Fourier domain.

$$G^*(\omega) = \frac{k_B T}{\pi \cdot R \cdot i\omega \langle \Delta\tilde{r}^2(\omega)\rangle} \tag{7.7}$$

If the medium is homogeneous on the length scale of the tracer particles, and the Stokes equation for the mobility of the particles is valid, and assuming that the Stokes- Einstein relation can be generalized to viscoelastic fluids, then in the general case, both the viscous and elastic moduli can be determined from the mean squared displacement using the method introduced by Mason [1]; [65]. The agarose gel we study in bulk is expected to be heterogeneous and the Stokes equation is unlikely to hold. In this case, the method gives effective moduli which characterize the response of the particles to the viscoelastic environment. The method convert the mean square displacement data obtained from the light scattering experiments to the viscous and elastic moduli, using a modified algebraic form of the generalized Stokes-Einstein relation that was originally suggested by Mason [1]. We calculate

$$G^*(\omega) \approx \frac{k_B T}{\pi \cdot R \cdot MSD \cdot \Gamma[1+\alpha(\omega)]} \tag{7.8}$$

where the gamma function $\Gamma$ is represented by:

$\Gamma[1+\alpha] \approx 0.457(1+\alpha)^2 - 1.36(1+\alpha) + 1.90$

and $\alpha$ is the slope in double logarithmic scale of the MSD versus time plot.

Then the moduli $G'$ and $G''$ are:

$$G'(\omega) = |G^*(\omega)|\, cos(\pi\alpha(\omega)/2) \tag{7.9}$$

$$G''(\omega) = |G^*(\omega)|\, sin(\pi\alpha(\omega)/2) \tag{7.10}$$

The notation used is $G'$ or G1 and $G''$ or G2.

### 7.3.5. Comparison with macrorheological measurements

A complete characterization of the gels makes it necessary to combine the results obtained from the two techniques used in this dissertation.

The rheological measurements have been performed on several milliliters of agarose material in the mechanical rheometer by applying a small amplitude oscillatory shear strain,

$$\gamma(t) = \gamma_0 sin\,(\omega t) \tag{7.11}$$

where $\gamma_0$ is the amplitude and $\omega$ is the frequency of oscillation, and measuring the resultant shear stress.

The upper range is limited by the onset of inertial effects, when the oscillatory shear wave decays appreciably before propagating throughout the entire sample. If the shear strain amplitude is small, the structure is not significantly deformed and the material remains in equilibrium; in this case, the affine deformation of the material controls the measured stress.

The time-dependent stress is linearly proportional to the strain, and is given by:

$$\sigma(t) = \gamma_0 \left[G'\,(\omega)\, sin\,(\omega t) + G''\,(\omega)\, cos\,(\omega t)\right] \tag{7.12}$$

$G'$ is the response in phase with the applied strain and is called the elastic or storage modulus, a measure of the storage of elastic energy by the sample. $G''$ is the response out of phase with the applied strain, and in phase with the strain rate, and is called the viscous or loss modulus, a measure of viscous dissipation of energy.

Next Figures show the Rheological data reported in terms of the complex shear modulus defined as

$$G^*(\omega) = G'(\omega) + iG''(\omega) \tag{7.13}$$

In microrheology, the complex shear modulus of the systems has been obtained from the time dependence of the average mean square displacement, MSD, of the particles using the generalized Stokes-Einstein equation. The elastic and viscous moduli at different temperatures for the sol gel transition in the agarose 2, 4 and 5 g/L are presented in Figures 7.17,7.18,7.19. At high temperature shows the sol state where the viscous component is the important part of the complex modulus. When the temperature is low and the gel is created the effect of the elastic component becomes significant and it can be observed the crossover from the elastic and viscous components. As the system is converted into a gel is the viscous component the one that becomes negligible and the elastic is reliable and consistent. A further observation is that the values of the moduli grow up with the gel formation. As it can be observed the agreement between those moduli obtained using DWS and those using mechanical rheometry is quite good, with values of the same order of magnitude and with a similar dispersion for each technique.

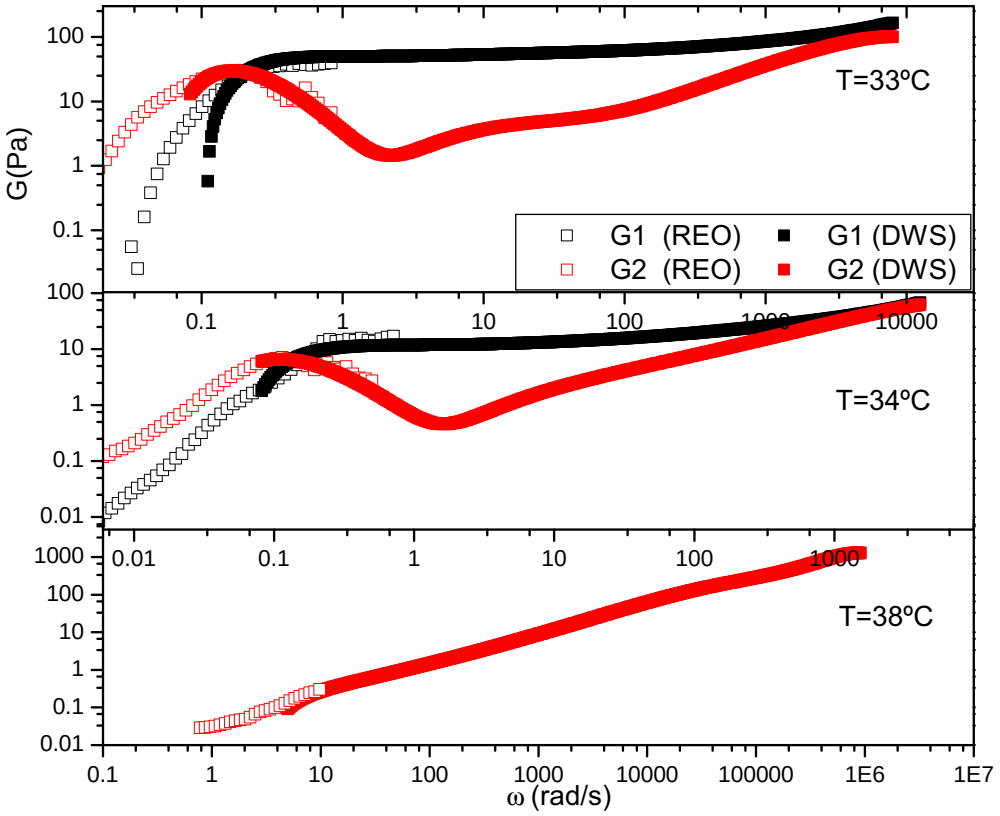


**Figure 7.17:** Elastic G' and viscous G" components for the agarose 2g/L system at different temperatures

Figures 7.17,7.18,7.19 show the frequency $\omega$ dependence of the storage $G'$ and loss $G''$ modulus for various agarose samples concentrations. With the increase of the frequency, both $G'$ and $G''$ increased in the low frequency region, and $G'$ continued to rise, while $G''$ declined after the crossover frequency. The sample shows liquid-like behavior ($G' < G''$) before the crossover and solid-like behavior ($G' > G''$) thereafter. Finally, $G'$ reaches a plateau ($G_0$), while G" increases again after reaching a minimum. This trend fits with the viscoelastic characteristics of agarose gels that follow the single-element Maxwell model [66], [67].

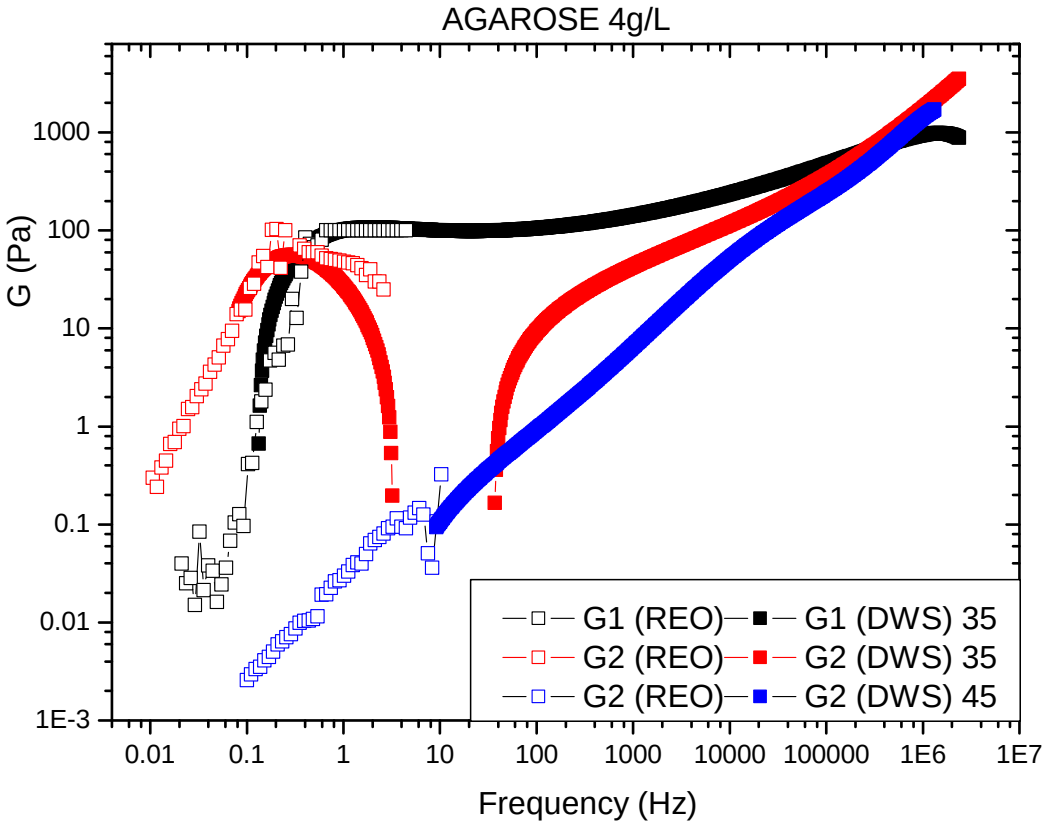


**Figure 7.18:** Elastic G' and viscous G" components for the agarose 4g/L system at different temperatures

For viscoelastic fluids Maxwell behavior is usually demonstrated in a Cole-Cole plot since G' and G" are proportional to each other. The Cole-Cole plots in which $\eta''(\omega)$ is plotted vs $\eta'(\omega)$ (or $G'(\omega)$ is plotted vs $G''(\omega)$) reduce to straight lines at the gel point. The ratio of the two moduli is independent of frequency.

For a Maxwell fluid this plot is characterized by a semicircle at low and intermediate frequencies. The moduli $G'$ and $G''$ vary as $\omega^2$ and $\omega$ in the low frequency region, and deviation from the rules occurs in the high frequency region.

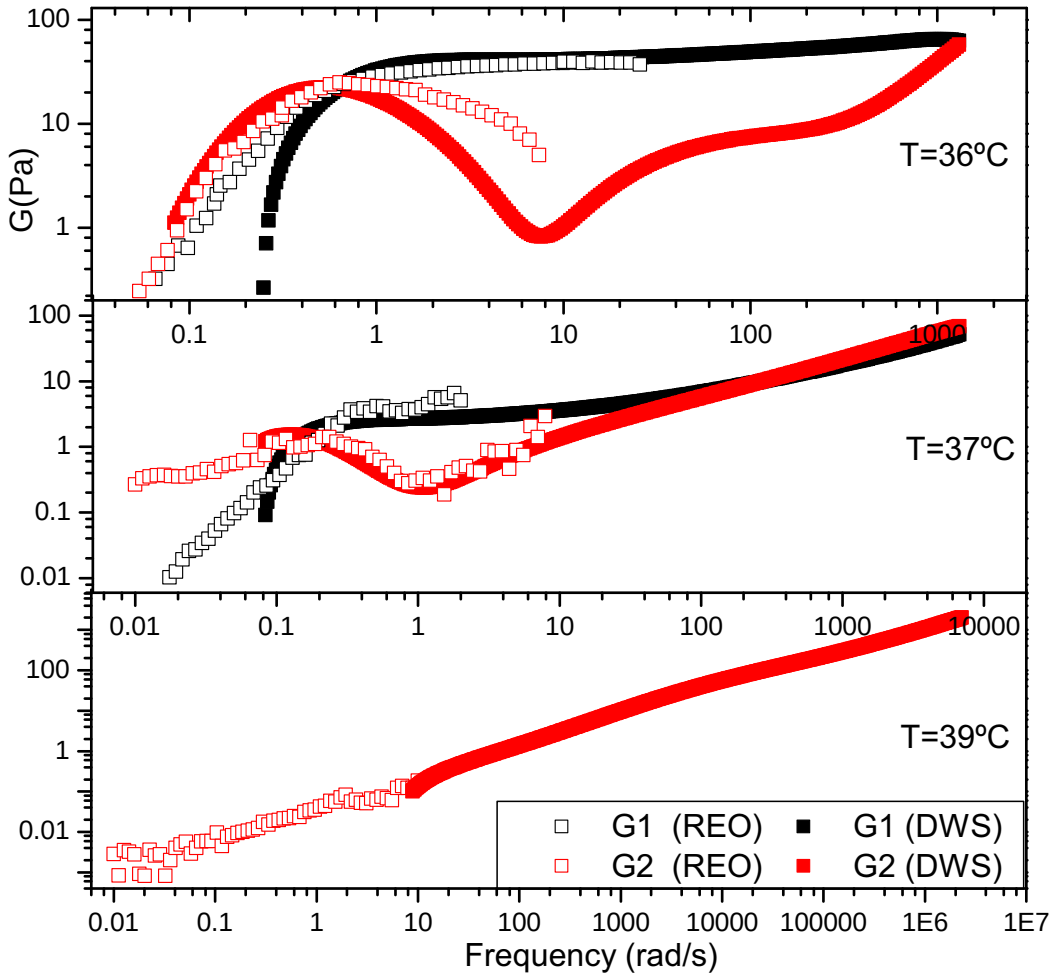


**Figure 7.19:** Elastic G' and viscous G" components for the agarose 5g/L system at different temperatures

As shown in Figure 7.20, the shape of the curve follows semicircular behavior perfectly, which indicates the formation of the gel at low and medium frequency, whereas the degree of deviation from the semicircular behavior at high frequency can be obtained by measuring the deviation of the data points.

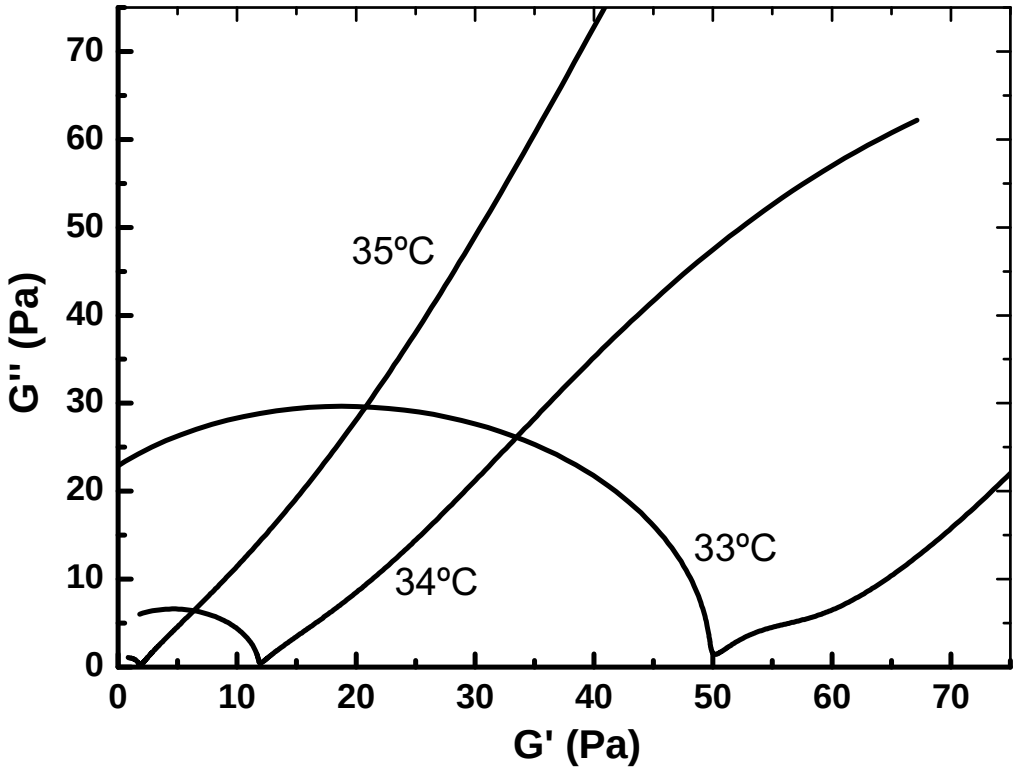


**Figure 7.20:** Cole-Cole plot from DWS at different temperatures for the agarose 2g/L

## 7.4. Viscoelastic models

It is necessary to relate the MSD curves with the complex shear modulus $G^*(\omega)$. For that a rheological model has to be assumed. One model that predicts the behavior described above is the extended Maxwell one, that corresponds to the initial Maxwell model with an extra viscous component.

The classical way to introduce the rheological properties of viscoelastic fluids, is to compare any elementary fluid element to a monodimensional mechanical system composed by springs and dashpots [68].

Maxwell proposed a viscoelastic model from non Newtonian behaviour of fluid which consists in a viscous damper and an elastic spring connected in serie [Maxwell, 1867]. A spring and dahshpot in series is called a Maxwell element (see Figure 7.21). The spring constant is denoted by $G$ so that the force applied to the spring is $G\gamma_1$ where $\gamma_1$ is the strain of the spring from its equilibrium state. The force applied to the dashpot is $\eta\frac{\partial\gamma_2}{\partial t}$ where $\eta$ is the viscosity and $\frac{\partial\gamma_2}{\partial t}$ is the velocity, that is to say the time rate of change of $\gamma_2$, which is the strain of the

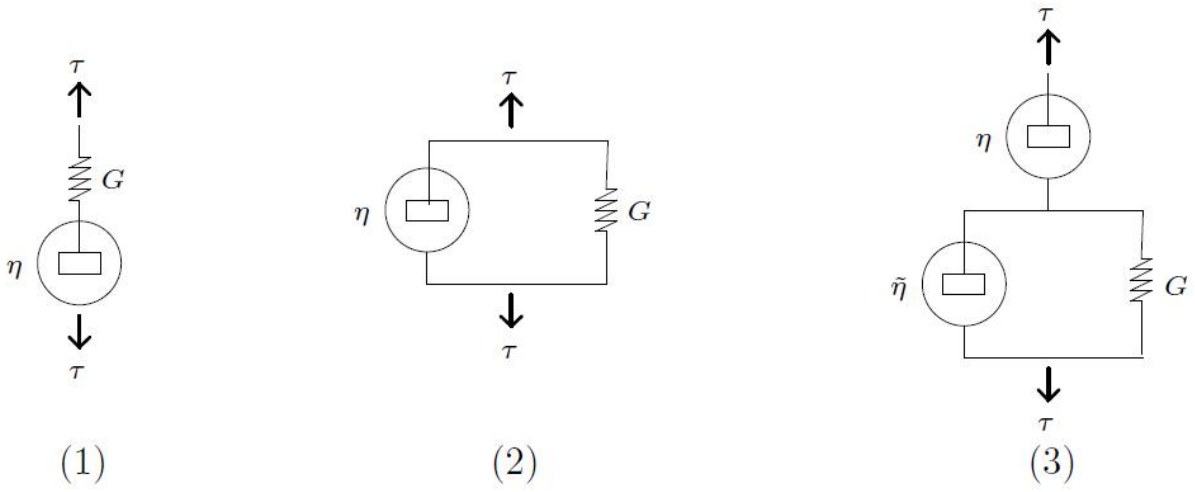


**Figure 7.21:** Maxwell (1), Voigt (2) and Extended Maxwell (3) models

dashpot. Because they are in series, the two forces are equal and we deduce

$$\lambda \frac{\partial \tau}{\partial t} + \tau = \eta \frac{\partial \gamma}{\partial t} \tag{7.14}$$

where $\lambda = \eta/G$ is a relaxation time, $\gamma = \gamma_1 + \gamma_2$ the total strain and $\tau$ the total stress to which is submitted the system. We can say that this system has instantaneous elasticity in the sense that there is an initial resistance due to the spring.

A Voigt model is a spring and a dashpot in parallel. In this case, the two forces must be added to obtain the total stress, and we have $\gamma_1 = \gamma_2$.

It is deduced the following relation

$$\tau = G\gamma + \eta \frac{\partial \gamma}{\partial t} \tag{7.15}$$

where $\gamma = \gamma_1 = \gamma_2$. This element is instantaneously viscous and this model is relevant for viscoelastic solids but not for fluids.

Extended Maxwell, that is also known as Jeffreys model, is a dashpot and a Voigt model in series and is widely used in the physical models for fluids. It is the model that we use in this Thesis. The total strain $\gamma$ in an extended Maxwell element is the sum of the strain in the first dashpot (of viscosity $\eta$) and the one in the Voigt element. Hence, it cab be written $\gamma = \gamma_1 + \gamma_2$

Because these two elements are serial, the forces in both elements are the same:

$$\tau = \eta \frac{\partial \gamma_1}{\partial t} = G\gamma_2 + \tilde{\eta} \frac{\partial \gamma_2}{\partial t} \tag{7.16}$$

After eliminating $\gamma_1$ and $\gamma_2$, it is obtained an equation connecting the force $\tau$ and the strain $\gamma$:

$$\frac{\eta+\widetilde{\eta}}{G}\frac{\partial\tau}{\partial t}+\tau=\eta\left(\frac{\partial\gamma}{\partial t}+\frac{\widetilde{\eta}}{G}\frac{\partial^2\gamma}{\partial t^2}\right) \tag{7.17}$$

We may define a relaxation time as $\lambda=\frac{\eta+\widetilde{\eta}}{G}$ and a retardation time $\widetilde{\lambda}=\frac{\widetilde{\eta}}{G}$.

In order to apply these simple 1D models of mechanical systems to fluid elements, we use the fact that the evolution of the strain $\gamma$ of an elementary fluid element is linked to the velocity field of the fluid.

For a Maxwell material the modulus decomposition is:

$$G^*=G'-iG''=G_0\frac{\omega^2\tau^2}{1+\omega^2\tau^2}-iG_0\frac{\omega\tau}{1+\omega^2\tau^2} \tag{7.18}$$

Figure 7.22 shows the components of the complex modulus that have a dependence with frequency following the extended Maxwell model. The storage modulus $G'$ is proportional to $\omega^2$ in the limit of low frequency, and attains a constant value at high frequency. The loss modulus G" is proportional to $\omega$ at low frequency and at high frequency where the Maxwell time $\tau$ characterizes the crossover from elastic to viscous behavior.

The MSD of the particles in a Jeffrey fluid is given by equation 7.19 [Rusakov, 2010 and 2013] [69, 70] resulting from the viscoelastic Langevin equation:

$$MSD=\frac{6K_BT}{\tau k(1+q)}\left(t+\frac{\tau_M q}{1+q}\left[1-e^{-(1+q)\frac{t}{\tau_M}}\right]\right) \tag{7.19}$$

The physical meaning in this scheme of Jeffrey, the friction force is represented by two simultaneously operating mechanisms. One is responsible for viscous (Newtonian) friction with a zero relaxation time and the other is responsible for delayed (Maxwellian) friction with the characteristic time defined via a renormalized dynamic elasticity. Then, the Jeffrey rheological scheme is a phenomenological model of the complex medium that consists of two interacting continua simple viscous and viscoelastic fluids. This behavior may be expected from moderately concentrated polymer solutions in low molecular solvents and (with a correction for the enlarged scale of base units) from some micellar systems.

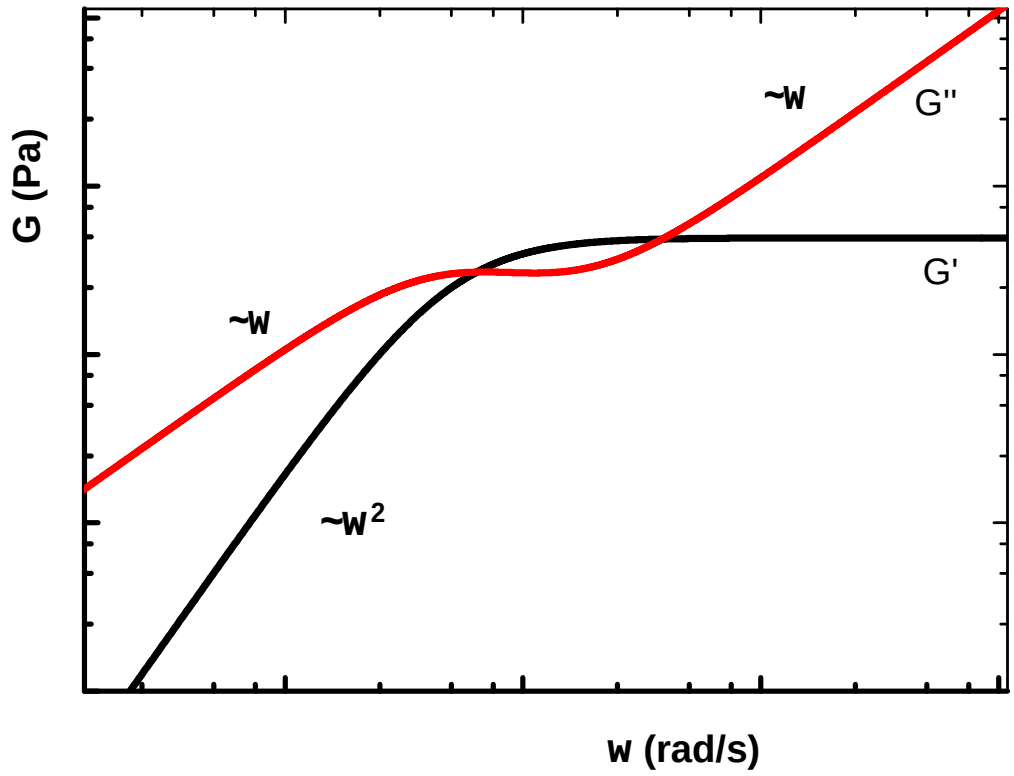


**Figure 7.22:** Elastic and viscous moduli as a function of angular frequency for the extended Maxwell fluid

The Newtonian element has the response time $\tau_N$, while that of the Maxwellian element is $\tau_M$, their ratio being $q = \tau_M/\tau_N$. Complete domination of one of the relaxation modes turns a Jeffrey into a Newtonian (q = 0) or a Maxwell (q = $\infty$) fluid. The elasticity and friction coefficients are introduced as $K = 6\pi GR$. With G the elastic modulus and R the radius of the particles.

In order to fit the experimental mean square displacement, [71], [72] the initial model for Brownian particles is given by the expression 7.20.

$$MSD = 6D_0t = 6\delta^2\left(1 - e^{-\frac{D_0}{\delta^2}t}\right) \tag{7.20}$$

Where $D_0$ is the short time diffusion coefficient, and $D_m$ the long time one, $\delta$ is the amplitude of the motion named cage size, and it is related to the elastic modulus $G'$ by equation 7.21

$$G_0 = \frac{k_BT}{6\pi R\delta^2} \tag{7.21}$$

If the longer times are considered a new term which is included in equation 7.20 and becomes

$$MSD = 6\delta^2 \left(1 - e^{-\frac{D_0}{\delta^2}t}\right)\left(1 + \frac{D_m}{\delta^2}t\right) \tag{7.22}$$

And a more accurate expression to describe the MSD of the particles in the dynamic heterogeneity of these complex systems introduces an exponent $\alpha$ following the Kohlrausch-Williams-Watts (KWW) idea of the stretched exponential.

$$MSD = 6\delta^2 \left(1 - e^{\left(-\frac{D_0}{\delta^2}t\right)^{\alpha}}\right)^{\frac{1}{\alpha}}\left(1 + \frac{D_m}{\delta^2}t\right) \tag{7.23}$$

Figure 7.23 shows a set of experimental results together with the best fit to Jeffrey´s model (curve marked $\alpha$ =1). Similar results were obtained for the rest of the samples. In order to overcome this problem, it is introduced an ad-hoc extension of the Maxwell model, leading to equation 7.23.

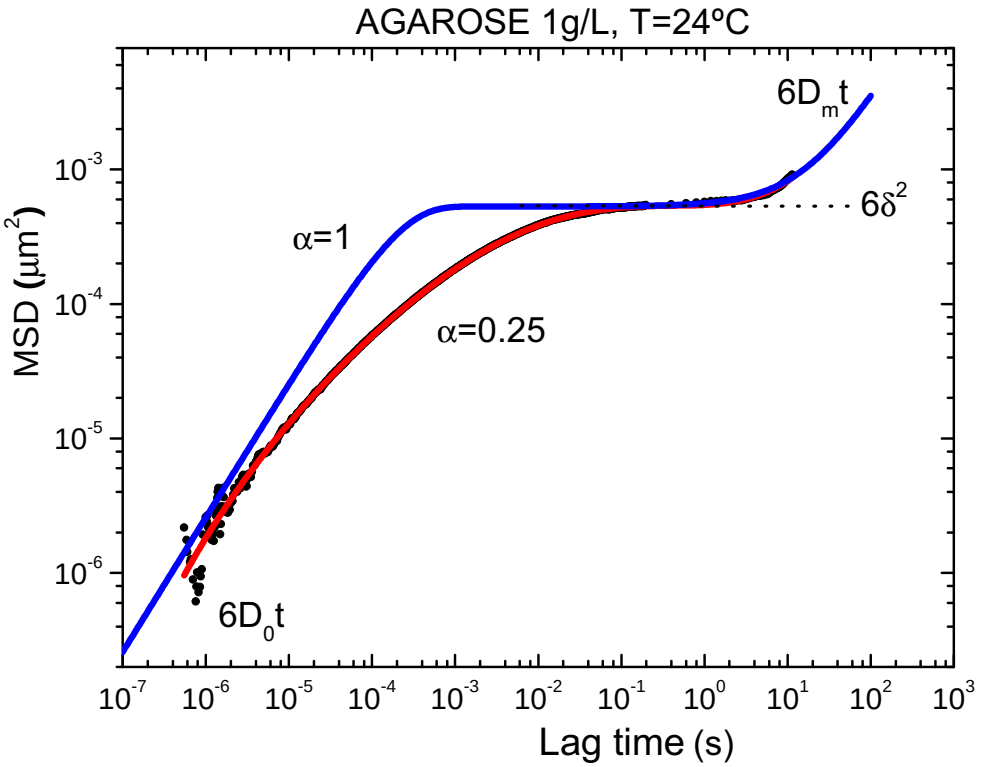


**Figure 7.23:** Curve of MSD as a function of lag time of PS latex in agarose 1g/L. Blue line is a fit obtained with Jeffrey equation 7.19, so that $\alpha$ =1. Red line corresponds to the best fit curve using the model equation 7.23.

It is possible to show that for $\alpha$ =1, this equation is equivalent to Jeffrey´s model. Figure 7.23 shows the best fit obtained with equation 7.23. From the low and high time limits $D_0$ and $D_m$ can be obtained, respectively, and from the plateau, $\delta$. It must be remarked that a very good quality of fits were obtained using equation 7.23 for all the temperatures, concentrations and for the two types of particles. Of course, reliable values of $D_m$ and $\delta$ can only be obtained when both the plateau and the long diffusive branch are observed.

Figure 7.24 represents the evolution of the cage size $\delta$ when temperature increases delta values for all the samples increases too till a moment in which they reach a constant value when the gel is formed and the threshold becomes so rigid that the particles cannot move randomly anymore.

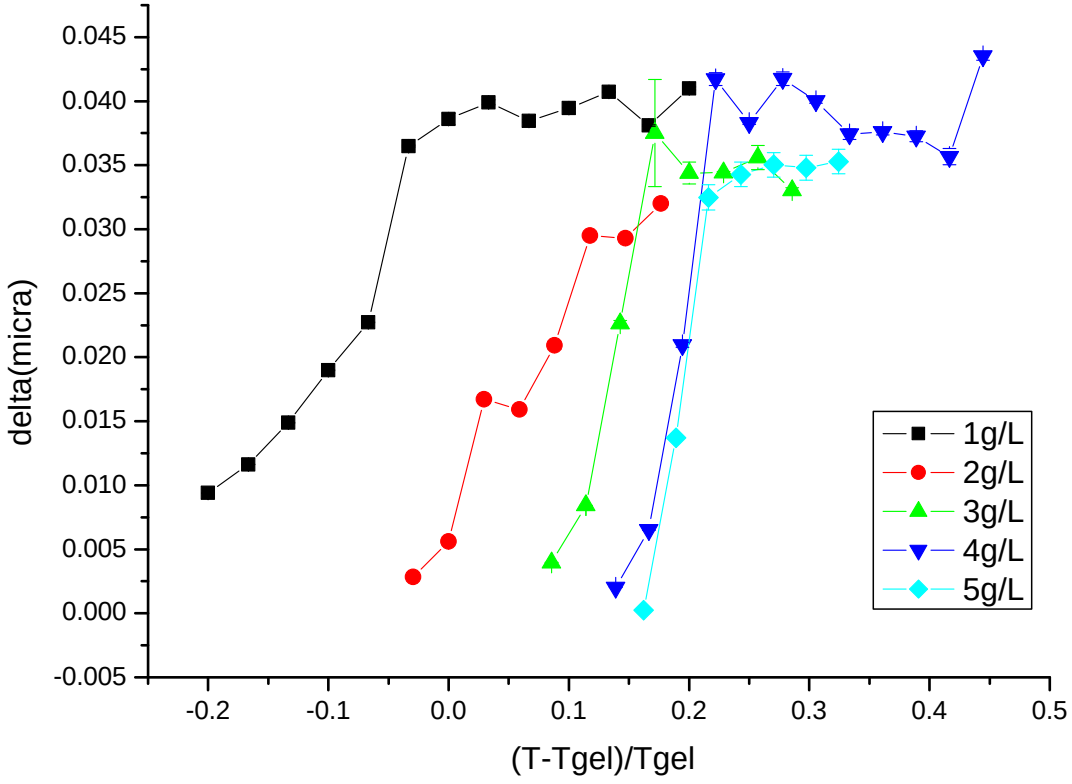


**Figure 7.24:** Evolution of the cage size $\delta$ parameter involved in equation 7.23 in the agarose solutions.

Figure 7.24 also shows that delta increases sharply with temperature until a plateau is reached in the fluid state. Even though the plateau is the same for all the concentrations studied, there has not been possible to build a master curve using the gelling temperature as the reducing parameter. Notice that the plateau modulus $G_0 = K_B T/(6\pi R\delta^2)$ strongly increases as the gelling temperature is approached from the sol state.

In Figure 7.25, represents the calculated diffusion coefficients in water obtained by

the Stokes-Einstein equation and those obtained in the agarose gel. The results of $D_0$ obtained in the gel are quite close to those calculated from the Stokes-Einstein equation in water. This seems to mean that at the lowest temperatures the short time range of the MSD curve essentially corresponds to the Brownian motion of particles within the gel network cages. However, above the gelling temperature, particles move in a viscous polymer solution and therefore $D_0$ decreases. $D_m$ has a steeper slope that reveals the behavior at longer times and could give a qualitative value of the viscosity by applying the Stokes-Einstein equation but taking into consideration that in the sol state the MSD curve has no relevant appearance and in the strong gel state the prediction of the equation is not very reliable. However, it is possible to see a change in the evolution of the $D_m$ data that shows the changes taking place in the system.

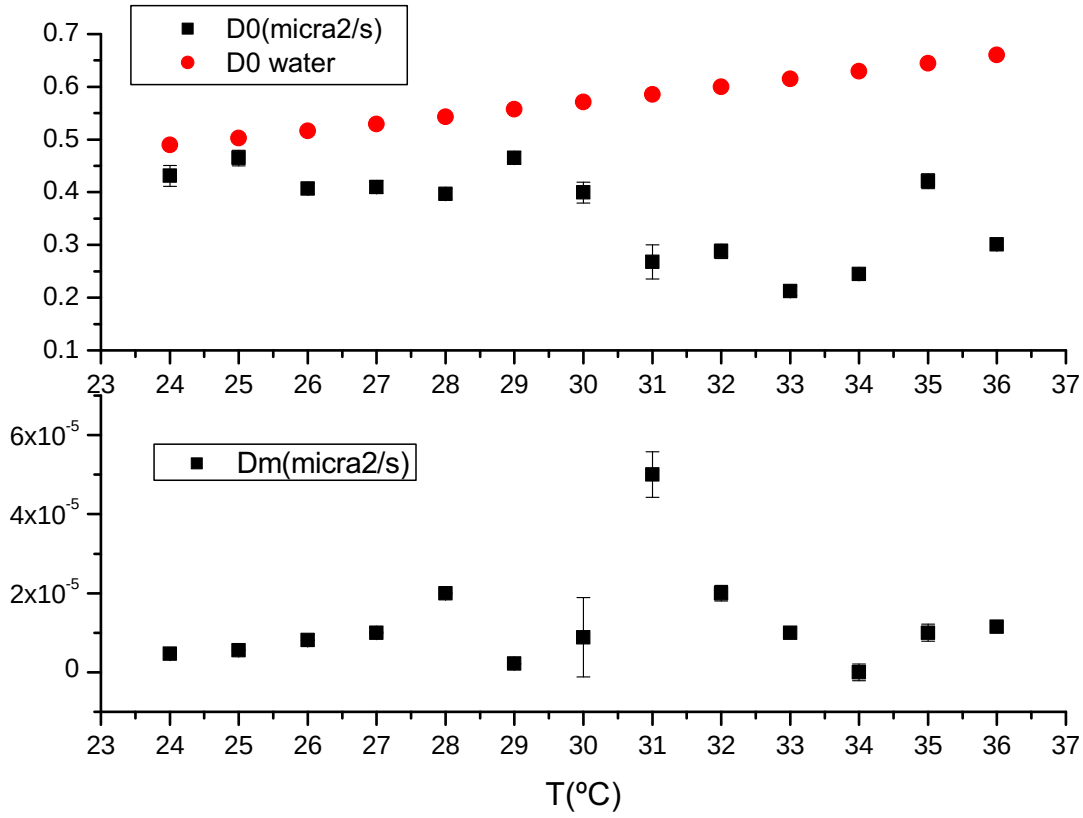


**Figure 7.25:** Evolution of the diffusion coefficients at short time $D_0$ and long time $D_m$ involved in equation 7.23 compared with the theoretical diffusion coefficient in water obtained by the Stokes Einstein equation in an agarose concentration of 1g/L.

The alpha parameter accounts for the width of the time relaxation distribution of the gel relaxation. To some extend it is analogous to the beta parameter of the Kohlrausch-Williams-Watts (KWW) function frequently used for describing the glass transition. Hence one can expect values of alpha close to unity at

high temperatures (near Maxwell like relaxation) and decreases as the system approaches the temperature gel (Figure 7.26). Values of $\alpha = 0.25$ correspond to very broad time relaxation distributions. It is noteworthy that the high temperature values of alpha are well below unity for an agarose concentration less than 3 g/L, which is reasonable for viscoelastic polymer solutions [73].

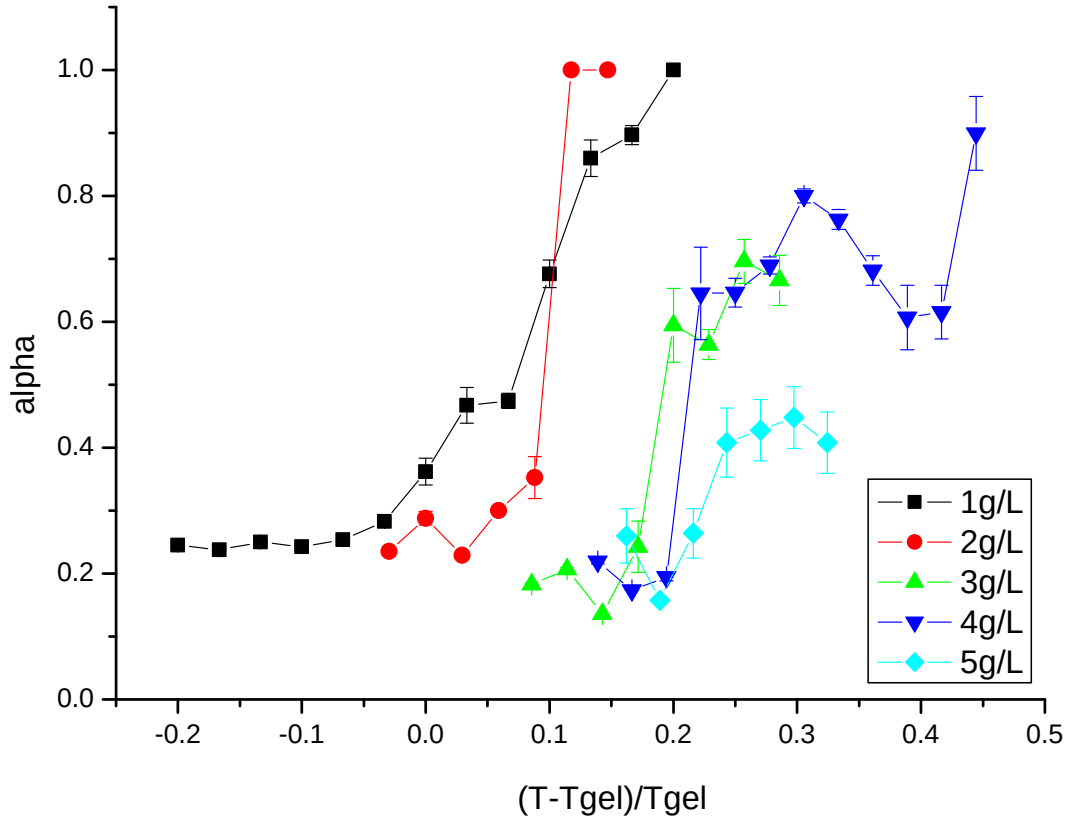


**Figure 7.26:** Evolution of the exponent $\alpha$ involved in equation 7.23 in the agarose solutions.

## 7.5. Kinetic effects in the gel formation

Gel properties close to the gelation point are strongly dependent on the gelation kinetics which in turn is strongly dependent on how close the sample is to the gelation point. Here particular care has been taken to ensure that

i) at each temperature, measurements are made until the time variation dependence becomes negligible, and

ii) the thermal history of the samples in the DWS equipment and in the torsion rheometer are as close as possible to each other.

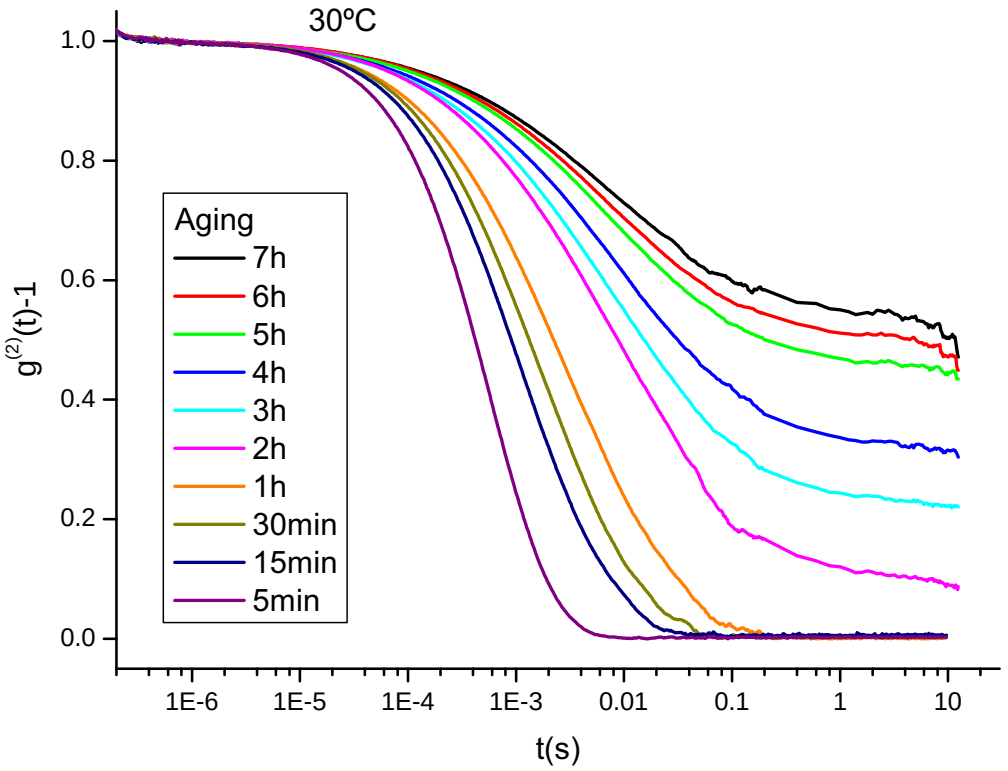


**Figure 7.27:** ICF vs t for an agarose concentration of 1g/L and at 30°C as a function of time

Kinetic of agarose gelation with time was studied for all the samples. Figure 7.27 and 7.28 show the evolution of the intensity autocorrelation function (ICF) for two different temperatures and for a 1g/L agarose solution. At the highest temperature the system does not present a significant evolution with aging time because it remains in the liquid sol phase however at 30°C it is possible to observe a significant evolution of the ICF along 7 hours period.

The same measurements made with the diffusing wave spectroscopy technique were also performed with the macrorheometer. The results show that for a temperature close to the gelling point, Figures 7.29) and 7.30, the results also show a time evolution, whereas at 36°C the results remain constant over a 7 hours period superimposing the moduli curves over each other (Figure 7.31). The valid frequency interval depends on the rheometer qualifications, and goes on from approximately 0.01 to 5 Hz.

The results shown are the expected for a viscoelastic fluid as it is clearly reflected in the Figure 7.31 explained below, at low frequency (long times), and at a constant strain rate it will produce a small deformation and the system will behave like a liquid and because of this $G'$ is lower than $G''$. But at high frequency (short times) the deformation is faster and it behaves like a solid with $G'$ higher than

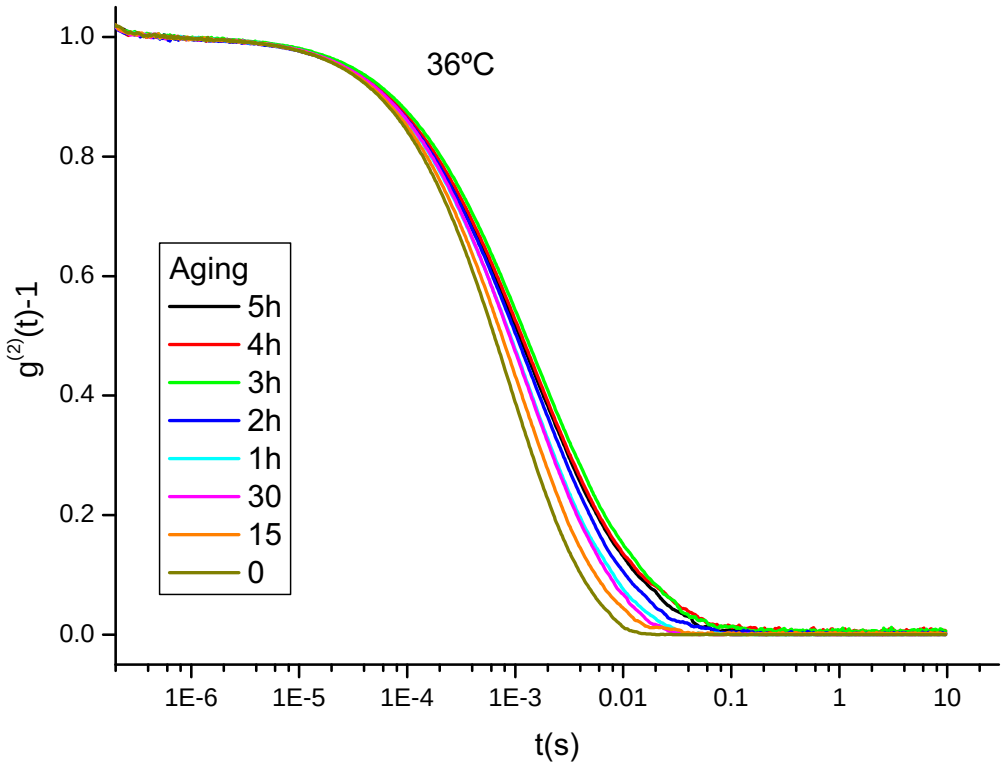


**Figure 7.28:** ICF vs t for an agarose concentration of 1g/L and at 36°C as a function of time

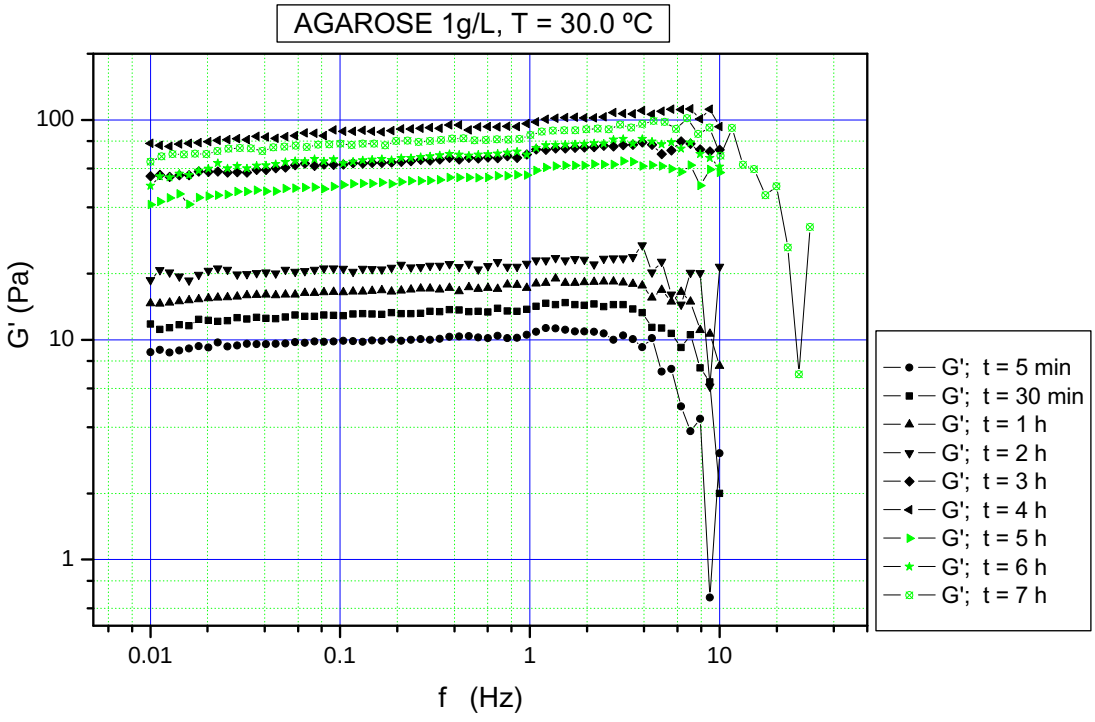


**Figure 7.29:** Rheometer frequency sweep for storage G' moduli for an agarose concentration of 1g/L at temperature 30°C as a function of aging time

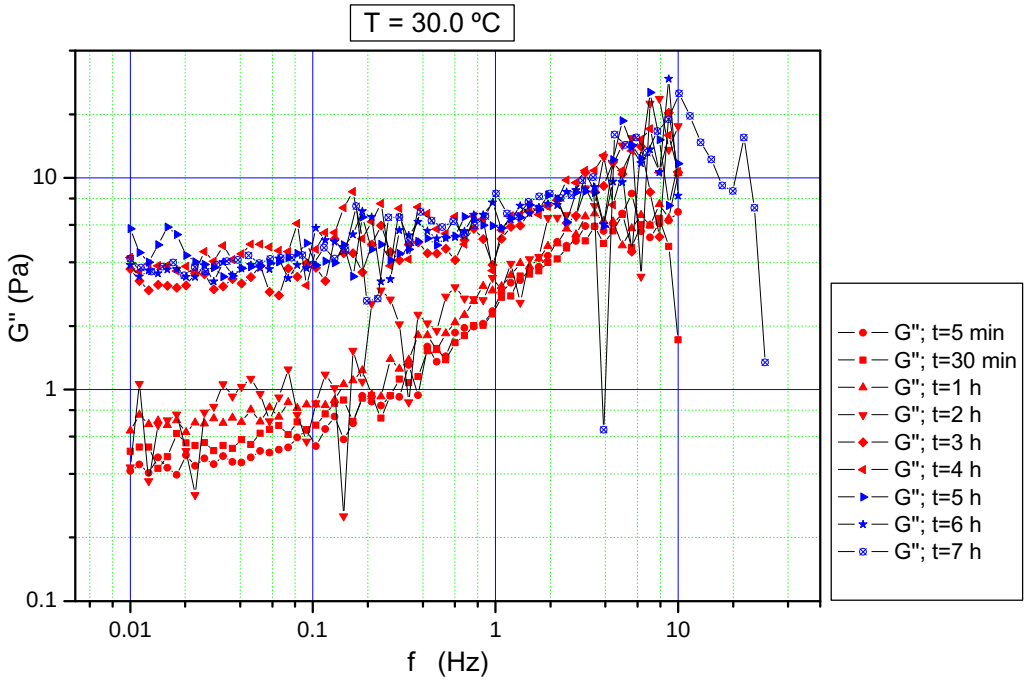


**Figure 7.30:** Rheometer frequency sweep for storage a) and loss b) moduli for an agarose concentration of 1g/L at temperature 30°C as a function of aging time

$G''$.

According to the percolation theory of gelation, [20], a power-law dependence of the elastic $G'$ and viscous $G''$ moduli on the frequency is expected for polymer systems near the point of the sol-gel transition (gelation point). As the system approaches the gelation point, the agreement with a simple power law form $G' = G'_0\omega^{n'}$; $G'' = G''_0\omega^{n''}$ is predicted to improve and, in fact, the values of $n'$ and $n''$ approach each other. The percolation theory is applicable to aging time and it predicts the equilibrium state for the sample when both curves are crossed (Figure 7.32). The time at which this theory predicts the equilibrium depends on the approach to the gel point where the equilibration time has been estimated as the highest; however for temperatures well within the liquid and in the gel states the equilibrium temperature reaches faster (Figure 7.33).

As shown in Figure 7.34 and 7.35, the power law exponents show that agarose forms a gel when a homogeneous solution is cooled from a liquid to a temperature below the ordering temperature, which is the gelling temperature and it depends on polymer concentration. In the present case, it is observed that the gelling temperature decreases gradually with the gel concentration.

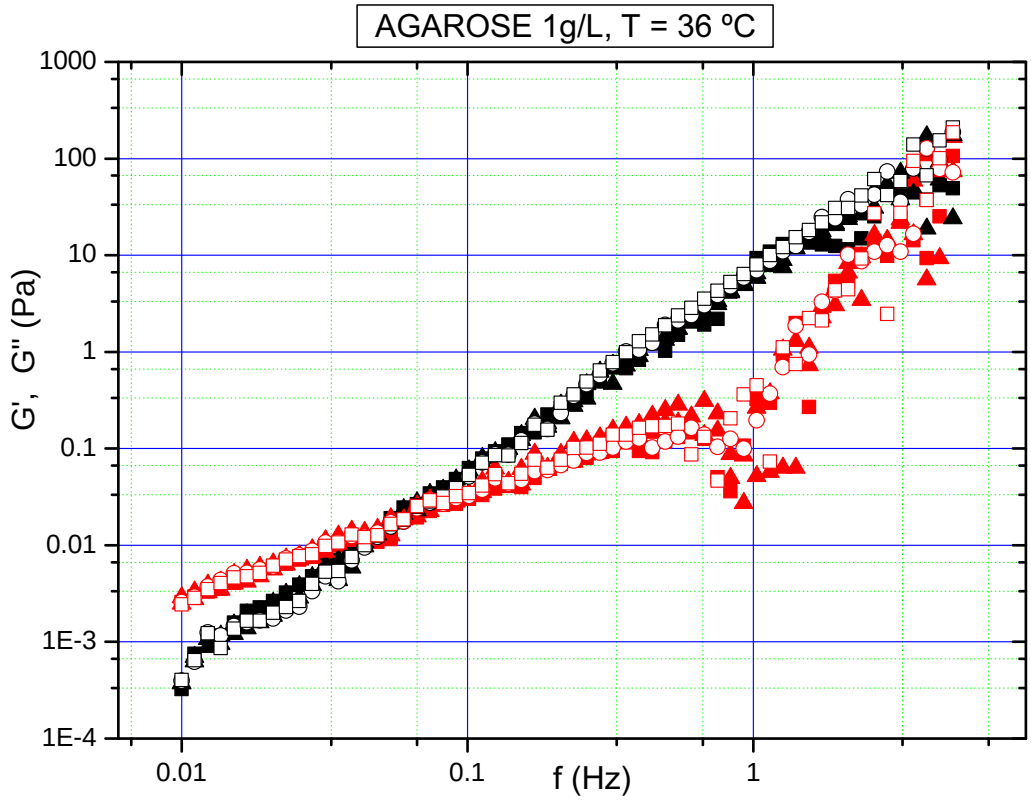


**Figure 7.31:** Rheometer frequency sweep, G" red points, G' black points for an agarose concentration of 1g/L at temperature 36°C as a function of aging time (5 min to 7 hours superimposing G´and G´´curves over each other, respectively)

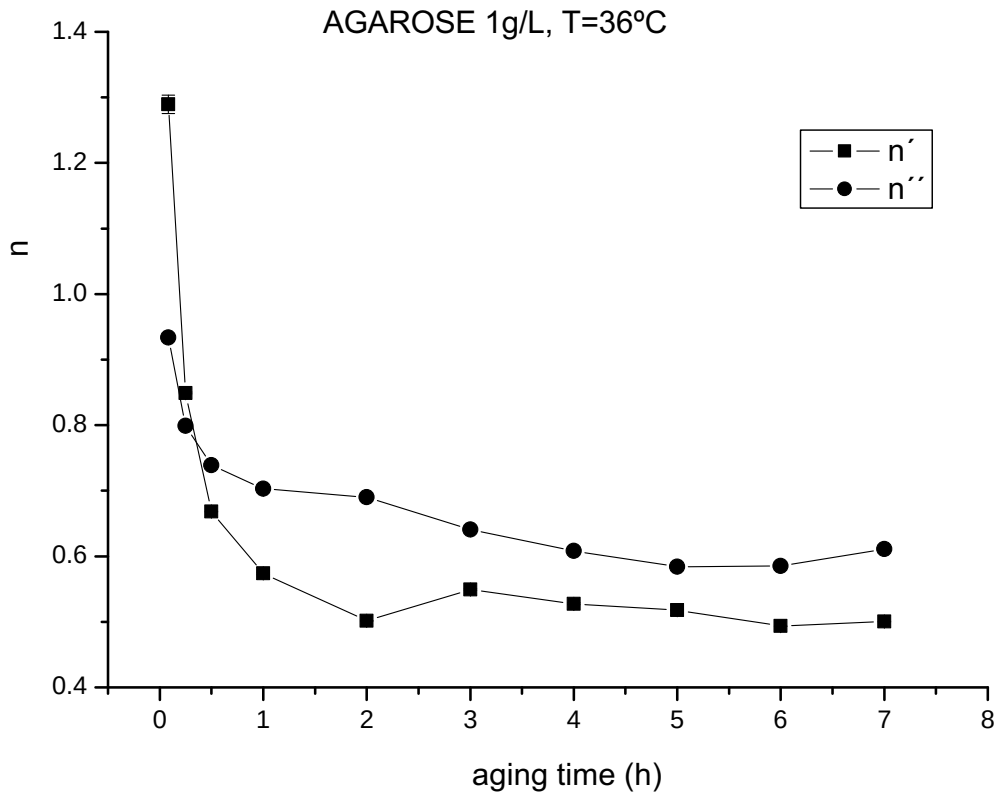


**Figure 7.32:** Power law exponents for agarose 1g/L at 30°C as a function of aging time

Results of the power law exponents in the agarose concentration ranging from 1 to 5 g/L allow to predict the gelation temperature from their crossover. The temperatures obtained by this method using both the macro (rheometer) and microrheological (DWS) viscoelastic moduli curves are the same and are presented in Table 7.1 and showed in Figure 7.35. Winter and Chambon have proposed a reliable criterion for determination of gel point temperature Tgel based on the temperature dependence of the loss tangent $tan\delta = G''/G'$ at different oscillation frequencies [74], so then, Tgel is the temperature at which $tan\delta$ becomes frequency independent and all curves at different oscillation frequencies coincide at this point.

The gel temperature values obtained are in agreement with the values reported in the literature [75],[76],[77].

Figure 7.36 shows the results obtained for a concentration of agarose of 5 g/L. The occurrence of a critical gelation temperature at which the $tan\delta$ is independent of the frequency is remarkable. Similar results were obtained for the other concentrations and the values obtained for Tgel are collected in table 7.1. The results are analogous to those obtained by the percolation theory.

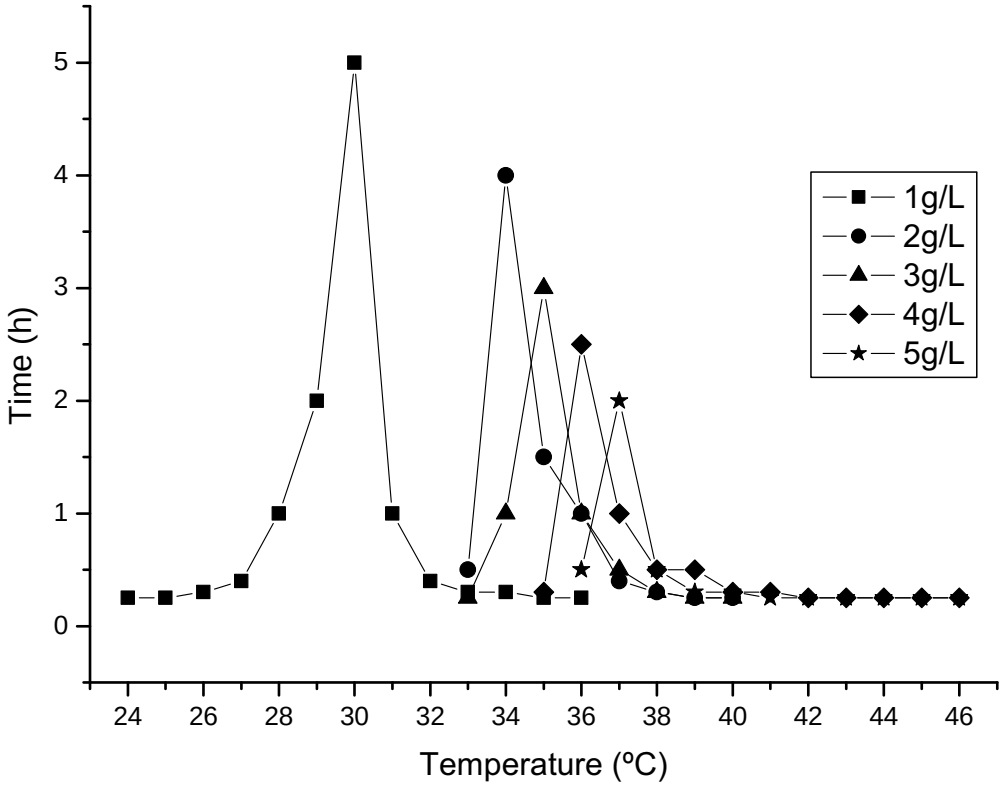


**Figure 7.33:** Effect of temperature on the agarose gelation kinetics

**Table 7.1:** Gelation temperature for agarose obtained by microrheology (DWS), macrorheology (rheometer) using Percolation Theory. The experimental error in the determination of the temperature gel (Tgel) is of the order of $\pm 1^{o}C$

| Agarose concentration (g/L) | Tgel (°C) |
|---|---|
| 1 | 30 |
| 2 | 34 |
| 3 | 35 |
| 4 | 36 |
| 5 | 37 |

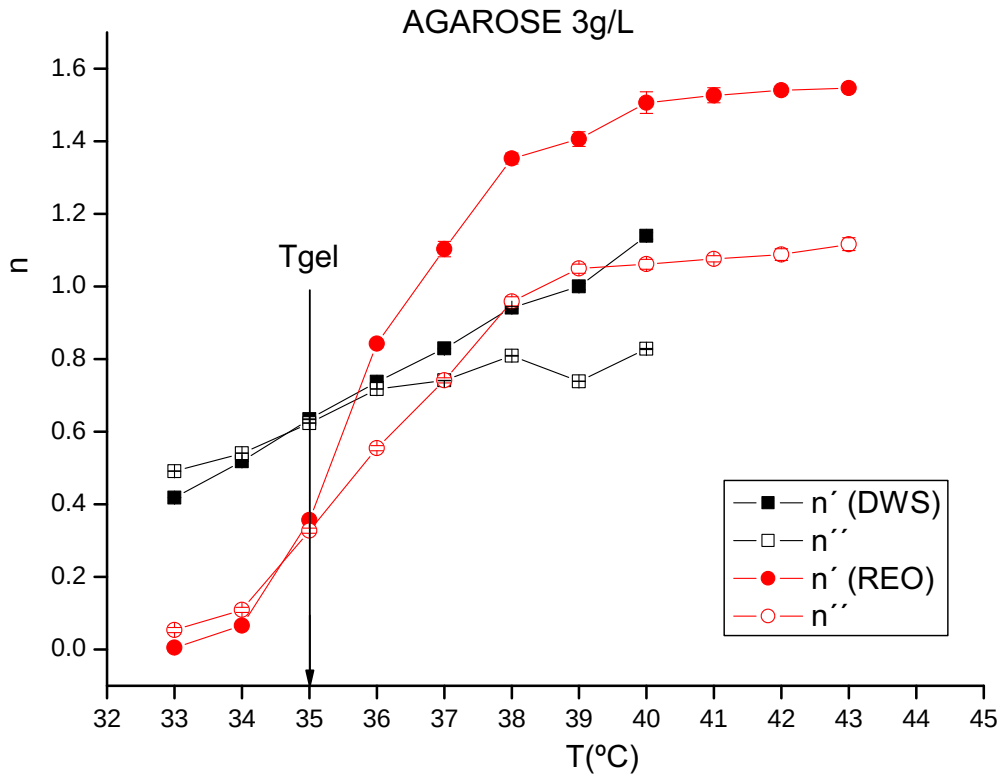


**Figure 7.34:** Power law exponents for agarose 3g/L as a function of temperature

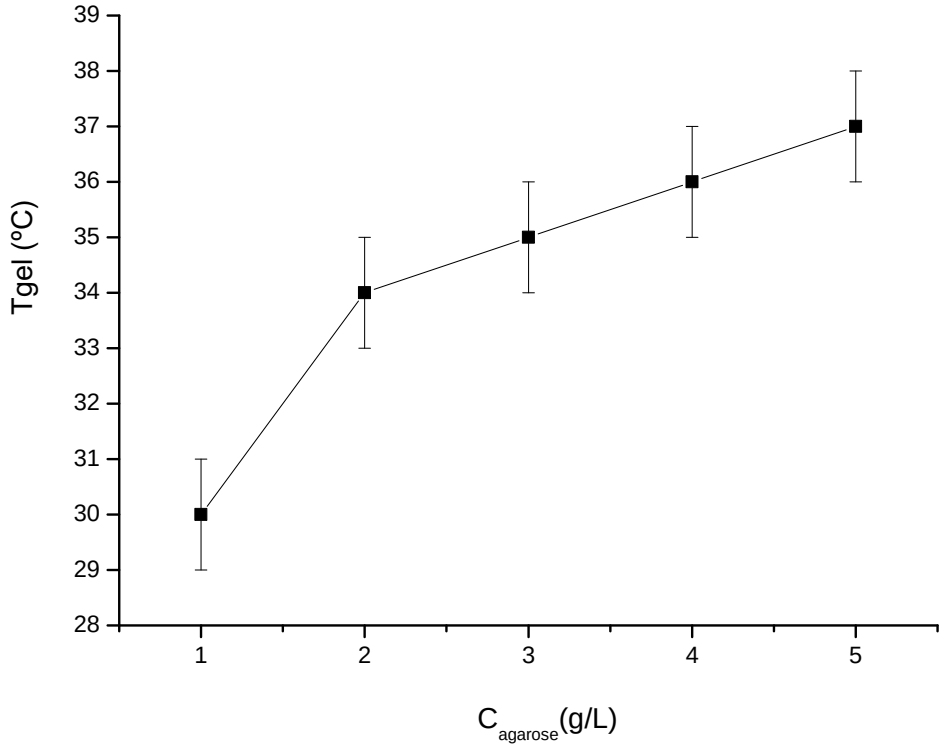


**Figure 7.35:** Concentration dependence of the agarose gelling temperature

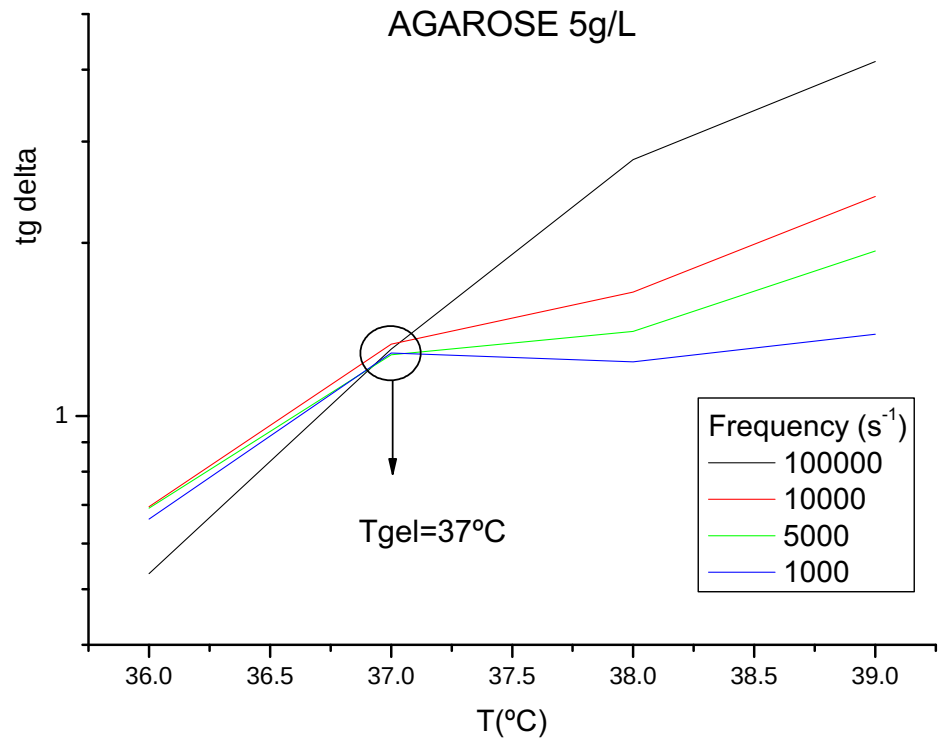


**Figure 7.36:** Representation of $tan\delta$ as a function of temperature with frequency variation for an agarose concentration of 5g/L

## 7.6. Viscosity

In a viscoelasticity fluid like agarose, viscosity is obtained from the viscous modulus, $G'' = \eta \cdot \omega$ and has an evolution with frequency.

Figure 7.37 shows the viscosity curves of agarose solutions from low to high concentration obtained at 37°C. The shape of the curves is characteristic of pseudoplastic liquids with some remarks: the first Newtonian plateau cannot be observed at low frequency. A shear thinning at intermediate shear rates is observed and finally, the second Newtonian plateau is found at high shear rates for all the samples, except for the less concentrated sample where the viscosity in practically constant in the hole region. A similar behavior is obtained for the viscosity curves at other temperatures.

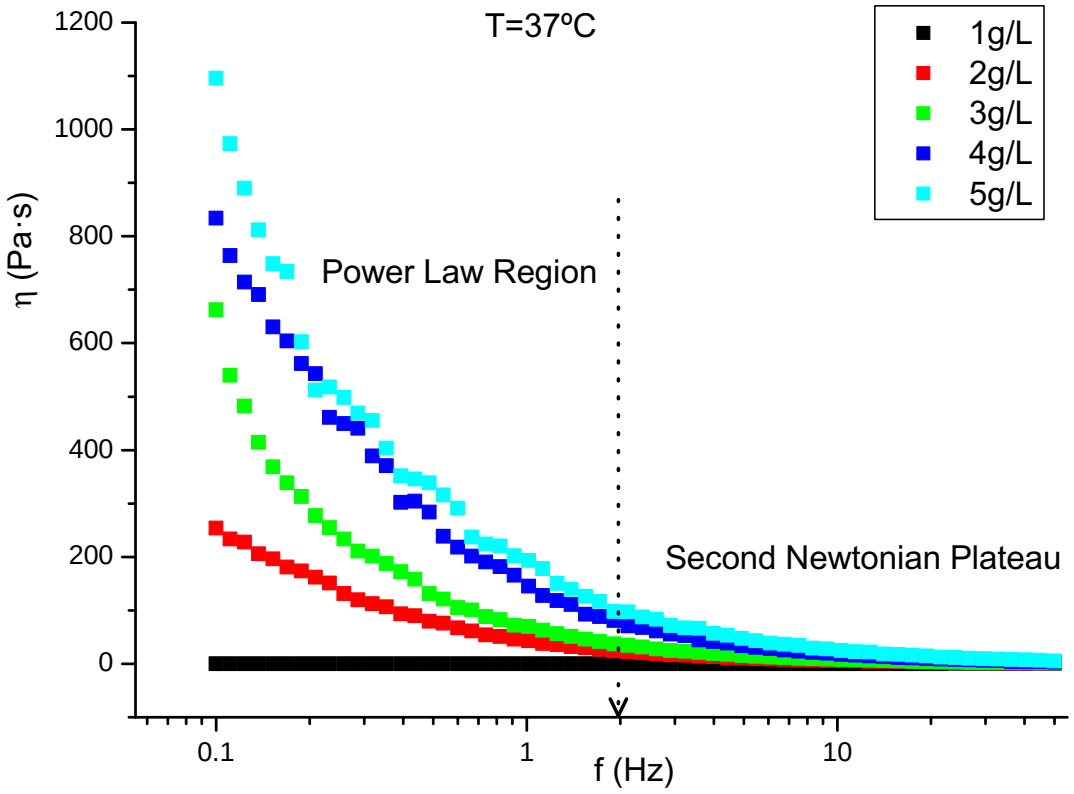


**Figure 7.37:** Viscosity curves at a temperature of 37°C for agarose solutions

The dependence of the viscosity with frequency has not the typical behaviour expected from Maxwell classical theory, negative slope of 2. In Figure 7.38, the viscosity determined at a fixed frequency of 10000 rad/s (corresponding to valid zone for all the samples in DWS, so that, the fall of the autocorrelation function) is plotted as a function of temperature for agarose aqueous solutions of different concentrations.

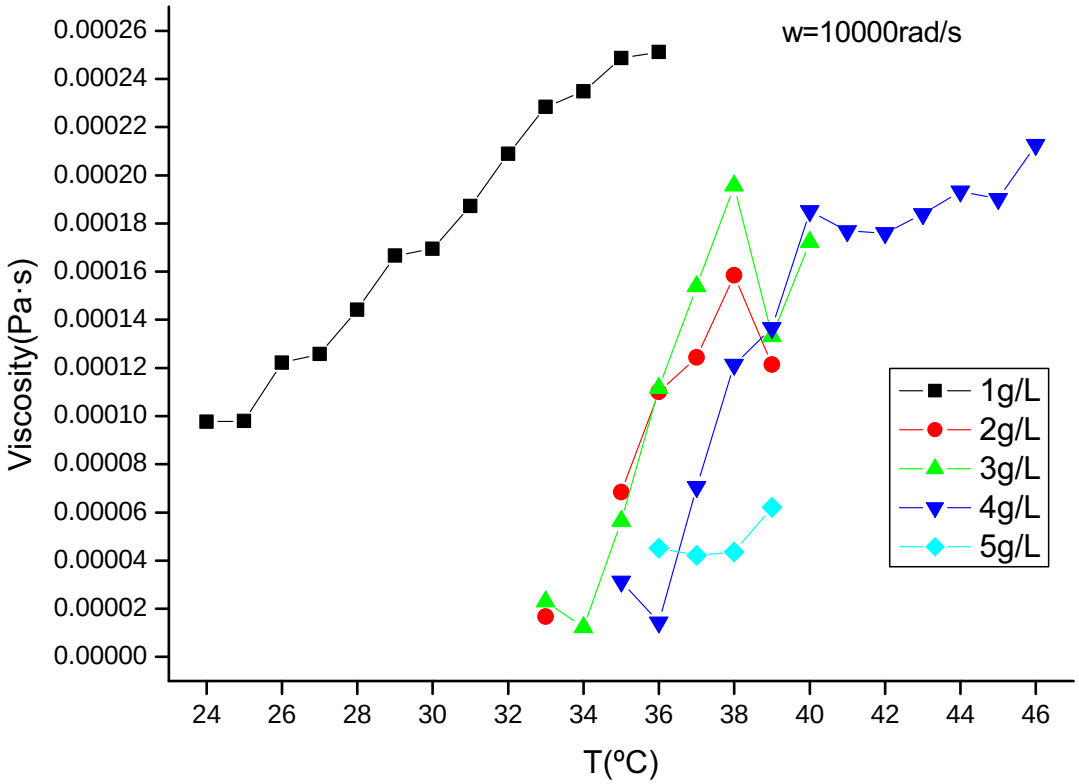


**Figure 7.38:** Viscosity values at a frequency of 10000rad/s as a function of temperature for agarose concentration of 1,2,3,4,5 g/L

## 7.7. Conclusions Agarose

Agarose is a natural polymer that present viscoelastic properties.

It was probed that Kinetics of agarose gelation is important in the microrheology with a remark time evolution of the agarose samples close to the gelling point. It was possible to predict the equilibrium stage for the sample with the percolation theory.

The viscosity of the agarose reveals a shape with the frequency characteristic of pseudoplastic liquids.

When using a smaller particles as tracers, a second decay is observed at high temperatures in the intensity autoccorrelation funscions, so we have observed the typical behavior in non ergodic systems. This novity has an effect in the MSD, so the second decay observed in the intensity autocorrelation function is corresponded with the increase in the last part of the MSD curve.

Several rheological models have been assumed that predicts the viscoelastic behavior, so one we call extended Maxwell, that corresponds to a Maxwell model in parallel with an viscous element and a streched exponent, is which better fit the MSD curves.

# Chapter 8

# MICRORHEOLOGY OF PLURONIC F127 SOLUTIONS

## 8.1. Introduction

Pluronic polyol F127 is one of a series of commercially available block polymers, derived from a propyleneglycol initiator, which are made by the sequential addition of propylene and ethylene oxides.

The Pluronic F127, also known as poloxamer 407, consists of approximately 70% by weight of ethylene oxide and 30% of propylene oxide. These products are called block polymers because they are composed af a propylene oxide block (PO) surrounded by two ethylene oxide blocks (EO). Pluronic F127 has the chemical formula $(EO)_{100}(PO)_{65}(EO)_{100}$

The polymer is soluble in water, and the mixtures has a lower critical solution temperature.

The thermogelification results from the interaction between the different molecules of Pluronic. The increment of the temperature modifies the hydration spheres around the hydrophobic units which in turn induces higher interactions between these different units [78]. This made Pluronic F127 attractive in formulating thermoreversible gels for ophthalmic and controlled delivery of many drugs.

Pluronic F127 has been studied in the literature due to capability to form gels in aqueous mixtures [79, 80]. Pluronics tend to form micellar aggregates with spherical, cylindrical or lamellar shapes depending on pluronic molecular structure, temperature, solvent, concentration and the pressence of salt. Aggregates formed by pluronics consist of a hydrophobic core formed by PO blocks and of a hydrophilic shell composed by the EO chains. increasing the polymer concentration a reversible sol-gel transition occurs

Solutions of Pluronic F127 in a concentration range of about 18 to 30%w/v are

liquids at low temperatures ($\leq 5^oC$) and are easily introduced into the DWS cells. A self-supporting, gel-like liquid crystalline phase is formed as the temperature is raised to $20^oC$.

## 8.2. Gel preparation

The microrheology and the gel-sol transition temperature was studied as a function of polymer concentration. The concentration range was adjusted such that the transition temperatures can be observed between 15 and 65°C. which corresponds to a concentration range of 7 to 25% w/v according to the literature [81], [82].

The solutions of were prepared using a secuence of cooling and stirring, but the pluronic forms a gel when the temperature is raised to $20^oC$. A weighed amount of pluronic is slowly added to cold water in a beaker containing a magnetic stirring bar, while providing gentle mixing. This enables each flake to become hydrated on the surface and increases the rate of disolution, whereas rapid addition of the pluronic to the water results in formation of a large ball requiring many hours for disolving. The container may be left in the quiescent state in the refrigerator overnight to effect complete solution.

The gels that form are reversible, that is, by placing the gel in the refrigerator, the solid state reverts to the liquid phase and a gel is formed again when the temperature is raised to $20^oC$. The gel can be cooled down many times and there will be no change in properties.

The pluronic F127 will form a soft gel at upper 15%w/v concentration and at temperatures upper 20°C.

## 8.3. Measurements conditions

At a concentration of 15% or higher in aqueous solution Pluronic F127 is transformed from a low viscosity solution to a semisolid gel upon heating from 4°C to temperature greater than 23°C and this thermogelation is reversible upon cooling. The phenomenon of thermogelling is characterized by a solgel transition temperature. This means that below this temperature, the sample is fluid allowing a comfortable and precise delivery, above this transition temperature, the solution becomes gel according to the increment of temperature.

The pluronic F127 used in these experiments was purchased from Sigma-Aldrich and used as received with no further treatment.

The experimental conditions are similar to that described for the Agarose in the previous chapter, with an important difference: For DWS experiments the temperature sweeps are now started from low to high temperature.

Two different types of monodisperse spherical particles as probes for the DWS measurements: Polystyrene with diameter 977 nm and titanium dioxide particles with diameter 127 nm. They were dispersed in water to obtain a suitable particle concentration for the DWS measurements.

Bulk shear measurements were made with the parallel plate geometry (40 mm diameter and GAP 1 mm) using a silicon oil as recover to prevent solvent evaporation. Oscillatory experiments were performed ar a stress of 0.1 Pa, good with the linear viscoelastic regime for the system wich was stablished via strain sweeps. The measurements of the elastic and viscous moduli was performed as a function of the temperature from 16 to 65°C at a heating rate of 1°C.

## 8.4. Effect of the particle size

In order to see the effect in the viscoelastic properties two types of particles are used, Polystyrene spherical particles with diameter 977 nm and titanium dioxide particles with diameter 127 nm, and were diluted in water to obtain a suitable particle solution concentration to measure in DWS.

For homogeneous viscoelastic media, the effect of the particle radius R on tracer mobility must obey a scaling rule, MSD $\sim$ 1/R. In all the experiments done, R $\gg$ $a$, where $a$ is the typical length scale of microscopic sample inhomogeneity, for example the mesh size of the hydrogels, or pore size in porous medium. As a result, the product (MSD·R) should be constant.

In the chapter of glicerol it was found that the optimal PS concentration for measured in DWS was 1%v/v, now we have to find the optimal concentration for the $TiO_2$ particles.

Assuming that the Stokes-Einstein equation holds the radius ratio $\frac{R_{PS}}{R_{TiO_2}}$ should be equal to the inverse of the diffusion coeficient ratio $\frac{D_{TiO_2}}{D_{PS}}$, like equation 8.1 expresses and the Figure 8.1 shows.

Figure 8.1 illustrates the normalized results obtained for the particle suspensions measured. It can be observed that the results for the $TiO_2$ particle suspensions of all the concentrations 1, 2, 3, 4 and 5%v/v are relatively close to those of the PS particles.

From the experimental results, the ratios of the radii of the particles and that of the diffusion coeficients calculated as the average of the different concentrations have been calculated. The results are:

$$\frac{R_{PS}}{R_{TiO_2}} = \frac{977}{127} = 7.7 \pm 0.5 \approx \frac{D_{TiO_2}}{D_{PS}} = \frac{28}{3.3} = 8.5 \pm 1 \tag{8.1}$$

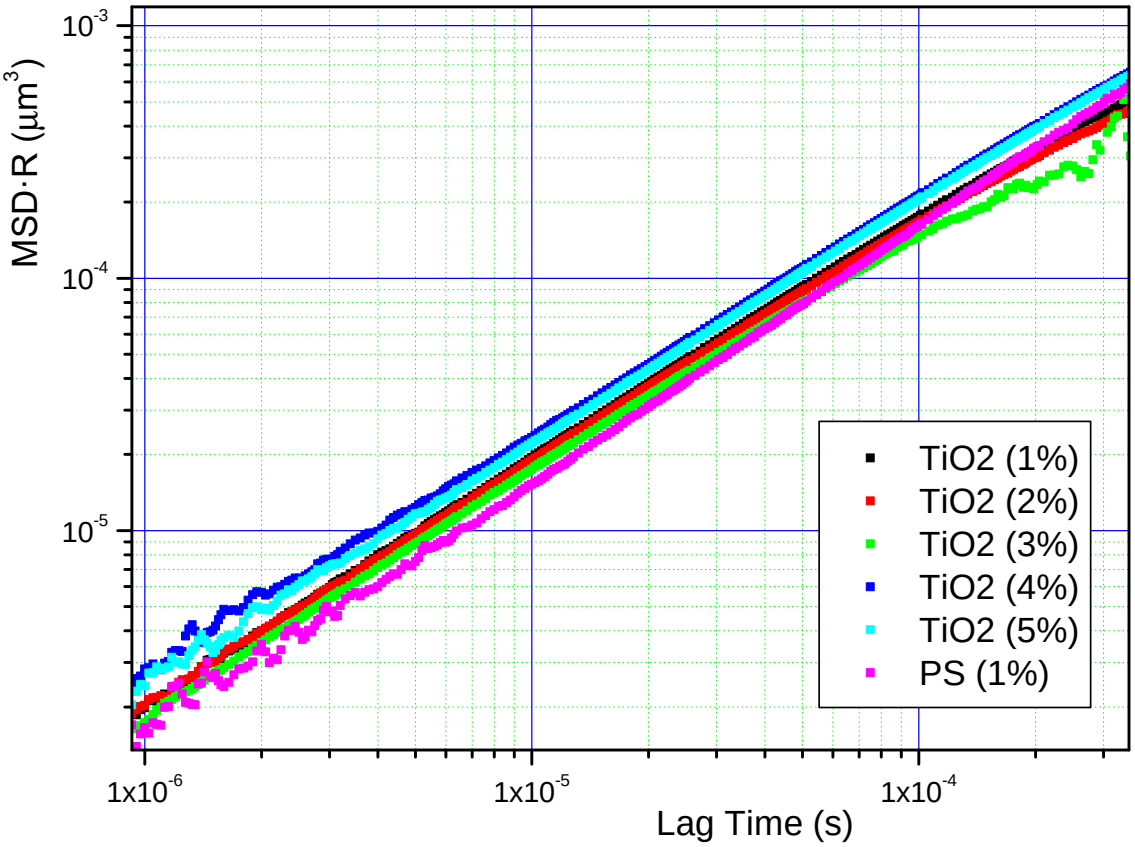


**Figure 8.1:** MSD·R for PS and $TiO_2$ in water solution

## 8.5. Autocorrelation functions

The intensity autocorrelation function for the pluronic F127 are shown in Figures 8.2 to 8.7, decays over the timescale that increase with the pluronic concentration of $10^{-4}$ to 1 s before finally decaying to zero. As reflected, for the low concentrations 7, 15 and 17%w/v the samples are homogenous liquid and not form a rigid gel.

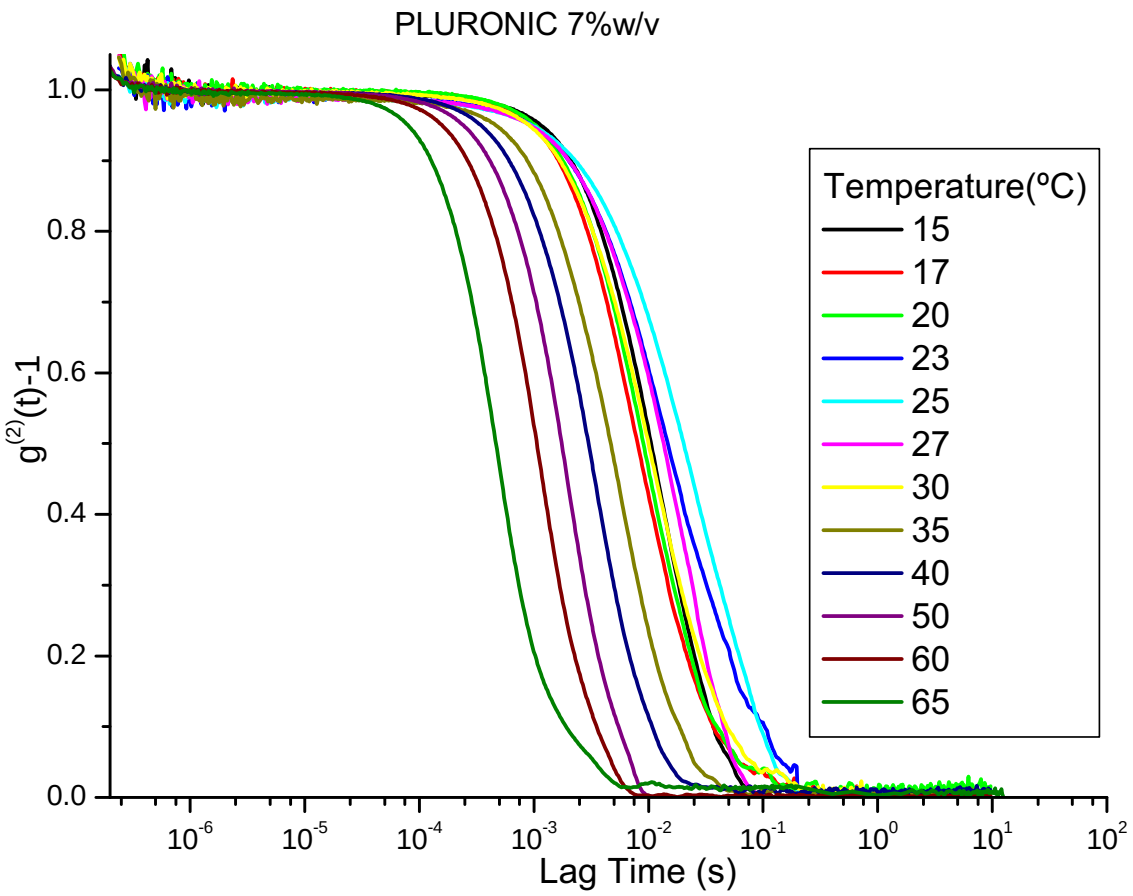


**Figure 8.2:** Intensity Autocorrelation function of the Pluronic F127 gel at 7 %w/v with PS particles in the range 15-65°C

Next concentrations, 18%w/v present sol-gel-sol reversion in the temperature range studied 15-65°C, higher concentrations 20 and 25 %w/v form also gels but it is not possible to see the reversion with the bigger particles of PS, maybe for the reason this change is produced at a higher temperature or have not a reversion point before the melting point. However, with the smaller $TiO_2$ particles, the reversion can be observed at this higher concentrations.

Figure 8.8 presents the ICF for a pluronic 20%w/v with the $TiO_2$ particles, and the curves at low temperature decays faster till reaching a temperature of 40°C, and then going back from 40 to 65°C.

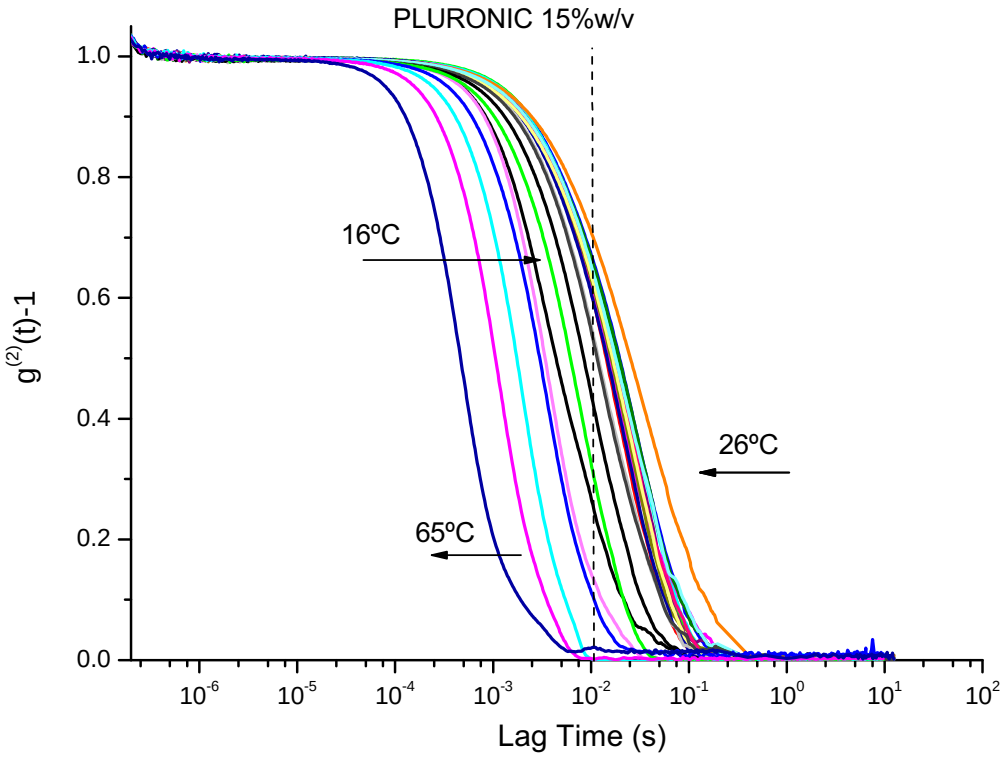


**Figure 8.3:** Intensity Autocorrelation function of the Pluronic F127 gels at 15%w/v with PS particles in the range 15-65°C

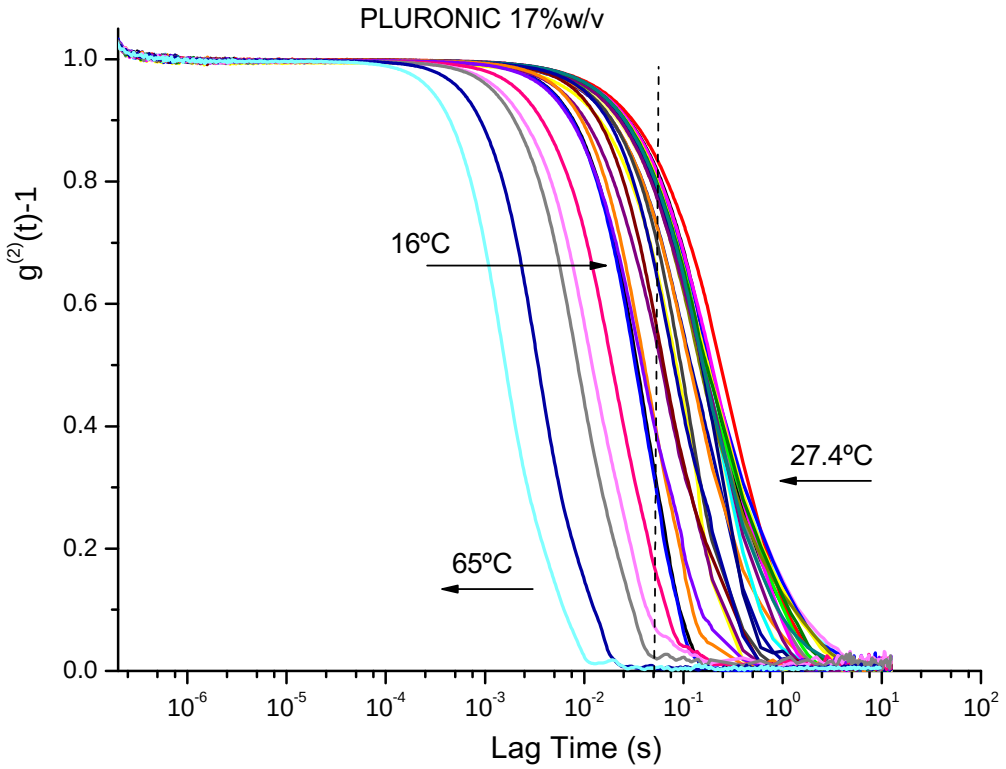


**Figure 8.4:** Intensity Autocorrelation function of the Pluronic F127 gels at 17 %w/v with PS particles in the range 16-65°C

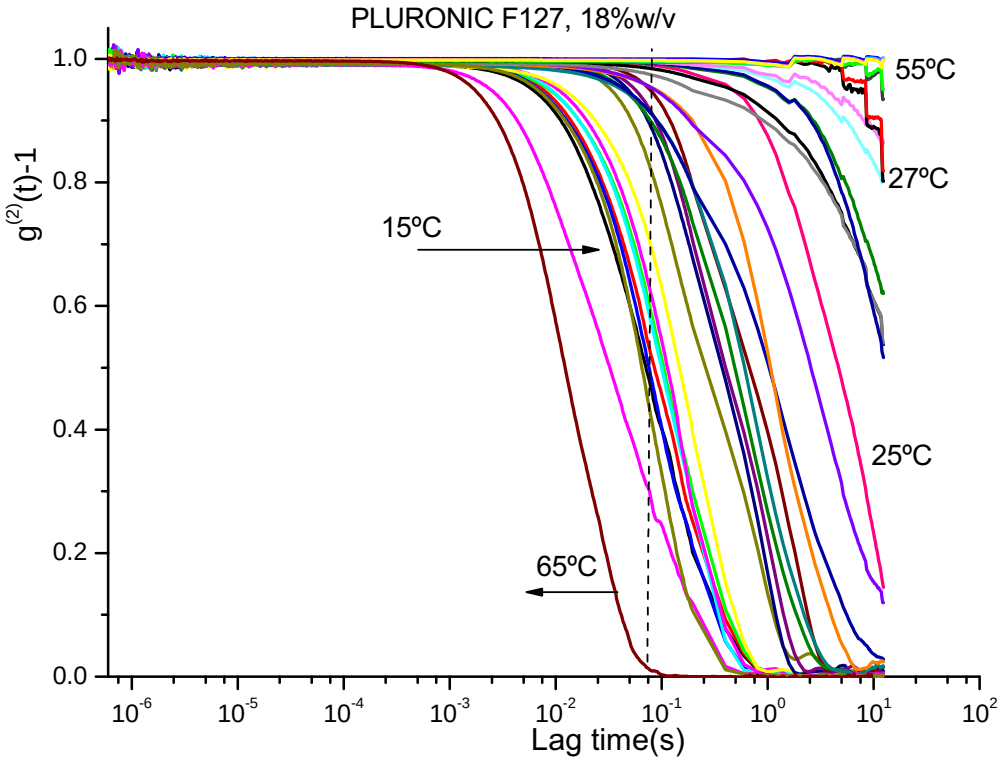


**Figure 8.5:** Intensity Autocorrelation function of the Pluronic F127 gels at 18 %w/v with PS particles in the range 16-65°C

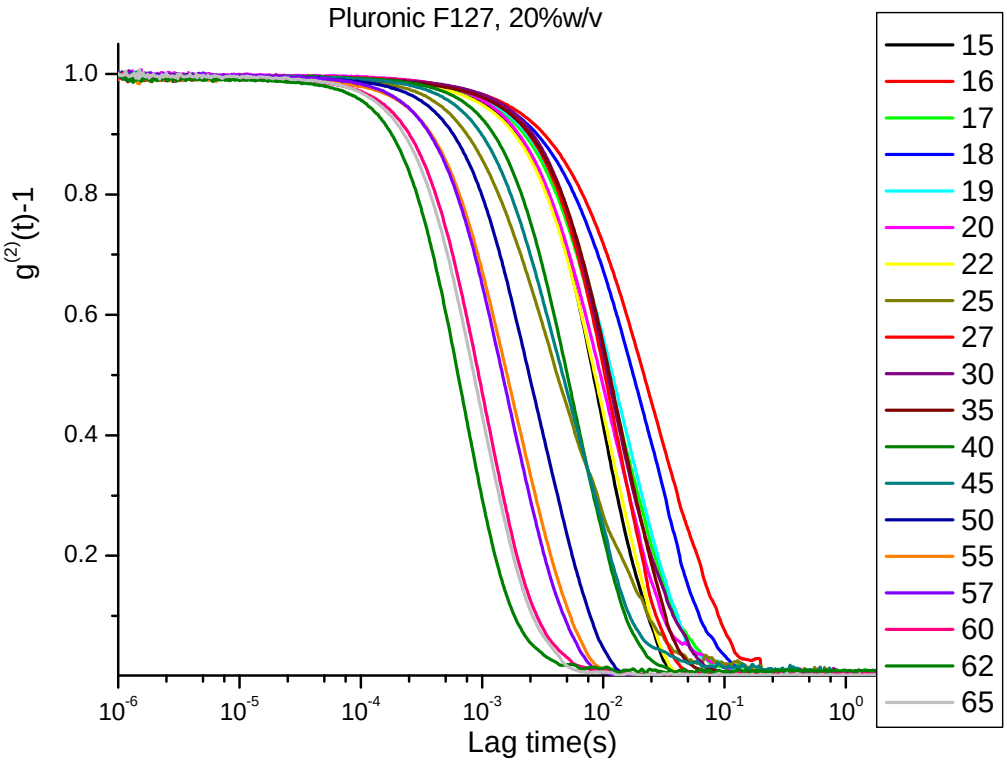


**Figure 8.6:** Intensity Autocorrelation function of the Pluronic F127 gels at 20 %w/v with PS particles in the range 15-65°C

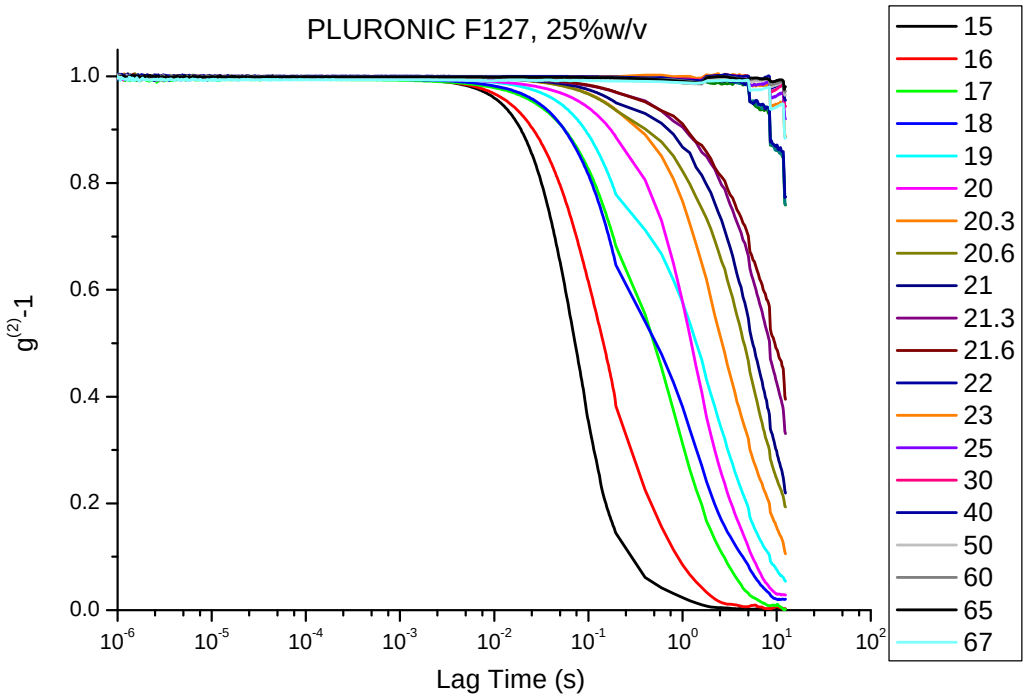


**Figure 8.7:** Intensity Autocorrelation function of the Pluronic F127 gels at 25 %w/v with PS particles in the range 15-65°C

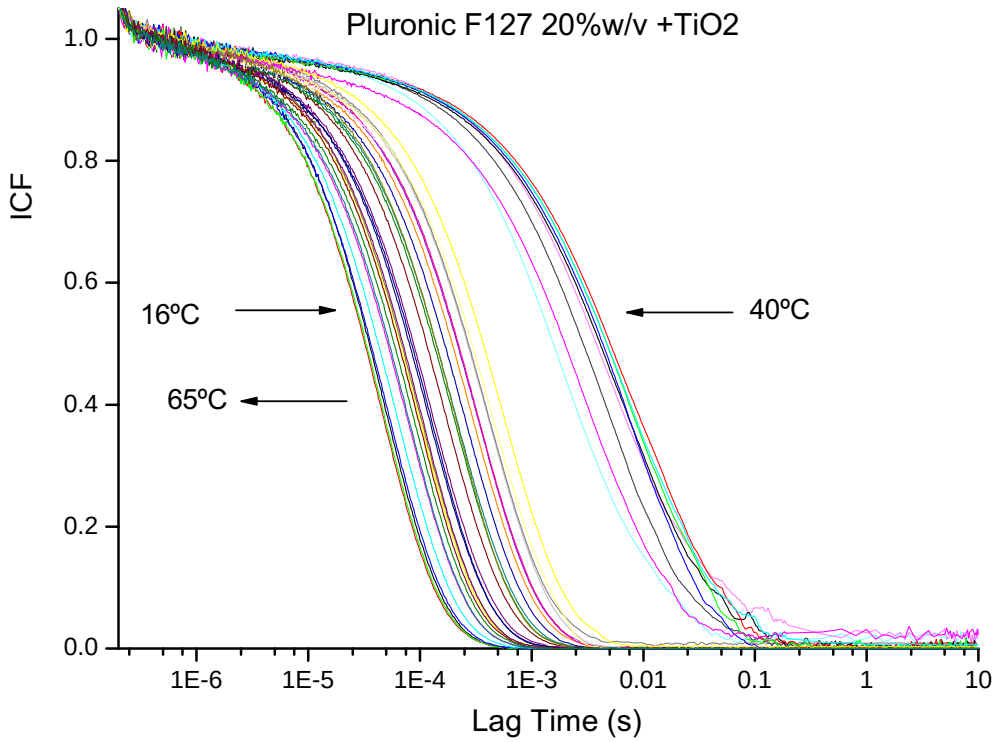


**Figure 8.8:** Intensity Autocorrelation function of the Pluronic F127 gel at 20 %w/v with TiO2 particles in the range 15-65°C

## 8.6. Mean square displacements

The data of the mean square displacements (MSD) of the polystyrene particles in the pluronic are logarithmically spaced and cover a large range in time.

MSD derived from the autocorrelation function given by expression 5.23.

$$g^2(t) - 1 = \left( \int_0^\infty P(s) \cdot e^{-\frac{s}{l^*} \cdot k^2 \cdot MSD} \, ds \right)^2 \tag{8.2}$$

The Figures 8.9 to 8.11, the MSD for polystyrene particles point out that the pluronic solutions are viscoelastic. At short time scales the MSD increases slowly, indicating nearly elastic motion, whereas at long time scales, the value of the MSD increases steeply, indicating viscous flow.

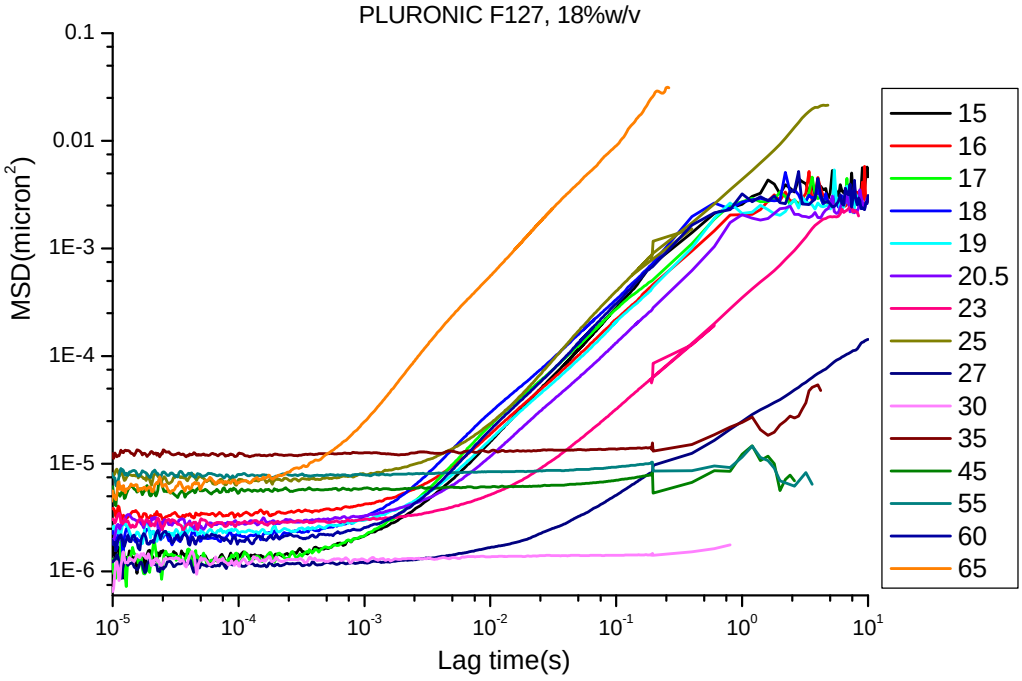


**Figure 8.9:** Mean square displacement of the Pluronic F127 gel 18 %w/v with PS particles in the range 15-65°C

The use of the $TiO_2$ particles, extends the time scale to short times, see Figure 8.12 showing the gelification of the pluronic in this time region. The behavior is cyclic, it starts from a diffusive to a subdiffusive when temperature is increasing from 16 to 40°C as the sol-gel transition takes place. For higher temperatures (40 to 65°C) the system reenters the sol state or forms a soft gel. The reentrant sol-gel-sol(or soft gel) transition has already been observed for the Pluronic F127 system [81].

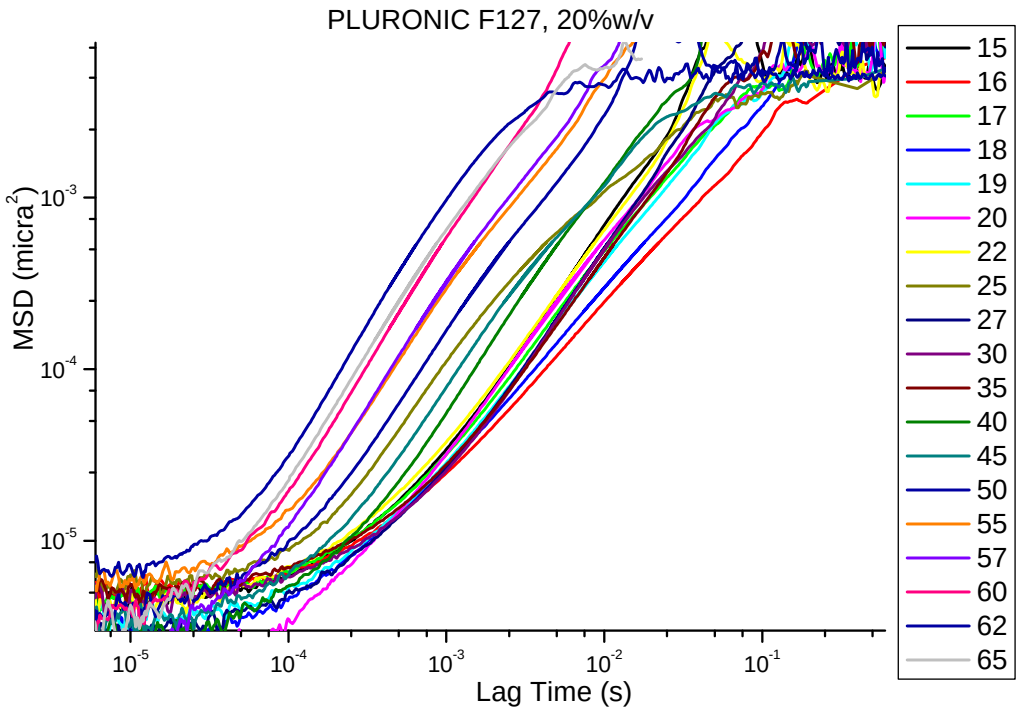


**Figure 8.10:** Mean square displacement of the Pluronic F127 gel at 20 %w/v with PS particles in the range 15-65°C

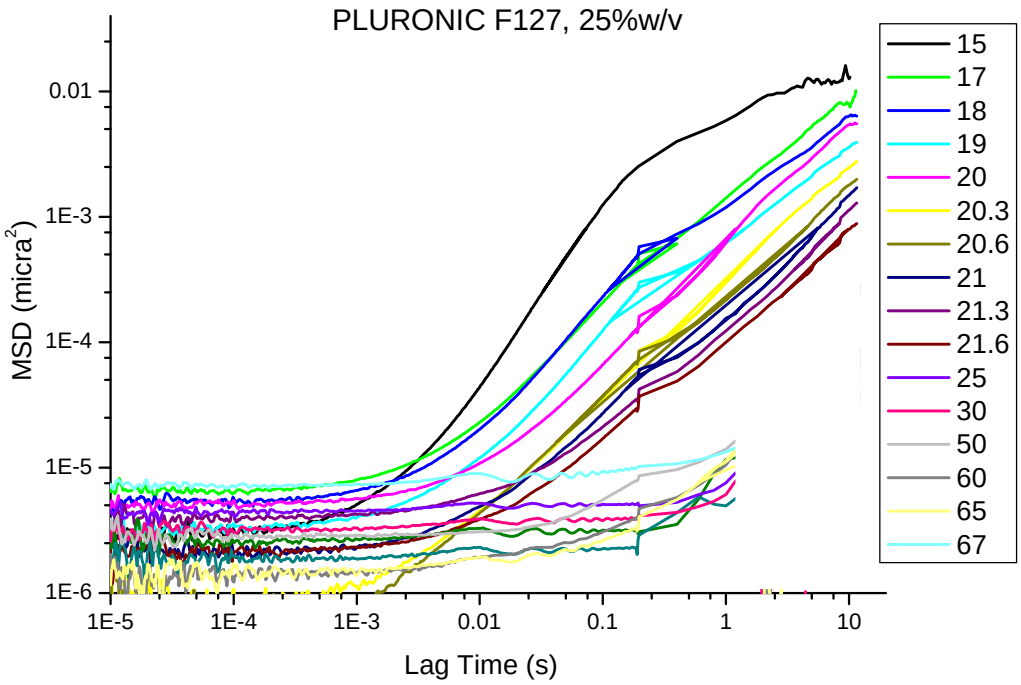


**Figure 8.11:** Mean square displacement of the Pluronic F127 gel 25 %w/v with PS particles in the range 15-65°C

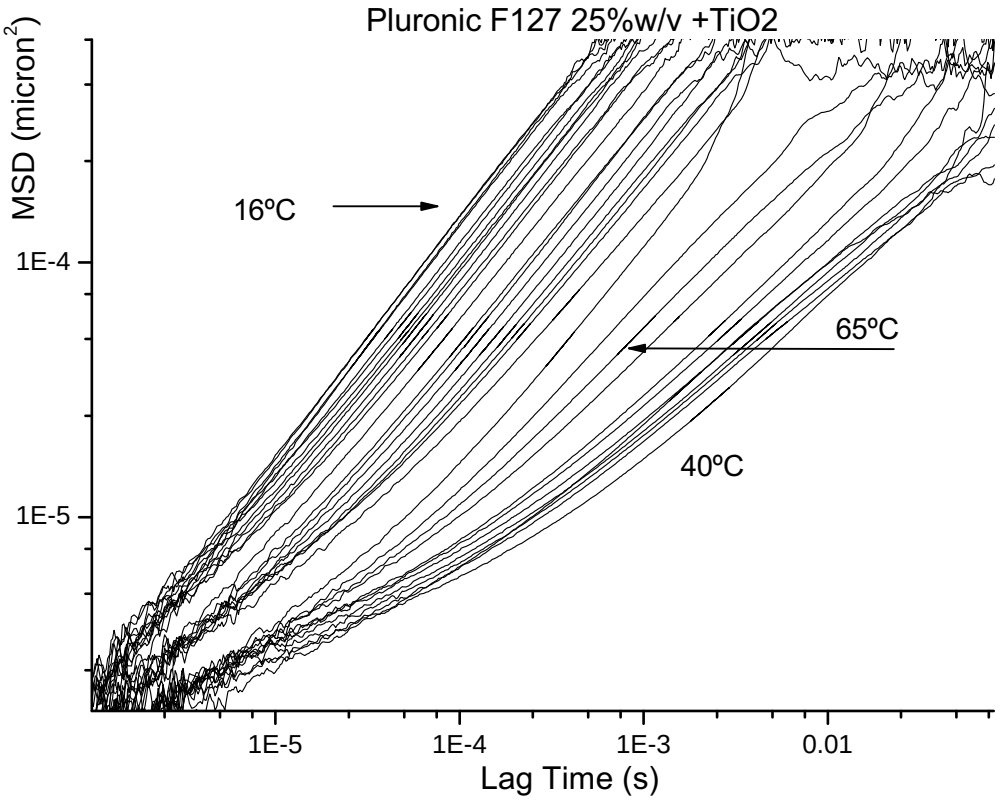


**Figure 8.12:** Mean square displacement of the Pluronic F127 gels at 25 %w/v with $TiO_2$ particles in the range 15-65ºC

## 8.7. Comparison the micro and macrorheological measurements

In this section we discuss both the results obtained by DWS and by an oscillatory rheometer. Figure 8.13 shows the results from low to high concentrations for pluronic 17%w/v. The results show that the behavior is essentially viscous, the linear response regime is preponderated and the storage modulus $G''$ in the decomposition components of the complex modulus $G^* = G' - iG''$ is the reliable component with the information for this state in which it is majority in the liquid phase. The notation used is $G'$ or G1 and $G''$ or G2.

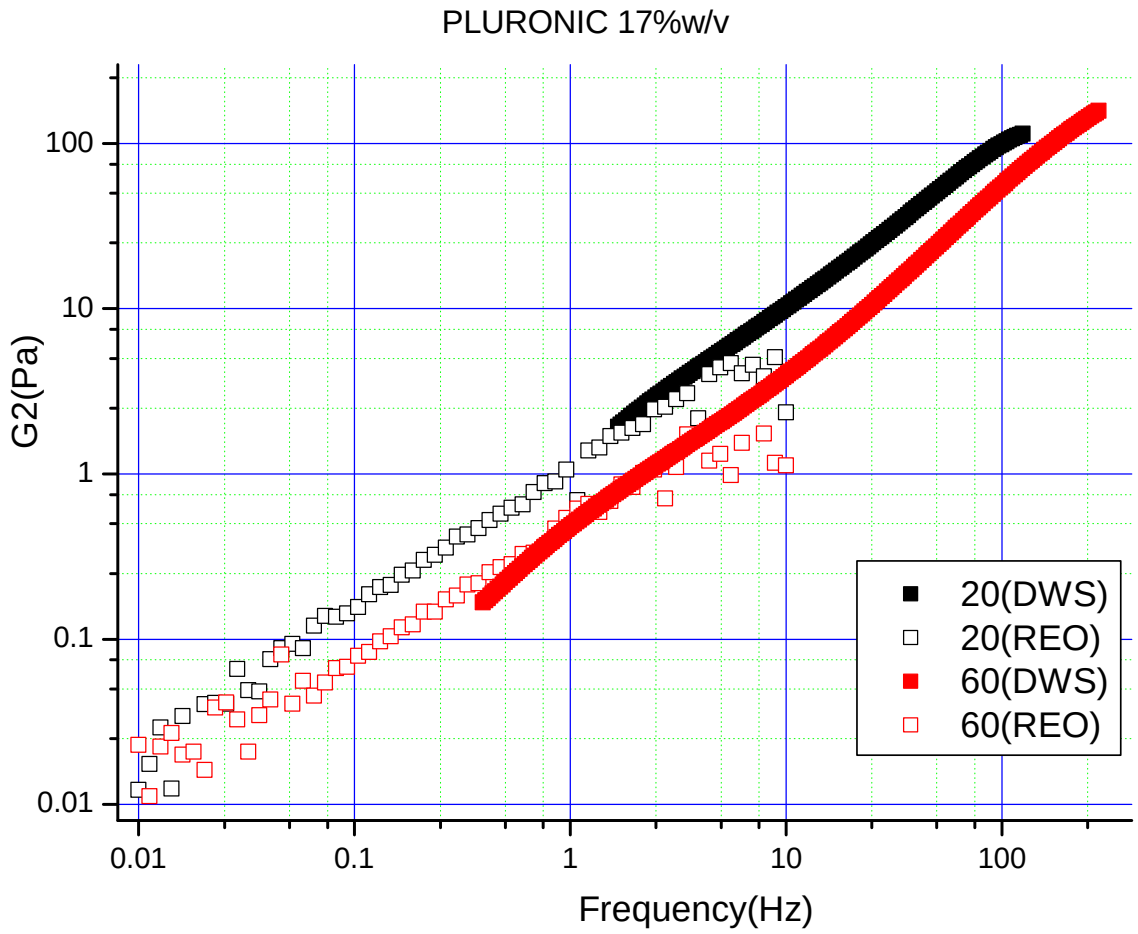


**Figure 8.13:** Viscous G2 component for the Pluronic F127 gel at different temperatures, 20 and 60°C

We will discussed the behavior of the system corresponding to 18%w/v over the 15 to 65°C temperature range. We have chosen this concentration because, at it will be seen, the Pluronic solution shows the reentrant sol-gel-sol transition as temperature is raised.

At low temperature the system behaves as a liquid, see Figures 8.14 and 8.15, and as the temperature is rised the system forms a gel. At this point the effect of the elastic component becomes significant until it dominates the mechanical behavior, see Figures 8.16 to 8.19. Further rising of the temperature brings the system again to a liquid state, with the elastic component becoming again negligible, see Figure 8.20.

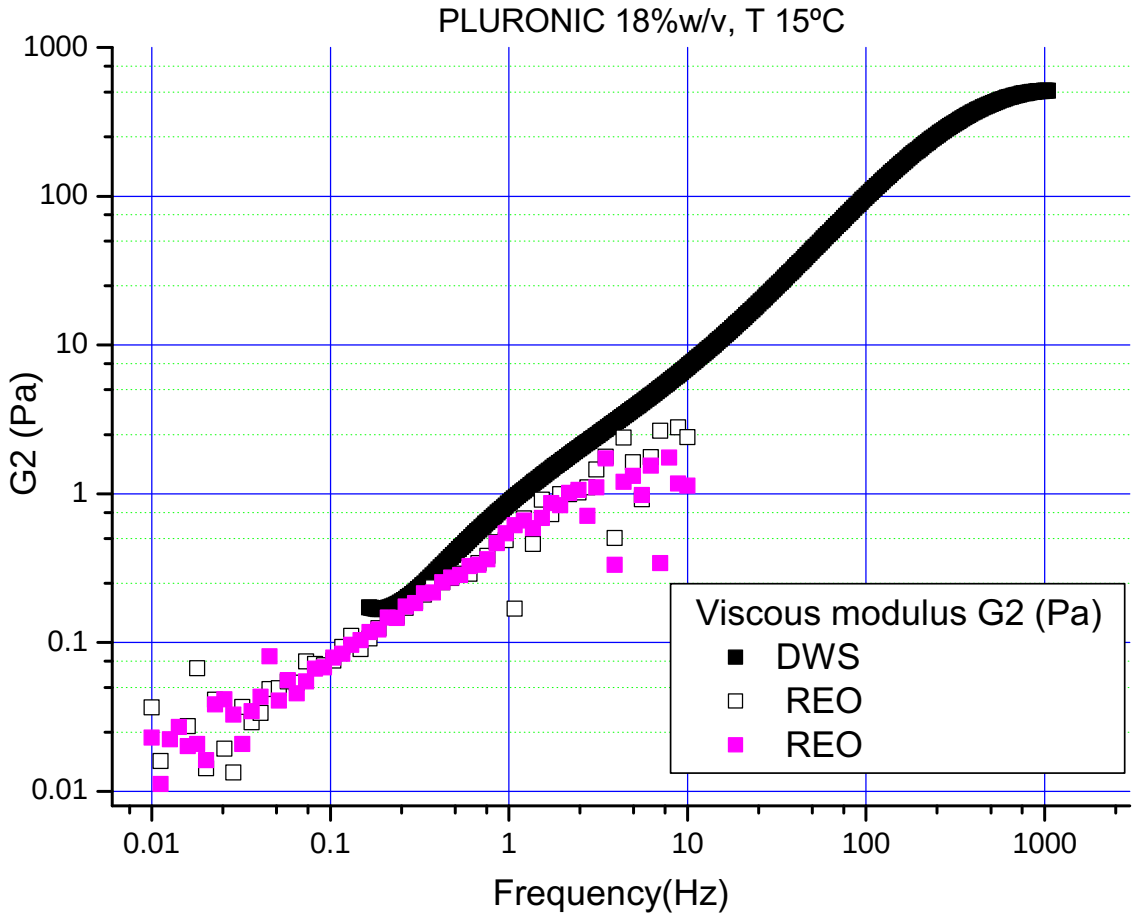


**Figure 8.14:** Viscous modulus G2 for the Pluronic F127 gel at 15°C

As it can be observed the agreement between the values of the complex shear moduli obtained by DWS and by mechanical rheometry is reasonable good in the frequency range of both techniques overlaping.

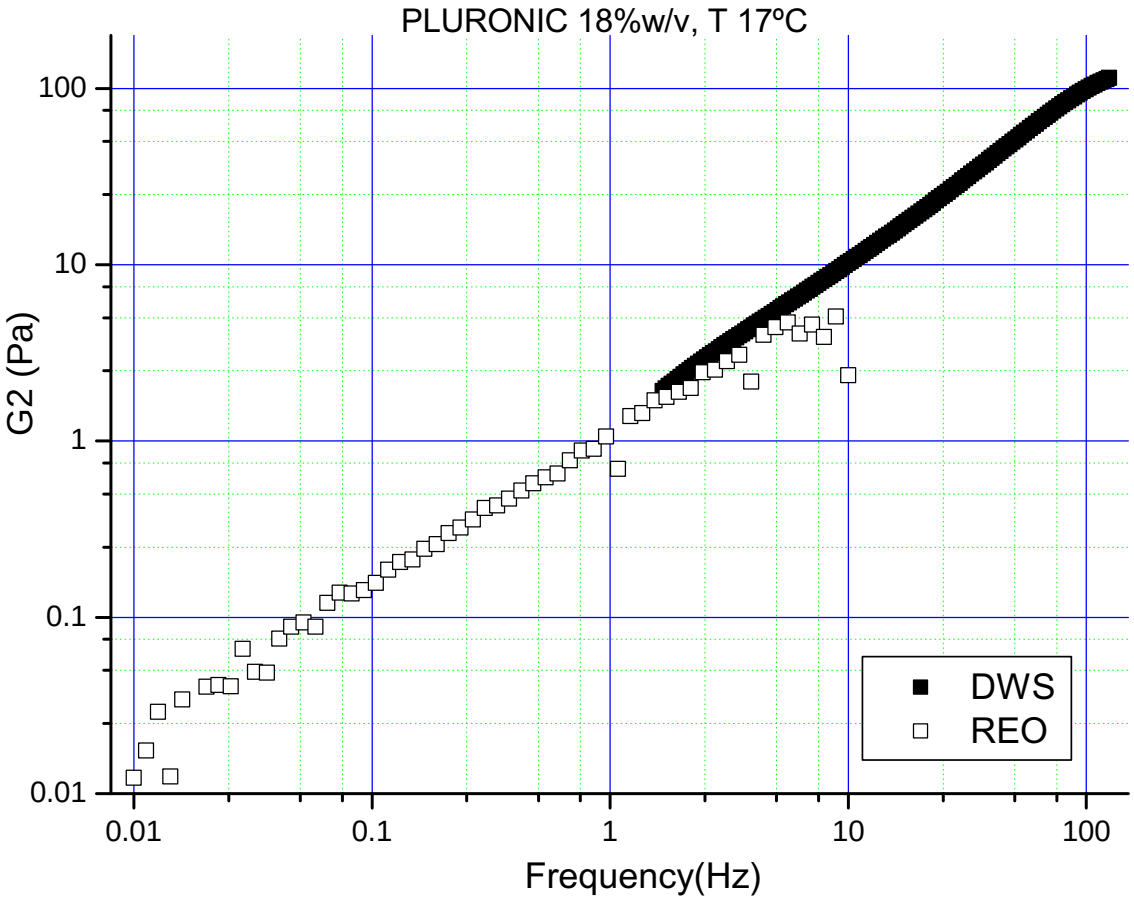


**Figure 8.15:** Viscous G2 component for the Pluronic F127 gel at 17°C

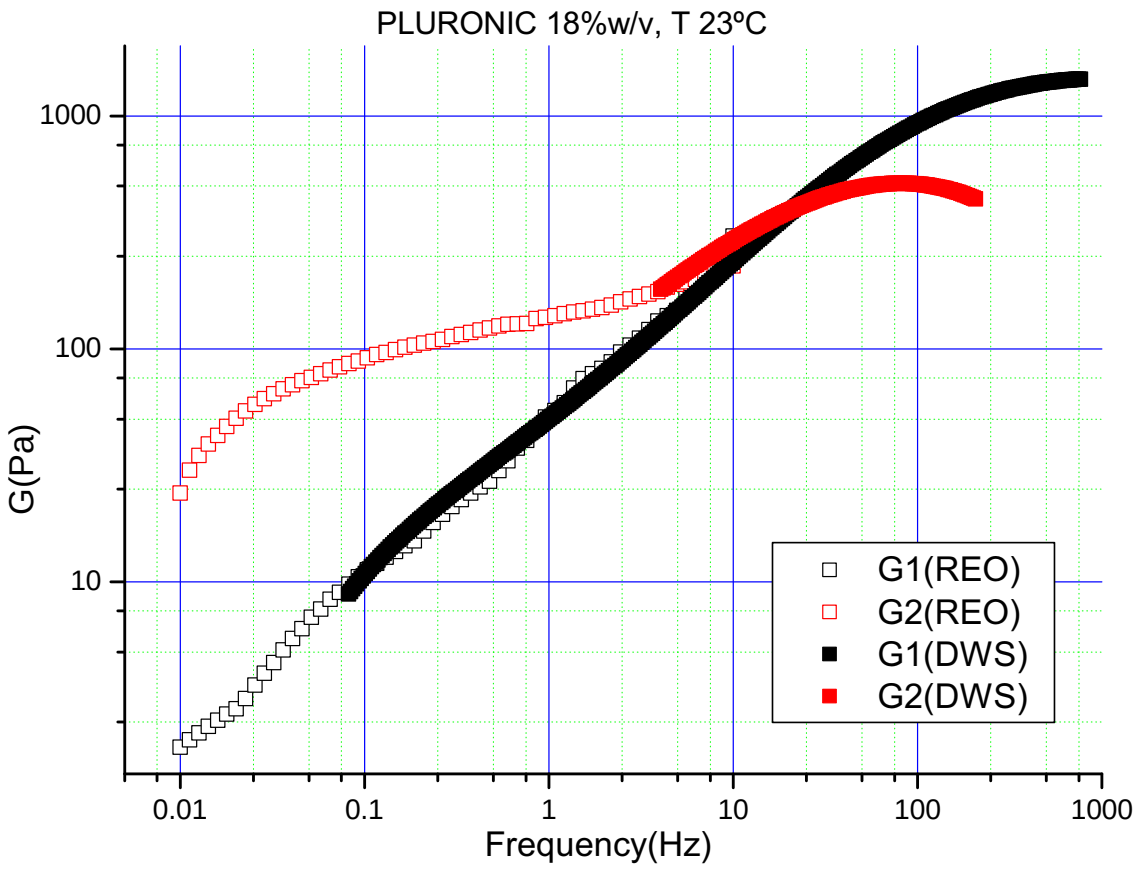


**Figure 8.16:** Viscoelastic moduli for the Pluronic F127 gel at 23°C

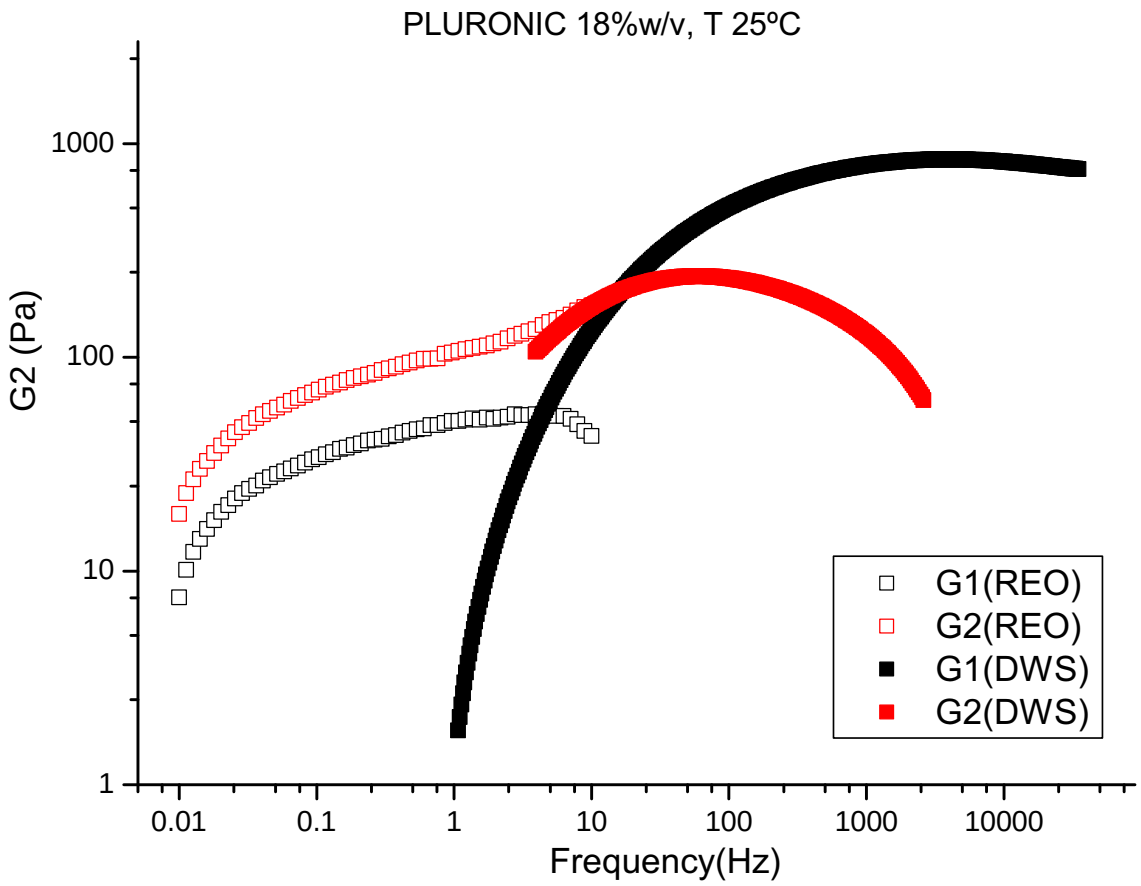


**Figure 8.17:** Viscoelastic moduli for the Pluronic F127 gel at 25°C

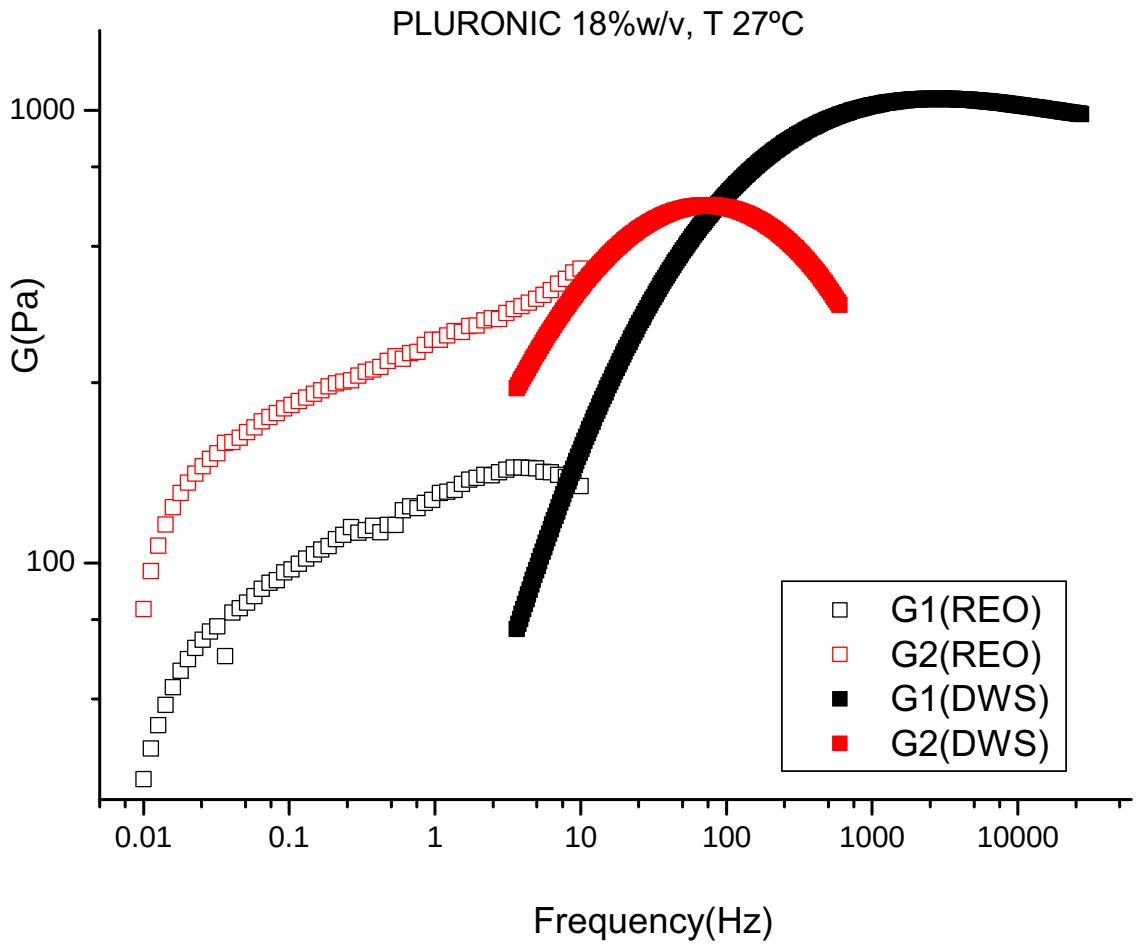


**Figure 8.18:** Viscoelastic moduli for the Pluronic F127 gel at 27°C

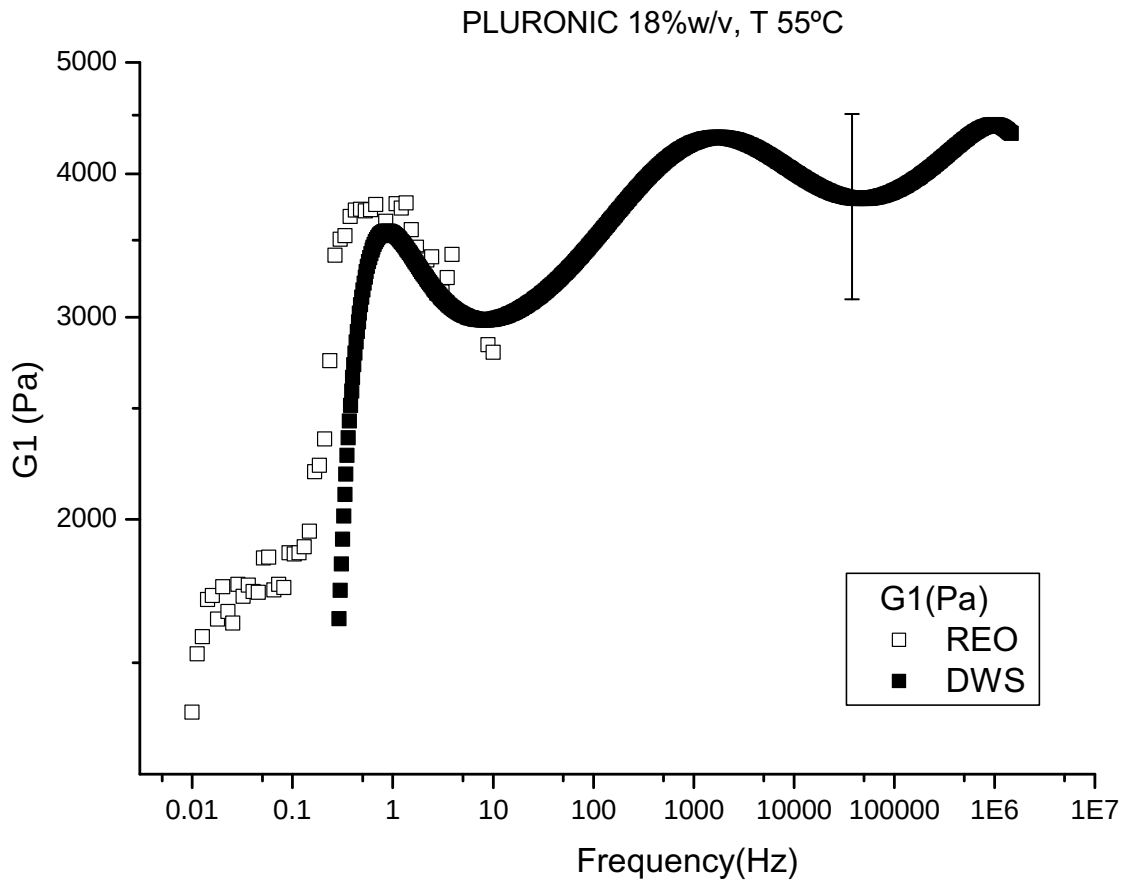


**Figure 8.19:** Elastic modulus G1 for the Pluronic F127 gel at 55°C

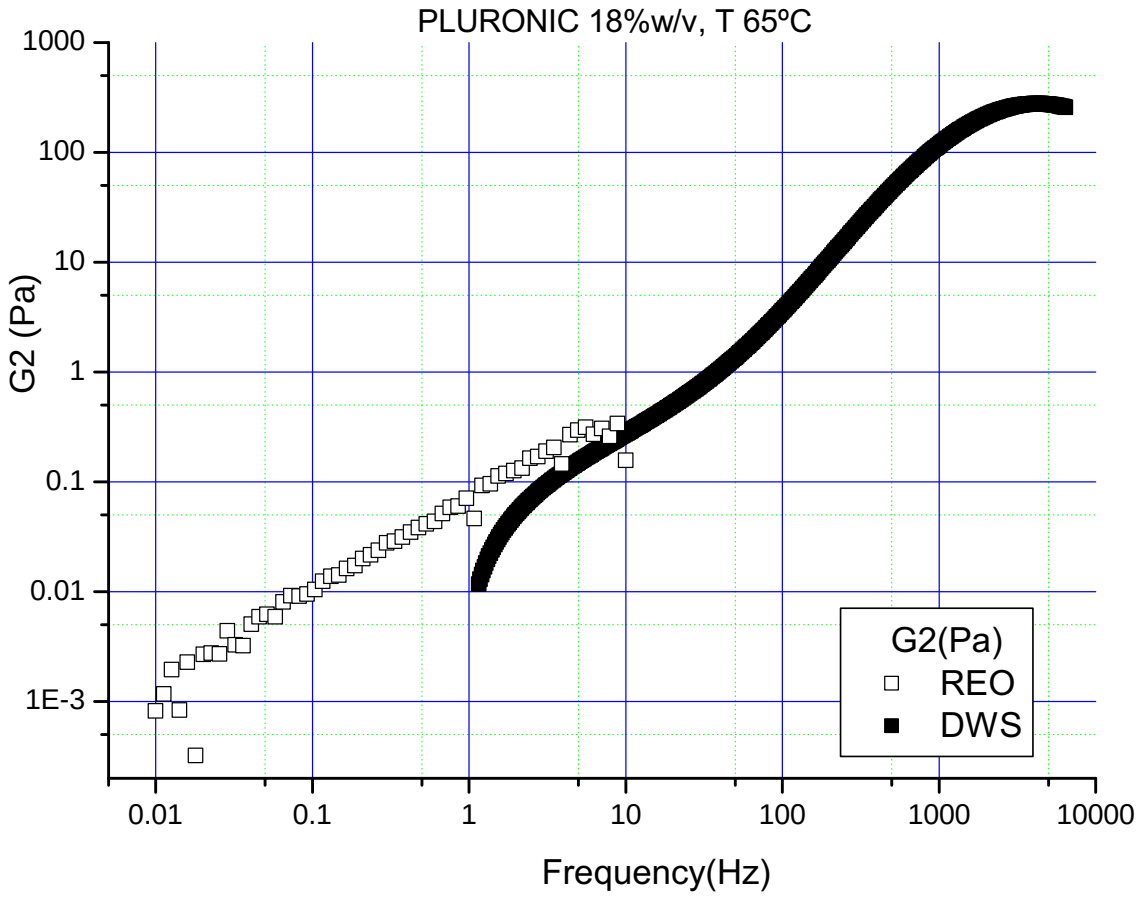


**Figure 8.20:** Viscous modulus G2 for the Pluronic F127 gel at 65°C

## 8.8. Microrheology

Now we will discuss the previous results in terms of the ad-hoc extension of the Maxwell model (see equation 8.3).

$$MSD = 6\delta^2 \left(1 - e^{\left(-\frac{D_0}{\delta^2}t\right)^{\alpha}}\right)^{\frac{1}{\alpha}} \left(1 + \frac{D_m}{\delta^2}t\right) \tag{8.3}$$

First of all it has to be remarked that the shape of the MSD curves for the Pluronic F127 apparently are different than for the agarose, for example see Figure 7.23, so it seems have an inverted from from that from the agarose with a concave shape, now pluronic have an MSD convexe. This means a distorsion in the paramenters involved in the extended Maxwell equation. A complete fit for the Pluronic F127 MSD is shown in Figure 8.21.

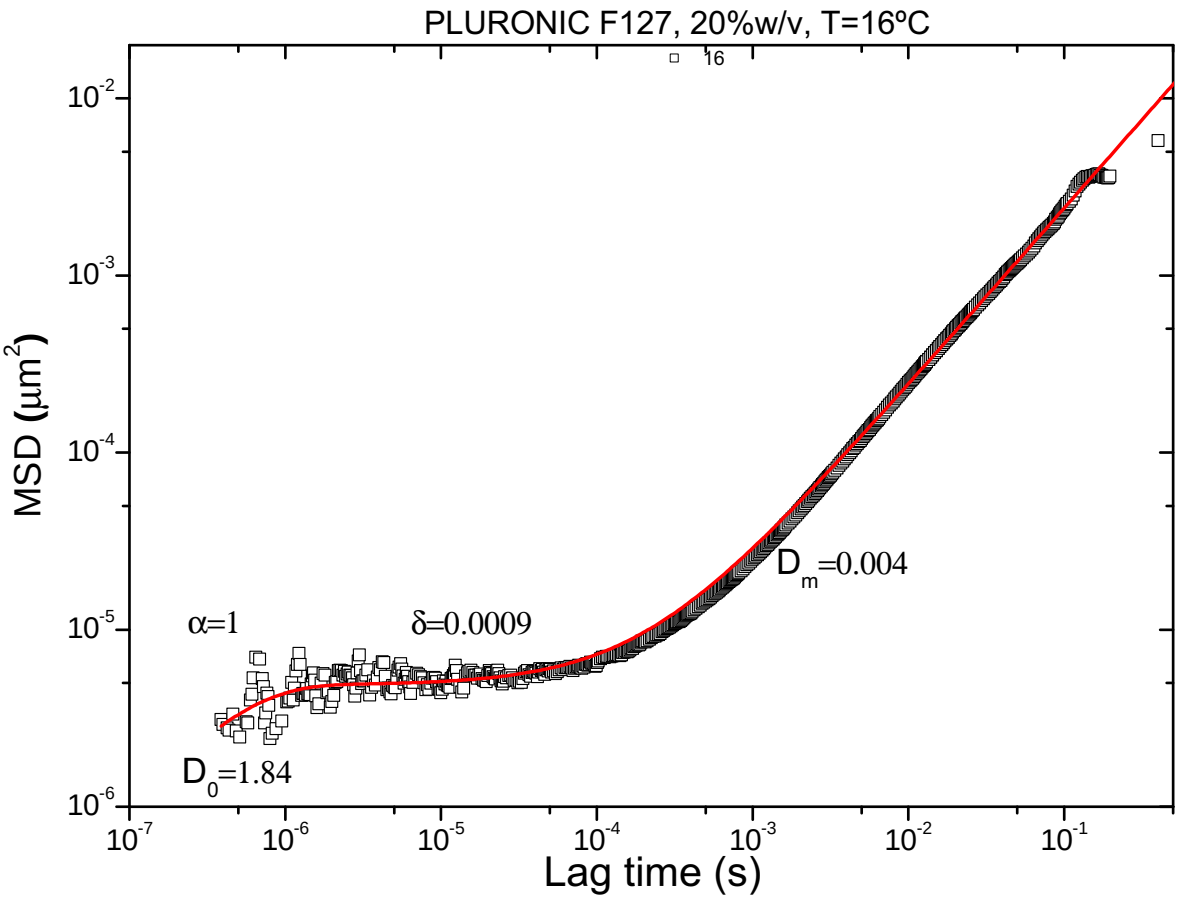


**Figure 8.21:** Curve of MSD as a function of Lag time of PS particles in Pluronic F127 gel at 20%w/v and 16°C

Since the short time part of the MSD curve is not observed, it has not been possible to determine the coefficient $D_0$.

Figure 8.22 shows the temperature dependence of the delta parameter and of the elastic modulus $G_0 = (k_B T)/(6\delta^2)$. The behavior of the diffusion coefficient $D_m$ is shown in Figure 8.23.

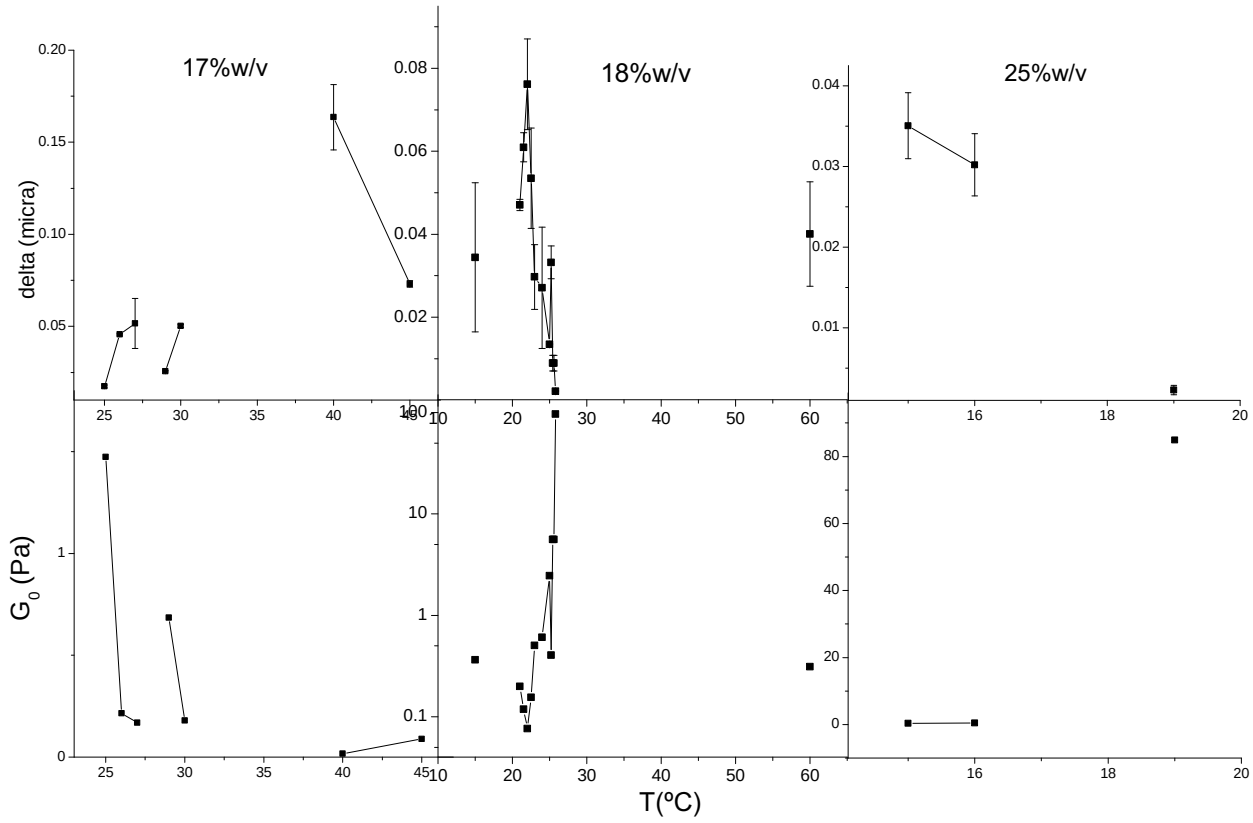


**Figure 8.22:** Evolution of the cage size $\delta$ parameter involved in equation 8.3 in Pluronic F127 solutions

Also, the viscosity is calculated from $G'' = \eta \cdot \omega$. Once, an Ahrrenius fit is probed for the viscosity data to see the variation with temperature taking into account that is valid for sol state, so we are in the Newtonian region that can be seen in Figure 8.24 and in Figure 8.25.

A molecular view of liquids can be used for a qualitative picture of the process of decrease in the bulk viscosity of a simple fluid with temperature. As the temperature increases, the time of interaction between neighbouring molecules of a liquid decreases because of the increased velocities of individual molecules. The macroscopic effect is that the intermolecular force appears to decrease and so does the bulk viscosity. The actual process can be quite complex and is typically represented by simplified mathematical or empirical models, so it is used the Arrhenius model.

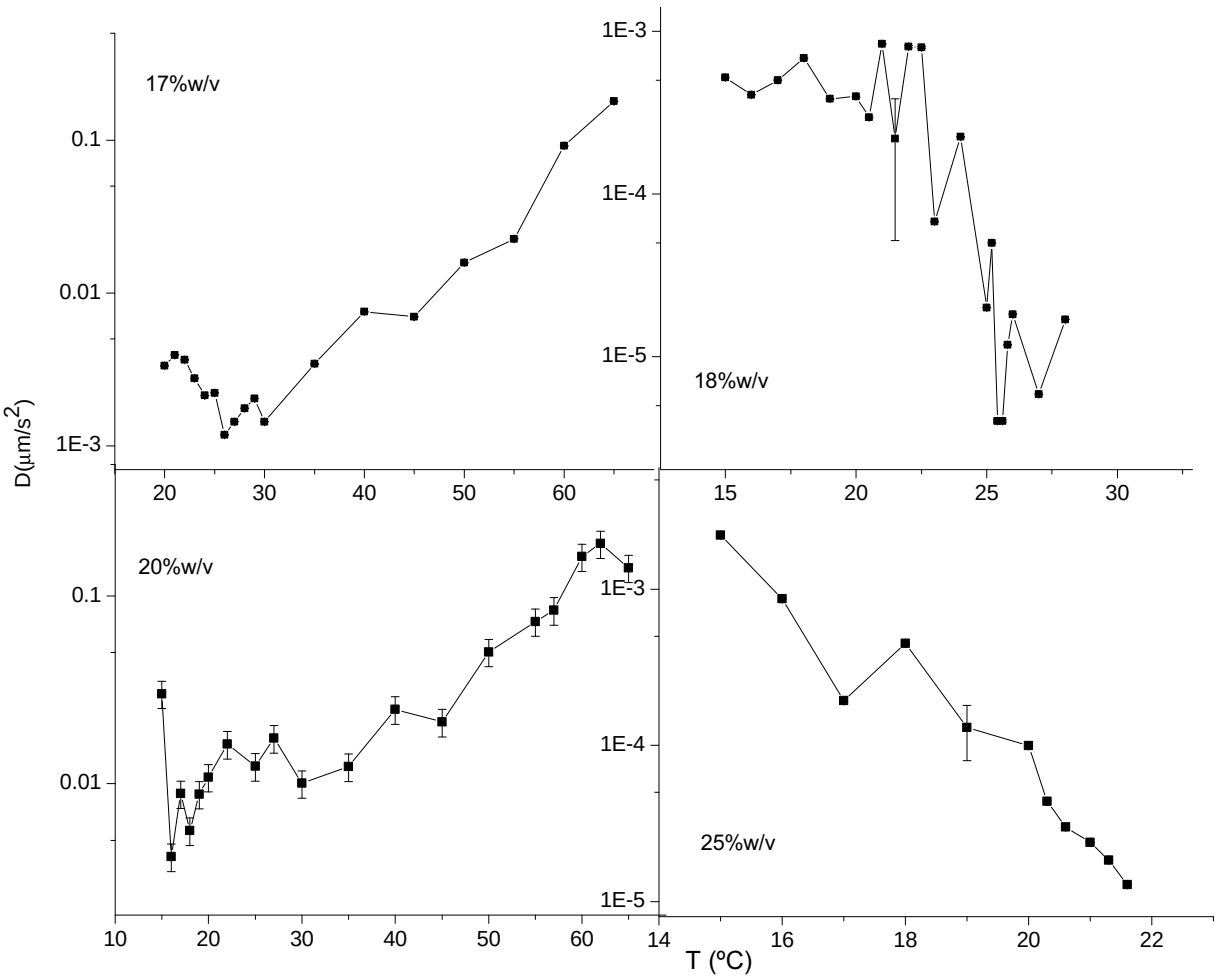


**Figure 8.23:** Evolution of the diffusion coefficient in Pluronic F127 gels

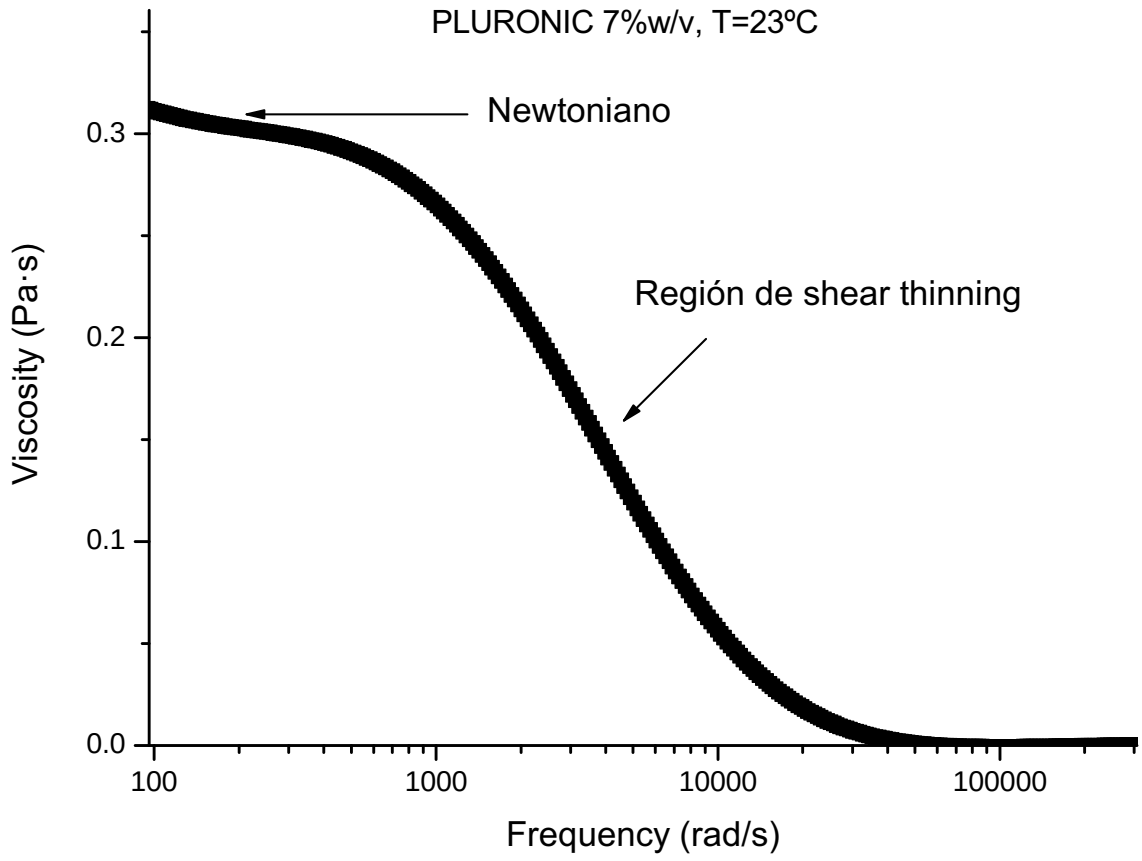


**Figure 8.24:** Newtonian behaviour in the sol state of the Pluronic F127 solutions

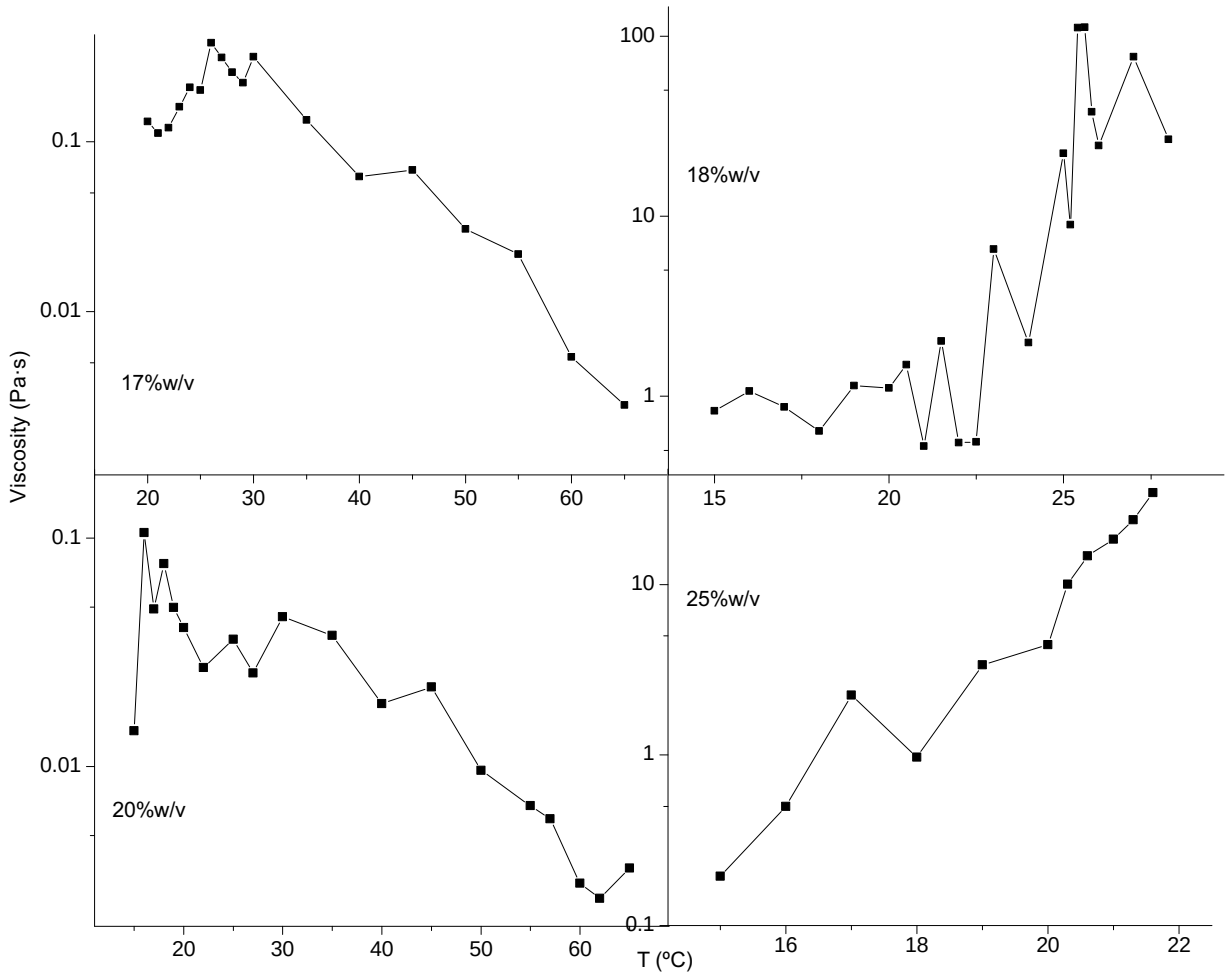


**Figure 8.25:** Evolution of viscosity with temperature in Pluronic F127 gels

This model is based on the assumption that the fluid flow obeys the Arrhenius equation for molecular kinetics:

$$\eta = A \cdot e^{\frac{Ea}{RT}} \tag{8.4}$$

where $T$ is temperature, $A$ is the preexponential factor, $Ea$ is the activation energy and R is the universal gas constant.

The Ahrrenius fit is quite reproducible for the viscosity of the pluronic samples like it is presented in Figure 8.26.

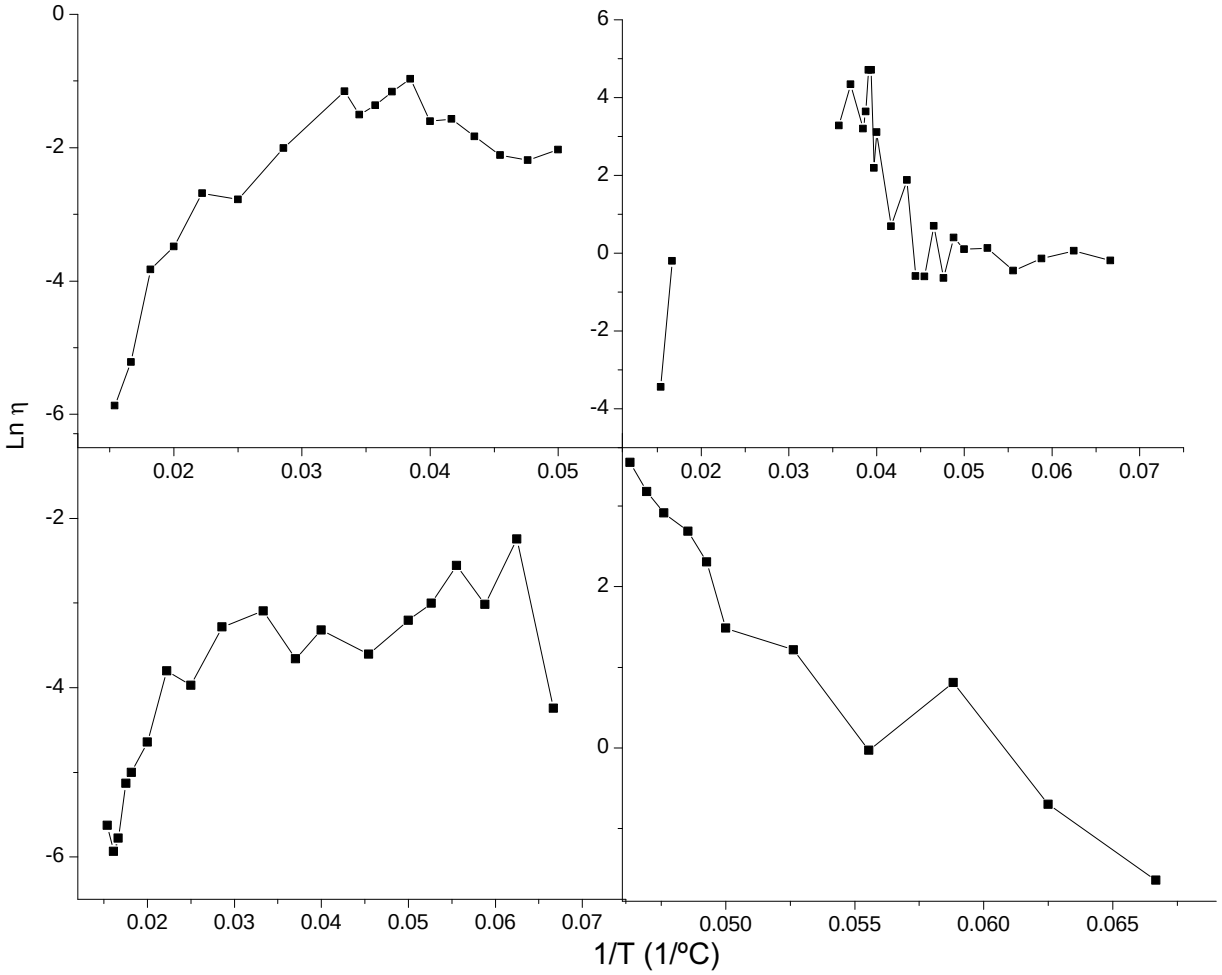


**Figure 8.26:** Ahrrenius fit for the viscosity of the pluronic samples

## 8.9. Conclusions Pluronic F127

Block copolymer Pluronic F127 is a very useful surfactant and has a qualify optimal concentration to be used as diagnostic drug. This concentration and an area range are that here have been studied to see the viscoelastic properties. The pluronic present a gel transition from low to high temperature making a loop at high temperature, instead of the agarose that the gel transition occurs from high to low temperature and without loop.

The intensity autocorrelation functions and the mean square displacements in the Pluronic show a signature of viscoelasticity. The shape of the Mean square displacement of the Pluronic F127 has a different form to the agarose, so it seems have an inverted from from that from the agarose with a concave shape, now pluronic have a convexe MSD shape. This means a distorsion in the paramenters involved in the extended Maxwell equation. At short time scales the MSD increases slowly, indicating nearly elastic motion; however, at long time scales, the value of the MSD increases steeply, indicating viscous flow.

The Ahrrenius fit is quite reproducible for the viscosity of the pluronic samples in the viscous region.

# Chapter 9

# MICRORHEOLOGY OF HYALURONIC ACID

## 9.1. Introduction

Hyaluronic acid (HA) is a natural polysaccharide present in eukaryotes cells and it is also synthesized by some bacteria.

Traditionally hyaluronic acid was extracted from animal cells, it was used the rooster combs, vitreous body, umbilical cord and now it is mainly produced via microbial fermentation with lower production costs and less environmental pollution. Hyaluronic Acid has been successfully produced on an industrial scale using Streptococcus sp. bacteria as the main producer.

Hyaluronic acid was first isolated by Karl Meyer and John Palmer in 1934 from bovine vitreous humor [83]. Human umbilical cord was shown by them to be a rich source of hyaluronic acid [84]. Before, in 1880, Portes reported that mucin from the vitreous body differs from other mucoids in cornea and cartilage and named it hyalomucine [85].

The chemical structure of HA consists of repeating monomer units of D-glucuronic acid and N-acetylglucosamine (Figure 9.1).

Solutions of HA are viscoelastic due to chain entanglement. HA is a highly hydrated polymer and the chains form an entangled network at relatively low concentration. This is essential for its lubricating function in joints, muscles and other tissues unions.

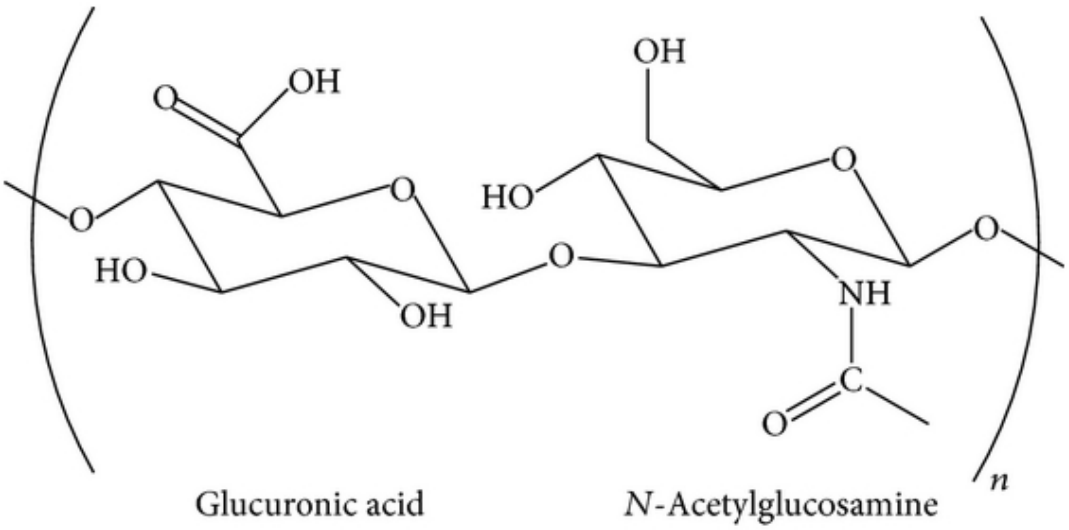


**Figure 9.1:** Hyaluronic acid structure

## 9.2. Gel preparation and experimental details

Hyaluronic acid was purchased from Sigma Aldrich (Germany) in sodium salt form. The comercial form is a powder so the preparation method is to weigh the amount of the hyaluronic acid into the proper destiled water volume, to obtain a weigh/volume concentration. To achieve an easier dissolution of the HA, the water should be cold, and when the hyaluronic acid is dissolved, it is kept in the fridge overnight, about 12 hours. HA aqueous solutions were investigated in the concentration range from 1 to 15 g/L, at different temperatures from 16 to 60°C and in presence of two types of salts: sodium chloride NaCl (monovalent cation) and calcium chloride $CaCl_2$ (divalent cation).

Two types of particles: titanium dioxide particles, $TiO_2$, diameter 127 nm (Degusa, Germany) and Polystyrene particles of 977 nm in diameter (kindly provided by the University of the Basque Country), which used for the DWS experiments as in the previous chapters for the Agarose and the Pluronic F127.

The details of the DWS sample preparation are the same than the described in the Agarose chapter.

## 9.3. Temperature influence

The rheological properties hve been studied in the temperature range of 16 to 60°C for each HA concentration. The results shown that the hyaluronic acid is

stable in this range of temperature with no relevant changes in the ICF´s shape.

HA solutions shows to have a simple viscoelastic behaviour following a Kelvin-Voigt model (see the model in Agarose chapter 7.21), as indicated by the linear shape of $G'' = \eta \cdot \omega$ and $G'$ is constant with frequency. This corresponds to single exponential decay of the intensity autocorrelation functions, and linear MSD curves. This results are shown in Figure 9.2 for the ICF, in Figure 9.3 for the MSD and Figure 9.4 for the viscoelastic moduli, all of then using $TiO_2$ particles in a 5% volume fraction.

The behavior using PS particles in the HA is the same as the represented by the $TiO_2$ particles, this comparison is more relevant when a salt is introduced, and it is showed and discussed next in the Comparison PS-$TiO_2$ particles section.

Figure 9.5 compares the results for the different concentrations at a fixed temperature, in this case 16°C. Because of the non dependence on the temperature the behavior for the rest of the concentrations and temperatures are the same.

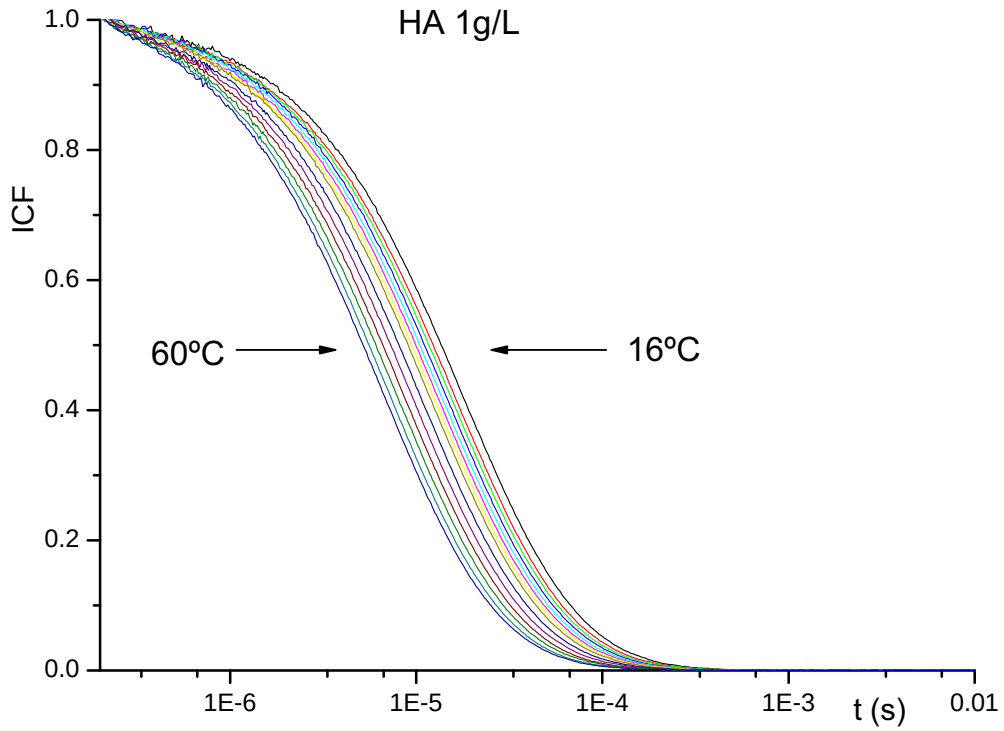


**Figure 9.2:** ICF of HA at 1 g/L with $TiO_2$ particles in the range 16-60°C. Temperatures correspond from right to left at 16,18,20,22,24,26,28,30,35,40,45,50,55,60°C

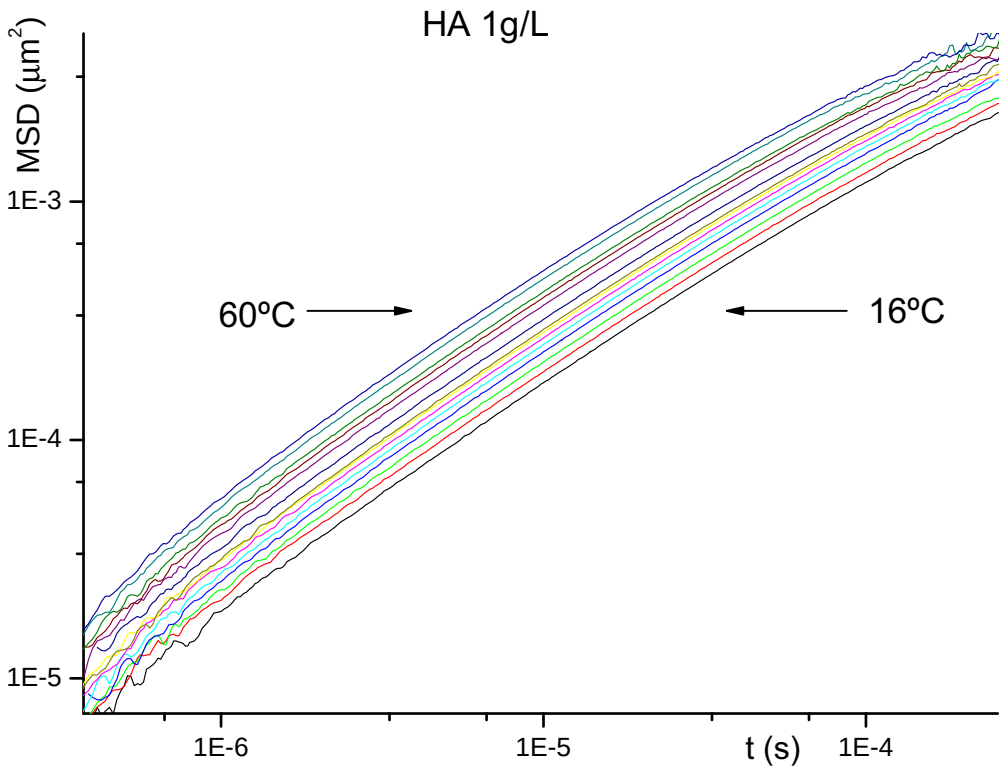


**Figure 9.3:** MSD of HA at 1 g/L with $TiO_2$ particles in the range 16-60°C.Temperatures correspond from right to left at 16,18,20,22,24,26,28,30,35,40,45,50,55,60°C

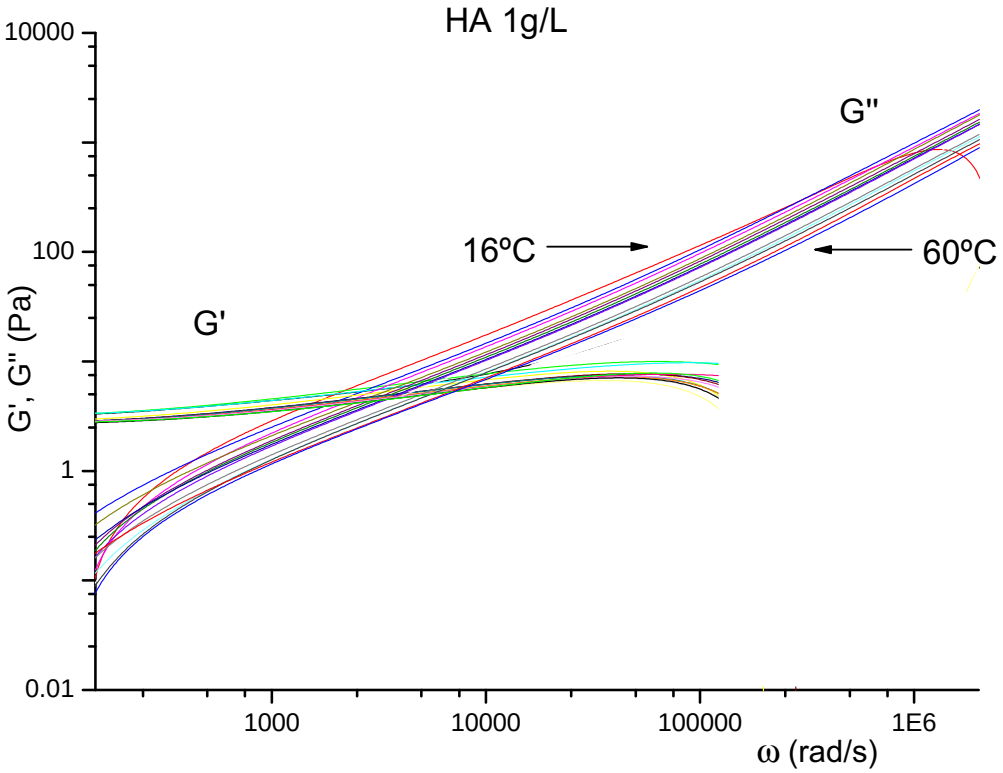


**Figure 9.4:** Viscoelastic moduli of HA at 1 g/L with $TiO_2$ particles in the range 16-60°C.Temperatures correspond from right to left at 16,18,20,22,24,26,28,30,35,40,45,50,55,60°C. It looks like a Kelvin-Voigt Model

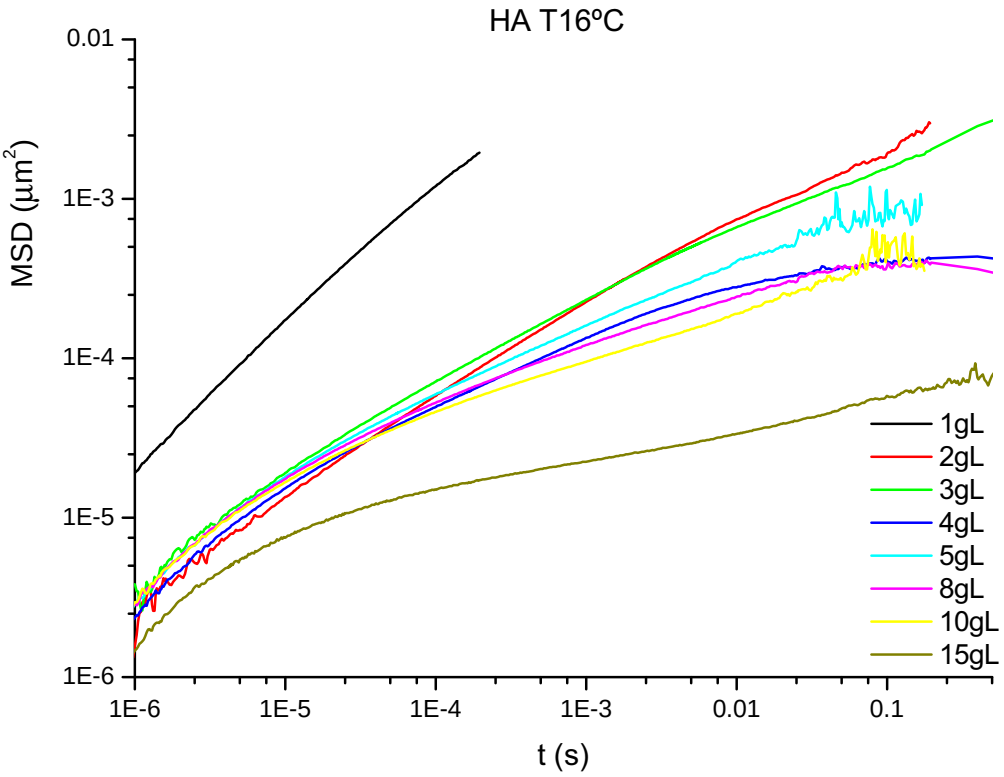


**Figure 9.5:** MSD at different concentration of HA from 1 to 15 g/L at a fixed temperature of 16°C

## 9.4. Effect of the ionic force

The ionic force influence is studied in this system because of it is neccessary to add salts in the HA medium to make it a viscoelastic material.

The higher HA concentations, 10 and 15 g/L, are selected for studying the influence of the ionic stregth on the viscoelastic behavior. Figure 9.6 shows the variation of the ICF as the salt sodium clhoride is added. It is observed that increasing the concentration of NaCl slows down the fluctuation's decay, and the shape of the ICF departs more from a single exponential function. This influence is further increased when a divalent cation is used, $CaCl_2$, as shown in Figure 9.7.

No changes in the shape of the ICF are observed till the stronger salt $CaCl_2$ and low temperature, from 30°C to 16°C, are used, because of this, it is decided to used a stronger salt and to get down the temperature to try observing more changes, so the same experiment were made with the calcium clhoride showing the results in the Figure 9.7.

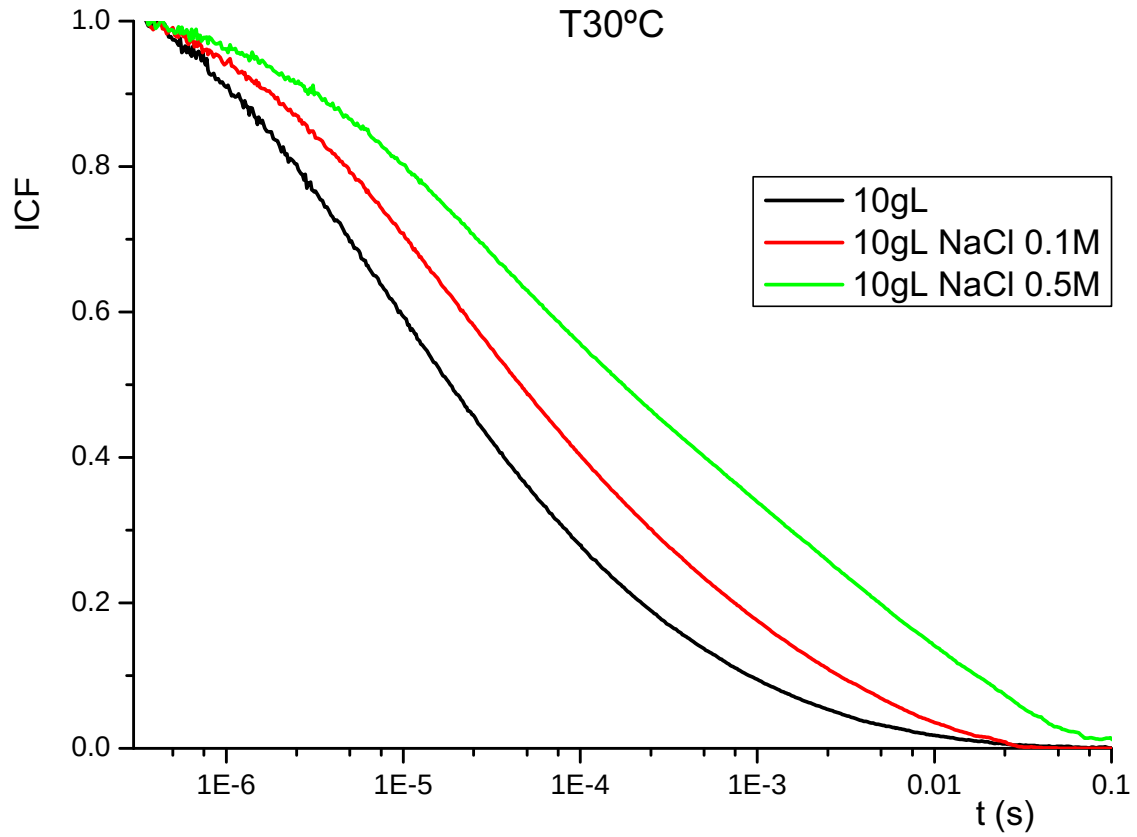


**Figure 9.6:** ICF at different concentration of NaCl in an 10g/L HA at temperature of 30°C. $TiO_2$ nanoparticles were used as probes

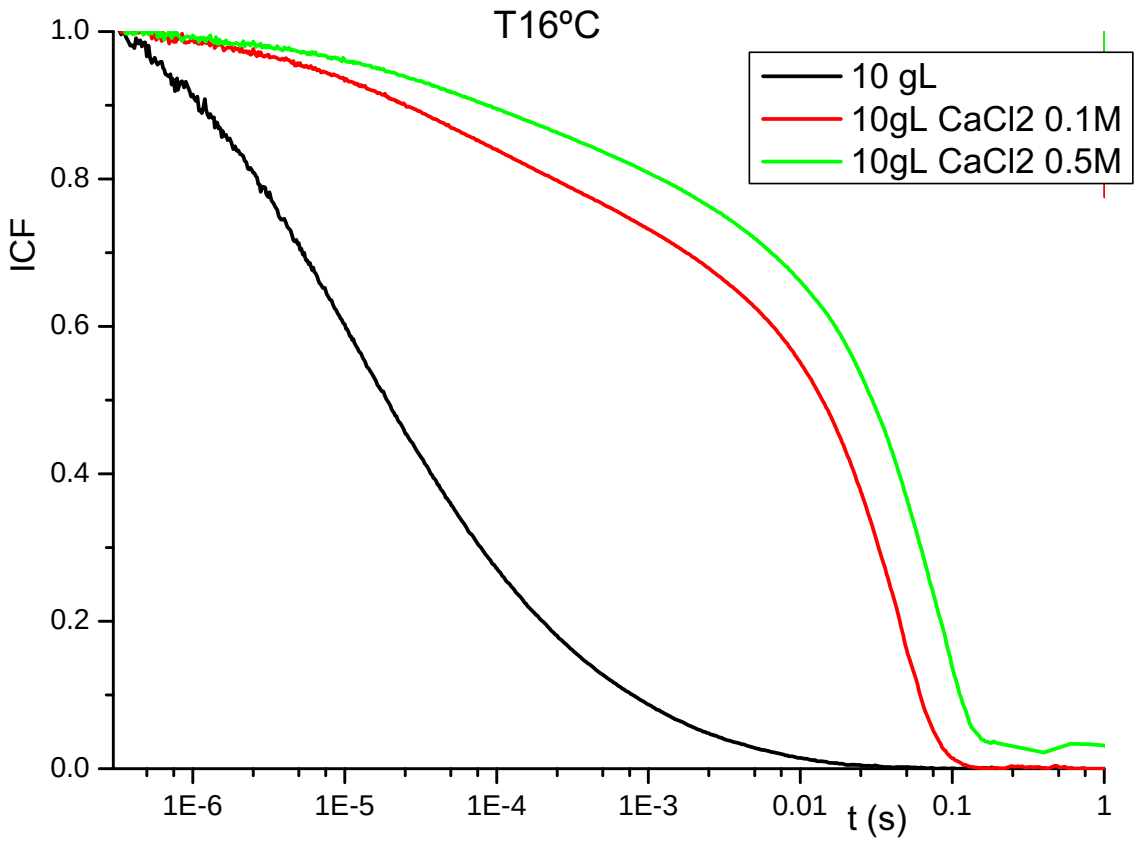


**Figure 9.7:** ICF at different concentration of $CaCl_2$ in an 10g/L HA at temperature of 16°C using $TiO_2$ particles

## 9.5. Comparison PS-$TiO_2$ particles

In the study of the Agarose solutions it was point out that there was a specific interaction between the polymer and the $TiO_2$ nanoparticles. The consequence was the failure of the Stokes-Einstein relationship. Since the nature of such specific interactions has not been unvealed and it was not found for the Pluronic F127 solutions, it is important to compare the results obtained for the PS microparticles and $TiO_2$ nanoparticles for Hyaluronic acid, because if its backbone has a different chemical nature.

The comparison of the results for the solutions without $CaCl_2$, in Figures 9.7 and 9.8, and 9.9 and 9.10, respectively, point out that the ICF decays at longer times when the PS particles are used.

Although the presence of $CaCl_2$ has a clear effect on the ICF, Figures 9.8 and 9.9 show that a five fold change of the salt concentration has little influence. In the case of $TiO_2$ nanoparticles the conclusion is very different.

In addition to the shift of the ICF on the time axis, also its shape is clearly modified.

We can conclude that, with different concentrations of salt it has been observed variation in the gelling capacity of the Hyaluronic acid. This behaviour has been observed in meat proteins [86].

By one hand, the gel strength increases by increasing the concentration of the monovalent sodium chloride 0.1 to 0.5M.

Otherwise, it was found that adding divalent cations diminished the strength and cohesiveness of gels [87, 88].

This behavior is also observed in some biological proteins, pectins, alginates. The effect is because divalent cations cause changes in the protein-protein interactions. It has been reported that the addition of sodium tripolyphosphate to saline soluble proteins, decreases the thermal aggregation. This possibly due to the ability to maintain phosphate molecules of protein in soluble state.

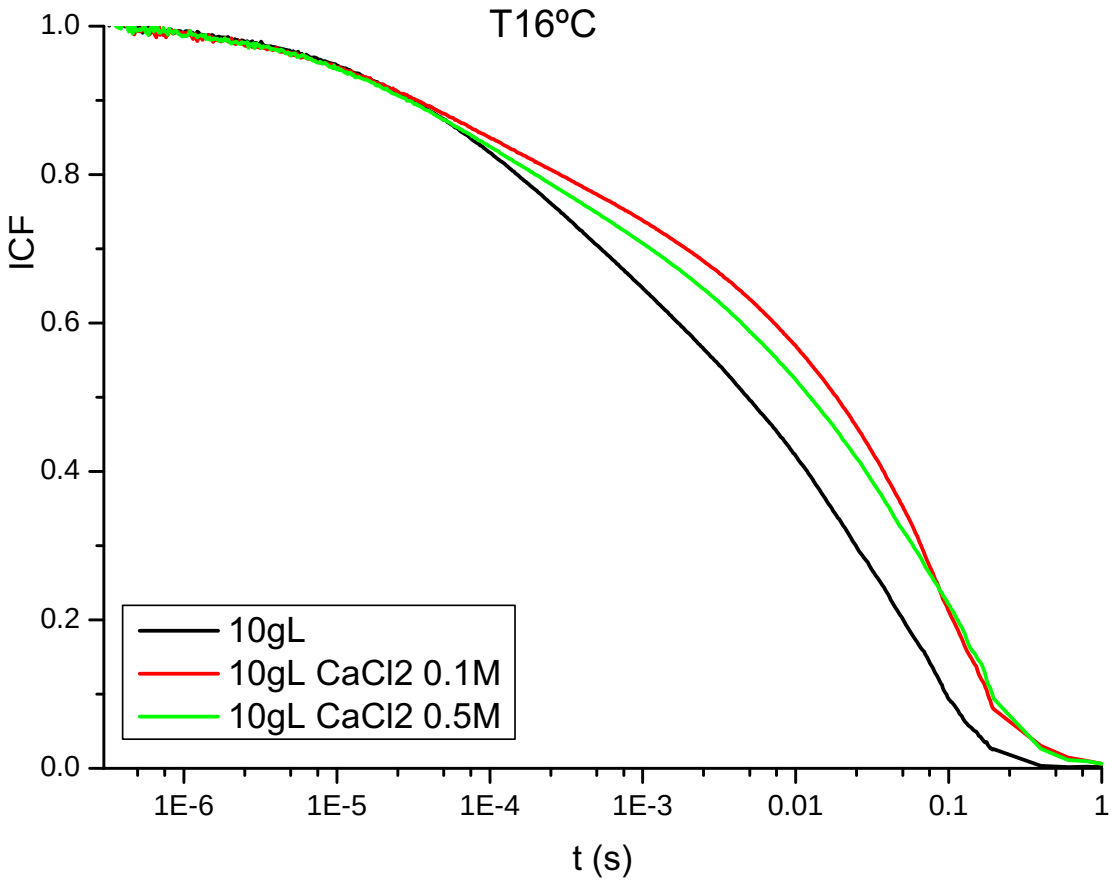


**Figure 9.8:** ICF at different concentration of $CaCl_2$ in an 10g/L HA at temperature of 16°C using PS particles

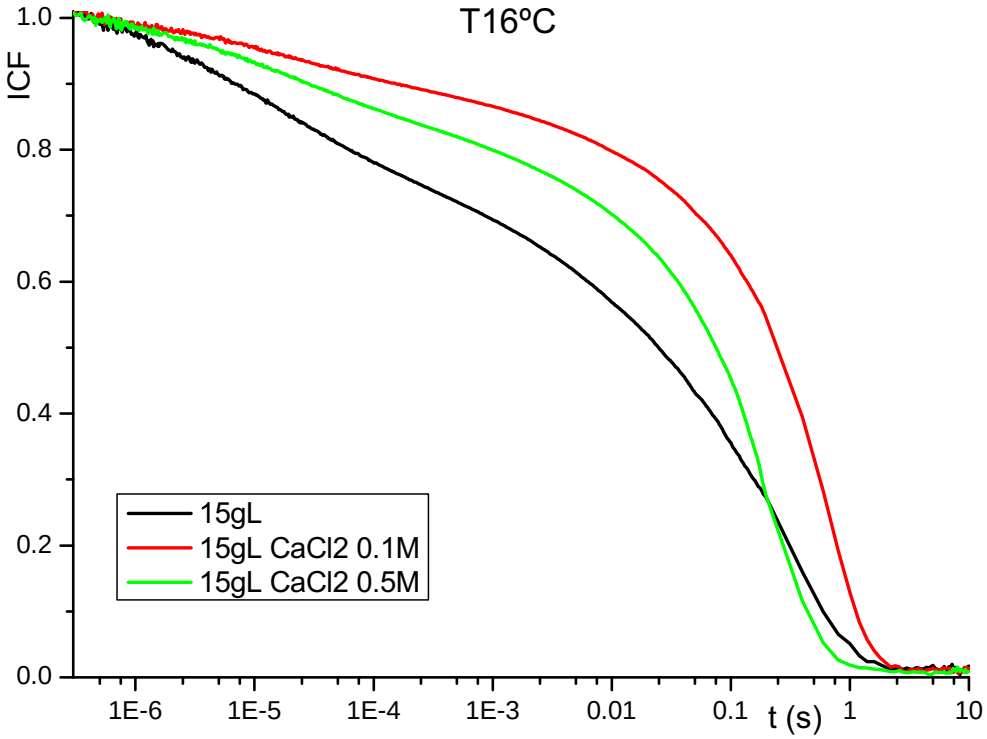


**Figure 9.9:** ICF at different concentration of $CaCl_2$ in an 15g/L HA at temperature of 16°C using TiO2 particles

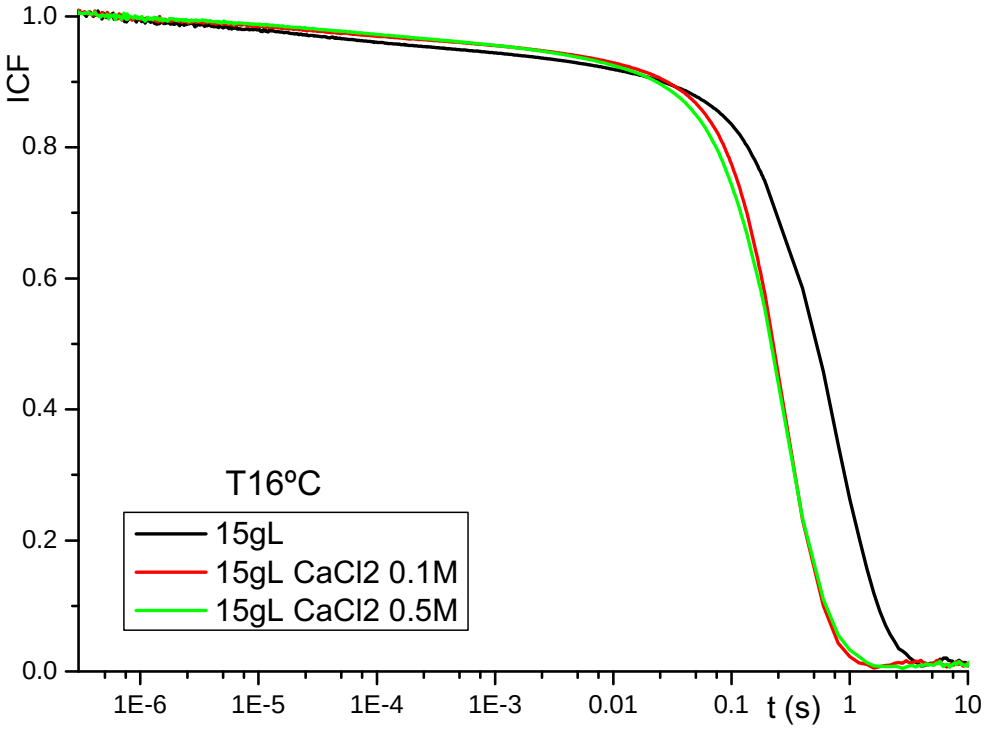


**Figure 9.10:** ICF at different concentration of $CaCl_2$ in an 15g/L HA at temperature of 16°C using PS particles

For the highest HA concentrations of 10 and 15 g/L, there are reliable the effect of the particle size in the form of the ICF, observing two aspects, a stronger effect in the decay that deforms the previous ICF decay without salt and also with the monovalent salt, Figure 9.2 and Figure 9.9 respectively, and a later decay for the PS particles, that means that the bigger particles move slowly in the gel of hyaluronic acid, Figures 9.8 and 9.10.

Going to the MSD which are presented using the $TiO_2$ nanoparticles and the PS microparticles and also for both with the two types of salts NaCl and $CaCl_2$, Figures 9.11 and 9.12 respectively. The most significant changes produce for the high HA concentration using the smaller particles and with the $CaCl_2$ salt, like it can be seen in the Figure 9.13, so it reveals that the ionic force has an important effect in the viscoelasticity properties in the hyaluronic acid gel.

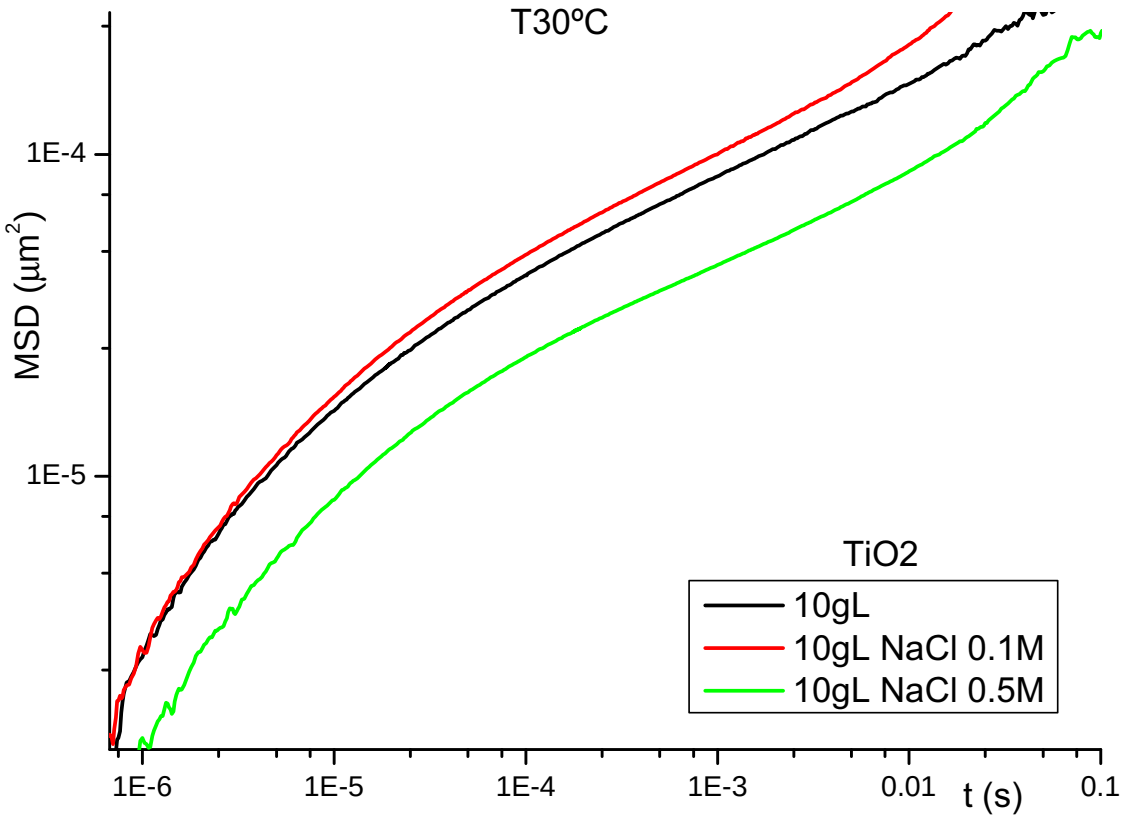


**Figure 9.11:** MSD for an 10g/L HA with NaCl at temperature of 30°C using $TiO_2$ particles

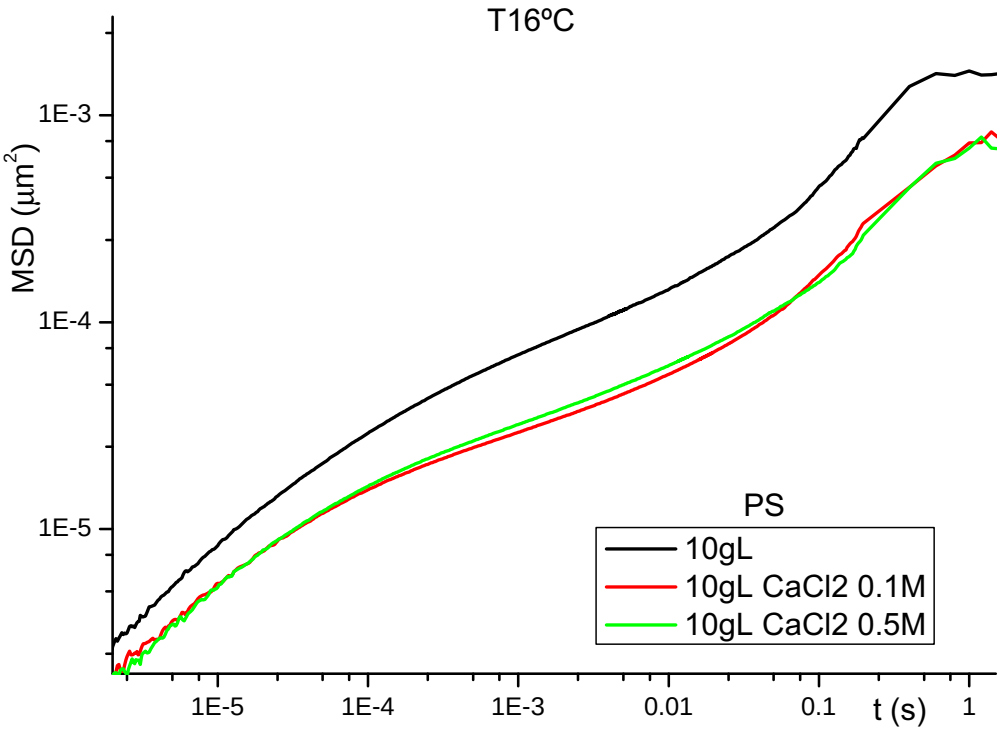


**Figure 9.12:** MSD for an 10g/L HA with $CaCl_2$ at temperature of 16°C using PS particles

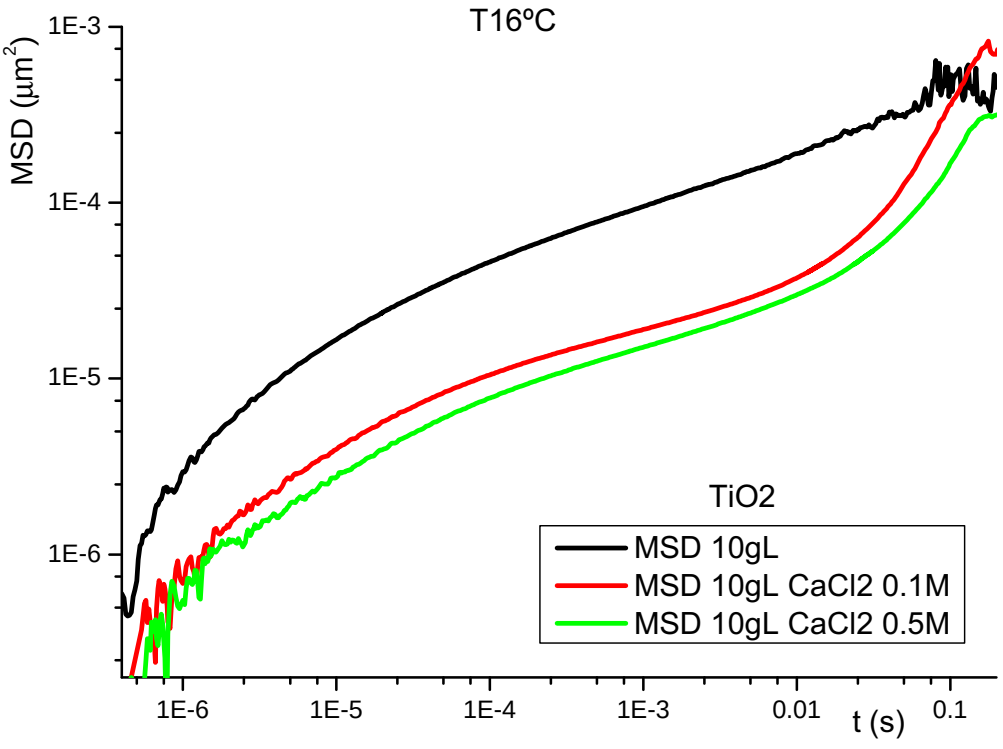


**Figure 9.13:** MSD for an 10g/L HA with $CaCl_2$ at temperature of 16°C using $TiO_2$ particles

Figure 9.14 shows the MSD for the PS and $TiO_2$ particles in HA at 15 g/L without any salt, and it reveals the hoped behavior, so the smaller particles move faster that the bigger ones.

This trend constinues this way for the $TiO_2$ nanoparticles when using $CaCl_2$ 0.1M, but when the concentration of this salt is 0.5M the movement of the particles of PS is faster at lower times. This behavior may be due to the divalent cation effect.

For lower concentrations the effect is the same but not so remarkable like in the higher ones.

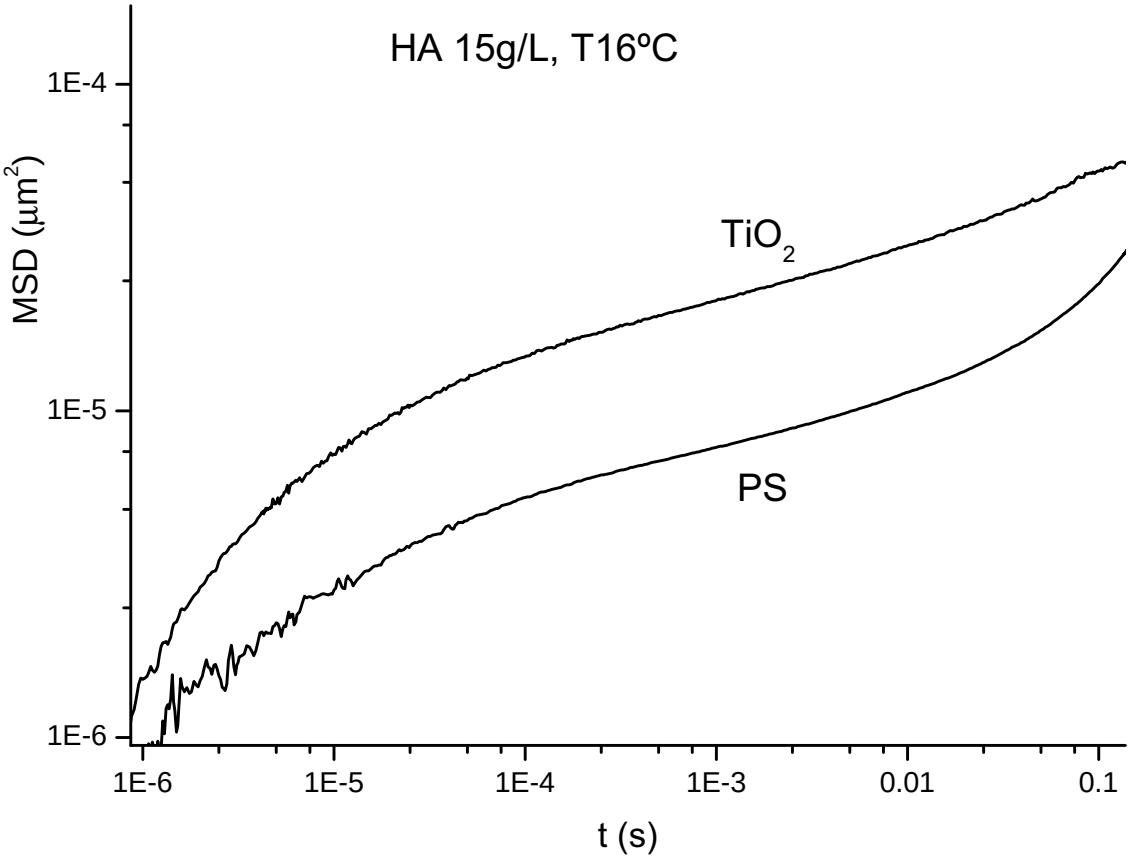


**Figure 9.14:** MSD for an 15g/L HA at temperature of 16ºC without salt

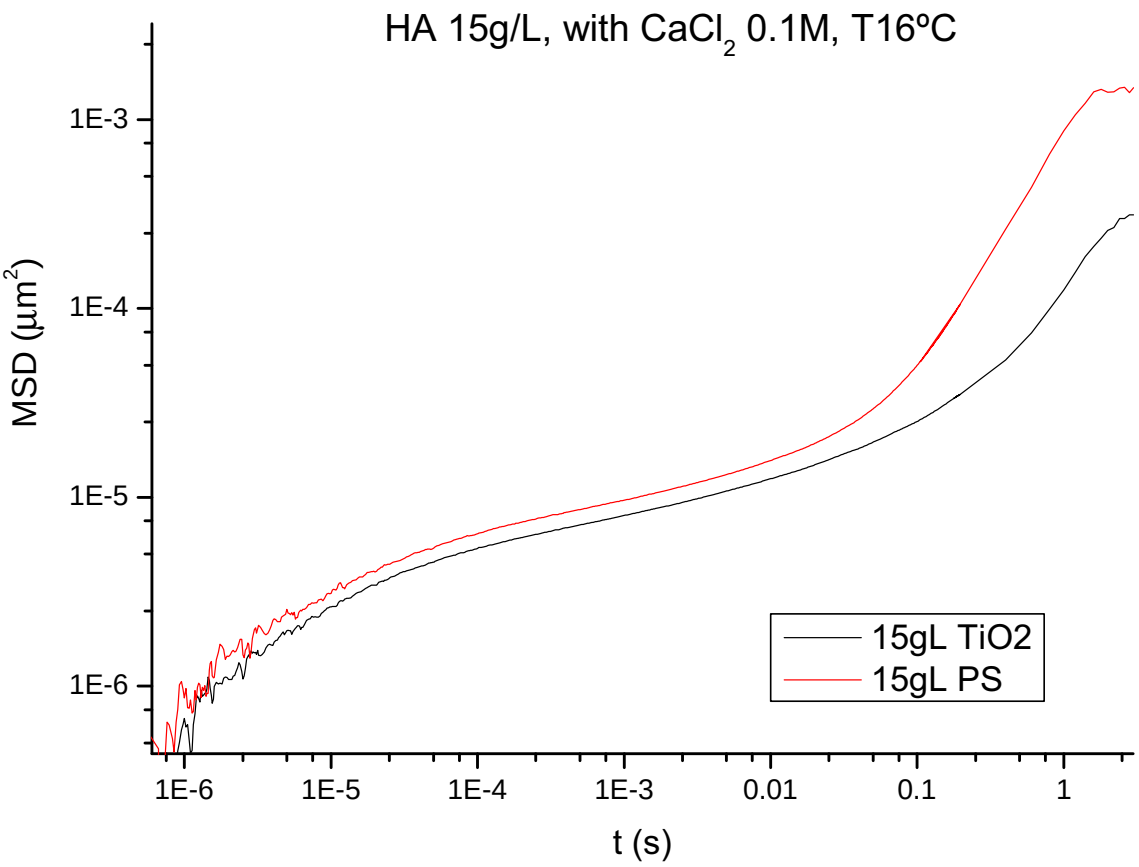


**Figure 9.15:** MSD for an 15g/L HA with $CaCl_2$ 0.1 M at temperature of 16°C

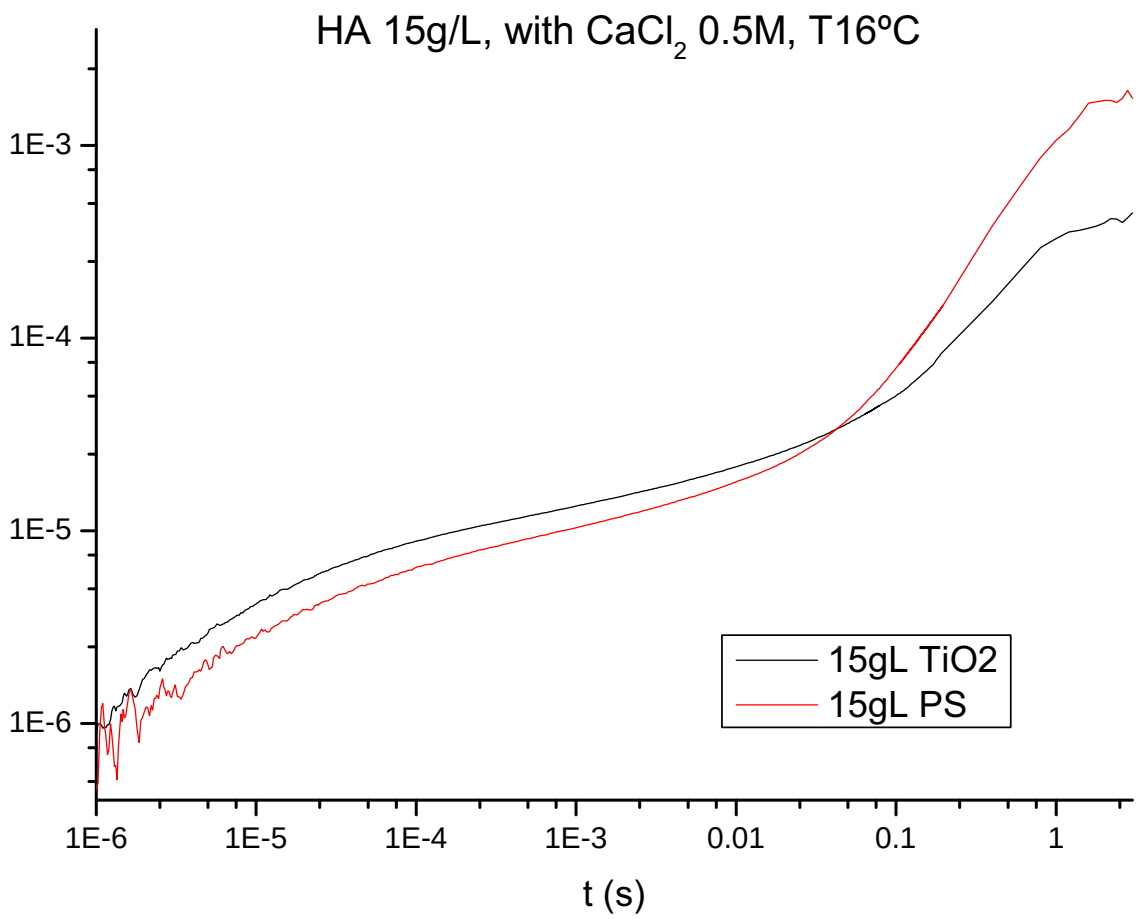


**Figure 9.16:** MSD for an 15g/L HA with $CaCl_2$ 0.5 M at temperature of 16°C

## 9.6. Viscosity

In a viscoelasticity fluid like Hyaluronic acid, viscosity is obtained from the viscous modulus, $G'' = \eta \cdot \omega$ and has an evolution with frequency.

Figure 9.17 shows the viscosity curves of hyaluronic acid solutions from low to high concentration obtained at 16°C. The shape of the curves is characteristic of pseudoplastic liquids with some remarks: the first Newtonian plateau cannot be observed at low frequency. A shear thinning at intermediate shear rates is observed and finally, the second Newtonian plateau is found at high shear rates for all the samples, except for the less concentrated sample where the viscosity in practically constant in the hole region. A similar behavior is obtained for the viscosity curves at other temperatures.

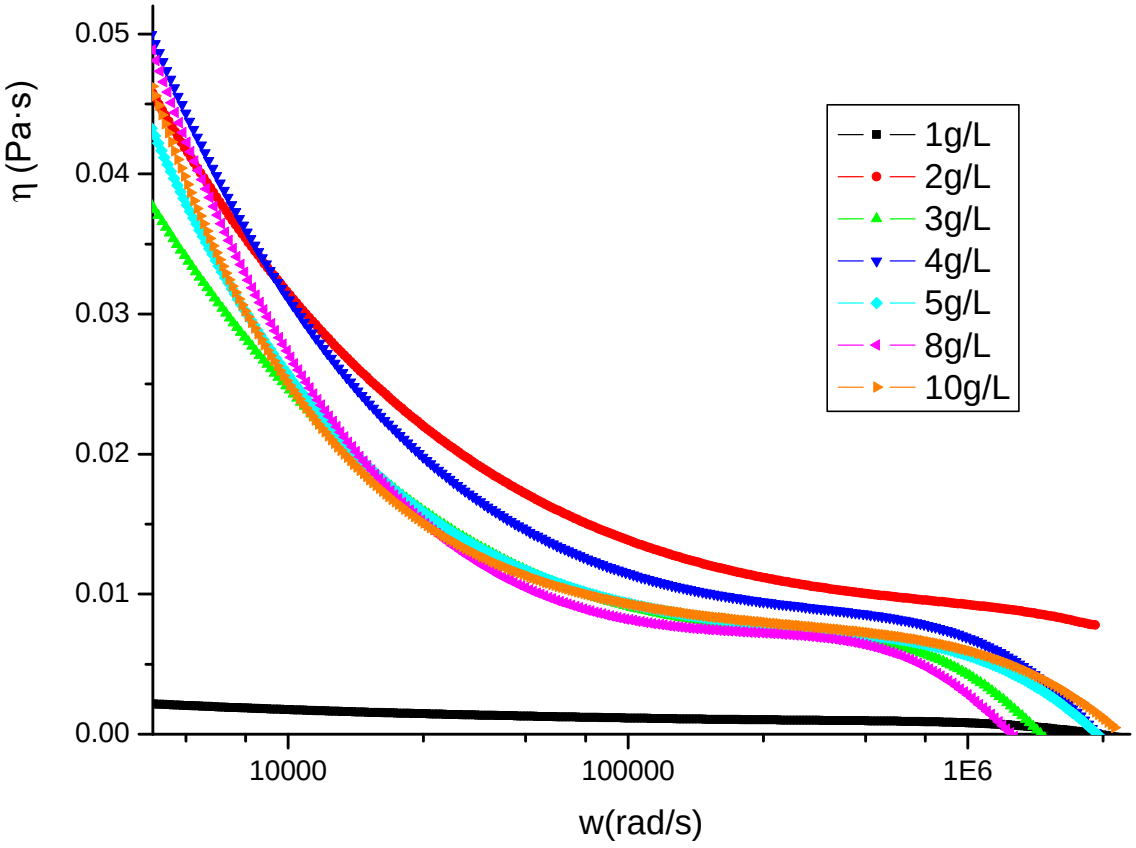


**Figure 9.17:** Viscosity curves at a temperature of 16°C for hyaluronic acid solutions

## 9.7. Rouse-Zimm theory to model Viscoelastic moduli

Following the bibliography from Oelschlaeger et al [89], they use a development in the Rouse-Zimm model for viscoelastic properties to be studied.

The first theories on the viscoelastic behavior of dilute emulsions given by Oldroyd [90],[91] also appeared in the fifties they were not accompanied by the appropriate experimental effort. The reason for this can be attributed to an experimental difficulty concerning ordinary emulsions. The largest relaxation time $\tau$ for an emulsion droplet with an interfacial tension $\gamma$ can be estimated as $\tau = R \cdot \eta/\gamma$, where R is the radius of the droplet and $\eta$ the viscosity of the emulsion.

In an harmonically oscillating shear experiment with angular frequency $\omega$ the reciprocal wave number is

$$\frac{\lambda}{2\pi} = \frac{1}{\omega}\sqrt{\frac{2}{\rho}\frac{G'^2 + G''^2}{\sqrt{G'^2 + G''^2} + G'}} \tag{9.1}$$

where G' and G" are the real and imaginary parts of the complex modulus respectively and $\lambda$ is the chain length and $\rho$ is the density of the liquid. For dilute emulsions or suspension at $\omega = 1/\tau$ this $\lambda$ length is at low volume concentrations about $10^{-6}$m. Consequently no bulk properties can be measured for ordinary emulsions in a dynamic shear experiment. This equation is only valid for dilute suspension, and can not reproduce the results for gels, therefore we not apply it, but it written here because in one of the first theories in viscoelastic fluids.

In the seventies the situation changed. On large scale information on so called microemulsions became available. If droplets of these emulsions are almost spherical they have a radius between $10^{-8}$ and $10^{-6}$m while their interfacial tension is very small ($10^{-4} - 10^{-7}$ N/m). In addition it turned out to be possible to make emulsions with a radius of about $5 \cdot 10^{-8}$ m [92]. In the mean time adequate apparatus development [93] enhanced the possibilities for the investigation of emulsions. As well for emulsions with small radius as for microemulsions corroborations could be given for the notion of linear viscoelastic behaviour of emulsions due to interfacial tension effects. A striking feature of some microemulsion results in particular was that the complex modulus showed more than two relaxation times which could not be accounted for by Oldroyd's theories. There may be several explanations for this phenomenon. In some papers the concept of the influence of thermal fluctuations of the droplet surfaces are pursued [94], but a complete theory cannot be given easily.

In the fifties fundamental research on the linear viscoelastic behaviour of (semi)dilute polymer solutions got great impetus to which Rouse [95] and Zimm

[96] theoretical work and the possibility of the measurement of the complex modulus of these systems significantly contributed. In the Rouse model, each molecular chain is subdivided into several submolecules that are each large enough that they obey Gaussian statistics. Each submolecule is represented by a spring, which accounts for ist elasticity, while its mass, which is responsible for the ehnergy dissipated by the moving submolecule in the viscous medium, is represented by a bead. The Rouse theory predicts that the diffusion coefficient of the chains in very dilute solutions is

$$D = \frac{k_B T}{M\xi} \tag{9.2}$$

where M is the molecular wieght of the chain and $\xi$ is the friction coefficient per submolecule. This expression takes not into account the hydrodynamic interactions.

The theory of Zimm uses the assumptions of the Rouse theory and considers hydrodynamic interactions between the moving submolecules and the solvent.

In terms of number density of Kuhn monomers (N), the overlap concentration c* is

$$c* = \frac{N}{R^3_{dilute}} \tag{9.3}$$

with N is the number of Kuhn monomers in the chain and $R_{dilute}$ is the dilute solution size of the chain.

Neutral polymers quite generally,

$$R_{dilute} \sim N^{\nu} \tag{9.4}$$

and

$$c* = \frac{N}{R^3_{dilute}} \sim N^{1-3\nu} \tag{9.5}$$

with $\nu = 1/2$ for a theta-solvent, $\nu = 0.588$ for good solvent and $\nu = 1$ for polyelectrolytes without salt; the three universality classes for polymer solutions. A theta-solvent is a solvent in which polymer coils act like ideal chains, assuming exactly their random walk coil dimensions therefore in a good solvent.

Rubinstein and Colby [97] showed that for the pure Zimm and pure Rouse models, an approximate form for the viscoelastic modulus of a power law and an exponential cutoff:

$$G' \sim G'' \sim \omega^n \tag{9.6}$$

while $G' \sim \omega^2$ and $G'' \sim \omega$ in the limit of low frequencies, as for any viscoelastic liquid.

Comparing our results with those in the work by Oelschlaeger et al [89] in their study of sodium hyaluronate with DWS and rheometry covering the frequency range from $10^{-1}$ to $10^7$ rad/s. This work is center in the application of the Rouse -Zimm model for viscoelastic moduli, we add ICF and MSD comments and extended Maxwell model fitting.

The frequency range studied in our DWS experiments goes from $10^{-1}$ up to $10^6$ rad/s. We do not measure with the macrorheometer because of it is just done in this work and we foccus our interest on managing viscoelastic models.

Concerning the variation of G' and G", similar results ot the Oelschlaeger study were obtained for the systems investigated here. It is expected and observed Rouse-Zimm slope upper a frequency $\omega > 10^4$ rad/s and the Kuhn slope at upper $\omega > 10^5$ rad/s.

Viscoelastic moduli from these samples show an evolution represented in the next Figures 9.18 and 9.20.

Figure 9.20 colects the viscoelastic moduli for both $TiO_2$ and PS particles. It is observed when $CaCl_2$ is used, that the shape of the curves is turned into a viscoelastic model following the extended Maxwell model represented by the Figure 9.19.

Figures 9.21 and 9.22 show this dependence for our hyaluronic acid system evaluated with the $TiO_2$ and PS particles, and the influence of the ionic force, so that $CaCl_2$ 0.1 M and 0.5 M are probed and the Rouse-Zimm model is adjusted.

Describing the results colected in the Figures 9.21 and 9.22 it can be seen that at low frequencies, $\omega < 10$ rad/s, the flow regime with $G' \sim \omega^2$ and $G'' \sim \omega$ is observed. At intermediate frequencies it is found that this dependence disappears, G' increases slightly with $\omega$ while G" presents a minimum and then increases almost in an approximate exponentially. It is at high frequencies, $\omega > 10^4\, rad/s$, where the response is first dominated by the Rouse-Zimm modes with a scaling exponent $G' \, or \, G'' \sim \omega^{0.5}$ and at even higher frequencies, $\omega > 10^5\, rad/s$, internal bending modes of single Kuhn segments dominate with G"$\sim \omega^{0.8-0.9}$. This results are similar to those predicted theoretically by Gittes [6] and by Morse [98].

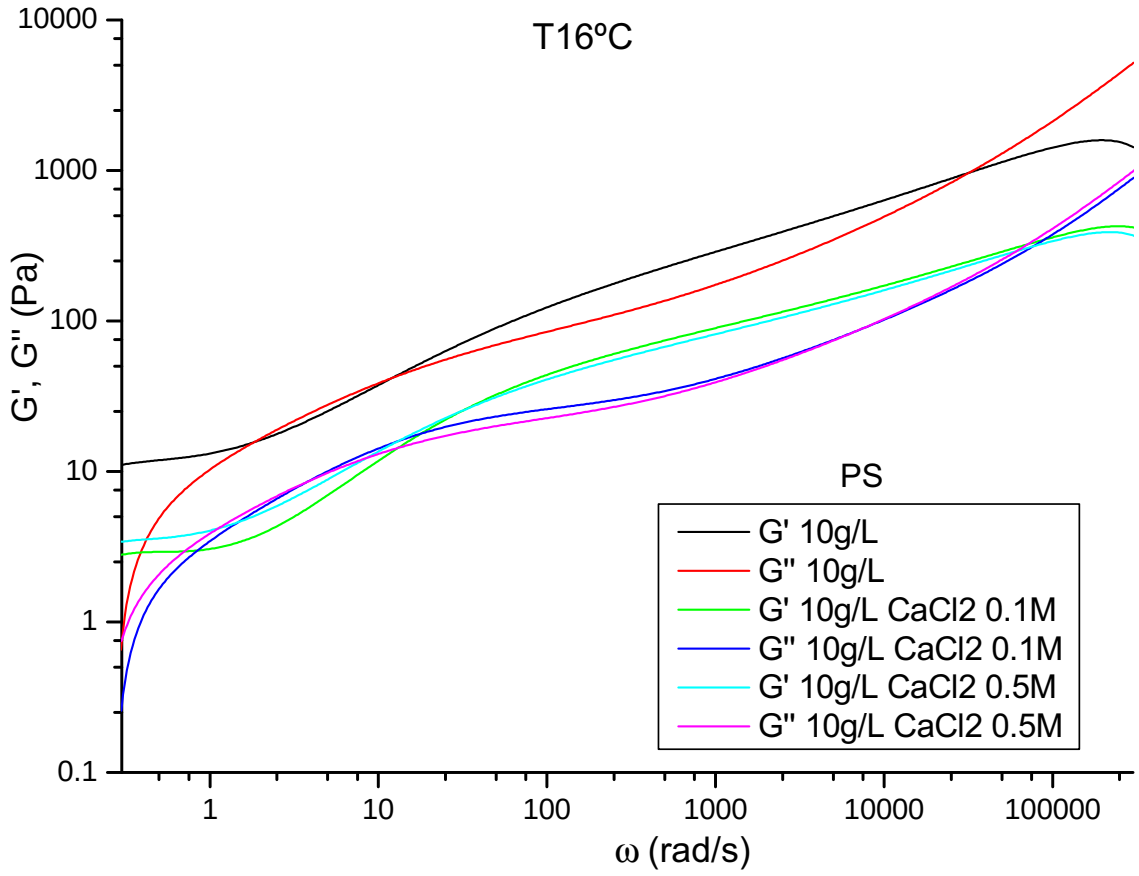


**Figure 9.18:** Viscoelastic moduli of 10g/L HA in presence of NaCl at T16°C

## 9.8. Extended Maxwell model

The MSD obtained from the equation 5.23 are fitted with the developped Maxwell model 8.3 used in the previous chapter with the Agarose and the Pluronic F127 and the results confirm that the extension of the Maxwell model is a general and consistent model that can fit the viscoelastic behavior and calculate microrheological properties in the hyaluronic acid gels.

$$g^2(t) - 1 = \left( \int_0^\infty P(s) \cdot e^{-\frac{s}{l^*} \cdot k^2 \cdot MSD} \, ds \right)^2 \tag{9.7}$$

$$MSD = 6\delta^2 \left( 1 - e^{\left(-\frac{D_0}{\delta^2} t\right)^\alpha} \right)^{\frac{1}{\alpha}} \left( 1 + \frac{D_m}{\delta^2} t \right) \tag{9.8}$$

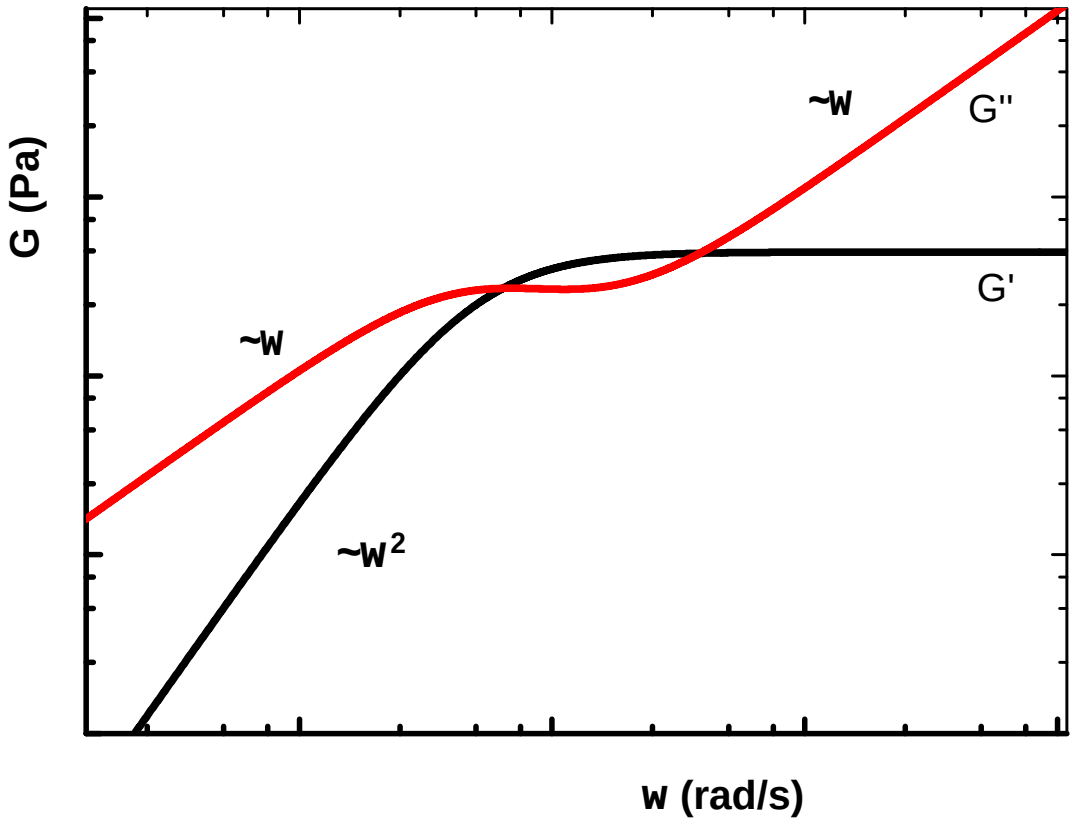


**Figure 9.19:** Elastic and viscous moduli as a function of angular frequency for the extended Maxwell fluid

Figure 9.25 represents the evolution of the cage size $\delta$ when hyaluronic acid concentration increases, $\delta$ values for all the samples decreases, except the first point that may be an artefact. This means that when the gel is forming, the threshold becomes rigider and the particles move less random. These results agree with those obtained in the Agarose and Pluronic F127.

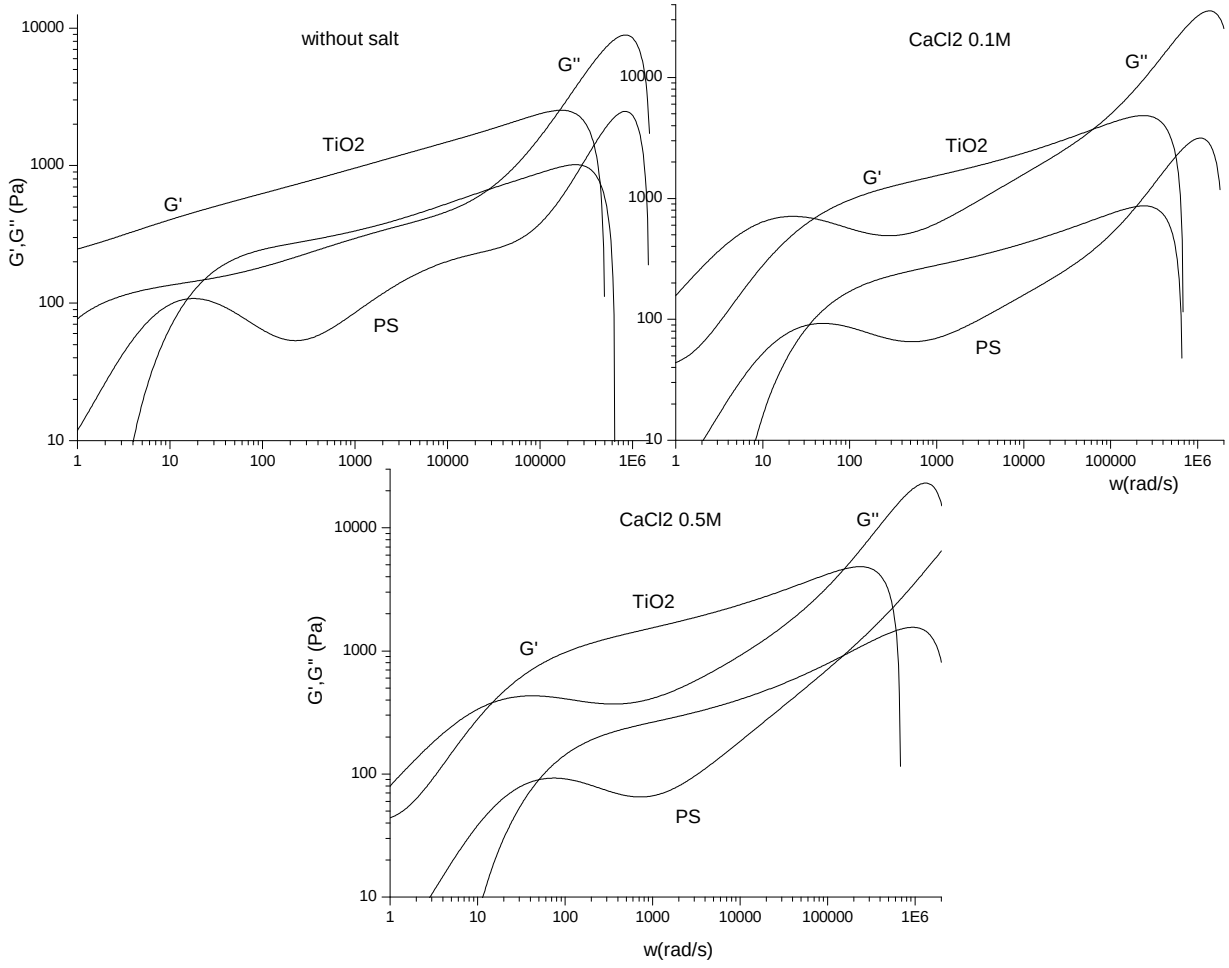


**Figure 9.20:** Viscoelastic moduli of 15g/L HA in presence of $CaCl_2$ T16°C

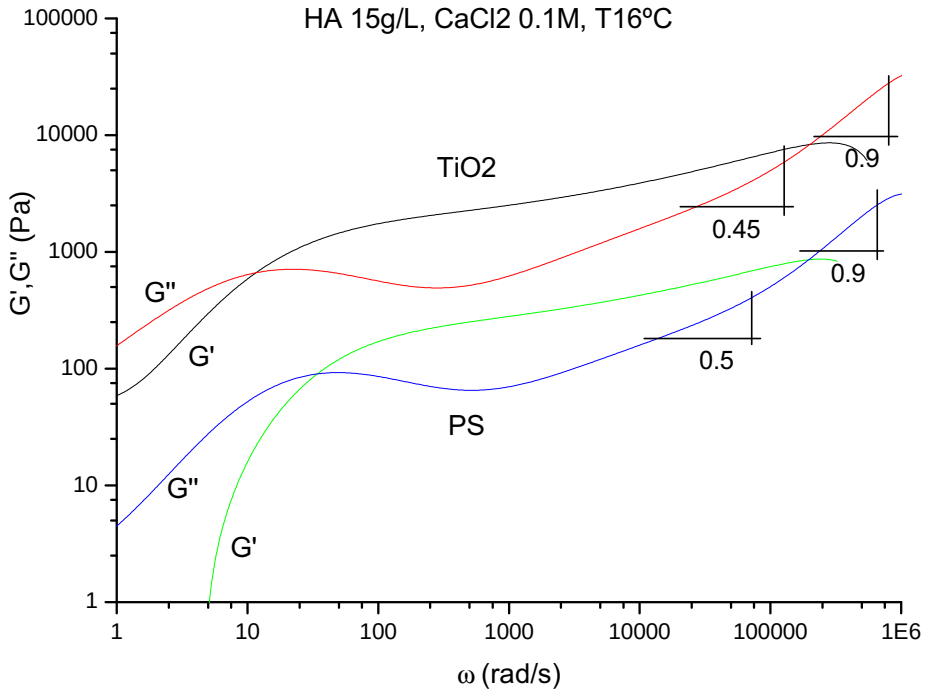


**Figure 9.21:** Rouse-Zimm slope of 15g/L HA in presence of $CaCl_2$ 0.1M T16°C

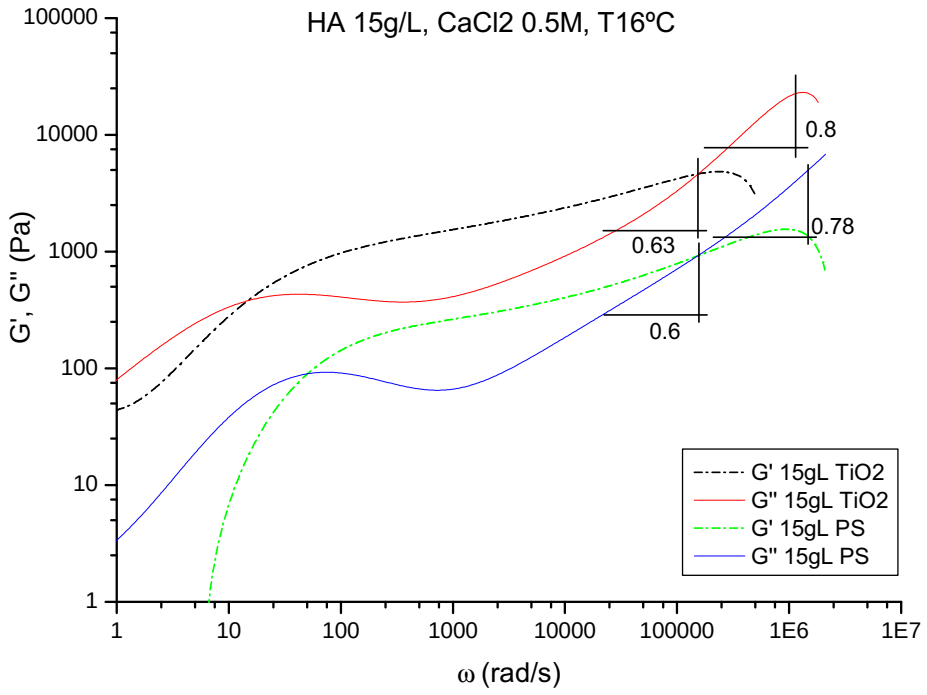


**Figure 9.22:** Rouse-Zimm slope of 15g/L HA in presence of $CaCl_2$ 0.5M T16°C

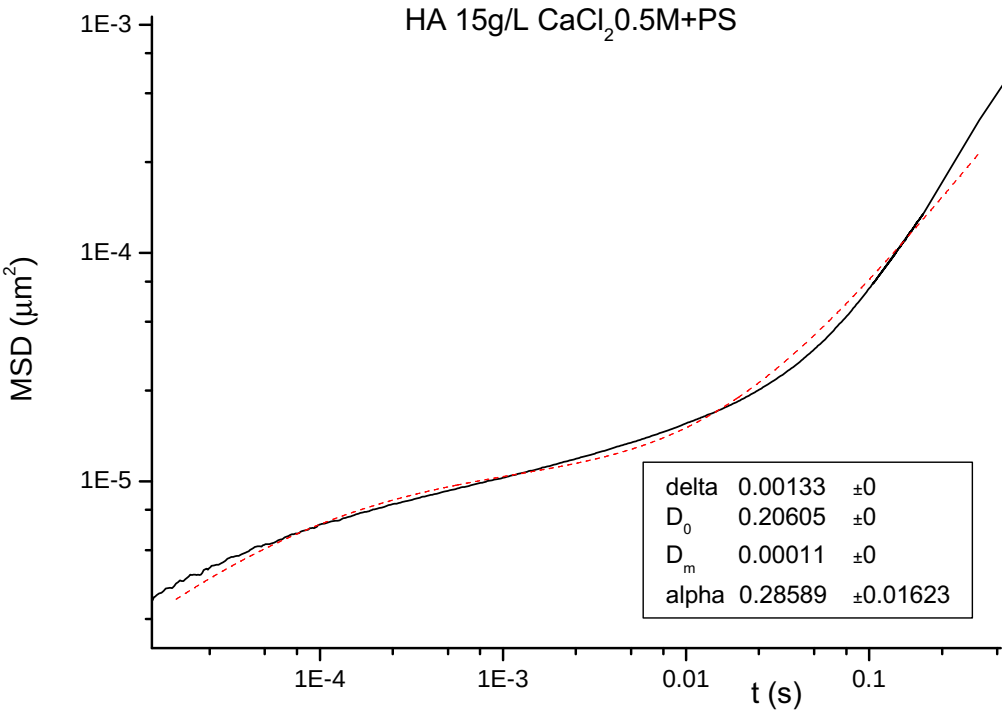


**Figure 9.23:** Maxwell fit of 15g/L HA in presence of $CaCl_2$ 0.5M with PS

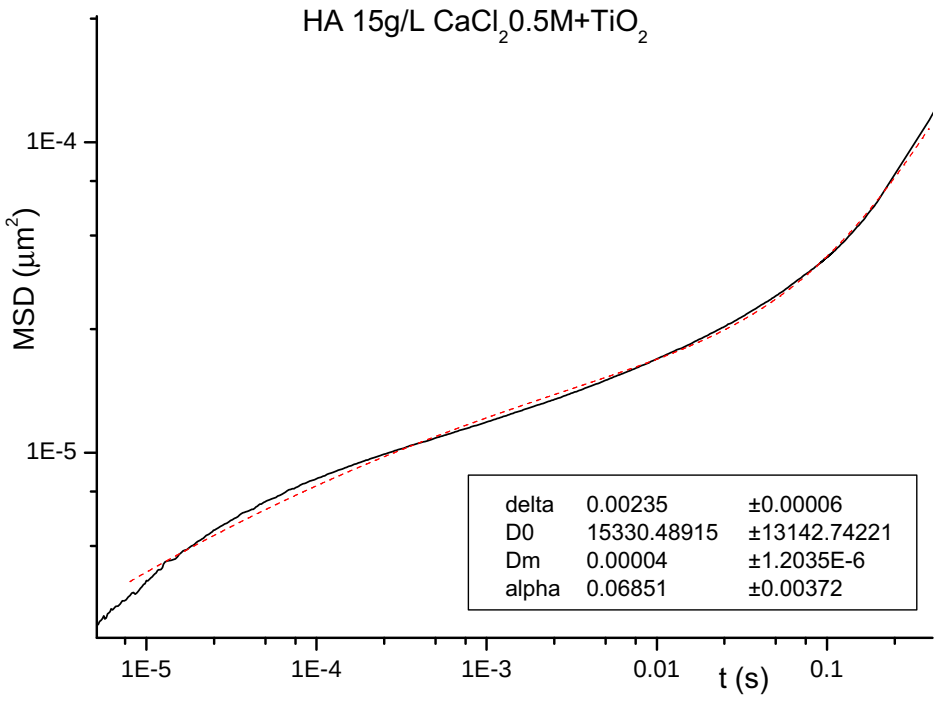


**Figure 9.24:** Maxwell fit of 15g/L HA in presence of $CaCl_2$ 0.5M with $TiO_2$

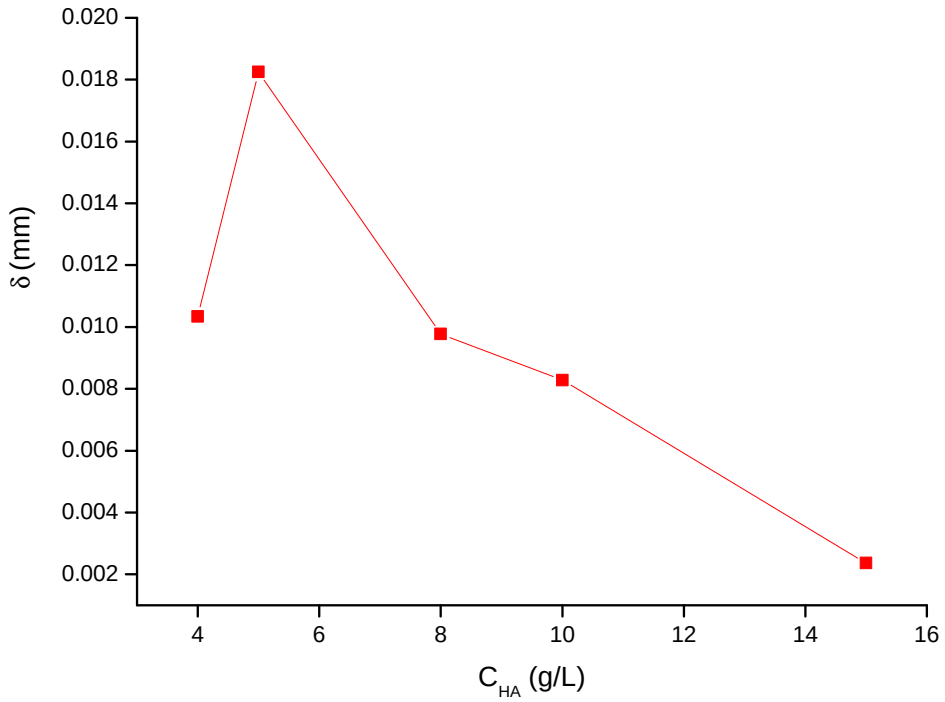


**Figure 9.25:** Evolution of delta parameter involved in Maxwell fit with concentration in presence of $CaCl_2$ 0.5M at T 16°C

The alpha parameter accounts for the width of the time relaxation distribution of the gel relaxation. Hence it is expected values of alpha increasing with concentration, and Figure 9.26 represents this trend. Values of $\alpha$ near 0.2 correspond to very broad time relaxation distributions.

It could not be possible to discuss an evolution in the parameters $D_0$ and $D_m$ because they remain constant in the equation fitting.

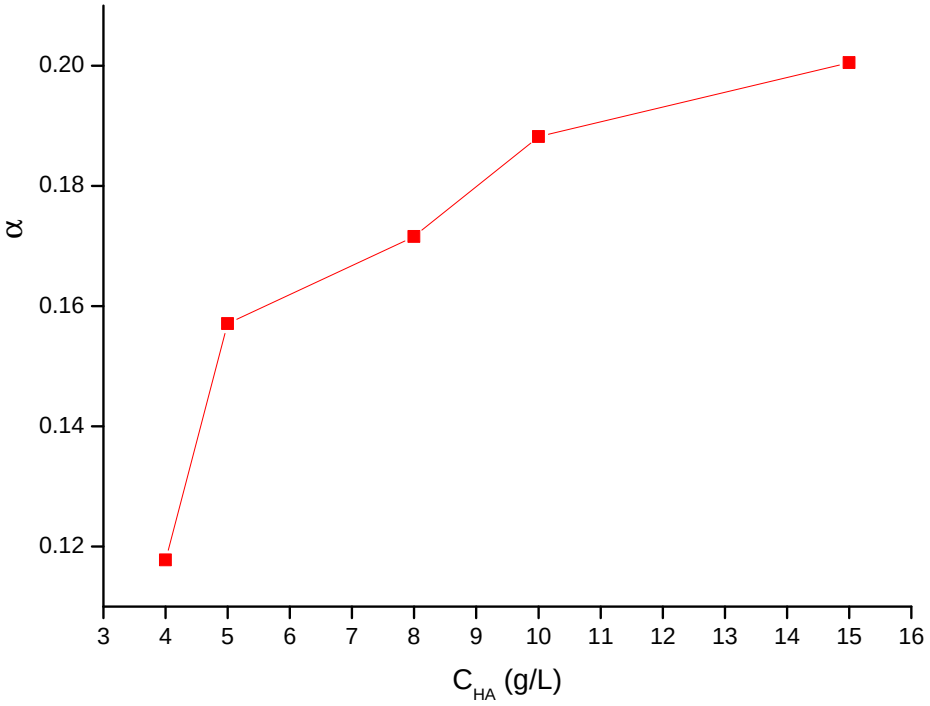


**Figure 9.26:** Evolution of alfa parameter involved in Maxwell fit with concentration in presence of $CaCl_2$ 0.5M at T 16°C

## 9.9. Conclusions Hyaluronic Acid

Hyaluronic acid has been conducted to new results in the viscoelastic behaviour that is the purpose in this dissertation.

It has been found that hyaluronic acid is stable in the entire temperature range which can be measured on the DWS. To observe viscoelastic behavior in the hyaluronic acid it is neccesary to change the ionic force in the medium. In this way, two types of salts are used in several concentration to try reach a limit in the bulk hyaluronic acid viscoelastic behavior. This has the conclusion that heavy salt is needed to observe stronger changes in viscoelastic proterties.

The develop in the Rouse-Zimm model is consistent when fitting the viscoelastic curves.

Also the developed Maxwell model can explain the viscoelastic behavior and calculate microrheological properties in the hyaluronic acid gels.

# Part III

# CONCLUSIONES

En el presente trabajo de Tesis Doctoral se ha llevado a cabo un estudio del comportamiento reológico y microreológico de diferentes sistemas con propiedades viscoelásticas. Estos sistemas son de interés en diferentes áreas tecnológicas.

Aunque en cada capítulo se han explicado las conclusiones concretas, esta sección pretende ser una recopilación de las principales conclusiones generales deducidas de los resultados obtenidos.

1. El estudio de un sistema viscoso, **glicerol** y mezclas glicerol más agua, se emplearon todos los tipos de técnicas microreológicas disponibles en el laboratorio: DLS, DWS y videomicroscopía para comprobar la compatibilidad de resultados y elegir uno de ellos para proseguir la investigación al profundizar a los sistemas viscoelásticos. DWS resultó ser la técnica más adecuada ya que es menos exigente en cuanto a la filtración de las meustras, lo que facilita el trabajo con los sistemas que forman geles, el manejo es más sencillo y permite un tratamiento de los datos más detallado.

2. Los resultados obtenidos han puesto de manifiesto que las partículas dispersadas en las mezclas agua+glicerol tienen un movimiento Browniano, como es de suponer en un líquido Newtoniano.

   Los valores de viscosidad obtenidos por DWS concuerdan con los obtenidos mediante un viscosímetro Ubbelohde y por DLS. Como cabe esperar, la viscosidad disminuye al aumentar la concentración de agua.

3. Las funciones de autocorrelación de intensidades obtenidas a partir de DLS se pueden describir mediante exponenciales simples. A partir de ellas se obtuvo el coeficiente de difusión y la dependencia temporal del desplazamiento cuadrático medio de las partículas en el seno del fluido. Estas funciones fueron analizadas con el método de Cumulantes y con el CONTIN, que dieron los mismos resultados.

4. Se realizó un estudio detallado de la técnica DWS en la agarosa, el pluronic F-127 y el ácido hialurónico, y se completó el rango de frecuencias estudiado con un reómetro oscilante convencional. Se observó la compatibilidad de ambas técnicas macro y micro en el intervalo de frecuencias común a ambas técnicas.

   Se llevó a cabo una caracterización de diferentes concentraciones de las disoluciones a distintas temperaturas. Se obtuvo el módulo complejo de cizalla en todas las muestras tanto en estado sol como gel. Los resultados han permitido confirmar la validez de un modelo de Maxwell extendido para describir las tres regiones de comortamiento encontradas en todo el intervalo de frecuencias.

5. Para comprender el comportamiento de los geles, se emplearon dos tipos de partículas: látex de poliestireno de 977 nm de diámetro y dióxido de titanio de 127 nm de diámetro. La formación de la fase gel empleando las partículas de $TiO_2$ ha dado lugar a resultados que no son compatibles con la ecuación de Stokes- Einstein. Este inusual comportamiento es debido a una interacción específica o a una reacción que se produce entre las moléculas del gel y las partículas. Esta interacción o reacción no ha sido identificada todavía, y es una de las perspectivas futuras de esta Tesis.

6. Se ha estudiado la cinética de gelificación de las disoluciones de **Agarosa** mediante DWS y el reómetro convencional. Como era de esperar la cinética se ralentiza mucho a medida que el sistema se aproxima a la transición sol-gel.

   Se ha comprobado que el mecanismo de gelificación de la agarosa concuerda con las predicciones de la Teoría de la Percolación, que ha permitido obtener la temperatura de gelificación para cada una de las concentraciones estudiadas.

7. Las funciones de autocorrelación de intensidades muestran una transición desde un decaimiento monoexponencial hasta otro descrito por una exponencial extendida a medida que el sistema se aproxima desde el estado sol hacia el gel.

8. Las curvas de MSD obtenidas a partir de las correspondientes funciones de autocorrelación representan las tres regiones que recoge el modelo viscoelástico de Maxwell desarrollado, dos zonas una incicial y final donde el gel sige un movimiento generalmente difusivo, y una zona intermedia.

   Los resultados obtenidos por microreología a frecuencias altas concuerdan con los obtenidos a baja frecuencia por reología convencional.

9. El **Pluronic F127** tiene el estado sol a baja temperatura y forma el gel a medida que la temperatura aumenta, entorno a la temperatura ambiente. Posteriormente, el sistema vuelve al estado sol a temeraturas próximas a 55°C (transición reentrante).

10. Las curvas de MSD vs tiempo del Pluronic F-127 presentan una curvatura contraria a las de agarosa en el intervalo de frecuencias estudiado curvas convexas. Lo que no se apreció para el Pluronic fue la influencia de una cinética. Se obtuvo el módulo de cizalla en todo el intervalo de frecuencias y se comprobó que la viscosidad a frecuencia cero sigue la ley de Ahrrenius.

11. El sistema **Ácido Hialurónico** + $H_2O$, solo forma gel a fuerzas iónicas altas. De este modo se han estudiado dos sales (NaCl y $CaCl_2$) a

diferentes concentraciones. A igual concentración de sal, el comportamiento viscoelástico es más evidente con el cloruro cálcico.

Los resultados de $G'(\omega)$ y $G''(\omega)$ se ajustan igual de bien con el modelo de Maxwell que con el modelo de Rouse-Zimm que tienen en cuenta estos detalles de fuerza iónica que el ácido hialurónico requiere y que en Maxwell no intervienen.

Al contrario que en los geles de agarosa, el MSD de las nanopartículas de $TiO_2$ es mayor que el de las micropartículas de PS. El comportamiento obtenido es el esperado de a mayor tamaño de las partículas menor movimiento en la red del gel según la ecuación de Stokes-Einstein.

# Part IV

# CONCLUSIONS

In the present manuscript a thorough study of the viscoelastic behavior of different systems used in many technological products and processes, such as Food Science, Cosmetics or Pharmaceutical industry has been carried out.

Despite the fact that in each chapter the particular conclusions have been explained, in this section a compilation of the main general conclusions deduced from the results of the present thesis are listed.

1. First of all, concerning results package 1, devoted to the microrheology of **glycerol**, it must be stressed that all of the different types of microrheological techniques were for the first time employed in this study: dynamic light scattering (DLS), diffusing wave spectroscopy (DWS), videomicroscopy, viscometry and reometry. All were found to be coherent and selective in the system under the conditions tested. DWS presented the best treatment and consistency among all the different light scattering techniques proved, because ot this, in the next systems is DWS the one selected.

   The system glycerol is a preliminary project to try the viscoelastic properties of a system to be investigated. Therefore, the initial system which should be studied is a viscous one where the viscosity can be changed in its magnitude.

2. Aqueous mixtures of glycerol have been explored to obtain the rheological properties. The results achieved confirm that the glycerol system has a Newtonian behaviour even at the experimental frequencies in DLS ($\sim$ kHz).

   Further studies revealed that polystyrene latex particles have a Brownian motion in the solution of glycerol. The viscosity of the solvent was also determined by a glass capillary-type viscometer. Dynamic Light Scattering is resulted to be precise in evidencing the viscous properties of this fluid that is transparent. The behaviour of the surrounding medium, glycerol-water mixtures, is viscous and particles undergo diffusive motion in a stochastic process.

3. In glycerol solutions the experimental normalized intensity autocorrelation function $g^{(2)}(t)$ obtained is an exponentially decaying function, from which the diffusion coefficient may be related through the Siegert relation with the electric field autocorrelation function $g^{(1)}(t)$ and this in terms of the mean square displacement MSD.

   It was proved that autocorrelation functions decay faster with higher observation angle, because of their dependence on the scattering vector. The linear dependence of the decay rate on the scattering vector demonstrates the diffusive character that this mode shows.

Samples with a higher decay rate correspond with mixtures of low-glycerol concentration, which provide a higher diffusion coefficient and consequently a lower viscosity. The decay rate decreases as the glycerol content increases in the mixture, so that, it is checked that viscosity is higher as more quantity of glycerol.

Cumulant and CONTIN data analysis performed for DLS data turned out to be suitable methods for the studied system, giving a similar diffusion coefficient for the latex particles.

4. Regarding the second results package devoted to the viscoelastic systems, a detailed study of the analysis of each system was conducted, and in this case based principally in DWS and reometry to complete the low frequency range.

5. An exhaustive characterization of the particles was carried out to unveil the different results obtained from the agarose with the two different types of monodisperse spherical particles used as probes: polystyrene and titanium dioxide particles with diameters 977 nm and 127 nm, respectively.

6. The formation of a new structure $TiO_2$-Agarose is the reason of the unusual and special behavior of the microrheological properties.

7. Kinetic of **Agarose** gelation with time showed that at the highest temperature the system does not present a significant evolution with aging time because it remains in the liquid phase. However, around the gelling point a significant evolution in the kinetic was observed.

   Agarose mechanism of gelation was identified to the percolation theory, and a power-law dependence of G´ and G´´ on the frequency was obtained. As the system approaches the gelation point, the agreement with a simple power law form $G = G_0 w^n$ was predicted to improve and, in fact, the values of the exponents approach each other. This fact confirm that agarose forms a gel when a homogeneous solution is cooled from a liquid to a temperature below the ordering temperature (coil-helix transition), which is around 35°C and it depends on polymer concentration.

8. The viscoelastic behavior is checked in the Agarose, the intensity autocorrelation functions at the fluid phase decay exponentially which is typical for a system that undergoes diffusion due to Brownian motion and this functions change and no longer decay to zero due to the slower motion of the clusters formed during the sol-gel transition. Using titanium dioxide particles 127 nm diameter, a second decay is observed at high temperatures that reveal the non ergodic behavior in the agarose.

9. MSD curves for the agarose represented the three regions described for a mathematical enhanced Maxwell model in viscoelastic systems.

   Rheological data combined with DWS technique showed the agreement between them, they give data numbers of the same order of magnitude.

10. The third system analyzed was the **Pluronic F127** via a novel method consisting in a secuence of cooling and stirring till the gel formation. This preparation route also results in the difference in the gel transition that occurs from low to high temperature, instead the agarose.

    The remark in the viscoelastic behavior respect the agarose is the shape of the MSD for Pluronic F127 that is different from that agarose.

    An Ahrrenius fit was probed for the viscosity data as a molecular view that can be used for a qualitative picture of the process of decrease in the bulk viscosity of a simple fluid with temperature.

11. Regarding the **Hyaluronic acid**, it was stable with temperature and to observe viscoelastic behavior it was neccesary to change the ionic force in the medium. In this way, two types of salts were used in several concentration to try reach a limit in the bulk hyaluronic acid viscoelastic behavior. The heavy salt was needed to observe stronger changes in viscoelastic proterties.

    A develop in the Rouse-Zimm model was applied when fitting the viscoelastic curves giving consistent results.

    Also the expanded Maxwell model can explain the viscoelastic behavior and calculate microrheological properties in the hyaluronic acid gels.

    Unlike in the agarose gels, the MSD of the $TiO_2$ nanoparticles is greater than the PS microparticles. The behavior obtained is that expected to larger particle moving slower than in the gel network according to the Stokes-Einstein equation.

# Part V

# BIBLIOGRAPHY

# Bibliography


[1] T. G. Mason, Estimating the viscoelastic moduli of complex fluids using the generalized stokes-einstein equation. *Rheologica Acta*, 2000, **39**, 371.

[2] T. Gisler and D. A. Weitz, Tracer microrheology in complex fluids *Current Opinion in Colloid and Interface Science.*, 1998, **3**, 586.

[3] V. Breedveld and D. J. Pine, Microrheology as a tool for high-throughput screening. *Journal of Materials Science,*, 2003, **38(22)**, 4461.

[4] T. A. Waigh, Microrheology of complex fluids. *Reports on Progress in Physics*, 2005, **68(3)**, 685.

[5] H. Freundlich and W. Seifriz, Zeitschrift für fysikalische chemie. *Polymer*, 1922, **104**, 233.

[6] F. Gittes and F. C. MacKintosh, Dynamic shear modulus of a semiflexible polymer network. *Physical review E*, 1998, **58**, R1241.

[7] F. C. MacKintosh and C. F. Schmidt, Microrheology *Current Opinion in Colloid and Interface Science.*, 1999, **4**, 300.

[8] A. Einstein, Zur theorie der brownschen bewegung. *Angewandte Chemie International Edition*, 1905, **17**, 549.

[9] A. Einstein, Über die von der molekularkinetischen theorie der wärme geforderte bewegung von in ruhenden flüssigkeiten suspendierten teilchen. *Angewandte Chemie International Edition*, 1906, **19**, 371.

[10] J. E. Mark, W. Graessley, K. Walters, K. Ngai, L. Mandelkern, E. Samulski, J. Koenig, and G. Wignall, *Physical properties of polymers.*, Cambridge, 2004.

[11] D. López, Geles poliméricos y sus aplicaciones. *Revista de plásticos modernos*, 2002, **84**, 557.

[12] J. M. Guenet, *Thermoreversible gelation of polymers and biopolymers.*, Academic press, 1992.

[13] T. Tanaka, Collapse of gels and the critical endpoint. *Physical review letters*, 1978, **40**, 820.

[14] G. M. Kavanagh and S. B. Roos-Murphy, Rheological characterisation of polymer gels. *Progress in Polymer Science*, 1998, **23**, 533.

[15] P. Flory, Molecular size distribution in three dimensional polymers. i. gelation. *Journal of the American Chemical Society*, 1941, **63**, 3083.

[16] P. Flory, Constitution of three-dimensional polymers and the theory of gelation. *Journal of Physical Chemistry*, 1942, **46**, 132.

[17] W. Stockmayer, Theory of molecular size distribution and gel formation in branched-chain polymers. *Journal of Chemical Physics*, 1943, **11**, 45.

[18] A. Miranda, M. Millán, and I. Caraballo, Study of the critical points in lobenzarit disodium hydrophilic matrices for controlled drug delivery. *Chemical and Pharmaceutical Bulletin*, 2006, **54**, 598.

[19] D. Stauffer and A. Aharony, *Introduction to Percolation Theory.*, Burgess Sciencie Press. London, 1991.

[20] H. H. Winter and M. M, Rheology of polymers near liquid-solid transitions. *Rheologica Acta*, 1997, **39**, 371.

[21] H. Leuenberger, R. Leu, and Bonny, Application of percolation theory and fractal geometry to tablet compaction. *Drug Development and Industrial Pharmacy*, 1992, **18**, 723.

[22] H. Leuenberger, B. Rohera, and C. Haas, Percolation theory - a novel approach to solid dosage form design. *International Journal of Pharmaceutics*, 1987, **38**, 109.

[23] I. Caraballo, M. Fernández-Arévalo, M. A. Holgado, and A. M. Rabasco, Percolation theory: Application to the study of the release behaviour from inert matrix systems. *International Journal of Pharmaceutics*, 1993, **96**, 175.

[24] J. Brady, *General chemistry principal and structure.*, John Wiley and sons, 2007.

[25] Y. Marcus, *Ion solvation*, John Wiley and sons, 1985.

[26] G. Knothe, J. Krahl, and J. V. Gerpen, *The Biodiesel Handbook.*, AOCS Press, 2010.

[27] M. Pagliaro, R. Ciriminna, H. Kimura, M. Rossi, and C. Della Pina,

From glycerol to value-added products. *Angewandte Chemie International Edition*, 2007, **46**, 4434.

[28] BASF Pluronic f-127 product specification. Technical report, Sigma-Aldrich, 2007.

[29] F. Lixin, M. Degen, N. Grupido, S. Bendle, and P. Pennartz, Simple linear viscoelastic models of dilute solutions of polymer molecules and emulsion droplets. *Materials Science and Engineering: A*, 2010, **528**, 127.

[30] D. Rassing and D. Attwood, Ultrasound velocity and light scattering studies on the polyoxyethylene-polyoxypropylene copolymer pluronic f127 in aqueous solution. *International Journal of Pharmaceutics*, 1983, **13**, 47.

[31] M. Vadnere, G. Amidon, S. Lindenbaum, and J. L. Haslam, Thermodynamic studies on the gelsol transition of some pluronic polyols. *International Journal of Pharmaceutics*, 1984, **22**, 207.

[32] L. Klouda and A. G. Mikos, Thermoresponsive hydrogels in biomedical applications. *European Journal of Pharmaceutics and Biopharmaceutics*, 2008, **68**, 34.

[33] G. Wanka, H. Hoffman, and W. Ulbricht, The aggregation behavior of poly-(oxyethylene)-poly-(oxypropylene)-poly-(oxyethylene)-block-copolymers in aqueous solution. *Journal of Colloid and Interface Science*, 1990, **268**, 101.

[34] G. Wanka, H. Hoffman, and W. Ulbricht, Phase diagrams and aggregation behavior of poly(oxyethylene)-poly(oxypropylene)-poly(oxyethylene) triblock copolymers in aqueous solutions. *Macromolecules*, 1994, **27**, 4145.

[35] B. Jeong, S. W. Kim, and Y. H. Bae, Thermosensitive sol-gel reversible hydrogels. *Advanced Drug Delivery Reviews*, 2002, **54**, 37.

[36] B. Weissman and K. Meyer, The structure of hialobiuronic acid from umbilical cord. *Journal of American Chemical*, 1954, **76**, 1753.

[37] J. E. Scott, F. Heatley, and W. E. Hull, Secondary structure of hyaluronate in solution. a 1h nmr investigation at 300 and 500 mhz in [ 2h 6 ] diethyl sulphoxide solution. *Biochemical Journal*, 1984, **220**, 197.

[38] J. E. Scott and F. Heatley, Hyaluronic form specific stable tertiary structure in aqueous solution: A13c-nmr study. *Proceedings of the National Academy of Sciences*, 1999, **96**, 4850.

[39] R. H. Mikelsaar and J. E. Scott, Molecular modelling of secondary and

tertiary structures of hyaluronan compared with electron microscopy and nmr data. *Glycoconjugate Journal*, 1994, **11**, 65.

[40] C. Nagorski, D. Opalensky, and F. A. Bettelhein, A study of collagen-hyaluronan interaction through swelling in poliacrylamide gels. *Research communications in molecular pathology and pharmacology*, 1995, **89**, 179.

[41] E. K. Forrest, M. Heidelberger, and H. Dawson, A serologically inactive polysaccharide elaborated by mucoid strains of group a hemolytic streptococcus. *The Journal of Biological Chemistry*, 1937, **118**, 61.

[42] S. Roseman, F. E. Moses, J. Ludowieg, and A. Dorfman, The biosynthesis of hyaluronic acid by group a streptococcus: i. utilization of 1-c14-glucose. *The Journal of Biological Chemistry*, 1953, **203**, 213.

[43] W. A. Pierce and A. G. White, Hyaluronic acid formation by streptococcus pyogenes. *Proceedings of the Society for Experimental Biology and Medicine*, 1954, **87**, 50.

[44] K. Sugahara, N. B. Schwartz, and A. Dorfman, Biosynthesis of hyaluronic acid by streptococcus. *The Journal of Biological Chemistry*, 1979, **254**, 6252.

[45] H. A. Barnes, F. J. Hutton, and K. Walters, *An introduction to rheology.*, Elsevier, 1989.

[46] B. Bird, W. Stewart, and E. Lightfoot, *Fenómenos de transporte.*, Limusa Wiley, 2006.

[47] G. Hauke, *Fenómenos de transporte.*, Copy center. Zaragoza, 2000.

[48] F. Chambon and H. H. Winter, Stopping of crosslinking reaction in a pdms polymer at the gel point. *Polymer Bulletin*, 1985, **13**, 499.

[49] E. Gross, Change of wavelength of light due to elastic heat waves at scattering in liquids. *Nature*, 1930, **126**, 201.

[50] B. J. Berne and R. Pecora, *Dynamic light scattering with applications to chemistry, biology and physics.*, New York, 2000.

[51] G. D. J. Phillies, Interpretatio of light scattering spectra in terms of particle displacements. *The Journal of Chemical Physics*, 2005, **122**, 224905.

[52] D. E. Koppel, Analusis of macromolecular polydispersity in intensity correlation spectroscopy: The method of cumulants. *Journal of Chemicals Physics,*, 1972, **57**, 4814.

[53] S. W. Provencher, Inverse problems in polymer characterization: Direct analysis of polydispersity with photon correlation spectroscopy. *Makromolekulare Chemie*, 1979, **180**, 201.

[54] S. W. Provencher, A constrained regularization method for inverting data represented by linear algebraic or integral equations. *Computer Physics Communication*, 1982, **27**, 213.

[55] S. W. Provencher, Contin: A general purpose constrained regularization program for inverting noisy linear algebraic and integral equations. *Computer Physics Communication*, 1982, **27**, 229.

[56] J. Jakes, Testing of the constrained regularization method of inverting laplace transform on simulated very wide quasielastic light scattering autocorrelation functions. *Czechoslovak Journal of Physics*, 1988, **126**, 1305.

[57] G. Maret and P. E. Wolf, Multiple light scattering from disordered media: the effect of brownian motion of scatterers. *Zeitschrift für Physik B*, 1987, **65**, 409.

[58] D. J. Pine, D. A. Weitz, P. M. Chaikin, and E. Herbolzheimer, Diffusing wave spectroscopy. *Physical Review Letters*, 1988, **60**, 1134.

[59] E. Riande, R. Díaz-Calleja, M. Prolongo, R. Masegosa, and S. C, *Polymer Viscoelasticity.*, New York, 2000.

[60] M. P. Van Albada, B. A. Van Tiggelen, A. Lagendijk, and A. Tip, Speed of propagation of classical waves in strongly scattering media. *Physical Review Letters*, 1991, **66**, 3132.

[61] L. Minini Rivas, Purificación y estudio de la estabilidad termodinámica de la proteína antena ficocianina Master's thesis, Universidad De La República. Uruguay, 2012.

[62] M. L. Gardel, M. T. Valentine, and D. A. Weitz, *Microscale Diagnostic Techniques.*, Springer-Verlag, 2005.

[63] T. G. Mason, H. Gang, and D. A. Weitz, Rheology of complex fluids measured by dynamic light scattering. *Journal of Molecular Structure*, 1996, **383**, 81.

[64] D. Van den Ende, E. Purnomo, M. H. G. Duits, W. Richterung, and F. Mugele, Aging in dense suspensions of soft thermosensitive microgel particles studied with particle-tracking microrheology. *Physical Review E*, 2010, **81**, 011404.

[65] T. G. Mason, K. Ganesan, J. H. Van Zanten, D. Wirtz, and S. C. Kuo, Particle tracking microrheology of complex fluids. *Physical Review Letters*, 1997, **79**, 3282.

[66] T. Lu, J. Huang, Z. Li, S. Jia, and H. Fu, Effect of hydrotropic salt on the assembly transitions and rheological responses of cationic gemini surfactant solutions. *The Journal of Physical Chemistry B*, 2008, **112**, 2909.

[67] D. Acharya, M. Hossain, T. Sakai, and H. Kunieda, Phase and rheological behaviour of viscoelastic wormlike micellar solutions formed in mixed nonionic surfactant systems. *Physical Chemistry Chemical Physics*, 2004, **6**, 1627.

[68] D. D. Joseph, *Fluid Dynamics of Viscoelastic Liquids.*, Springer, 1990.

[69] Y. Raikher and V. Rusakov, Theory of brownian motion in a jeffreys fluid. *Journal of Experimental and Theoretical Physics*, 2010, **111**, 883.

[70] Y. Raikher, V. Rusakov, and R. Perzynski, Brownian motion in a viscoelastic medium modelled by a jeffreys fluid. *Soft Matter*, 2013, **9**, 10857.

[71] L. S. Ornstein and G. E. Uhlenbeck, On the theory of the brownian motion. *Physical Review,*, 1930, **36**, 823.

[72] P. N. Pusey and W. Van Megen, Dynamic light scattering by non-ergodic media. *Physica A,*, 1989, **157**, 705.

[73] M. Bellour, M. Skouri, J. Munch, and P. Hebraud, Brownian motion of particles embedded in a solution of giant micelles. *The European Physical Journal E*, 2002, **8**, 431.

[74] K. T. Nijenhuis and H. H. Winter, Mechanical properties at the gel point of a crystallizing poly (vinyl chloride) solution. *Macromolecules*, 1989, **22**, 411.

[75] S. Boral, A. Saxena, and H. B. Bohidar, Universal growth of microdomains and gelation transition in agar hydrogels. *Journal of Physical Chemistry B*, 2008, **112**, 3625.

[76] E. Fernández, D. López, C. Mijangos, M. Duskova, M. Ilavsky, and K. Dusek, Rheological and termal properties of agarose aqueous solutions and hydrogels. *Journal of polymer science: Part B: Polymer physics*, 2002, **46**, 322.

[77] P. Aymard, D. Martin, K. Plucknett, T. Foster, A. Clark, and N. I, Influence of thermal history on the structural and mechanical properties of agarose

gels. *Biopolymers*, 2001, **59**, 131.

[78] G. Dumortier, J. L. Grossiod, M. Zuber, G. Couarraze, and J. C. Chaumeil, Rheological study of a thermoreversible morphine gel. *Drug Development and Industrial Pharmacy*, 1991, **17**, 1255.

[79] I. Boucenna, M. Guedeau, A. Lapp, P. Colinart, A. Proag, L. Royon, and A. Mourchid, Temperature directed-assembly of coated-laponite nanoparticles in pluronic micellar solutions. *Soft Matter*, 2013, **9**, 170.

[80] J. Escobar-Chávez, M. López-Cervantes, A. Naïk, Y. Kalia, D. Quintanar-Guerrero, and A. Ganem-Quintanar, Applications of thermo-reversible pluronic f-127 gels in pharmaceutical formulations. *Journal of Pharmacy and Pharmaceutical Sciences*, 2006, **9(3)**, 339.

[81] I. Schmolka, Artificial skin i. preparation and properties of pluronic f127 gels for treatment of burns. *Journal of Biomedical Materials Research*, 1972, **6**, 571.

[82] BASF Pluronic f-127 surfactant viscosity as a function of temperature and concentration. Technical report, BASF The chemical company, 2006.

[83] K. Meyer and J. W. Palmer, The polysaccharide of the vitreous humor. *The Journal of Biological Chemistry*, 1934, **107**, 629.

[84] K. Meyer and J. W. Palmer, The polysaccharide of the vitreous humor. *The Journal of Biological Chemistry*, 1936, **114**, 689.

[85] H. G. Garg and C. A. Hales, *Chemistry and Biology of Hyaluronan.*, Elsevier, 2004.

[86] J. Bello Gutiérrez, *Ciencia bromatológica.*, Ediciones Díaz de Santos, 2000.

[87] N. S. Chang and R. J. Boackle, Hyaluronic acid-complement interactions–ii. role of divalent cations and gelatin. *Molecular Immunology*, 1985, **22**, 843.

[88] M. I. Nieto, I. Santacruz, and R. Moreno, Consolidación de materiales cerámicos por gelificación de polisacáridos. *Rev. LatinAm. Metal. Mat*, 2014, **34**, 2.

[89] C. Oelschlaeger, M. Cota Pinto Coelho, and N. Willenbacher, Chain flexibility and dynamics of polysaccharide hyaluronan in entangled solutions: A high frequency rheology and diffusing wave spectroscopy study. *Biomacromolecules*, 2013, **14**, 3689.

[90] J. G. Oldroyd, The elastic and viscous properties of emulsions and suspensions. *Proceedings of the Royal Society of London A*, 1953, **218**,

122.

[91] J. G. Oldroyd, The effect of interfacial of stabilizing films on the elastic and viscous properties of emulsions. *Proceedings of the Royal Society of London A*, 1955, **232**, 567.

[92] M. Oosterbroek, J. Mellema, and J. S. Lopulissa, Linear viscoelasticity of emulsions. *Journal of Colloid and Interface Science*, 1981, **84**, 27.

[93] M. Oosterbroek, H. A. Waterman, S. S. Wiseall, E. G. Altena, J. Mellema, and G. A. M. Kip, Automatic apparatus, based upon a nickel-tube resonator, for measuring the complex shear modulus of liquids in the khz range. *Rheologica acta*, 1980, **19**, 497.

[94] J. Mellema, C. Blom, and J. Beekwilder, Simple linear viscoelastic models of dilute solutions of polymer molecules and emulsion droplets. *Rheologica Acta*, 1987, **26**, 418.

[95] P. E. Rouse, A theory of the linear viscoelastic properties of dilute solutions of coiling polymers. *Journal of Chemical Physics*, 1953, **21**, 1272.

[96] B. H. Zimm, Dynamics of polymer molecules in dilute solution: Viscoelasticity, flow birefringence and dielectric loss. *Journal of Chemical Physics*, 1956, **24**, 269.

[97] M. Rubinstein and R. Colby, *Polymer Physics.*, Oxford Univ. Press, New York., 2003.

[98] D. C. Morse, Viscoelasticity of tightly entangled solutions of semiflexible polymers. *Physical review E*, 1998, **58**, R1237.

[99] Z. Akcasu, Interpretation of dynamic scattering from polymer solutions. *Polymer*, 1980, **86**, 866.

[100] T. G. Mason and D. A. Weitz, Optical measurements of frequency dependent linear viscoelastic moduli of complex fluids. *Physical Review Letters*, 1995, **74**, 1250.

[101] Y. Hemar and N. Pinder, DWS microrheology of linear polysaccharide. *Biomacromolecules*, 2006, **7**, 674.

[102] A. Eshuis and J. Mellema, Viscoelasticity and microstructure of non-ionic microemulsions. *Colloid and Polymer Science*, 1984, **262**, 159.

[103] F. Scheffold, S. E. Skipetrov, S. Romer, and P. Schurtenberger, Diffusing wave spectroscopy of nonergodic media. *Physical Review E*, 2001, **63**, 061404.

[104] D. Lopez and R. Castillo, Microrheology of solutions embedded with thread-like supramolecular. *Soft Matter*, 2011, **7**, 5926.

[105] E. Sarmiento, D. Lopez, and R. Castillo, Microrheology and characteristic lengths in wormlike micelles made of a zwitterionic surfactant and sds in brine. *The Journal of Physical Chemistry B*, 2010, **114**, 12193.

[106] J. Galvan-Miyoshi, J. Delgado, and R. Castillo, Diffusing wave spectroscopy in maxwellian fluids. *The European Physical Journal E*, 2008, **26**, 369.

[107] Z. Gaygadzhiev, M. Corredig, and M. Alexander, Diffusing wave spectroscopy of the colloidal interactions ocurring between casein micelles and emulsion droplets: comparios to hard sphere behavior. *Lagmuir*, 2008, **24**, 3794.

[108] W. Brown, *Dynamic Light Scattering. The method and some applications. Monographs on the physics and chemistry of materials.*, Oxford, 1993.

[109] T. H. Larsen. *Microrheology of responsive hydrolgels.* PhD thesis, University of Delaware, 2008.

[110] W. P. Jackson. *Characterization of Soft Polymers and Gels using the Pressure-Bulge Technique.* PhD thesis, 2008.

[111] V. Zivkovic. *Study of granular temperature in dense fluidized beds by diffusing wave spectroscopy.* PhD thesis, University of Edinburgh, 2009.

BIBLIOGRAPHY

# Part VI

# CURRÍCULUM

# CURRÍCULUM

**Nuria Mancebo Radio** obtuvo el título de Ingeniera Química en el año 2008. Un año más tarde realizó el Máster de Formación del Profesorado en la Universidad Complutense de Madrid. En 2010 consiguió una beca predoctoral FPI del entonces Ministerio de Ciencia e Innovación, actualmente recogido en el Ministerio de Economía y Competitividad que le permitió iniciar su carrera investigadora bajo la dirección del profesor Dr. Francisco Ortega Gómez y del profesor Dr. Ramón González Rubio. Ese mismo año obtuvo el Máster en Ciencia y Tecnología Químicas por la Universidad Complutense de Madrid en el Departamento de Química Física I. Ha realizado una estancia predoctoral Alemania en el laboratorio de reconocido prestigio internacional en el área de dispersión de luz, de tres meses de duracción bajo la supervisión del profesor Dr. Georg Maret.